

Ciprofloxacin Metal Complexes and Linked Dimers as Potential Antimicrobial Agents

Abbey Jane Telfer

MSc

University of York

Chemistry

December 2020

Abstract

Antimicrobial resistance is one of the biggest threats to public health globally. Modifications to ciprofloxacin, a commercially available fluoroquinolone antibiotic, could overcome increasing antimicrobial resistance and increase its antimicrobial activity.

Ciprofloxacin contains several potential donor atoms, which can be used to coordinate to a metal ion. Coordination of ciprofloxacin to bioavailable metal ions such as iron(III) could promote bacterial uptake of the metallo-ciprofloxacin complex, making it a more effective antimicrobial agent over ciprofloxacin. The coordination of ciprofloxacin to metal ions with antimicrobial properties such as bismuth(III) could also further enhance the antimicrobial properties. Presented are two novel iron(III)-ciprofloxacin complexes, a novel zinc(II)-ciprofloxacin complex and a bismuth(III)-ciprofloxacin complex. The metallo-ciprofloxacin complexes presented have been characterised using a variety of techniques, including X-ray crystallography, X-ray fluorescence (XRF), fourier-transform infrared spectroscopy (FTIR), elemental analysis, solid state nuclear magnetic resonance (ssNMR) and melting point.

Another modification that can be made to the structure of ciprofloxacin is to design and synthesise a linked dimers. A dimeric compound could bridge across the binding sites of the intracellular target enzyme, DNA gyrase. Previously reported fluoroquinolone dimers have been found to possess enhanced antimicrobial properties as well as anti-tumour properties. Presented are two ciprofloxacin dimers, the first featuring an ethylenediaminetetraacetic acid (EDTA) linker and the second a diethylenetriamine pentaacetate (DTPA) linker. The EDTA and DTPA linkers have also been suggested to have antimicrobial properties due to their metal-chelating properties and therefore could further enhance the effectiveness of the ciprofloxacin dimers presented. The linked ciprofloxacin ligands presented have been characterised using nuclear magnetic resonance (NMR), High-performance liquid chromatography (HPLC), FTIR, elemental analysis and melting point.

Table of Contents

Abstract.....	2
Table of Contents.....	3
List of Tables	7
List of Figures	8
Acknowledgements.....	12
Declaration.....	13
1. Introduction	14
1.1 History of fluoroquinolones	14
1.2 Fluoroquinolones: mechanism of action and structure-activity relationship	16
1.3 Metallo-fluoroquinolones	17
1.3.1 Choice of bacteria to assess antimicrobial effectiveness	19
1.3.2 Choice of fluoroquinolone	20
1.3.4 Choice of metal	22
1.3.5 Type of bonding	25
1.3.6 Metal-to-ligand ratio.....	27
1.3.7 Summary and conclusions	30
1.4 Complexes of fluoroquinolone dimers	30
1.4.1 DNA gyrase: fluoroquinolone drug target	31
1.4.2 Antimicrobial properties	32
1.4.3 Anti-tumour properties.....	34
1.4.4 Summary and conclusions	35
2.1 Aims and objectives	36
2.2 Introduction	36
2.3 Iron(III)-ciprofloxacin	42
2.3.1 Preliminary experiments.....	44
Optimum metal-to-ligand ratio for coordination of iron(III) to ciprofloxacin	44
Optimum pH for complexation	47
2.3.2 Crystallisation Techniques	48
Solvent Layering.....	48
Vapour Diffusion	48
2.3.3 Synthesised iron(III)-ciprofloxacin complexes	49
2.3.3.1 Iron(III) chloride-ciprofloxacin complex.....	49
2.3.3.2 Iron(III) sulfate-ciprofloxacin complex.....	57

2.3.3.3 Summary of conclusions from crystallographic information.....	65
2.4 Bismuth-ciprofloxacin complex.....	66
2.4.1 1:4 bismuth(III)-ciprofloxacin.....	66
2.4.2 1:3 bismuth(III)-ciprofloxacin.....	67
2.5 Zinc-ciprofloxacin.....	69
2.2 Other attempts at metallo-FQ complexation	74
2.3 Conclusions	74
2.4 Future work.....	75
3. Ciprofloxacin Dimers.....	76
3.1 Aims and objectives	76
3.2 Introduction	76
3.4 EDTA-ciprofloxacin dimer	83
3.5 DTPA-ciprofloxacin dimer	91
3.6 Conclusions	97
3.7 Future Work.....	98
4. Overall summary, conclusions and future work	99
4.1 Metallo-ciprofloxacin complexes.....	99
4.2 Linked dimeric ciprofloxacin compounds	100
5. Experimental	101
5.1 <i>General Remarks</i>	101
5.1.1 Materials	101
5.1.2 Instruments.....	101
5.2 <i>Methods</i>	102
5.2.1 Job's Plot	102
5.2.2 Metallo-fluoroquinolone precursors	102
5.2.3 Metallo-fluoroquinolone synthesise.....	104
5.2.4 Dimer complex synthesise	107
5.2.5 Crystallisation Methods	113
Abbreviations.....	114
6. Appendices.....	115
6.1 Ciprofloxacin sodium salt.....	115
6.1.1 FTIR.....	115
6.1.2 ¹ H NMR.....	116
6.1.3 COSY	117
6.1.4 ¹³ C NMR.....	118
6.1.5 ¹⁹ F NMR	119

6.1.6 mass spectrometry.....	120
6.2 Bismuth oxynitrate.....	121
6.2.1 FTIR.....	121
6.3 1:2 iron(III)-ciprofloxacin.....	122
6.3.1 FTIR.....	122
6.3.2 X-ray crystal structure data and refinement.....	123
6.3.3 X-ray crystal structure bond lengths.....	125
6.3.4 X-ray crystal structure bond angles	126
6.4 1:1/1:2 Iron(III)-ciprofloxacin salt	128
6.4.1 FTIR.....	128
6.4.2 X-ray crystal structure bond lengths.....	129
6.4.3 X-ray crystal structure bond angles	132
6.5 1:3 bismuth(III)-ciprofloxacin.....	136
6.5.1 FTIR.....	136
6.5.2 ¹ H NMR.....	137
6.5.3 COSY	138
6.5.4 ¹³ C NMR.....	139
6.5.5 ¹⁹ F NMR	140
6.6 1:2 zinc(II)-ciprofloxacin.....	141
6.6.1 FTIR.....	141
6.6.2 ¹³ C ssNMR	142
6.6.3 ¹⁹ F ssNMR	143
6.7 Ciprofloxacin methyl ester	144
6.7.1 FTIR.....	144
6.7.2 ¹ H NMR.....	145
6.7.3 ¹³ C NMR.....	146
6.7.4 ¹⁹ F NMR	147
6.7.5 mass spectrometry.....	148
6.8 EDTA-ciprofloxacin dimer sodium salt	149
6.8.1 FTIR.....	149
6.8.2 ¹ H NMR.....	150
6.8.3 COSY	151
6.8.4 ¹⁹ F NMR	152
6.8.4 mass spectrometry.....	153
6.9 DTPA-ciprofloxacin methyl ester dimer	154
6.9.1 mass spectrometry.....	154

6.10 DTPA-ciprofloxacin dimer sodium salt.....	155
6.10.1 FTIR.....	155
6.10.2 ¹ H NMR.....	156
6.10.3 COSY.....	157
6.10.4 ¹³ C NMR.....	158
6.10.5 ¹⁹ F NMR.....	159
References	160

List of Tables

Table 1: MIC values of [Bi(norfloxacin) ₃ (H ₂ O) ₂] and norfloxacin against fluoroquinolone resistant strains of <i>H. pylori</i>	20
Table 2: The stability constants (K) for a range of fluoroquinolone-metal ion complexes calculated using capillary zone electrophoresis at 298 K with a 30 kV separation potential and pH 3.25 for Fe(III) and Al(III) complexes, 8.02 for the Mg(II) complexes.	22
Table 3: Pearson classification of a selection of Lewis acid metal ions, categorised as soft, intermediate and hard.	23
Table 4: stability constants from fluorescence of 1:1 metal(II)-Nalidixic acid complexes from two different studies.	24
Table 5: enthalpy (kJ mol ⁻¹) of reactions between Ca(II)/ Mg(II) metal ions with ciprofloxacin (5) calculated from the temperature dependence of the stability constants of the reactions. ΔH ₁ represents the enthalpy change on the coordination of a single ciprofloxacin ligand and ΔH ₂ represents the enthalpy change on the coordination of a second ciprofloxacin ligand to the metal(II)-ciprofloxacin complex.	26
Table 6: the percentage reduction in minimum inhibitory concentration (MIC) for [Bi(norfloxacin) ₃ (H ₂ O) ₂] and [Bi(norfloxacin) ₄ (H ₂ O) ₂] against <i>Escherichia coli</i> , <i>Bacillus pumilis</i> , <i>Staphylococcus aureus</i> and <i>Staphylococcus epidermidis</i>	28
Table 7: values for stability constants K ₁ and K ₂ for the above reactions for a range of metal(II) ions in the complexation of 1:1 metal(II)-nalidixic acid and 1:2 metal(II)-nalidixic acid according to the above reactions at pH 6.4.	29
Table 8: summary of findings reported in the literature on different combinations of metals, fluoroquinolones (FQ) and metal-fluoroquinolone ratios.	30
Table 9: a summary of relevant data from the results of a ciprofloxacin compound search using the CSD. The complexes included in this table are metallo-ciprofloxacin complexes whereby ciprofloxacin coordination to the metal ion takes place through the ketone and carboxylate oxygen donor atoms of the ciprofloxacin ligands*.	37
Table 10: formal charges (q) and ionic radii (r) ⁸¹ of selected metal ions, used to calculate charge densities (ρ) of the metal ions.	39
Table 11: selected bond lengths for 1:2 iron(III)-ciprofloxacin (1).	51
Table 12: selected bond angles for the crystal structure of (1).	51
Table 13: selected bond lengths for ciprofloxacin (2).	55
Table 14: summary of unsuccessful attempts at synthesis of metallo-fluoroquinolones.	74
Table 15: summary of current literature on fluoroquinolone dimer molecules and their antimicrobial/ anti-tumour properties.	82
Table 16: summary of the EDTA-ciprofloxacin dimer sodium salt ¹ H NMR chemical shifts and associated data (integration and multiplicity) as well as any ¹ H- ¹ H coupling observed in the COSY NMR spectrum recorded in sodium hydroxide and DMSO- <i>d</i> ₆	90
Table 17: summary of the DTPA-ciprofloxacin dimer sodium salt ¹ H NMR chemical shifts and associated data (integration and multiplicity) as well as any ¹ H- ¹ H coupling observed in the COSY NMR spectrum recorded in DMSO- <i>d</i> ₆ and sodium hydroxide.	96

List of Figures

Figure 1: pharmacophore of fluoroquinolones.....	14
Figure 2: structures of fluoroquinolones marketed in the early 1980s norfloxacin (1), pefloxacin (2), enoxacin (3), fleroxacin (4), ciprofloxacin (5) and ofloxacin (6).	15
Figure 3: timeline showing the development of quinolone generations with examples and their structures for each.....	16
Figure 4: fluoroquinolone pharmacophore with labelled structure activity relationship and alternate substituents that could improve the potency in each position.	17
Figure 5: a general reaction scheme of fluoroquinolone with a metal M(III) cation to form a metallo-fluoroquinolone in hydrochloric acid. The scheme shows how fluoroquinolones can coordinate to metals: through the carboxylate/ ketone groups in positions 3 and 4 respectively.	18
Figure 6 : structure of complex formed by zinc(II) ions from biomolecules and levofloxacin in blood plasma exhibiting coordination via nitrogen atoms in the 1-methylpiperazine group in the R ₂ position.....	18
Figure 7: general structure of coordination of norfloxacin to a metal cation (2+) through the two oxygen donor atoms in the β-ketone carboxylate group.	19
Figure 8: structures of ciprofloxacin (top left), lomefloxacin (top right) and levofloxacin (bottom).....	25
Figure 9: reported structures of Bi(III)(norfloxacin) ₃ (H ₂ O) ₂ (7) and Bi(III)(norfloxacin) ₄ (H ₂ O) ₂ (8).	28
Figure 10: structure of fluoroquinolone target molecule; DNA gyrase. DNA gyrase is a dimer protein composed of the monomers gryA and gryB.	31
Figure 11: left: structure of the DNA gyrase dimer. Right (top): a close-up of the two recognition helices at the 'head dimer interface', viewed from the top with the side chains of residues 81, 87, 122 shown (generated with MolScript). Right (bottom): linked fluoroquinolone dimer.....	32
Figure 12: piperazinyl linkers used in effective antibiotic fluoroquinolone dimers: (7) p-xylene (8) m-xylene (9) 2,6-dimethylpyridine (10) (E)-but-2-ene (11) 1,1-biphenyl. Fluoroquinolones with piperazinyl groups in the R ₂ position can be bonded to linkers to form dimeric fluoroquinolone molecules, as shown in the molecule at the top of the figure. The linkers (structures 7-11) bond to fluoroquinolones in the positions labelled "FQ".....	33
Figure 13: synthesised fluoroquinolone dimer with linker at the C ₃ position, which has anti-tumour properties.	34
Figure 14: graph of the relationship between the mean M-O bond lengths in published metallo-ciprofloxacin complexes and the charge density (ρ) of metal ions. The error bars plotted are the mean maximum and minimum values from the published data. The metal-ketone (black) and metal-carboxylate oxygen (red) bond lengths are plotted separately for comparison.	40
Figure 15: graph showing the relationship between metal ion charge density (increasing from Sm(III) to Fe(III)) and the O-M-O bite angle in metallo-ciprofloxacin complexes.....	41
Figure 16: iron uptake mechanism in Gram positive bacteria whereby iron in heme, siderophore or transferrin is taken into the cell by membrane-anchored binding proteins and permease proteins and is then released as iron(III) after reacting with ATP in ATP-binding cassette proteins. This figure was adapted from a figure by K. D. Krewulak and H. J. Vogel.....	42
Figure 17: iron uptake mechanisms in Gram negative bacteria. Various outer membrane proteins are used to transport iron(III) in the form of transferrin, iron-bound siderophores and heme groups into the periplasm, which are then bound to periplasmic binding proteins which	

facilitate the transportation into the cytoplasm and through ATP-binding cassette proteins to release iron(III) into the cytoplasm. This figure was adapted from a figure by K. D. Krewulak and H. J. Vogel.....	43
Figure 18: protein structure of a porin by M. S. Weiss and G. E. Schulz (generated with Discovery Studio Visualizer).....	43
Figure 19: structure of $[\text{Fe}(\text{cfH})\cdot(\text{C}_2\text{O}_4)]\cdot(\text{cfH}_2^+)\cdot 5\text{H}_2\text{O}$, from crystallographic data reported by L.-C. Yu <i>et al.</i>	44
Figure 20: Job's plot graph showing the relationship between pH and molar fraction of ciprofloxacin on absorbance at 456 nm. The concentrations of the metal and ligand solutions were $1.81 \times 10^{-3} \text{ mol dm}^{-3}$ each in hydrochloric acid (0.1 M for pH 2 and 0.02 M for pH 3). The results plotted are the mean of the triplicate results at each pH, with the error bars showing \pm one standard deviation. The experimental procedure is detailed in section 6.2.1.....	45
Figure 21: Job's plot graphs showing extrapolated data points used to calculate the values of ϵ and subsequently K_{eq} for iron(III)-ciprofloxacin systems at pH 2 (left) and pH 3 (right).	46
Figure 22: scheme showing the varying pKa values of ciprofloxacin.....	47
Figure 23: solvent vapour diffusion crystallisation method set up using an open smaller sample vial (1.8 mL) half filled with the reaction mixture (approx. 1 mL), inside a tightly sealed larger sample vial (8mL) containing the antisolvent (approx. 1 mL).....	49
Figure 24: ORTEP representation of the asymmetric unit of 1:2 iron(III)-ciprofloxacin (1). Ellipsoids are plotted at 50 % probability	51
Figure 25: ball and stick representation of the asymmetric unit of (1) with the bond angle of O3-Fe2-O1 measured to be $84.99(6)^\circ$. Solvent atoms and hydrogen atoms have been removed for clarity.....	53
Figure 26: wire representation of (1) with the pi stacking distance of the aromatic rings of the ciprofloxacin ligands measured to be 3.850 \AA between the C2/C3/N1/C4/C9/C10 rings and 5.209 \AA between the C4/C5/C6/C7/C8/C9 rings, using calculated centroid atoms. Solvent atoms and hydrogen atoms have been omitted for clarity.....	53
Figure 27: ORTEP representation of the X-ray crystal structure of ciprofloxacin (2). Ellipsoids are plotted at 50 % probability. C15A, C17A and C18A have been omitted for clarity, these formed a minor structure within the crystal with a ratio of the occupancy of the major and minor structures of 0.931:0.069(3). This structure was collected and refined by Adrian C Whitwood.	55
Figure 28: X-ray crystal structure of $[\text{FeCl}(\text{H}_2\text{O})(\text{cfH})]$ (1), showing the intermolecular interactions. <i>Left</i> : ball and stick asymmetric unit of (1) with atom labels showing intermolecular interactions. <i>Right</i> : structure of (1) with ellipsoids plotted at 50 % probability, showing intermolecular interactions. In both diagrams solvent atoms have been removed for clarity.	56
Figure 29: ball and stick packing formation of (1).	56
Figure 30: ORTEP representation of the X-ray crystal structure of (3). Ellipsoids are plotted at 50 % probability. O20 and O19 (occupancy of 0.44(3)), C31A, C32A, C33A and C34A (occupancy of 0.684(6)), and C15A, C16A and C17A (occupancy of 0.361(6)) have been omitted for clarity. Data collected and refined by Theo Tanner.....	59
Figure 31: ORTEP representation of the X-ray crystal structure of the 1:2 iron(III)-ciprofloxacin complex found in (3), $[\text{Fe}(\text{SO}_4)_2(\text{cfH})_2]$, henceforth referred to as 3i . Ellipsoids are plotted at 50 % probability. O20 and O19 (occupancy of 0.44(3)), C31A, C32A, C33A and C34A (occupancy of 0.684(6)), and C15A, C16A and C17A (occupancy of 0.361(6)) have been omitted for clarity.	60

Figure 32: wire frame representation of 3i with measured bond angles for the O-M-O bite angles for each of the ciprofloxacin ligands. Solvent and hydrogen atoms have been omitted for clarity.....	61
Figure 33: wire frame representation of 3i , showing the measured distances between calculated centroids in the aromatic rings of the ciprofloxacin ligands. The hydrogen and solvent atoms have been removed for clarity.....	62
Figure 34: ORTEP X-ray crystal structure of the 1:1 iron(III)-ciprofloxacin structure found in (3) $[\text{Fe}(\text{SO}_4)(\text{H}_2\text{O})_3(\text{cfH})]^+$, henceforth referred to as 3ii . Ellipsoids are plotted at 50 % probability.	63
Figure 35: wireframe representation of 3ii with a measured O-M-O bite angle for the ciprofloxacin ligand. Hydrogen and solvent atoms have been removed for clarity.....	64
Figure 36: X-ray crystal structure of the 1:1 complex salt of $[\text{Fe}(\text{SO}_4)_2(\text{cfH})_2]^-$ 3i and $[\text{Fe}(\text{SO}_4)(\text{H}_2\text{O})_3(\text{cfH})]^+$ 3ii . Ellipsoids plotted at 50 % probability.	65
Figure 37: $[\text{Bi}(\text{H}_2\text{O})_2(\text{norfloxacin})_4]$ structure proposed by A. R. Shaikh <i>et al.</i> , for which an attempt at the synthesis of a bismuth(III)-ciprofloxacin complex was made.....	67
Figure 38: the proposed structure of $[\text{Bi}(\text{H}_2\text{O})_2(\text{cf})_3]$, synthesised by A. R. Shaikh <i>et al.</i>	68
Figure 39: XRF spectrum of the compound $[\text{Bi}(\text{H}_2\text{O})_2(\text{cf})_3]$. This spectrum confirms the presence of bismuth in the product obtained.....	69
Figure 40: proposed structure of the $[\text{Zn}(\text{H}_2\text{O})_2(\text{cf})_2]$ by Chohan <i>et al.</i>	70
Figure 41: XRF spectrum of the compound synthesised following the procedure reported by Chohan <i>et al.</i>	71
Figure 42: $^{19}\text{F}\{^1\text{H}, ^{13}\text{C}\}$ ssNMR spectrum of the synthesised zinc(II)-ciprofloxacin complex. Asterisks indicate spinning sidebands.	72
Figure 43: $^{13}\text{C}\{^1\text{H}\}$ ssNMR spectrum of the synthesised zinc(II)-ciprofloxacin complex. Asterisks indicate spinning sidebands.....	72
Figure 44: proposed structure of the repeated synthesis of a zinc(II)-ciprofloxacin structure, based on elemental analysis of the compound.	73
Figure 45: generic structure of dimeric ciprofloxacin compounds comprised of two ciprofloxacin molecules connected by a linker.....	76
Figure 46: schematic diagram showing the various types of DNA type II topoisomerases.....	78
Figure 47: structures of two anti-tumour drugs which target mammalian topoisomerase II. <i>Top</i> : doxorubicin. <i>Bottom</i> : mitoxantrone.	79
Figure 48: reported structures of fluoroquinolone dimers with increased anti-tumour properties in comparison to their fluoroquinolone monomers. <i>Top</i> : ciprofloxacin dimer with $\text{CH}_2\text{OCO}(\text{CH}_2)_{14}\text{COOCH}_2$ linker. <i>Middle</i> : ciprofloxacin dimer with $(\text{CH}_2)_{14}$ linker. <i>Bottom</i> : modified (ethyl group added to piperazinyl group) ciprofloxacin dimer with linker in the C ₃ position. ...	80
Figure 49: fluoroquinolone pharmacophore, for fluoroquinolone dimer linker position reference.....	81
Figure 50: proposed changes in stacking of EDTA-ciprofloxacin molecules as a result of different solvents.....	84
Figure 51: reaction scheme for the synthesis of the ciprofloxacin EDTA dimer sodium salt.	85
Figure 52: HPLC graphs for ciprofloxacin (<i>left</i>) and EDTA-ciprofloxacin dimer (<i>right</i>).	86
Figure 53: $^{19}\text{F}\{^1\text{H}\}$ NMR of EDTA-ciprofloxacin sodium salt, showing a single peak at -124.23 ppm with the zoomed in image of the peak in the top left.....	87
Figure 54: $^{19}\text{F}\{^1\text{H}\}$ NMR spectra for ciprofloxacin methyl ester (<i>top</i>) in chloroform- <i>d</i> , and the EDTA-ciprofloxacin dimer sodium salt (<i>bottom</i>) in DMSO- <i>d</i> ₆ /sodium hydroxide.	87
Figure 55: ^1H NMR of sodium hydroxide and acetone in DMSO, with the corresponding peaks labelled.....	88

Figure 56: numbered structure of the EDTA-ciprofloxacin dimer sodium salt.....	89
Figure 57: ^1H - ^1H COSY spectrum for the EDTA-ciprofloxacin dimer sodium salt in sodium hydroxide and $\text{DMSO-}d_6$	89
Figure 58: DTPA-ciprofloxacin dimer stacking interaction as a result of different solvents.....	91
Figure 59: reaction scheme for the synthesis of the ciprofloxacin DTPA dimer sodium salt.	92
Figure 60: $^{19}\text{F}\{^1\text{H}\}$ NMR spectrum of the DTPA-ciprofloxacin dimer sodium salt with an expanded image showing that there is only a singlet peak.....	93
Figure 61: stacked $^{19}\text{F}\{^1\text{H}\}$ NMR spectra of the EDTA-ciprofloxacin dimer sodium salt (<i>top</i>) and the DTPA-ciprofloxacin dimer sodium salt (<i>bottom</i>) showing that they contain a single peak at -124.23 ppm.	94
Figure 62: numbered structure of the DTPA-ciprofloxacin dimer sodium salt.....	95
Figure 63: COSY spectrum of the DTPA-ciprofloxacin dimer sodium salt in $\text{DMSO-}d_6$ and sodium hydroxide.	95
Figure 64: numbered ciprofloxacin structure for the assignment of NMR peaks in $[\text{Bi}(\text{ciprofloxacin})_3(\text{H}_2\text{O})]$	106
Figure 65: structure of 2-({2-[(carboxymethyl)(2-{4-[1-cyclopropyl-6-fluoro-3-(methoxycarbonyl)-4-oxo-1,4-dihydroquinolin-7-yl]piperazin-1-yl}-2-oxoethyl)amino]ethyl}{2-{4-[1-cyclopropyl-6-fluoro-3-(methoxycarbonyl)-4-oxo-1,4-dihydroquinolin-7-yl]piperazin-1-yl}-2-oxoethyl)amino)acetic acid, referred to as [EDTA(ciprofloxacin methyl ester) $_2$].	109
Figure 66: numbering scheme used for the NMR assignment of 7-[4-(2-{[2-({2-[(3-carboxy-1-cyclopropyl-6-fluoro-4-oxo-1,4-dihydroquinolin-7-yl]piperazin-1-yl)-2-oxoethyl}{(carboxymethyl)amino}ethyl{(carboxymethyl)amino}acetyl)piperazin-1-yl]-1-cyclopropyl-6-fluoro-4-oxo-1,4-dihydroquinoline-3-carboxylic acid, formed in an NMR tube with $\text{DMSO-}d_6$ and sodium hydroxide, referred to as [EDTA(ciprofloxacin) $_2$]. Spectra described below.	110
Figure 67: diagrams of crystallisation methods described in this section.....	113

Acknowledgements

I would like to thank Professor Anne-Katherine Duhme-Klair for giving me the opportunity and for supporting my research throughout my Masters to help me develop my skills as a chemist. I would also like to acknowledge Dr Anne Routledge for providing academic support throughout my time at York as my undergraduate supervisor and IPM. It has been a pleasure working as part of the AKDK group. Ben, Conor, James, Katie, Lisa, Luke, Nat, Ros, Thorsten and Tom have all been helpful, supportive and inspirational throughout my Masters.

I would like to acknowledge all the technicians at the University of York Chemistry Department. In particular, thank you to Dr Emma Dux, Dr Adrian Whitwood, Theo Tanner, Heather Fish, Karl Heaton and Dr Graeme McAllister for running samples and maintaining equipment used in the duration of my research for my Masters. A special thanks also to Chris Goult for assisting in ssNMR for this project as well as being part of my inspiration to continue into academic research.

Thank you to my friends and family who have supported me throughout my academic journey. I am blessed to have such a wonderful brother and parents who have encouraged me to “reach for the moon” and “be big”. The girls from home have been with me throughout all of the ups and downs of school and beyond, I’m so proud of how far Beth, Hannah, Holly and I have all come. Thank you to Alex and Melissa for sharing my experiences studying at York and becoming friends for life. My partner Sammy inspires me everyday, in the words of Michael Scott: “you complete me”.

I would also like to thank Professor Paul Walton and Dr Sofia Diaz-Moreno for offering me a PhD position; allowing me to continue my academic journey and giving me added motivation.

Thank you to everyone who has played a part in helping me to get to where I am today.

Declaration

I declare that this thesis is a presentation of original work and I am the sole author. This work has not previously been presented for an award at this, or any other, University. All sources are acknowledged as References.

1. Introduction

1.1 History of fluoroquinolones

Antimicrobial resistance is one of the biggest threats to public health globally¹. Fluoroquinolones are a group of molecules with a pharmacophore shown in figure 1. They have broad spectrum antimicrobial properties and are commercially available as oral antibiotics, often used to treat infections such as urinary tract infections, gastrointestinal infections, respiratory tract infections, sexually transmitted diseases and skin infections^{2,3}.

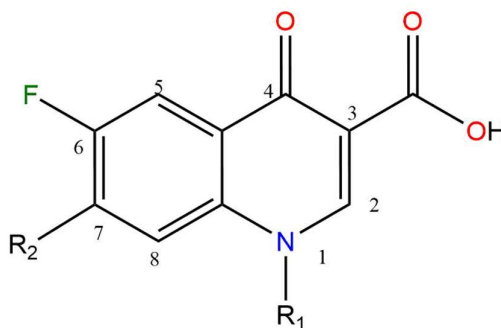


Figure 1: pharmacophore of fluoroquinolones.

The first fluoroquinolones developed were second generation quinolones. The first clinically-available fluoroquinolone was norfloxacin (1), patented in 1977⁴. The success of this drug saw the development of several more fluoroquinolone antibiotics within the next three years, many of which are still commonly used to treat infections today. These include: pefloxacin (2), enoxacin (3), fleroxacin (4), ciprofloxacin (5) and ofloxacin (6)⁵ (figure 2). Second generation quinolones can be subdivided into Class I and Class II fluoroquinolones, with Class II fluoroquinolones exhibiting higher serum, tissue, and intracellular drug concentrations compared with Class I second generation quinolones^{6,7}. Of the second generation quinolones listed (figure 2) ciprofloxacin (5) and ofloxacin (6) are Class II, whereas the (1)-(4) are Class I second generation quinolones. When these fluoroquinolones were first brought onto the market, there was virtually zero resistance, however for many infections, fluoroquinolones are now an ineffective treatment in more than half of patients globally⁸.

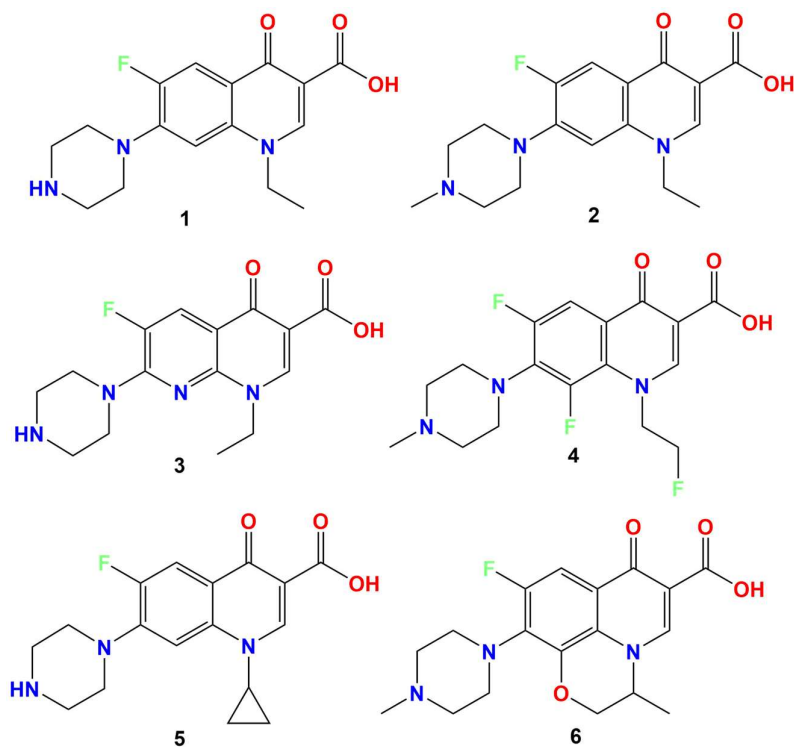


Figure 2: structures of fluoroquinolones marketed in the early 1980s norfloxacin (1), pefloxacin (2), enoxacin (3), fleroxacin (4), ciprofloxacin (5) and ofloxacin (6).

In 1985 third generation quinolones were being developed. Third generation quinolones are also fluoroquinolones but unlike the second-generation quinolones, they are active against *Streptococci* bacteria. This paved the way for fourth-generation quinolones; fluoroquinolones similar to the third generation quinolones but with increased antimicrobial activity in Gram-positive bacteria^{6,7} (figure 3) .

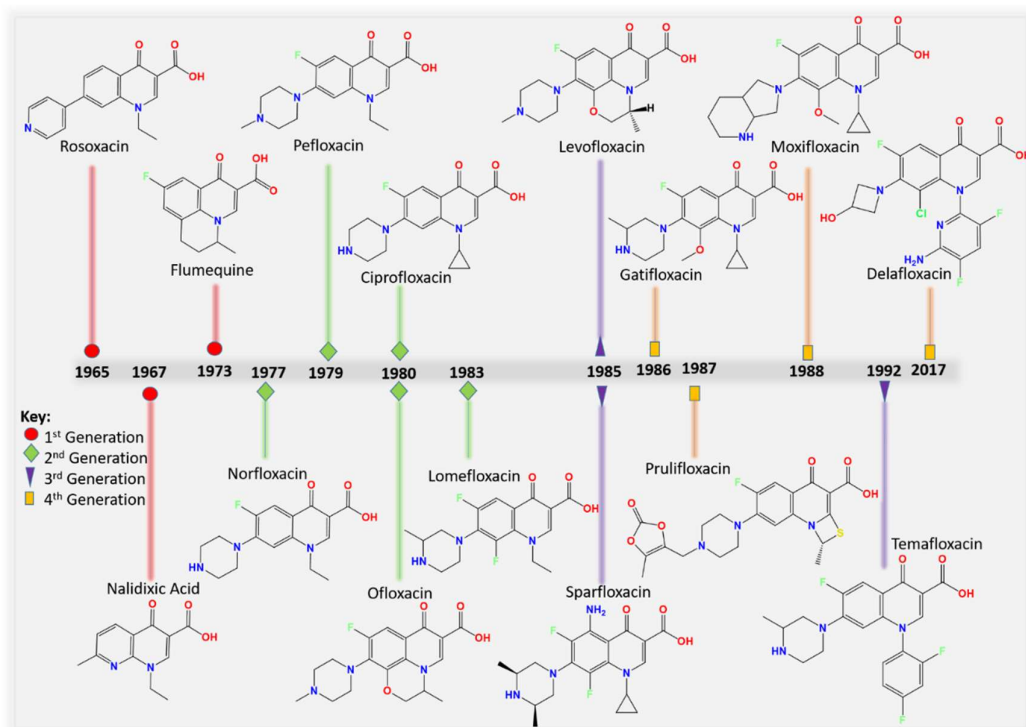


Figure 3: timeline showing the development of quinolone generations with examples and their structures for each.

1.2 Fluoroquinolones: mechanism of action and structure-activity relationship

Fluoroquinolones enter bacterial cells mainly *via* porins and passive diffusion and interact with DNA gyrase, the intracellular drug target⁹. DNA gyrase is an enzyme involved in the supercoiling of DNA in bacterial cells¹⁰.

A cyclopropyl group in the R₁ position (figure 1) has been found to be the optimum substituent due to its favourable steric, spatial and through-space interactions. This makes ciprofloxacin (5) one of the most potent fluoroquinolone antibiotics available. In position 2, a hydrogen atom is the optimal substituent, but antimicrobial activity has been demonstrated with small rings connecting to C₁ or C₃. The ketone/ carboxylic acid groups in positions 3 and 4 respectively are essential for binding to DNA gyrase and bacterial transport and therefore modifications should not be made here. It has been suggested that adding a nitrogen atom to the ring to replace C₅ could increase potency against Gram-positive bacteria, this is shown through the increase in antibacterial effectiveness from pefloxacin (2) to enoxacin (3). The fluorine substituent in position 6 is essential to the pharmacophore of fluoroquinolones and has been shown to

significantly increase effectiveness of the antimicrobial properties of quinolones. In position 7 five and six membered nitrogen containing rings have been shown to be most effective, such as the diazene ring in norfloxacin (**1**), enoxacin (**3**) and ciprofloxacin (**5**)^{11,12}.

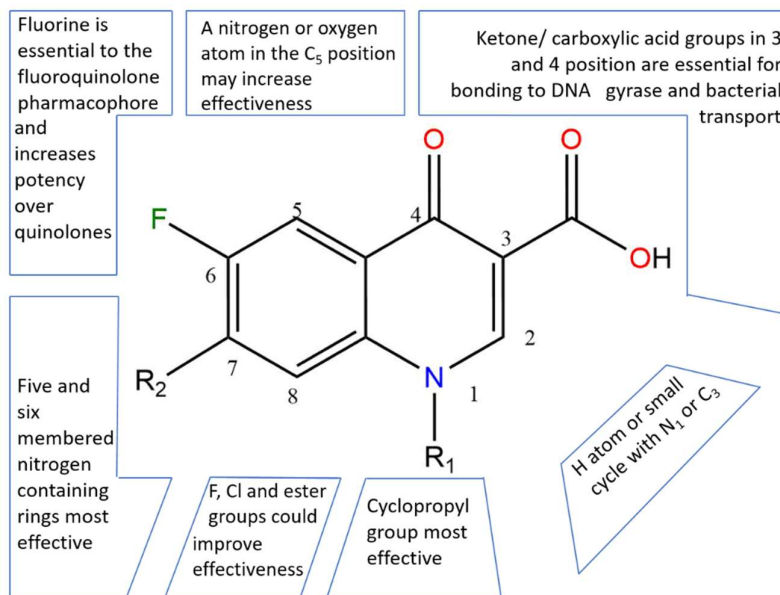


Figure 4: fluoroquinolone pharmacophore with labelled structure activity relationship and alternate substituents that could improve the potency in each position.

1.3 Metallo-fluoroquinolones

Fluoroquinolones contain several donor atoms which could potentially coordinate to metal ions. The pharmacophore of fluoroquinolones (figure 1) contains three oxygen atoms, which could coordinate to a metal ion: two in the carboxylate substituent on C₃ (when deprotonated) and one in the ketone group on C₄. “ The lone pair of electrons on the nitrogen atom in position 1 of the pharmacophore (figure 1) are sterically less available due to the R₁ substituent, meaning it is not a good donor atom. Donor atoms can be introduced into fluoroquinolone structures through the R₁ and R₂ substituents. A common R₂ substituent is a piperazine ring, as seen in norfloxacin (**1**), pefloxacin (**2**), enoxacin (**3**), fleroxacin (**4**), ciprofloxacin (**5**) and ofloxacin (**6**) (figure 2). A piperazine ring introduces two additional nitrogen atoms, capable of coordinating to a metal ion.

Coordination of fluoroquinolones to a metal most often occurs through the ketone and carboxylic acid groups in positions 3 and 4¹³. A coordinative bond is formed from the oxygen

from the OH group in the carboxylate substituent (formed by the loss of a proton) and a coordinative bond through the ketone oxygen (figure 5).

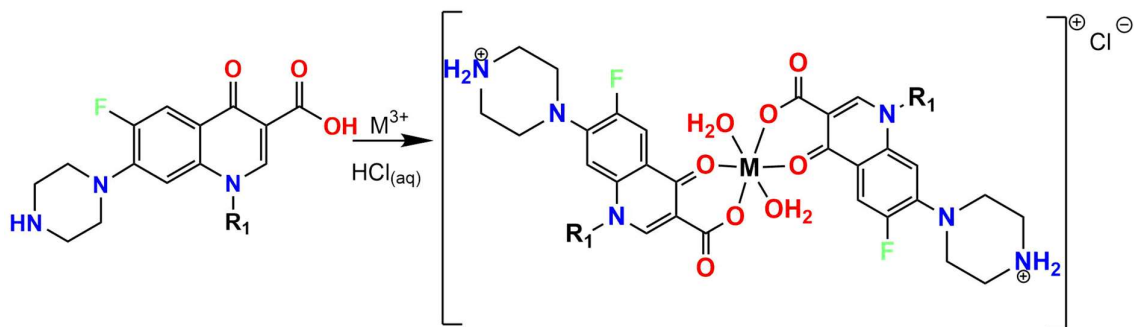


Figure 5: a general reaction scheme of fluoroquinolone with a metal M(III) cation to form a metallo-fluoroquinolone in hydrochloric acid. The scheme shows how fluoroquinolones can coordinate to metals: through the carboxylate/ ketone groups in positions 3 and 4 respectively.

It has been suggested that zinc(II) from biomolecules coordinates to the fluoroquinolone levofloxacin via the more rarely seen coordination through nitrogen atoms in the R_2 substituent, which is a 1-methylpiperazine group in levofloxacin (figure 6)¹⁴. This form of coordination through the nitrogen donor atoms from the R_2 group is also seen in a complex of platinum and ciprofloxacin¹⁵.

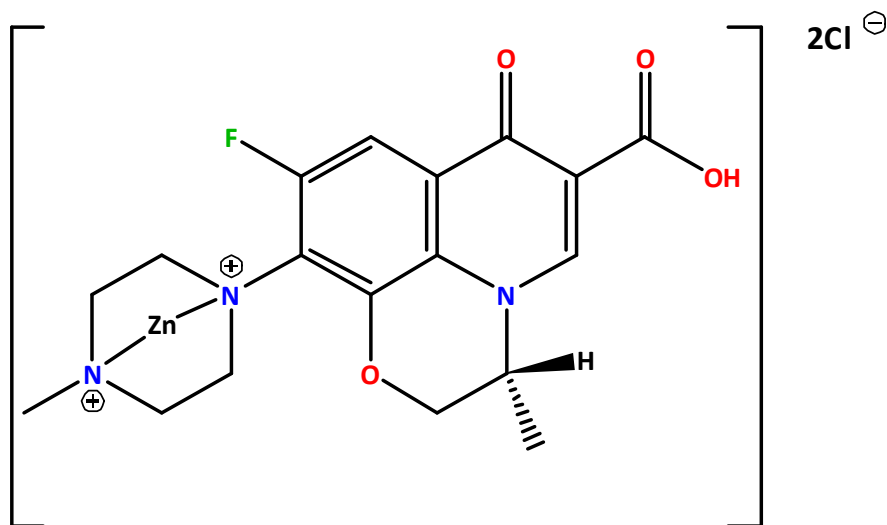


Figure 6 : structure of complex formed by zinc(II) ions from biomolecules and levofloxacin in blood plasma exhibiting coordination via nitrogen atoms in the 1-methylpiperazine group in the R_2 position¹⁴.

Additionally, there are examples of coordination of fluoroquinolones such as norfloxacin (**1**) to iron(III) and cobalt(II) through the two carboxylate oxygen atoms in the β -ketone carboxylate group. The novel iron(III) and cobalt(II) norfloxacin complexes were synthesised by F. Gao *et al.* in 1995, the proposed structure from UV-vis, NMR and elemental analysis characterisation is shown in figure 7^{16,17}.

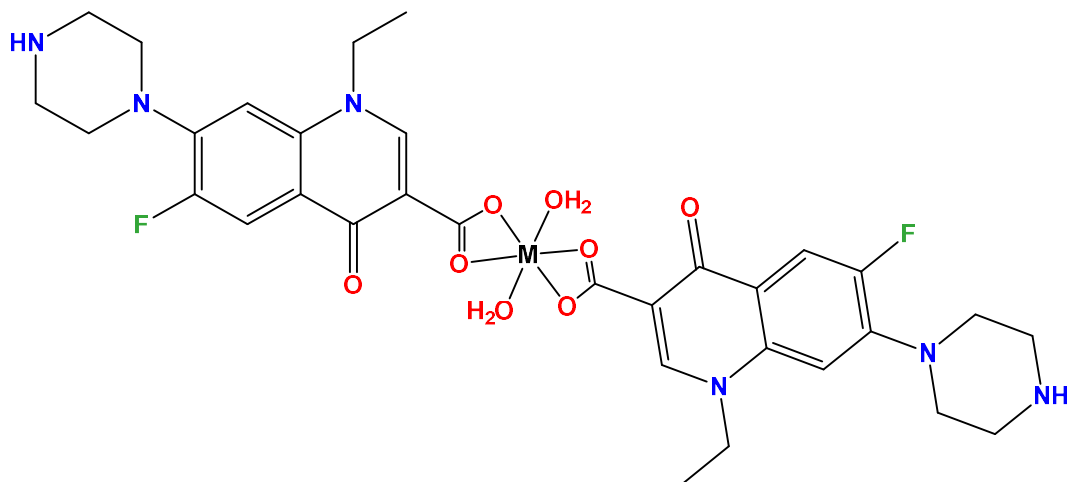


Figure 7: general structure of coordination of norfloxacin to a metal cation (2+) through the two oxygen donor atoms in the β -ketone carboxylate group^{16,17}.

1.3.1 Choice of bacteria to assess antimicrobial effectiveness

Across a range of metal and fluoroquinolone combinations, there is a large variation in effectiveness in different strains of bacteria. Whilst fluoroquinolones are broad spectrum antibiotics, metallo-fluoroquinolones could have more effective applications if used to treat specific bacterial strains. Metallo-fluoroquinolone complexes have potential to be effective against bacterial strains that are resistant to the parent fluoroquinolone drugs. Complexes of 1:3 bismuth(III)-norfloxacin and 1:4 bismuth(III)-norfloxacin were found to have lower minimum inhibitory concentration (MIC) values versus their parent fluoroquinolone over a range of clinically-relevant bacteria. Most notably these complexes were effective against strains of *Helicobacter pylori* which are resistant to fluoroquinolones, showing a sixteen fold decrease in the MIC values of the 1:3 bismuth(III)-norfloxacin versus norfloxacin (**1**) (table 1)^{18, 19, 20}.

Table 1: MIC values of [Bi(norfloxacin)₃(H₂O)₂] and norfloxacin against fluoroquinolone resistant strains of *H. pylori*.

	MIC (mg L ⁻¹) for strain No. of <i>H. pylori</i>		
	2304	2287	2662
[Bi(norfloxacin) ₃ (H ₂ O) ₂]	1.0	1.0	1.0
norfloxacin	16.0	16.0	16.0

Similarly, in a 1:1 copper(II)-ciprofloxacin complex, the antibacterial activity was found to be the same as ciprofloxacin administered on its own across a range of clinically-relevant bacteria apart from *Pseudomonas aeruginosa* and *Salmonella typhimurium*. In *P.aeruginosa* and *S.typhimurium* strains the copper(II)-ciprofloxacin complex increased the inhibition zone by 10 mm and 7 mm respectively²¹. The potential for metallo-fluoroquinolones to overcome fluoroquinolone resistance in bacteria demonstrates the importance of testing complexes on a wide range of clinically-relevant bacteria and the significant potential metallo-fluoroquinolones demonstrate against rising antimicrobial resistance.

Conversely, a study investigated the antimicrobial properties of tris(quinolono)metal(III) complexes of gallium(III) and iron(III) with each of the following nine fluoroquinolones in a 1:3 metal(III)-to-fluoroquinolone ratio: nalidixic acid, norfloxacin (**1**), fleroxacin (**4**), oxolinic acid, enoxacin (**3**), levofloxacin, pipermidic acid, ciprofloxacin (**5**) and lomefloxacin. The single disk method against pathogens associated with nosocomial diseases was used to evaluate the antimicrobial properties of these complexes compared to the equivalent concentration of fluoroquinolone if it were not coordinated to a metal ion, by measuring the inhibition zone sizes. The study concluded that the each one of the tris(quinolono)metal(III) complexes tested against each strain of bacteria showed no change in the antimicrobial properties when compared to the parent fluoroquinolone, including in *Klebsiella pneumoniae*, which had developed a resistance to nalidixic acid and subsequently was also resistant to [Ga(nalidixic acid)₃] and [Fe(nalidixic acid)₃]²².

1.3.2 Choice of fluoroquinolone

The type of fluoroquinolone influences the effectiveness of the metal-fluoroquinolone complexes. In a 1:1 copper(II)-ciprofloxacin complex, the MIC was found to be lower than ciprofloxacin in certain bacteria¹⁸, however in a 1:1 copper(II)-lomefloxacin complex there was no change in the MIC across a range of bacteria in comparison to lomefloxacin alone^{23, 24}.

The antimicrobial properties of a range of [bismuth(III)-(fluoroquinolone)₃(H₂O)₂] complexes found that for each strain of bacteria was most susceptible to a different complex. All of the [bismuth(III)-(fluoroquinolone)₃(H₂O)₂] complexes synthesised were found to have enhanced antimicrobial properties over the parent fluoroquinolone, across a range of clinically-relevant bacteria. The bismuth(III)-ciprofloxacin complex was found to be most potent against *E. coli* with MIC of 0.05 mg L⁻¹ whereas bismuth(III)-ofloxacin complex was the most potent against *S. aureus* (MIC: 0.125 mg L⁻¹) and *B. pumilus* (MIC: 0.045 mg L⁻¹) and bismuth(III)-sparfloxacin complex against *S. epidermidis* (MIC: 0.125 mg L⁻¹), suggesting that the choice of parent fluoroquinolone will alter the effectiveness of the metallo-fluoroquinolone complex against different strains of bacteria¹⁸.

In [iron(III)(fluoroquinolone)₃] complexes whereby the fluoroquinolones included: nalidixic acid, norfloxacin (**1**), fleroxacin (**4**), oxolinic acid, enoxacin (**3**), levofloxacin, piperimidic acid, ciprofloxacin (**5**) and lomefloxacin, there was a positive correlation with the antibacterial properties of the parent fluoroquinolone and the antibacterial properties of the iron(III)-fluoroquinolone complex suggesting the more potent the parent fluoroquinolone is, the more effective the metal complex will be²².

The choice of fluoroquinolone will also influence the stability of the complex. There is variation in stability constants (table 2) within a range of metal-fluoroquinolone combinations, which reflect the strength of the interaction between the fluoroquinolone ligand and the metal cation. Stability constants were calculated using capillary zone electrophoresis experiments at pH 3.25 for the iron(III) and aluminium(III) complexes and at 8.02 for the magnesium(II) complexes, as these were determined to be the optimum pH values for the respective metal complexes. All experiments were undertaken at 298 K and measured with a 30 kV separation potential. This study found that for Al(III) and Fe(III), coordination to norfloxacin appears to be the most favourable and lomefloxacin the least favourable, with a stability constant less than a third of that of norfloxacin in Al(III) and half in Fe(III). There is similarly a large range of stability constants when different fluoroquinolones are coordinated to Mg(II) however, a different pattern is observed with levofloxacin forming the most stable complex, suggesting that the oxidation state and metal ion also influences the stability of the complex formed²⁵.

Table 2: The stability constants (K) for a range of fluoroquinolone-metal ion complexes calculated using capillary zone electrophoresis at 298 K with a 30 kV separation potential and pH 3.25 for Fe(III) and Al(III) complexes, 8.02 for the Mg(II) complexes ²⁵.

Fluoroquinolone	K ± ΔK (L mmol ⁻¹)		
	Fe(III)	Al(III)	Mg(II)
ciprofloxacin	14.117 ± 0.223	14.184 ± 0.218	2.744 ± 0.074
norfloxacin	20.113 ± 0.181	34.091 ± 0.249	3.545 ± 0.038
ofloxacin	14.659 ± 0.225	17.901 ± 0.202	4.488 ± 0.021
levofloxacin	9.146 ± 0.199	24.275 ± 0.168	5.578 ± 0.019
lomefloxacin	8.910 ± 0.206	10.653 ± 0.194	3.674 ± 0.029
enrofloxacin	15.491 ± 0.149	10.564 ± 0.189	3.385 ± 0.200
sparfloxacin	17.781 ± 0.139	12.319 ± 0.192	1.360 ± 0.064

1.3.4 Choice of metal

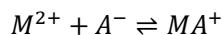
The properties of the metal ion used to coordinate to a fluoroquinolone are also significant. In metallo-fluoroquinolone complexes, the fluoroquinolone coordinates through donor atoms and the metal ion accepts electron density. Simplistically, this describes a reaction between a Lewis acid and a Lewis base, whereby the fluoroquinolone is the Lewis base and the metal ion is the Lewis acid. The softness (or hardness) of a species is classified by its size, charge or oxidation state, electronic structure, and the other attached groups and is often consistent with the electronegativity of a species²⁶. Soft species are often larger and more polarisable, whereas harder species are smaller and highly charged. The donor atoms we most commonly see coordinated to metal ions in metallo-fluoroquinolone complexes are the deprotonated oxygen from the carboxylate group at C₃ (RCO₂⁻) and the oxygen from the ketone on C₄ (R₂O) (figure 1). Both donor atoms are Lewis basic and are classified as hard bases²⁶. Hard Soft Acid Base theory suggests that hard Lewis acids prefer to bond to hard Lewis bases and soft Lewis acids prefer to bond to soft Lewis bases, meaning that the hard basic oxygen atoms in fluoroquinolones have a higher affinity with a hard acidic metal ion (table 3).

Table 3: Pearson classification of a selection of Lewis acid metal ions, categorised as soft, intermediate and hard²⁶.

Soft	Intermediate	Hard
Cu(I), Ag(I), Au(I)	Fe(II), Co(II), Ni(II), Zn(II), Cu(II)	Mg(II), Al(III), Se(III), Ga(III), Co(III), Fe(III)

Hard Soft Acid Base theory suggests why metallo-fluoroquinolone complexes are most often seen with hard metal ions such as metal(III) ions: iron(III), gallium(III), bismuth(III) and some complexes with intermediate metal(II) ions: copper(II) and zinc(II). It follows that studies of formation constants suggest that that coordination of ciprofloxacin (**5**) to metal ions increases according to the order: Ca(II) < Mg(II) < Zn(II) ~ Fe(II) < Cu(II) < Al(III) ~ Fe(III)²⁷.

The stability constants of metallo-fluoroquinolone complexes vary depending on the metal. Stability constants of various 1:1 metal(II)-nalidixic acid complexes were calculated from fluorescence data^{28,29}(table 4) for the reaction:



$$K_1 = \frac{[MA^{+}]}{[M^{2+}][A^{-}]}$$

Where: M^{2+} is the metal(II) ion

A^{-} is nalidixic acid

MA^{+} is the metal(II)-nalidixic acid complex

K_1 is the first equilibrium stability constant for the reaction

Even though all four metal(II) ions are classed as intermediate Lewis acids (table 3), there is a significant variation in the stability constants of the 1:1 complexes they form with nalidixic acid, suggesting certain metals are more suitable for complexation with fluoroquinolones than others. Fluorescence spectroscopy experiments suggest that metal(II) affinity for nalidixic acid follows: Zn(II) < Fe(II) < Co(II) < Cu(II)^{28,29}.

Table 4: stability constants from fluorescence of 1:1 metal(II)-Nalidixic acid complexes from two different studies ^{28, 29}.

Metal(II) ion	Log K ₁ ²⁸	Log K ₁ ²⁹
Fe(II)	3.86 ± 0.03	-
Co(II)	4.22 ± 0.02	4.4
Cu(II)	5.38 ± 0.03	5.5
Zn(II)	3.30 ± 0.03	3.8

This pattern conforms with the observations of the Irving-Williams series, whereby the trend in stability for divalent first row transition metals in high-spin octahedral complexes for the substitution of water for another ligand is as follows: Mn(II)<Fe(II)<Co(II)<Ni(II)<Cu(II)>Zn(II) ³⁰.

A careful consideration of side reactions and how the complex will react in a biological system is critical for any drug. It is important to use a metal that will be transported *in vivo* but also will limit side reactions, such as electron transfer reactions with biomolecules. Cobalt(II)-enoxacin (**3**) complexes have been shown to have an increased MIC across a range of clinically relevant bacteria in comparison to enoxacin on its own. This suggests that the chelation to the cobalt metal ion reduces the antimicrobial effectiveness of fluoroquinolones and therefore is not suitable for use in metallo-fluoroquinolone drugs ^{31, 32}. The reason for this could be due to cobalt's interaction with other biological molecules. A study found that there is a mechanism in which cobalt(II) ions chelated to ciprofloxacin ligands interact with adenosine triphosphate (ATP) and form an intermediate. This facilitates a reaction between ciprofloxacin and ATP ³³. This mimics competitive inhibition with other biological molecules and could explain why the cobalt-enoxacin complex has an increased MIC. Whilst metals that are biologically relevant may have transportation benefits for the metallo-fluoroquinolone complexes, caution should be paid to the side reactions they also facilitate.

1.3.5 Type of bonding

The positive metal ion is surrounded by the donor atoms from the fluoroquinolone ligands, creating an electrostatic attraction, thus coordinating the fluoroquinolone to the metal ion. As the number of fluoroquinolone ligands increases from one to three, the metallo-fluoroquinolone complexes tend towards an octahedral geometry, meaning that there is large repulsion between the metal ion d electrons and the p electron orbitals of the oxygen donor atoms from the carboxylate group in the C₃ position of fluoroquinolones. This means that there is very weak orbital overlap, making the fluoroquinolone ligands labile. If the fluoroquinolone ligands are labile, this could influence the mechanism of action of the drug complex *in vivo*; under biological conditions, the complex could dissociate, altering the metal-to-ligand ratio.

Titration and ¹H-NMR experiments suggest that the coordination ability of fluoroquinolones varies between species. Coordination to Al(III) ions increases as follows: levofloxacin > ciprofloxacin > lomefloxacin³⁴ (figure 8). The differences in strength of coordination between these three complexes could be due to the different substituents at C₈. Ciprofloxacin has no substituent whereas lomefloxacin has an electron withdrawing group and levofloxacin has an electron donating group in the C₈ position. The electron donating ability of the C₈ substituent of levofloxacin stabilises the complex formed with the Al(III) ion, whereas the electron withdrawing fluorine in the C₈ position of lomefloxacin destabilises the complex formed with Al(III).

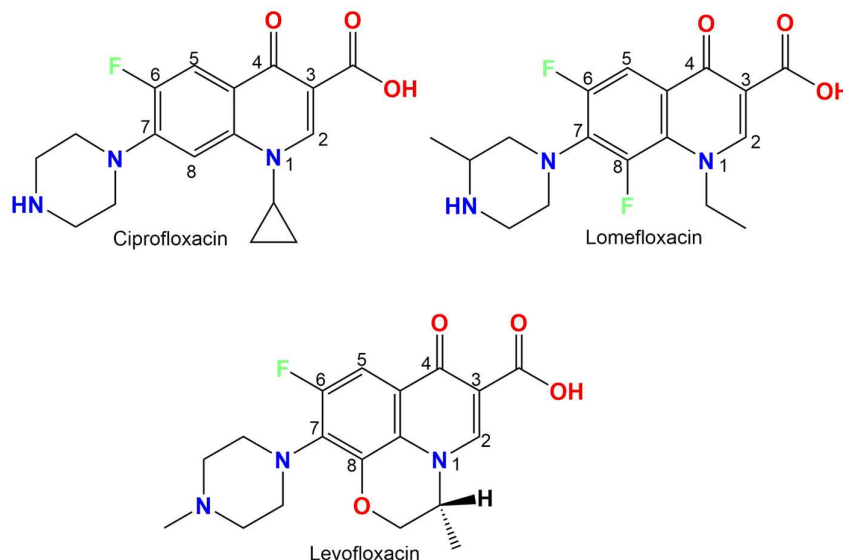


Figure 8: structures of ciprofloxacin (top left), lomefloxacin (top right) and levofloxacin (bottom)

The change in enthalpy on reaction of ciprofloxacin (**5**) and Ca(II) and Mg(II) ions has been calculated from experiments on the temperature dependence of the stability constants for these reactions (table 5)³⁵. The enthalpy change on the coordination of one ciprofloxacin ligand (ΔH_1) and of a second ciprofloxacin ligand to the metal(II)-ciprofloxacin complex (ΔH_2) are both negative, suggesting the formation of a bond between the metal(II) ion and the ciprofloxacin ligands. However, the magnitude of the enthalpy changes are very small relative to other bond enthalpies, with ΔH_1 being of a similar strength to a weak O-O bond for both metal(II) ions. Furthermore, the ΔH_2 values for both metal(II) complexes are even weaker. This is further evidence that fluoroquinolone ligands are coordinated to metal ions in metallo-fluoroquinolone complexes by relatively weak electrostatic attraction. This data also suggests that the second coordinated ciprofloxacin is more weakly coordinated to the metal(II) ion than the first ciprofloxacin ligand, which will be due to the weaker electrostatic attraction between the negatively charged oxygen donor atom on the carboxylate in the C3 position of ciprofloxacin and the [metal(II)(ciprofloxacin)]⁺ complex versus the same ligand interacting with a metal(II) ion. It is also important to note, that as explained in previous sections, metal(II) ions are normally of intermediate “hardness” (table 3) and therefore not as ideally suited for coordination with a hard oxygen donor atom from the carboxylate ion in ciprofloxacin as a hard metal ion such as a metal(III) ion.

Table 5: enthalpy (kJ mol⁻¹) of reactions between Ca(II)/ Mg(II) metal ions with ciprofloxacin (**5**) calculated from the temperature dependence of the stability constants of the reactions. ΔH_1 represents the enthalpy change on the coordination of a single ciprofloxacin ligand and ΔH_2 represents the enthalpy change on the coordination of a second ciprofloxacin ligand to the metal(II)-ciprofloxacin complex³⁵.

	Enthalpy (kJ mol ⁻¹)	
	ΔH_1	ΔH_2
Ca(II)	-157.86	-35.23
Mg(II)	-163.00	-29.02

Whilst bismuth(III)-fluoroquinolone complexes have been shown to be more effective against bacteria than the parent fluoroquinolone^{18, 19}, an ionic complex of bismuth and ciprofloxacin (**5**) showed no change to the MIC, and therefore no change in effectiveness against the MIC of ciprofloxacin over a range of clinically relevant bacteria³⁶. The difference in bonding of fluoroquinolones to the bismuth(III) ion is determined by X-ray crystallography and IR analysis.

X-ray crystallography structures show Bi(III)Cl₆ not coordinated to the fluoroquinolone in the ionic complex^{18, 19} and IR data showed the absence of a peak at 1725 cm⁻¹ (C=O in the carboxylate) and emergence of additional peaks at about 1520 and 1455 cm⁻¹ due to symmetrical and asymmetrical carboxylate stretching vibrations in complexes where the bismuth(III) ion is coordinated to the fluoroquinolone³⁶. Furthermore, when bismuth(III) and fluoroquinolones were tested uncoordinated as an admixture, this also had no effect on the MIC value, compared to the fluoroquinolone on its own^{37, 38, 39}. Therefore, the complexation of the metal and the fluoroquinolone is essential to the mechanism of action.

1.3.6 Metal-to-ligand ratio

The metal-to-ligand ratio affects the transportation of the drug through biological systems and may also affect the drug's ability to bind to the target enzyme. 1:2 and 1:1 copper(II)-ciprofloxacin complexes have been synthesised, exhibiting different antimicrobial properties. The 1:1 copper(II)-ciprofloxacin complex showed exactly the same MICs as ciprofloxacin on its own over a range of clinically relevant bacteria in all but three cases: *Enterococcus*, *Staphylococcus aureus* and *Bacillus pumilus*, where there was a 50% reduction in the MIC^{31, 18}. The 1:1 copper(II)-ciprofloxacin complex had the same MIC values as the 1:2 complex in antimicrobial tests on these three bacteria. However, the MIC of the 1:2 complex was higher than ciprofloxacin on its own against five of the other bacterial strains tested^{14, 31}. This suggests that not only does chelation to copper ions decrease the antimicrobial effectiveness of fluoroquinolones against some bacteria (further to the studies discussed on this section), but that there is influence of the metal-to-fluoroquinolone ratio in the antimicrobial activity of metallo-fluoroquinolone drugs.

Two separate studies investigated bismuth(III)-norfloxacin complexes with two water ligands. One study synthesised a 1:3 bismuth(III)-norfloxacin complex; Bi(norfloxacin)₃(H₂O)₂¹⁸, and the other a 1:4 bismuth(III)-norfloxacin complex; Bi(norfloxacin)₄(H₂O)₂¹⁹(figure 9). Both studies measured the minimum inhibitory concentrations of these complexes against a range of clinically-relevant bacteria, they both tested the MIC against *Escherichia coli*, *Bacillus pumilis*, *Staphylococcus aureus* and *Staphylococcus epidermidis*. Both complexes were found to have more effective antimicrobial properties than norfloxacin against the bacterial strains tested (other than the 1:3 complex against *E. coli* where the MIC was the same as norfloxacin). Each study found different MIC concentrations for norfloxacin for the same strains of bacteria, this

may be due to slightly different stains/ methods being used, therefore to compare the reported antimicrobial effectiveness we can use the percentage reduction in MIC of each complex, relative to the MIC of norfloxacin in the same bacteria from the investigation into each complex respectively. There is a greater percentage reduction in MIC across three out of the four bacterial strains in the 1:4 bismuth(III)-norfloxacin complex compared to the 1:3 bismuth(III)-norfloxacin complex. However the 1:3 bismuth(III)-norfloxacin complex has a greater percentage reduction (80%) in MIC compared to norfloxacin in *B. pumilis* than the 1:4 bismuth(III)-norfloxacin complex (50%) (table 6).

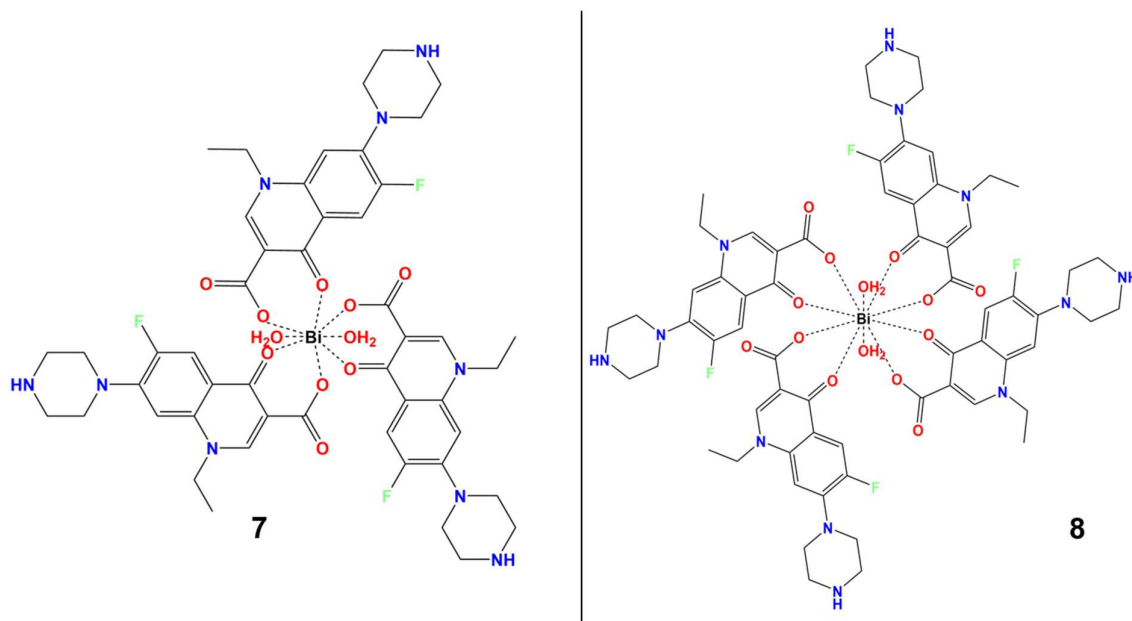
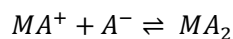
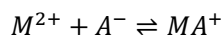


Figure 9: reported structures of $\text{Bi(III)(norfloxacin)}_3(\text{H}_2\text{O})_2$ ¹⁸ (**7**) and $\text{Bi(III)(norfloxacin)}_4(\text{H}_2\text{O})_2$ ¹⁶ (**8**).

Table 6: the percentage reduction in minimum inhibitory concentration (MIC) for $[\text{Bi(norfloxacin)}_3(\text{H}_2\text{O})_2]$ ¹⁸ and $[\text{Bi(norfloxacin)}_4(\text{H}_2\text{O})_2]$ ¹⁹ against *Escherichia coli*, *Bacillus pumilis*, *Staphylococcus aureus* and *Staphylococcus epidermidis*.

Bismuth(III):norfloxacin	Reduction in MIC compared to norfloxacin for different bacteria (%)			
	<i>E. coli</i>	<i>B. pumilis</i>	<i>S. aureus</i>	<i>S. epidermidis</i>
1:3	0	80	10	17
1:4	50	50	25	25

The stepwise equilibrium stability constants K_1 and K_2 have been calculated via fluorescence spectroscopy²⁸(table 7) for a range of metal(II) ions and their successive binding of nalidixic acid, according to the equations below:



Where: M^{2+} is the metal(II) ion

A^- is nalidixic acid

MA^+ / MA_2 are the metal(II)-nalidixic acid complex

With the stability constants K_1 and K_2 for the respective reactions given by:

$$K_1 = \frac{[MA^+]}{[M^{2+}][A^-]}$$

$$K_2 = \frac{[MA_2]}{[MA^+][A^-]}$$

Table 7: values for stability constants K_1 and K_2 for the above reactions for a range of metal(II) ions in the complexation of 1:1 metal(II)-nalidixic acid and 1:2 metal(II)-nalidixic acid according to the above reactions at pH 6.4²⁸.

Metal(II) ion	Log K_1	Log K_2
Fe(II)	3.86 ± 0.03	3.0 ± 0.1
Co(II)	4.22 ± 0.02	3.0 ± 0.1
Cu(II)	5.38 ± 0.03	4.1 ± 0.1
Zn(II)	3.30 ± 0.03	2.3 ± 0.1

The stability constants at pH 6.4 are lower for all the 1:2 metal(II)-nalidixic (K_2) acid than the 1:1 metal(II)-nalidixic acid (K_1), suggesting the 1:2 complexes are less likely to form than the 1:1 complexes²⁸.

1.3.7 Summary and conclusions

There are five key considerations when designing and synthesising metallo-fluoroquinolones. Firstly, it is important to consider the choice and combination of fluoroquinolone and metal, as well as the metal-to-fluoroquinolone ratio. It is essential that the metal and fluoroquinolone are strongly bound, however coordination of metal ions and fluoroquinolone ligands is often via weak electrostatic interactions and hence kinetically labile. Finally, once a suitable metallo-fluoroquinolone has been synthesised, it should be tested on a wide range of clinically relevant bacteria, including bacterial strains resistant to fluoroquinolone drugs, in order to fully evaluate its effectiveness and potential as an antibiotic.

Table 8: summary of findings reported in the literature on different combinations of metals, fluoroquinolones (FQ) and metal-fluoroquinolone ratios.

Metal (M)	Fluoroquinolone (F)	M:F	Effectiveness
Bismuth(III)	Ciprofloxacin (5)	1:3	Lower MIC than uncoordinated FQ, even in FQ resistant bacteria, <i>H.pylori</i> ^{18,19}
Bismuth(III)	Norfloxacin (1)	1:4	
Copper(II)	Ciprofloxacin (5)	1:1	Higher MIC than uncoordinated FQ ¹⁸
Copper(II)	Ciprofloxacin (5)	1:2	Lower MIC than uncoordinated FQ in certain bacteria, otherwise no change ³¹
Copper(II)	Lomefloxacin	1:1	Same MIC as uncoordinated FQ ²³
Cobalt(III)	Enoxacin (3)	1:1	Higher MIC than uncoordinated FQ ³¹
Zinc(II)	Ciprofloxacin	1:2	Lower MIC than uncoordinated FQ ^{40, 41, 42}

1.4 Complexes of fluoroquinolone dimers

Multi-component antibiotic systems are a promising approach in the development of new antibiotics⁴³. Dimeric compounds have been shown to demonstrate unique properties over their parent monomers in some bioactive compounds in which the biological target contains at least two binding sites. An example of this is the antimalarial drug, bisquinoline, which was found to be significantly more potent than the original chloroquinoline monomer⁴⁴. In theory, dimer-based drugs are able to bridge across a target molecule's binding sites⁴⁵, a potential solution to

overcome the unfavourable entropy cost of two monomers binding to a target molecule⁴⁶, similar to the chelation effect. Furthermore, as the target protein is a dimer, when one side of the dimer is bound, the other side will be held in proximity to the other target binding site, enhancing binding kinetics. The antimicrobial and anti-tumour properties of complexes of dimeric fluoroquinolones have been investigated.

1.4.1 DNA gyrase: fluoroquinolone drug target

In Gram-negative bacteria, DNA gyrase is the primary intracellular target for fluoroquinolones. DNA gyrase is a type II topoisomerase, an enzyme involved in the supercoiling of chromosomal DNA, an essential function in the division of bacteria. In Gram-positive bacteria Topoisomerase IV has also been suggested to be the primary intracellular target for fluoroquinolones. Topoisomerase IV facilitates the separation of bacterial genomes into daughter cells, another essential function for bacterial cell division^{10, 47}.

DNA gyrase exists as a tetramer of approximately 370 kDa, made up of two subunits of gyrA and two subunits of gyrB⁴⁸, shown in figures 10 and 11. Spontaneous mutation in the gyrA subunit is the most common route to fluoroquinolone resistance, although it has been suggested that mutations in both gyrA and gyrB subunits simultaneously is unlikely⁴⁹. This makes DNA gyrase a good target for a dimeric drug.

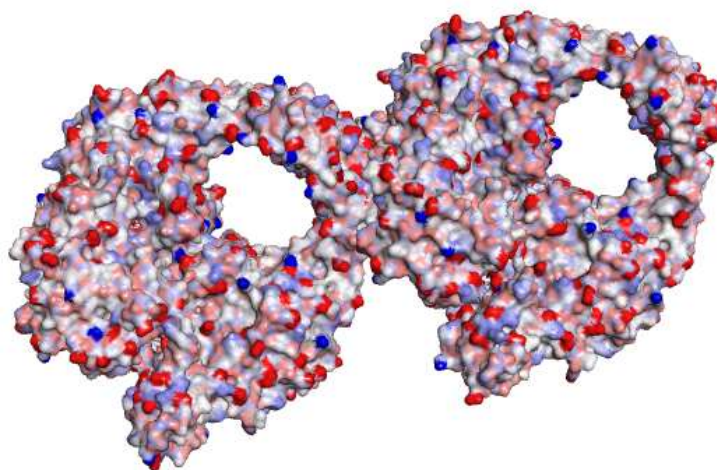


Figure 10: structure of fluoroquinolone target molecule^{50, 51}; DNA gyrase. DNA gyrase is a dimer protein composed of the monomers gyrA and gyrB⁴⁹.

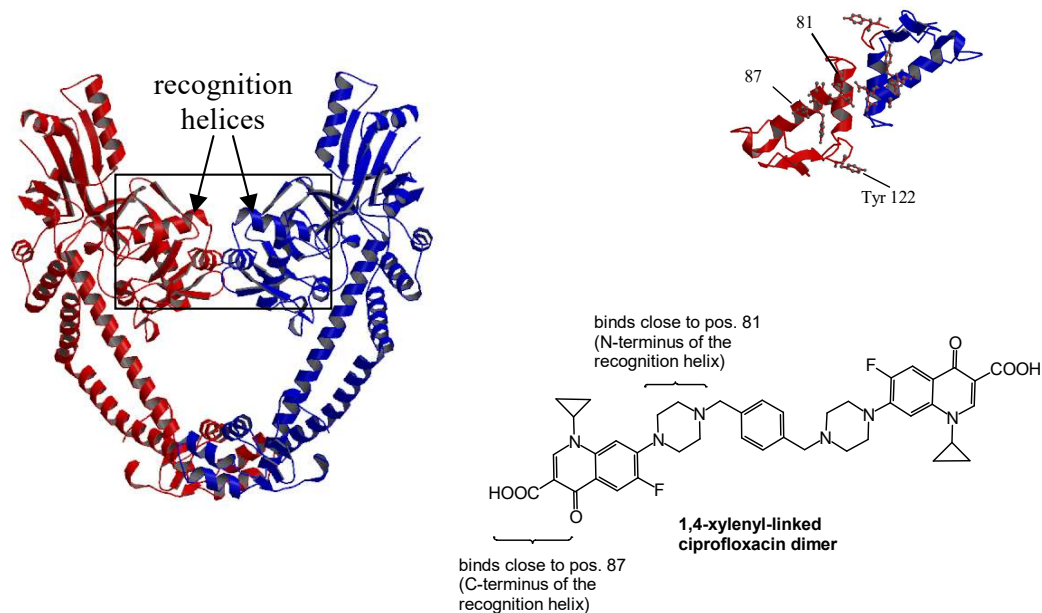


Figure 11: *left*: structure of the DNA gyrase dimer⁵³. *Right (top)*: a close-up of the two recognition helices at the 'head dimer interface', viewed from the top with the side chains of residues 81, 87, 122 shown (generated with MolScript). *Right (bottom)*: linked fluoroquinolone dimer⁵².

1.4.2 Antimicrobial properties

Both symmetric and asymmetric fluoroquinolone dimers have been synthesised using a range of fluoroquinolone monomers including ciprofloxacin, pipemidic acid, and norfloxacin. The antimicrobial properties of these molecules do not correlate with the relative antimicrobial properties of the parent fluoroquinolone⁵⁴. Asymmetric fluoroquinolone dimers are more effective against a range of strains of bacteria than symmetric complexes^{23, 43, 55}, if a strain of bacteria develops a resistance to one of the fluoroquinolone monomers, it may still be susceptible to the other fluoroquinolone in the asymmetric dimer. Complexes containing a ciprofloxacin monomer have been found to be the most potent^{45, 55}.

The effects of a range of different linkers used in fluoroquinolone dimers indicate that the linker plays a pivotal role in the antimicrobial effectiveness of the complexes. Different piperazinyl linkers (figure 12) have been found to have antibacterial properties in fluoroquinolone resistant strains of bacteria^{45, 54, 56}, a 100 fold reduction in MIC against strains of fluoroquinolone sensitive bacteria⁵⁶, and inhibited growth (but did not kill) strains of *Mycobacterium smegmatis*⁵⁷. Amino

acid-based linkers have also been suggested to show decreased degradation inside the bacterial cell, giving an increased concentration of the dimer in the cell, relative to the concentration of the dimer administered, thereby reducing the MIC⁵⁵. Although the successfulness of the linker is related to its combination of fluoroquinolones in a dimer, the same linker may not be as effective with a different combination of fluoroquinolones⁵⁴. This is due to the size of the complex, the linker needs to be able to bridge between the fluoroquinolone donor atoms between the DNA gyrase target sites. Different combinations of fluoroquinolones will alter the length of the molecule and therefore a suitably sized linker is required.

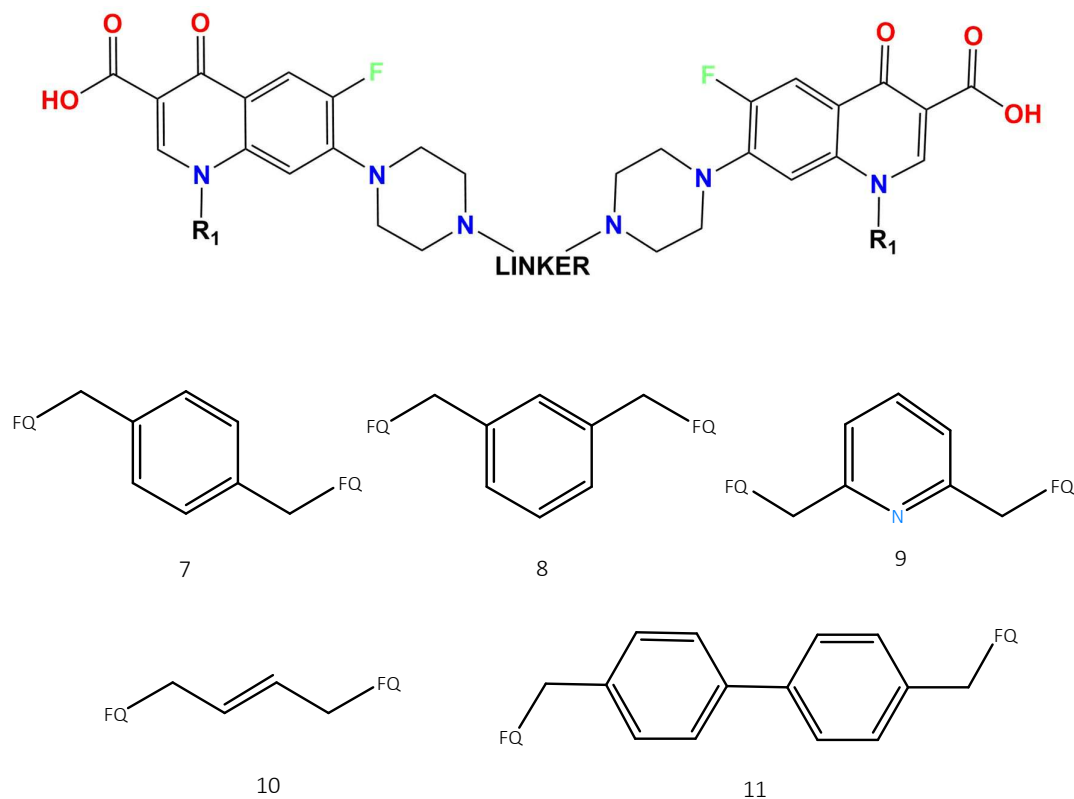


Figure 12: piperazinyl linkers used in effective antibiotic fluoroquinolone dimers: **(7)** *p*-xylene **(8)** *m*-xylene **(9)** 2,6-dimethylpyridine **(10)** (*E*)-but-2-ene **(11)** 1,1'-biphenyl. Fluoroquinolones with piperazinyl groups in the R₂ position can be bonded to linkers to form dimeric fluoroquinolone molecules, as shown in the molecule at the top of the figure. The linkers (structures **7-11**) bond to fluoroquinolones in the positions labelled "FQ".

Fluoroquinolone mechanism of action involves binding to DNA gyrase. DNA gyrase exists as a dimer, consisting of *gyrA* and *gyrB*⁴⁹, in bacterial strains which are fluoroquinolone resistant, it has been found that there is a mutation in either *gyrA* or *gyrB*, but not both^{53, 54}. This could explain why some of the discussed fluoroquinolone dimer complexes are effective against

strains of bacteria which are resistant to fluoroquinolones, as a dimer means that both gryA and gryB sites can be targeted simultaneously, therefore if there is a mutation in one subunit, the other can still bind effectively with a fluoroquinolone. Furthermore, a bulky sidechain at C₇ can also overcome efflux mutations in bacteria which are fluoroquinolone resistant⁴³.

1.4.3 Anti-tumour properties

An anti-tumour drug that also exhibits anti-microbial properties would have significant clinical advantages. Often, a side-effect of cancer treatments is a weakened immune system, which can lead to complications from greater pathogenic bacterial susceptibility⁵⁸. Fluoroquinolones with modifications at the piperazinyl ring, both when coordinated to a transition metal ion⁵⁸ and without metal ion coordination^{59,60} have been shown to have anti-tumour properties, through their interactions with human topoisomerase II. Topoisomerase II is a class of enzymes used in DNA replication in human cells and is often the intracellular target for anti-cancer drug compounds⁶¹.

Fluoroquinolone dimers have displayed anti-tumour properties, which are not observed in the parent fluoroquinolone monomers⁵⁵. Two ciprofloxacin dimers (with (CH₂)₁₄ and (CH₂OCO(CH₂)₁₄COOCH₂ piperazinyl linkers) were found to be ineffective as antibacterial agents but had an IC₅₀ < 10 μM MIC against tumour cells⁶².

A further fluoroquinolone dimer has also been synthesised with anti-tumour activity, but this dimer is linked through C₃ of the fluoroquinolone monomers rather than through the piperazinyl groups, as previously seen (figure 13)⁶³.

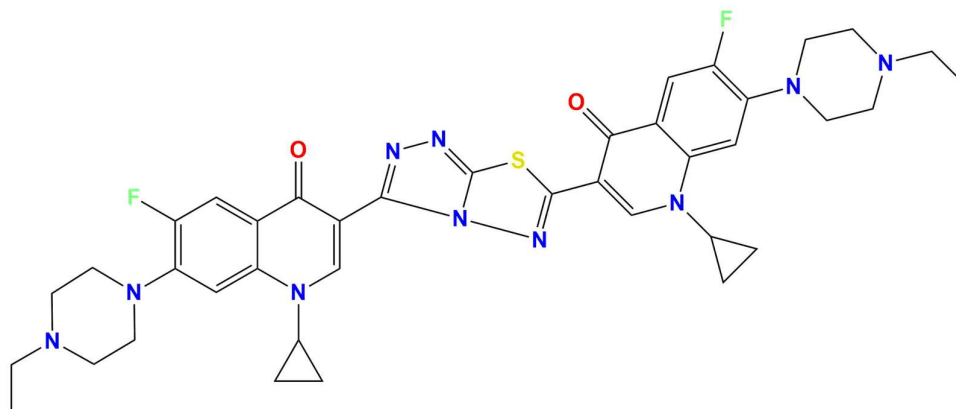


Figure 13: synthesised fluoroquinolone dimer with linker at the C₃ position, which has anti-tumour properties⁶³.

1.4.4 Summary and conclusions

Dimeric fluoroquinolone complexes have potential to overcome fluoroquinolone resistance and may have enhanced antimicrobial properties over their fluoroquinolone monomers. There is scope to synthesise a range of symmetric and asymmetric compounds with different combinations of fluoroquinolones and linkers^{23, 55, 43}. The linkers are also important to the effectiveness of the dimeric complexes^{45, 54, 56}. As well as antimicrobial properties, dimeric fluoroquinolone complexes may also exhibit anti-tumour properties^{55, 62, 63}, requiring further experimental investigation.

2. Metallo-ciprofloxacin complexes: results and discussion

2.1 Aims and objectives

The aim of this section of work was to synthesise and characterise metallo-fluoroquinolone complexes to provide a basis for further investigation of their antimicrobial properties. In order to achieve this aim, a review of the existing literature detailing the synthesis of metallo-fluoroquinolones was undertaken. Repeats of existing synthetic protocols for further characterisation and evaluation of the products were carried out, resulting in the synthesis of a 1:3 bismuth(III)-ciprofloxacin complex and a novel 1:1 zinc(II)-ciprofloxacin complex. In addition, by using literature information and preliminary experiments into suitable reaction conditions, the synthesis of novel iron(III)-ciprofloxacin complexes was achieved. The iron(III)-ciprofloxacin complexes were subsequently characterised and evaluated in comparison to literature metallo-ciprofloxacin complexes.

2.2 Introduction

Whilst there has been extensive research into metallo-fluoroquinolone complexes, there are few examples of X-ray crystal structures in which metal ions directly bound to fluoroquinolones. A literature search for X-ray crystal structures which contained ciprofloxacin was undertaken using the Cambridge Structural Database (CSD) from the physical sciences data-science service⁶⁴. A search of the compound name "ciprofloxacin" found 124 X-ray crystal structures. It was found that 23 of these structures were metallo-ciprofloxacin complexes with coordination to the metal ion through the oxygen donor atoms of the ketone and carboxylate group in ciprofloxacin. The metallo-ciprofloxacin complexes identified in the CSD search are summarised in table 9, along with key data such as the metal-ciprofloxacin bond lengths of the ketone and carboxylate groups, as well as the metal-ciprofloxacin bond angles between the ketone and carboxylate groups.

Table 9: a summary of relevant data from the results of a ciprofloxacin compound search using the CSD. The complexes included in this table are metallo-ciprofloxacin complexes whereby ciprofloxacin coordination to the metal ion takes place through the ketone and carboxylate oxygen donor atoms of the ciprofloxacin ligands*.

Metal	Metal-ciprofloxacin bond length/ Å		O-M-O Bond angle / °	Formula	References
	M-O (ketone)	M-O (carboxylate)			
Cd(II)	2.18(2)	2.23(2)	79.9(5)	Na ₂ [(Cd(cf) ₃)(Cd(cf) ₃ (H ₂ O))].12H ₂ O	65
Co(II)	2.0733(17)	2.0610(19)	86.80(7)	[Co(cf) ₂].4H ₂ O	66
Co(II)	2.044(1)	2.052(1)	/	[Co(cfH)(oba)(H ₂ O) ₂]	67
Co(II)	2.013(8)	2.038(8)	87.4(3)	[Co(CfH) ₂ (H ₂ O) ₂].9H ₂ O	65
Cu(II)	1.9407(19)	1.913(2)	94.03(9)	[Cu(cfH)(phen)Cl](BF ₄).4H ₂ O	68
Cu(II)	1.9454 (12)	1.9143 (13)	93.67 (5)	[CuCl(cfH)(phen)]Cl.2H ₂ O	69
Cu(II)	1.9290(15)	1.9333(16)	86.87(7)	[Cu(cfH) ₂ Cl ₂].2MeOH.6H ₂ O	70
Cu(II)	1.9381(17)	1.917(2)	92.97(8)	[Cu(cfH) ₂ (ClO ₄) ₂].6H ₂ O	31
Cu(II)	1.9393(3)	1.9128(3)	/	[Cu(cfH)(H ₂ O) ₃]SO ₄ .2H ₂ O	71
Cu(II)	1.9281(13)	1.9330(14)	86.73(6)	[Cu(cfH) ₂ (OH) ₂].2CH ₃ OH.6H ₂ O	72
Cu(II)	1.9121(18)	1.917(2)	92.86(8)	[Cu(cfH) ₂ (NO ₃) ₂].H ₂ O	73
Cu(II)	1.927(2)	1.907(3)	93.83(10)	[Cu(cfH) ₂ (BF ₄) ₂].6H ₂ O	74
Fe(III)	1.9989(16)	1.9678(18)	88.20(7)	[Fe(cfH).(C ₂ O ₄).(cfH ₂).5H ₂ O	66
Mg(II)	2.102(2)	2.038(2)	84.39(7)	[Mg(cfH) ₃](SO ₄).5H ₂ O	75
Mg(II)	2.041(1)	2.039(2)	86.04(5)	[Mg(H ₂ O) ₂ (cfH) ₂](NO ₃) ₂ .2H ₂ O	75
Mn(II)	2.1578(18)	2.139(2)	83.39(7)	[Mn(cfH) ₂].2H ₂ O	76
Ni(II)	2.003(1)	2.024(1)	/	[Ni(cfH)(oba)(H ₂ O) ₂]	67

Ru(II)	2.0897(17)	2.0875(17)	86.10(7)	[Ru(η^6 - <i>p</i> -cym)(cfA-H)Cl]	58
Sm(III)	2.345(3)	2.333(3)	72.43(10)	[Sm(cfH)(Ox) ₂]	77
Sn(II)	2.158	2.135	79.93	Ph ₂ Sn(cfH) ₂	78
Zn(II)	1.9994(12)	1.9423(13)	92.73(5)	[Zn(cfH)(Hbtc)].H ₂ O	79
Zn(II)	1.983(16)	2.013(17)	90.6(7)	[Zn(cfH) ₂ (H ₂ O) ₂].8H ₂ O	65
Zn(II)	2.028(2)	1.920(3)	92.89(10)	[Zn ₂ (cfH) ₂ (odpa)]	79

* ligand abbreviations: cfH= zwitterionic ciprofloxacin, phen=phenethylamine, oba=2-(oxalyl-amino)-benzoic acid, cym=cymene, cfA=7-(4-(decanoyl)piperazin-1-yl)-ciprofloxacin, odpa=octadecylphosphonic acid, Ox=oxalate, btc=trimesic acid.

The data obtained from the crystal structures of the metallo-ciprofloxacin complexes identified in the ciprofloxacin compound search was used to determine whether there is a correlation between the charge density of the metal ion in the complex and the strength of the metallo-ciprofloxacin coordination, evaluated using the metal-oxygen donor atom bond lengths. The volume charge density (ρ) of the metal ions was calculated using equation 1⁸⁰, giving the values for each of the metal ions found to be in metal-ciprofloxacin complexes as summarised in table 10. The ionic radii used in equation 1 are the Shannon-Prewitt radii⁸¹.

Equation 1

$$\rho = \frac{q}{\left(\frac{4}{3}\right)\pi r^3}$$

Where: r is the ionic radius

q is the formal charge

Table 10: formal charges (q) and ionic radii (r)⁸¹ of selected metal ions, used to calculate charge densities (ρ) of the metal ions.

<i>Metal ion</i>	Q	r/ Å	ρ/ Å⁻³
<i>Sm(III)</i>	+3	1.10	0.54
<i>Cd(II)</i>	+2	0.92	0.61
<i>Mn(II)</i>	+2	0.80	0.93
<i>Co(II)</i>	+2	0.79	0.96
<i>Zn(II)</i>	+2	0.74	1.18
<i>Cu(II)</i>	+2	0.71	1.33
<i>Mg(II)</i>	+2	0.71	1.33
<i>Sn(II)</i>	+2	0.69	1.45
<i>Ni(II)</i>	+2	0.69	1.45
<i>Ru(II)</i>	+2	0.68	1.52
<i>Fe(III)</i>	+3	0.72	1.92

The average lengths of the metal-ketone and metal-carboxylate bonds in the X-ray crystal structures of the metallo-ciprofloxacin complexes as a function of the estimated charge density of selected metals are shown in figure 14. Whilst it would be expected that the metal-carboxylate bond lengths would generally be shorter than the metal-ketone bond lengths because the oxygen donor atom in the carboxylate group has a formal negative charge, this is not observed across all of the metallo-ciprofloxacin complexes reported. It would also be expected that as the charge density of the metal ions increases, there would be a stronger coordination to the ciprofloxacin ligand, which would be reflected through a shortening of the M-O bond lengths. This trend is observed from Sm(II) to Cu(II) with both the metal-ketone and metal carboxylate bonds, as shown in figure 14. However, even though Mg(II) has the same calculated charge density as Cu(II), the averaged Mg(II) M-O bond lengths (for both ketone and carboxylate) are significantly longer. This could be because Mg(II) is an alkaline earth metal rather than a transition metal and does not have d electrons available to participate in bonding with a ciprofloxacin ligand. A lack of d electron availability to participate in bonding with a ciprofloxacin ligand could also explain the Sn(II) metallo-ciprofloxacin M-O bond length discrepancy as Sn(II) is a not a transition metal ion. As the charge density of the metal ions increases from Mg(II) to Fe(III), coordination to the ciprofloxacin ligand becomes more electrostatic than covalent. Differences in the observed and predicted trends in this data will

also arise from the influence of the coordination number, different types ligands or modifications to the ciprofloxacin ligands in the metallo-ciprofloxacin complexes which have been discussed.

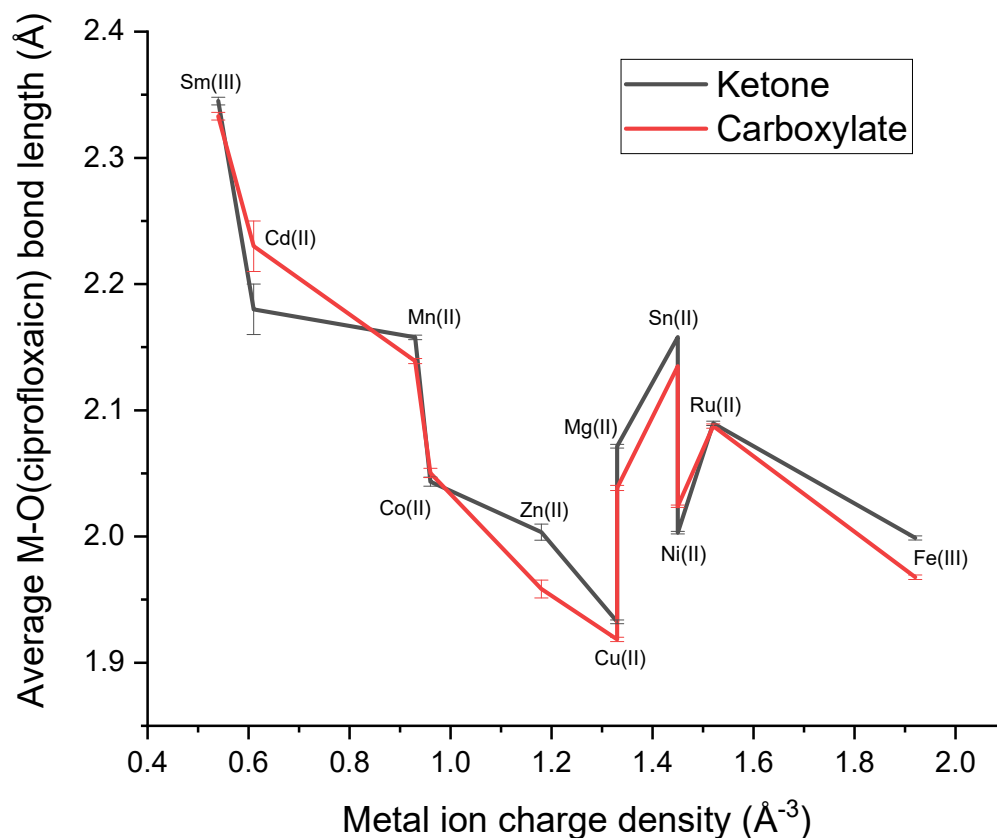


Figure 14: graph of the relationship between the mean M-O bond lengths in published metallo-ciprofloxacin complexes and the charge density (ρ) of metal ions. The error bars plotted are the mean maximum and minimum values from the published data. The metal-ketone (black) and metal-carboxylate oxygen (red) bond lengths are plotted separately for comparison.

The data summarised in table 9 also shows the bite angle for the O-M-O bonds of the metal ion and the ciprofloxacin oxygen donor atoms. When plotted against the metal ions in order of increasing charge density, there is a trend in the O-M-O bond angles as shown in figure 15. In perfectly octahedral complexes, it would be expected that the O-M-O bond angle would be 90° , however steric and electronic effects can cause distortion. The mean O-M-O bond angle in Cu(II) metallo-ciprofloxacin complexes appears to show the least distortion on the O-M-O bond angles with the mean bite angle of $91.14(8)^\circ$. The Sm(III) metallo-ciprofloxacin complex exhibits the most distortion of the metallo-ciprofloxacin complexes with a bite angle of $72.43(10)^\circ$. The bite angle increases as the charge density of the metal ions increases from Sm(III) to Zn(II), but

from Cu(II) to Fe(III) no trend is observed. Once again, this could be due to the influence of the coordination number, different types ligands or modifications to the ciprofloxacin ligands in the metallo-ciprofloxacin complexes.

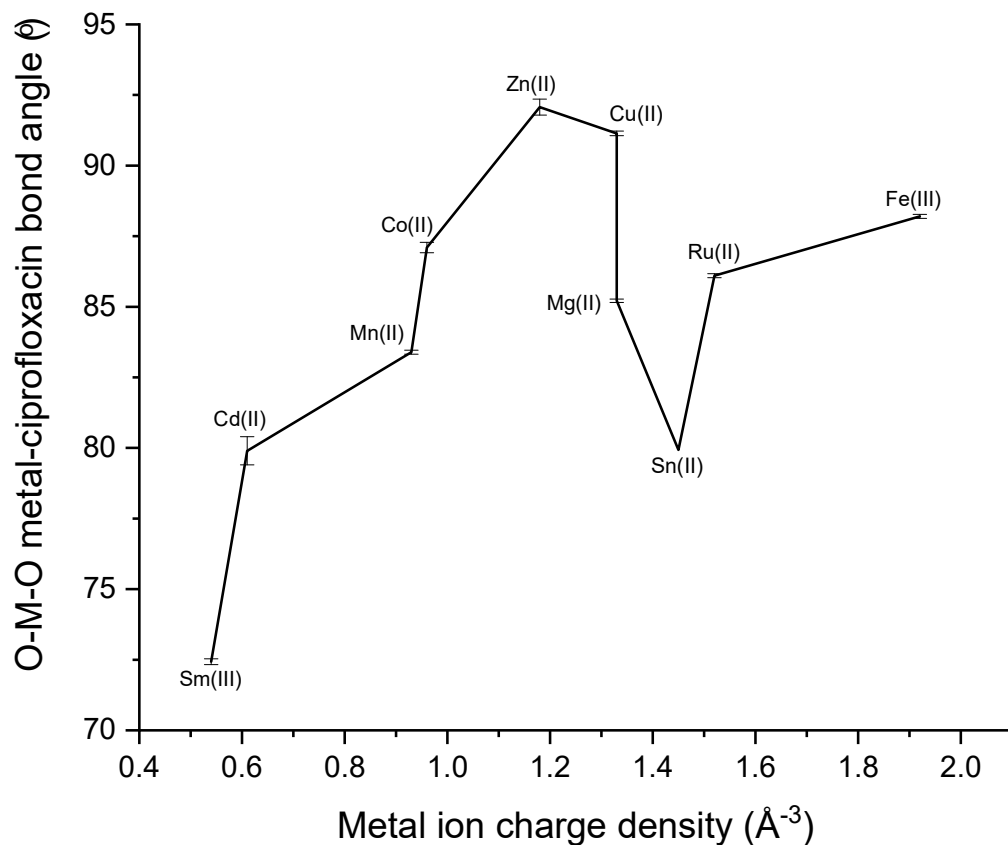


Figure 15: graph showing the relationship between metal ion charge density (increasing from Sm(III) to Fe(III)) and the O-M-O bite angle in metallo-ciprofloxacin complexes.

The results of the literature search for X-ray crystal structures of metallo-ciprofloxacin complexes using the CSD have shown that there is potential to coordinate ciprofloxacin ligands to a variety of metal ions. Whilst ciprofloxacin is known to have antimicrobial properties, other weakly coordinated ligands in the metallo-ciprofloxacin complexes could have additional antimicrobial effects *via* the formation of reactive oxygen species. Reactive oxygen species can kill cells if the oxidation process becomes uncontrolled and the production of reactive oxygen species is in fact a bacterial mechanism for stress stimulated self-destruction⁸². The remainder of this chapter will discuss the synthesis and characterisation of further metallo-ciprofloxacin complexes.

2.3 Iron(III)-ciprofloxacin

Iron is essential for fundamental biological processes in almost all living organisms, including bacteria. Iron is required for many metabolic functions such as DNA replication, oxygen transportation and immune responses⁸³. Both Gram negative and Gram positive bacteria have a variety of iron uptake pathways using various transport proteins, which are summarised in figures 16 and 17, using iron sources such as transferrin, hemophores and siderophores. Whilst bacteria have numerous iron uptake mechanisms, utilisation of these mechanisms would require the membrane receptors to recognise the iron(III)-ciprofloxacin complex, which is unlikely as these uptake pathways are specific.

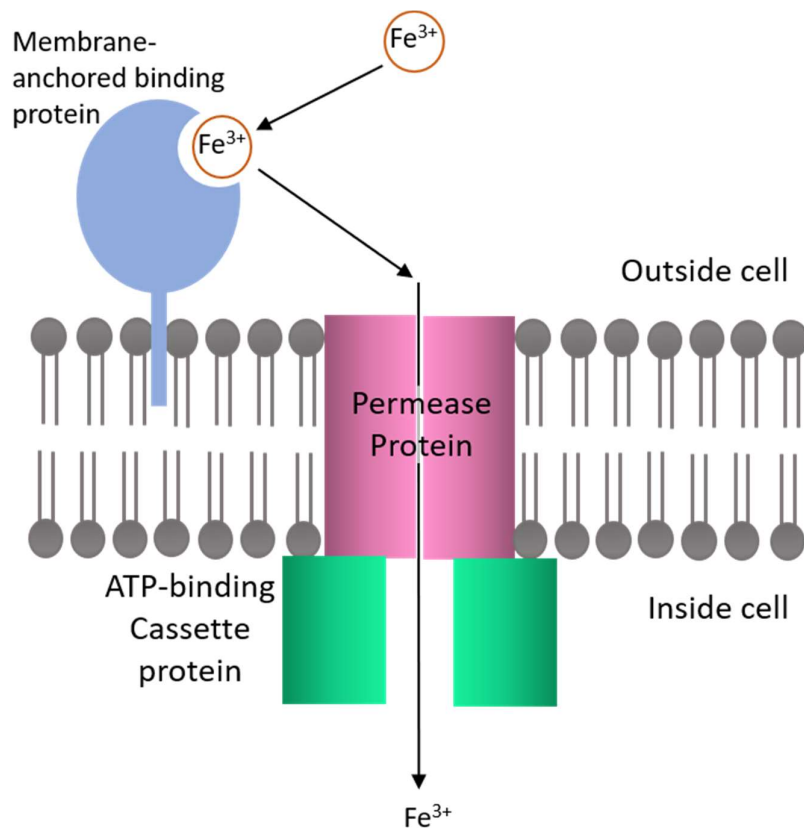


Figure 16: iron uptake mechanism in Gram positive bacteria whereby iron in heme, siderophore or transferrin is taken into the cell by membrane-anchored binding proteins and permease proteins and is then released as iron(III) after reacting with ATP in ATP-binding cassette proteins. This figure was adapted from a figure by K. D. Krewulak and H. J. Vogel⁸⁴.

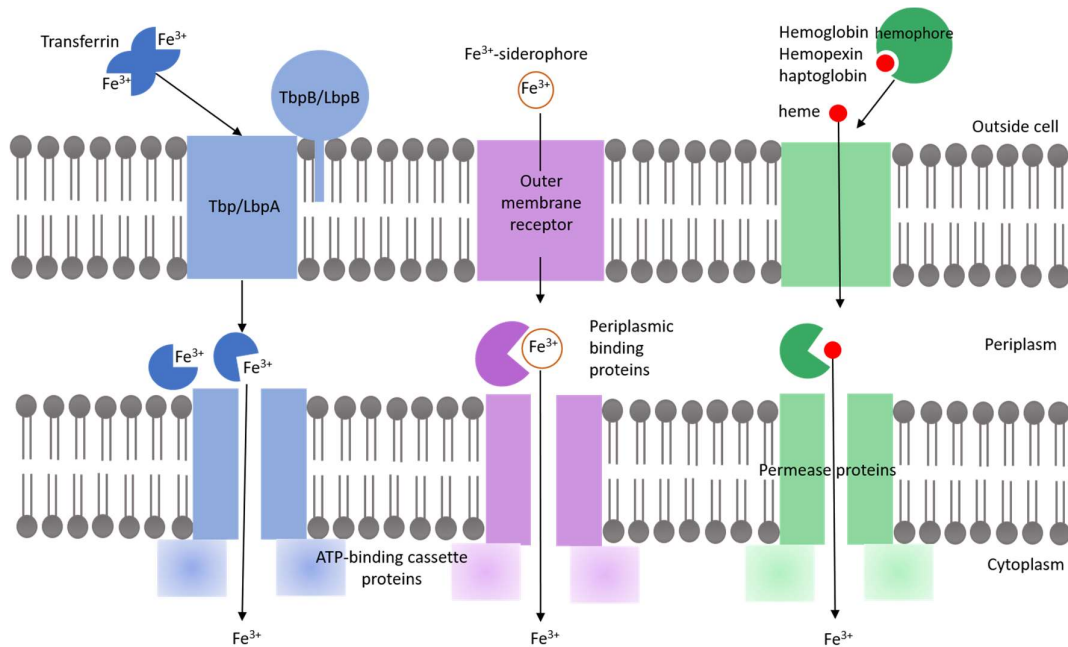


Figure 17: iron uptake mechanisms in Gram negative bacteria. Various outer membrane proteins are used to transport iron(III) in the form of transferrin, iron-bound siderophores and heme groups into the periplasm, which are then bound to periplasmic binding proteins which facilitate the transportation into the cytoplasm and through ATP-binding cassette proteins to release iron(III) into the cytoplasm. This figure was adapted from a figure by K. D. Krewulak and H. J. Vogel⁸⁴.

More likely uptake mechanisms into bacteria for the iron(III)-ciprofloxacin complexes will involve passive membrane diffusion and porins. Porins (figure 18) are beta barrel proteins found in the cell membrane (outer membrane of Gram-negative bacteria) and act as channels for passive diffusion.

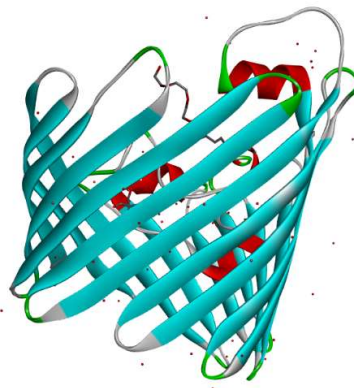


Figure 18: protein structure of a porin by M. S. Weiss and G. E. Schulz⁸⁵ (generated with Discovery Studio Visualizer).

Only one example of an X-ray crystal structure of an iron(III)-ciprofloxacin crystal structure was found in a search of CSD, this is $[\text{Fe}(\text{cfH})(\text{C}_2\text{O}_4)] \cdot (\text{cfH}_2^+) \cdot 5\text{H}_2\text{O}$ (figure 19), which has increased antimicrobial activity against *P. aeruginosa* than ciprofloxacin at every concentration tested (0.125, 0.25 and 0.5 $\mu\text{g mL}^{-1}$)⁶⁶, demonstrating the potential for iron(III)-ciprofloxacin complexes as antimicrobial agents.

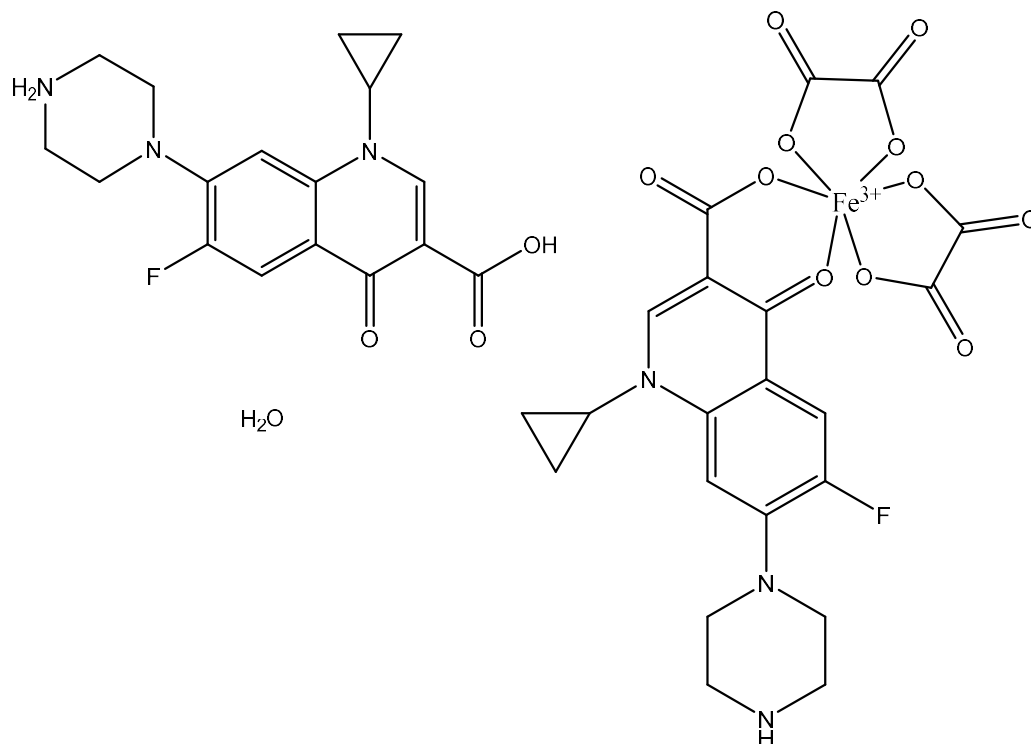


Figure 19: structure of $[\text{Fe}(\text{cfH})(\text{C}_2\text{O}_4)] \cdot (\text{cfH}_2^+) \cdot 5\text{H}_2\text{O}$, from crystallographic data reported by L.-C. Yu *et al.*⁶⁶

2.3.1 Preliminary experiments

Optimum metal-to-ligand ratio for coordination of iron(III) to ciprofloxacin

In order to determine the optimum metal-to-ligand ratio, a Job's plot style investigation was conducted using UV-vis spectroscopy, the results of which are plotted in figure 20. The absorbance at 456 nm was chosen for analysis as this absorption band occurred exclusively in the spectra of the solutions between 0.1 and 0.9 molar fraction of ciprofloxacin, suggesting that this absorption band corresponds to an electronic transition that is characteristic for the iron(III) ciprofloxacin complex. In the pH 2 solution, the maximum absorbance values at 456 nm, averaged over results in triplicate, occurred in the 0.5 molar fraction of the ciprofloxacin

solution. From this experiment it can be concluded that a 1:1 metal-to-ciprofloxacin ratio is the optimum ratio in a pH 2 solution. However, in pH 3 solutions of the same concentration, the maximum absorbance shifts further towards a 1:2 iron(III)-to-ciprofloxacin ratio, suggesting that the pH influences the ratio of iron and ciprofloxacin complexation.

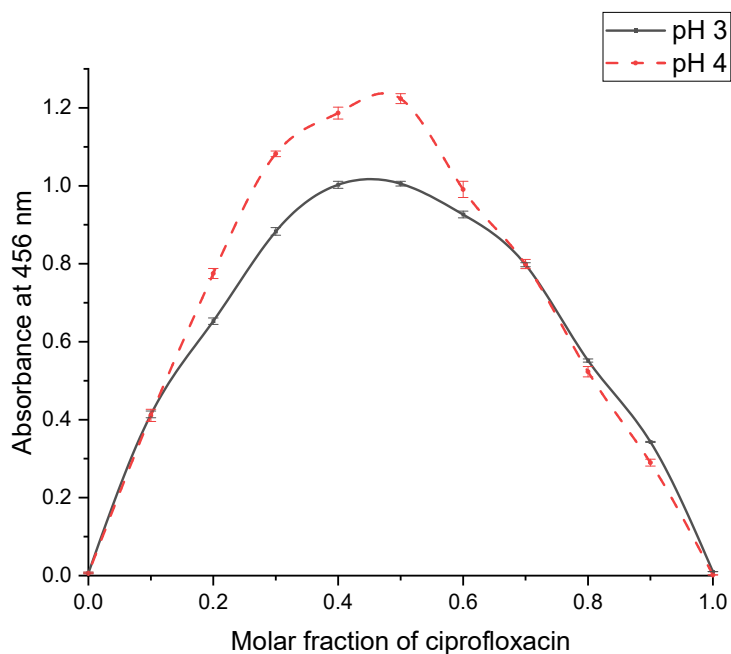


Figure 20: Job's plot graph showing the relationship between pH and molar fraction of ciprofloxacin on absorbance at 456 nm. The concentrations of the metal and ligand solutions were $1.81 \times 10^{-3} \text{ mol dm}^{-3}$ each in hydrochloric acid (0.1 M for pH 2 and 0.02 M for pH 3). The results plotted are the mean of the triplicate results at each pH, with the error bars showing \pm one standard deviation. The experimental procedure is detailed in section 6.2.1.

From this investigation, it can be concluded that the optimum metal-to-ligand ratio for iron(III)-ciprofloxacin ratio is dependent on the pH of the solution and further investigation into the pH is required. At pH 2, a 1:1 ratio should be employed, whereas a greater metal-to-ligand ratio may be appropriate in solutions of a higher pH.

Extrapolation of the data for each of the Job's plot graphs at pH 2 and 3 (figure 21) allowed for the calculation of the theoretical concentration of the iron(III) ciprofloxacin complex at 100% complexation¹³⁴. Using the theoretical concentration of the iron(III) ciprofloxacin complex at 100% complexation, a value for the molar extinction coefficient (ϵ) was calculated using equation 2 to be $2078.40 \text{ dm}^3 \text{ mol}^{-1} \text{ cm}^{-1}$ for pH 2 and $1705.50 \text{ dm}^3 \text{ mol}^{-1} \text{ cm}^{-1}$ for pH 3. The

calculated values for ϵ can then be used to calculate an equilibrium constant (K_{eq}) for the reactions at pH 2 and pH 3.

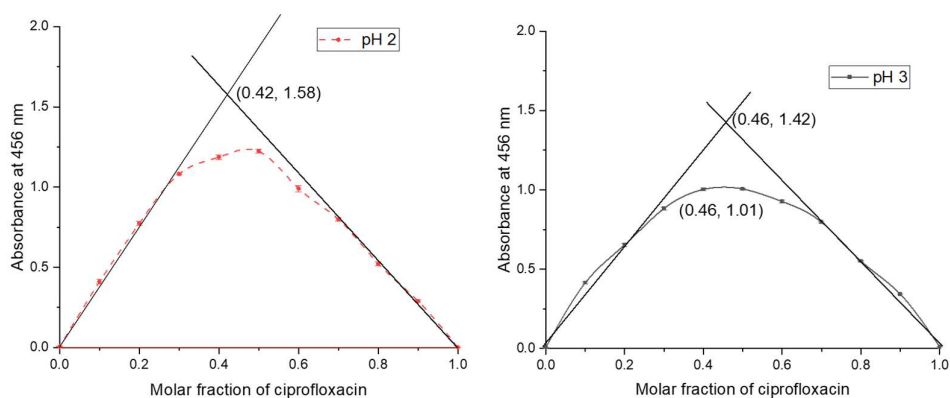


Figure 21: Job's plot graphs showing extrapolated data points used to calculate the values of ϵ and subsequently K_{eq} for iron(III)-ciprofloxacin systems at pH 2 (left) and pH 3 (right).

Equation 2

$$A = \epsilon cl$$

Using equation 3, K_{eq} is calculated to be $6664.97 \text{ mol}^{-1} \text{ dm}^3$ for the reaction at pH 2 and $6380.34 \text{ mol}^{-1} \text{ dm}^3$ at pH 3. Both values of K_{eq} demonstrate that under the Job's plot experimental conditions (room temperature, atmospheric pressure), the equilibrium favours the product (iron(III)-ciprofloxacin complex) over the reactants. Whilst the values for K_{eq} for both the pH 2 and pH 3 systems are of a similar magnitude, there is a greater value for K_{eq} calculated for the pH 2 system than the pH 3 system, evidencing that there is more iron(III)-ciprofloxacin complexation at pH 2 than pH 3.

Equation 3

$$K_{eq} = \frac{[ML]_{eq}}{[M]_{eq}[L]_{eq}} [M]_{eq} = [M]_0 - [ML]_{eq}$$

$$[M]_{eq} = [M]_0 - [ML]_{eq}$$

$$[L]_{eq} = [L]_0 - [ML]_{eq}$$

Optimum pH for complexation

Coordination to iron(III) is expected to occur at the hard oxygen donor atoms of the ketone/ carboxylate groups in ciprofloxacin. Figure 22 demonstrates that pH impacts the species of ciprofloxacin present. At pH 6.35 half of the carboxylic acid groups in ciprofloxacin are deprotonated⁸⁶, making it a better donor atom and therefore more likely to coordinate to iron(III); a hard metal ion. However, it is difficult to get iron(III) ions in solution in basic conditions, due to their Lewis acidic properties they tend to precipitate as hydroxides. Figure 22 also shows that around neutral pH, the zwitterion of ciprofloxacin is present which is insoluble. This knowledge directed the research into the investigation of metallo-fluoroquinolone complexation in acidic conditions.

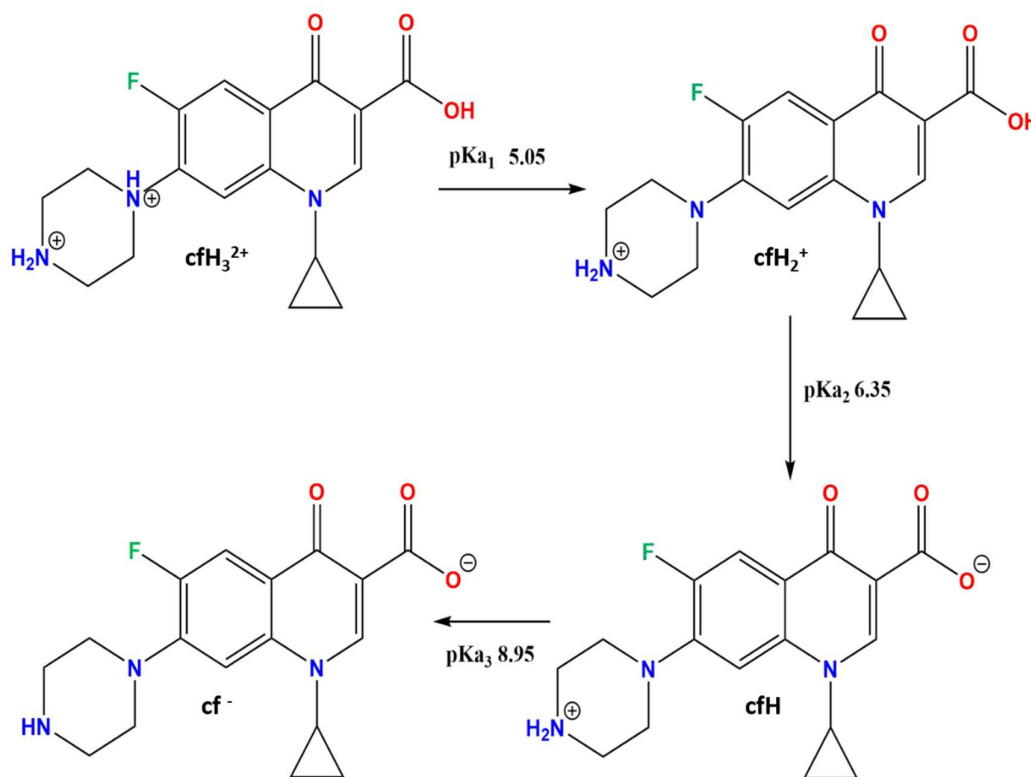


Figure 22: scheme showing the varying pKa values of ciprofloxacin⁸⁶.

Solutions with pH values of less than two could not be evaluated as ciprofloxacin was found to be fully protonated and insoluble below pH 2. Similarly, solutions with pH values greater than four could also not be investigated due to insolubility of both iron(III) and ciprofloxacin.

The findings from the Job's plot investigation into iron(III)-ciprofloxacin coordination presented in figure 20 show that pH influences the absorbance at 456 nm. Greater absorbance occurs for the solutions of the same concentration and the same molar fractions at pH 2 comparative to

pH 3. The positive correlation between absorbance and concentration, demonstrated in the Beer-Lambert Law (equation 2) suggests that there is a greater concentration of the iron(III)-ciprofloxacin complex in solution at pH 2 *versus* pH 3

These findings allude to a solution of pH 2 creating more optimum reaction conditions compared to a solution of pH 3. Using a pH probe, it was found that ciprofloxacin in 0.1 M hydrochloric acid solution has a value of pH 2 and therefore this provided the basis of the reaction conditions used for metallo-fluoroquinolone complexation.

2.3.2 Crystallisation Techniques

A critical objective of this research is to show that the metal ion is coordinated to the fluoroquinolone molecule in the synthesised complexes. This is important as literature suggests that merely the presence of unbound metals does not influence the effectiveness of fluoroquinolone antibiotics³⁷⁻³⁹. Given the poor solubility of the reagents and resulting complexes, characterisation is challenging. Creating a good quality crystal allows for a crystal structure to be generated to determine the structure of the complex.

Solvent Layering

Solvent layering is a commonly used crystallisation techniques. A range of anti-solvents were tested to find the most suitable. In the synthesis of the iron(III)-ciprofloxacin complex, acetone, acetonitrile and methanol were selected due to their miscibility with water (the solvent of the reaction mixture). Of the anti-solvents employed, solvent layering with acetone was the only anti-solvent to yield a precipitate. However, this technique yielded powders/ microcrystals, which were not suitable for analysis *via* X-ray crystallography. In order to create more useful crystals for analysis, experimentation with other crystallisation techniques were carried out in order to slow down the crystal growing process.

Vapour Diffusion

Vapour diffusion crystallisation was the most successful crystallisation technique and yielded crystals which were analysed using X-ray crystallography. Using the knowledge acquired from the solvent layering experiments, acetone was the antisolvent of choice for the iron(III)-ciprofloxacin experiments. Acetone is also volatile, a key feature required for an anti-solvent in vapour diffusion. The set up for this solvent diffusion method was using an open small sample vial (1.8 mL), half filled with the reaction mixture, inside a tightly sealed larger sample vial (8 mL)

containing the antisolvent, as shown in figure 23. This set up was more successful than solvent layering for creating crystals, but some of these crystals were still not of a quality that could be analysed using X-ray crystallography. Care was taken to ensure that the crystallisations were set up at room temperature in places where they would be undisturbed.

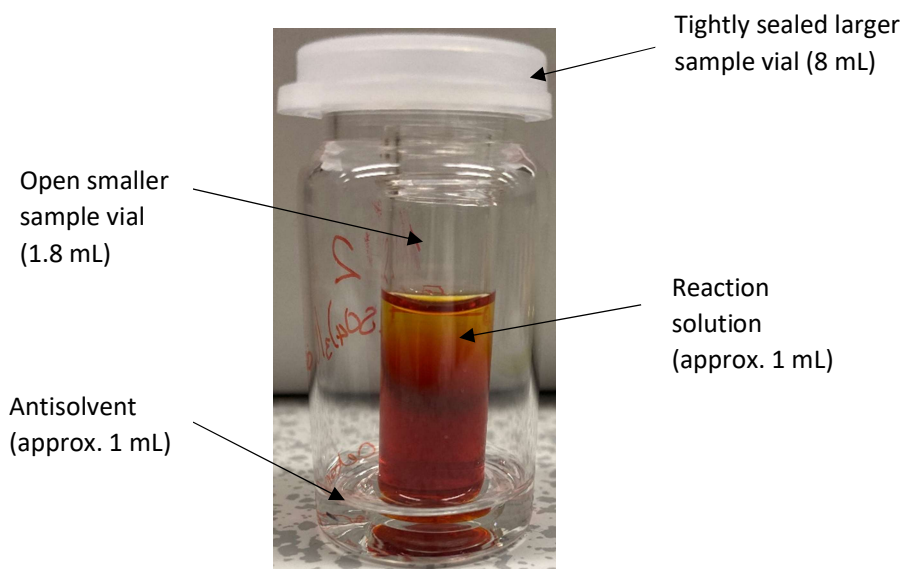


Figure 23: solvent vapour diffusion crystallisation method set up using an open smaller sample vial (1.8 mL) half filled with the reaction mixture (approx. 1 mL), inside a tightly sealed larger sample vial (8mL) containing the antisolvent (approx. 1 mL).

2.3.3 Synthesised iron(III)-ciprofloxacin complexes

Two different iron(III)-ciprofloxacin complexes have been synthesised using the information from the preliminary experiments into iron(III)-ciprofloxacin coordination, and their crystal structures have been analysed in comparison to a crystal structure of the isolated ciprofloxacin ligand (**2**). The first iron(III)-ciprofloxacin complex to be synthesised was $[\text{FeCl}(\text{H}_2\text{O})(\text{cfH})]$ (**1**). In order to remove the chloride ligand iron(III) sulfate was used as opposed to iron(III) chloride in the synthesis of the second iron(III)-ciprofloxacin complex, the complex salt $[\text{Fe}(\text{SO}_4)(\text{H}_2\text{O})_3(\text{cfH})]^+ [\text{Fe}(\text{SO}_4)_2(\text{cfH})_2]^-$ (**3**).

2.3.3.1 Iron(III) chloride-ciprofloxacin complex

The first complex to be successfully crystallised and analysed using X-ray crystallography was the 1:2 iron(III)-ciprofloxacin complex (**1**), the crystal structure is shown in figure 24. The crystal data

and refinement of **(1)** was generated by Dr Adrian C. Whitwood. This complex was formed using non-stoichiometric quantities of ciprofloxacin and iron(III) chloride hexahydrate (equation 4) and was crystallised using vapour diffusion with acetone. Single crystal X-ray diffraction shows that the 1:2 iron(III)-ciprofloxacin crystals have a monoclinic crystal system with an $I2/a$ space group. A discrete atom model was used to model disordered solvent and anions in this crystal and a solvent mask was used in order to account for the 64 electrons of disordered content per complex which lay in a solvent channel. The highly disordered solvent content of this crystal equated to a combination between 2 acetone and 6 water molecules. Three different 1:2 iron(III)-ciprofloxacin complexes exist in this crystal structure, with variation in the chloro/ aquo ligands. Present in the crystal are a combination on dichloro, diaquo and chloro/aquo complexes with a chloride to water ratio of 0.373:0.626(6). The second ciprofloxacin ligand is symmetry generated from the asymmetric unit using $3/2-X,+Y,1-Z$.

Equation 4

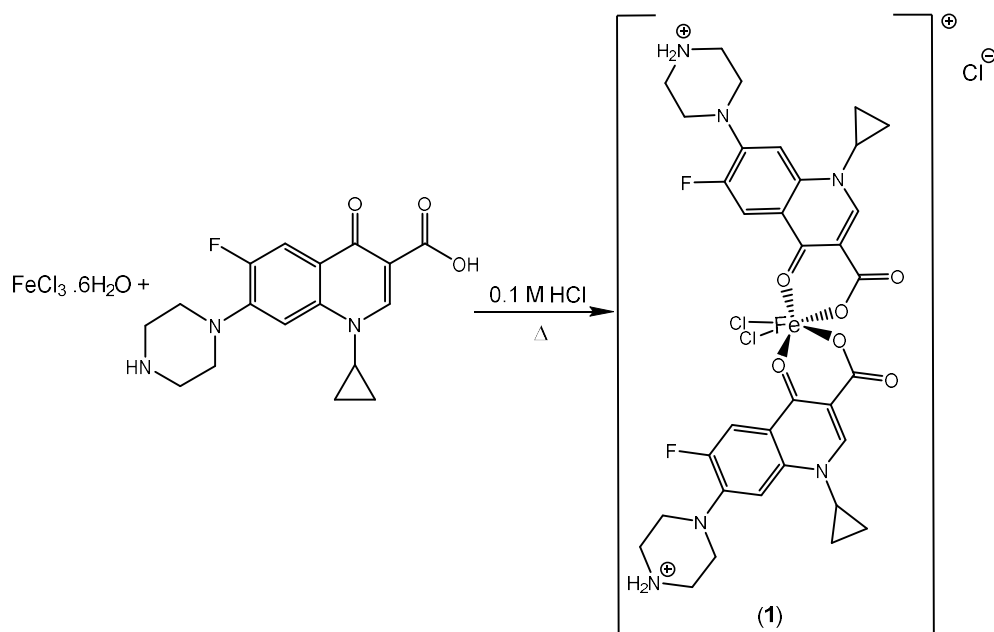


Table 11: selected bond lengths for 1:2 iron(III)-ciprofloxacin (**1**).

Atom	Atom	Length/Å	Atom	Atom	Length/Å
C1	O1	1.275(3)	Cl1	Fe2	2.293(3)
C1	O2	1.246(3)	Fe2	O1	1.997(16)
C3	O3	1.279(3)	Fe2	O3	2.029(15)

Table 12: selected bond angles for the crystal structure of (**1**).

Atom	Atom	Atom	Angle/°	Atom	Atom	Atom	Angle/°
O1	C1	C2	119.20(19)	O1	Fe2	Cl1	96.65(8)
O2	C1	C2	118.70(2)	O1	Fe2	O3	84.99(6)
O2	C1	O1	122.10(2)	O1	Fe2	O4	97.03(16)
O3	C3	C2	124.27(19)	O3	Fe2	Cl1	97.20(9)
O3	C3	C4	118.99(19)	O4	Fe2	O3	85.78(17)
C1	O1	Fe2	128.29(14)	C3	O3	Fe2	121.86(13)

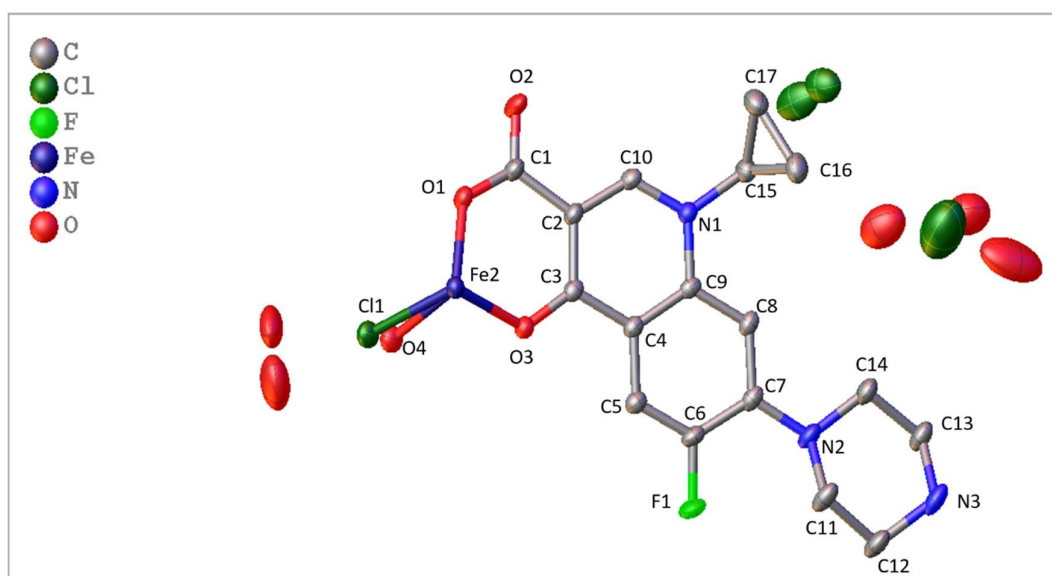


Figure 24: ORTEP representation of the asymmetric unit of 1:2 iron(III)-ciprofloxacin (**1**). Ellipsoids are plotted at 50 % probability

With a coordination number of six and metal-ligand bond angles around 90°, (**1**) has an approximately octahedral geometry. The bond lengths obtained for the 1:2 iron(III)-ciprofloxacin complex yielded from the reaction detailed in equation 4, shown in table 11, show that the longest bond in this structure is the Fe2-O3 bond (2.0292(15) Å). This coincides with what would be expected as this is a particularly weak coordination, as the O3 atom is from the ketone group on the ciprofloxacin ligand and does not have a formal negative charge and therefore does not engage strongly in electrostatic interactions.

The deprotonated O1 atom is a hard donor atom, which according to hard-soft acid-base theory, will have a high affinity for the iron(III) ion which is a hard acceptor. Furthermore, the deprotonated O1 has a negative charge and therefore mainly interacts with the positively charged iron(III) ion through strong electrostatic interactions. This explains why the Fe2-O1 bond is shorter and therefore stronger than the Fe2-O3 bond (1.997(16) Å *versus* 2.029(15) Å). The equivalent of M-O1 forming a shorter bond than M-O3 is also observed in a copper(II) complex with a modified ciprofloxacin ligand^{60, 87} in which the ciprofloxacin ligand is coordinated to the copper ion through the oxygen donor atoms in the β-ketone carboxylic acid group. The bond lengths of Fe2-O1 and Fe2-O3 are within error of the reported bond lengths of ciprofloxacin to iron(III) by Wallis *et al.* for their complex: [Fe(cf')(nta)]₃.5H₂O (this complex was not reported in CSD). The equivalent of the Fe2-O1 bond length in [Fe(cf')(nta)]₃.5H₂O was found to be 1.97(1) Å compared to 1.997(16) Å in (**1**). Similarly, the equivalent of the Fe2-O3 bond in [Fe(cf')(nta)]₃.5H₂O was found to be 1.942(8) Å compared to 2.029(15) Å in (**1**)¹³. The biological consequences of the strength of the coordination of the ciprofloxacin ligand to the iron(III) ion will depend on the mechanism of action of the drug molecule in bacterial cells. As the ciprofloxacin pharmacophore structure-activity-relationship requires the β-ketone carboxylic acid group for coordination to the intercellular target molecule; DNA gyrase and for bacterial transport, a more labile ciprofloxacin ligand could be advantageous.

The Fe2-Cl1 bond length (2.293(3) Å) in (**1**) is slightly longer than reported literature values for Fe(III)-Cl bonds^{88, 89}. The occasional occupancy of chloro ligands on the iron(III) ion poses as a problem as this means that there is not a uniform structure throughout the crystal and as such would reduce the accuracy of any biological assays.

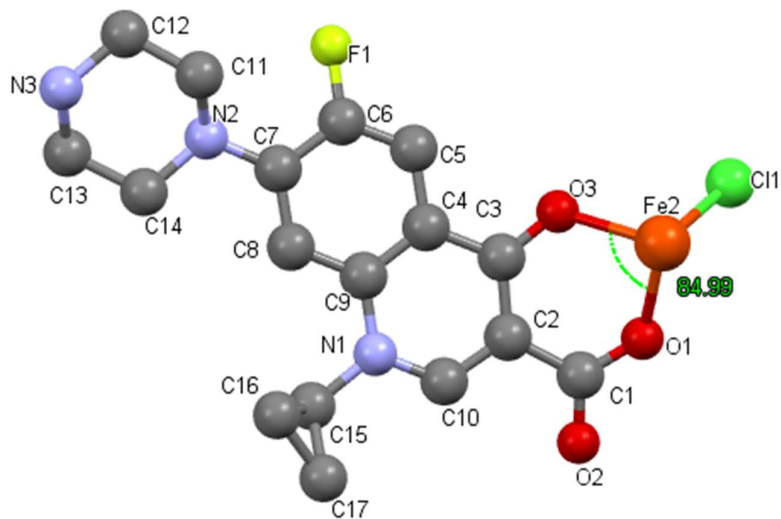


Figure 25: ball and stick representation of the asymmetric unit of (1) with the bond angle of O3-Fe2-O1 measured to be 84.99(6)°. Solvent atoms and hydrogen atoms have been removed for clarity.

Figure 25 shows that the O1-Fe(III)-O3 bond angle is 84.99(6)°, which is smaller than the 90° angle expected in the octahedral structure, meaning that there is distortion. Distortion could be caused by steric or electronic effects driven by the ligands.

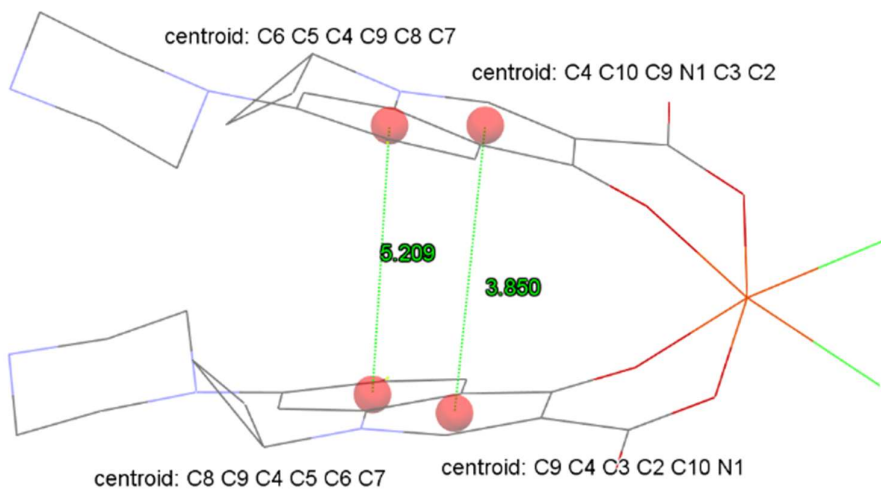


Figure 26: wire representation of (1) with the pi stacking distance of the aromatic rings of the ciprofloxacin ligands measured to be 3.850 Å between the C2/C3/N1/C4/C9/C10 rings and 5.209 Å between the C4/C5/C6/C7/C8/C9 rings, using calculated centroid atoms. Solvent atoms and hydrogen atoms have been omitted for clarity.

There is π - π stacking present in **(1)**. The ciprofloxacin ligands are stacked over each other due to the π - π stacking interactions between the aromatic rings in the ciprofloxacin ligands and also due to the drive for the hydrophobic ciprofloxacin ligands to align. Using calculated centroids, as displayed in figure 26, the π - π stacking distance of the C2/C3/N1/C4/C9/C10 aromatic rings of the ciprofloxacin ligands to be 3.850 Å. The distance between the C4/C5/C6/C7/C8/C9 aromatic rings in ciprofloxacin experience less π - π stacking interaction shown by the longer distance of 5.209 Å. The reasons for the reduced π - π stacking interaction in the C4/C5/C6/C7/C8/C9 aromatic rings in the ciprofloxacin ligands could be due to steric factors meaning that the rings simply do not align as well as the C2/C3/N1/C4/C9/C10 aromatic rings. Another explanation for the reduced π - π stacking interaction in the C4/C5/C6/C7/C8/C9 aromatic rings in the ciprofloxacin ligands is the fluorine substituent that is present, which is very electronegative and therefore reduces the electron density surrounding the aromatic ring. π - π stacking is not observed between intramolecular ciprofloxacin ligands in the metallo-ciprofloxacin structures found in the CSD search. This is because the complexes that were found in the CSD search either only had a single ciprofloxacin ligand, or because the ciprofloxacin ligands are trans to one another and therefore are not close enough nor have a favourable orientation to interact.

All of the bond lengths and angles of the ciprofloxacin ligand in **(1)** are comparable within error to those of the uncoordinated ciprofloxacin ligand **(2)**, with the exception of the carbonyl group bond lengths. In **(1)** there is a carboxylate group where there is a carboxylic acid group in **(2)**. In comparison to the uncoordinated ciprofloxacin ligand **(2)** shown in figure 27, the C1-O1 bond in **(1)** is significantly shorter (1.275(3) Å in **(1)** and 1.3329(15) Å in **(2)**) and the C1-O2 bond is significantly longer (1.246(3) Å in **(1)** and 1.2124 Å in **(2)**). The changes in the carboxylate bond lengths arise due to the coordination of the O1 ion to the iron(III) ion. Although the ketone oxygen atom in ciprofloxacin (O3) also takes part on coordination to the iron(III) ion, there is no significant difference between the C3-O3 bond lengths of the ketone in the coordinated and uncoordinated ciprofloxacin ligand (1.279(3) Å in **(1)** and 1.2700(15) Å in **(2)**), which further evidences that the O3 interaction with iron(III) is weak.

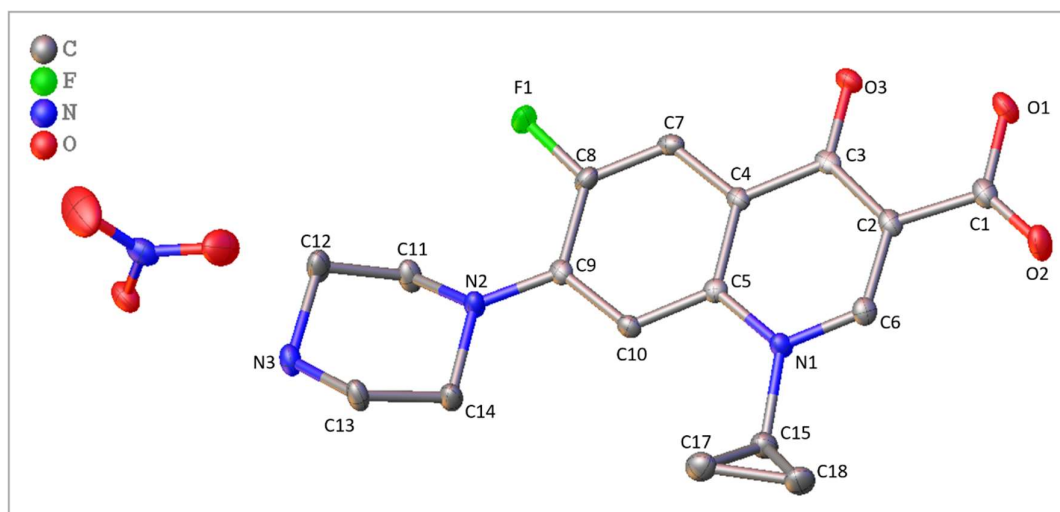


Figure 27: ORTEP representation of the X-ray crystal structure of ciprofloxacin (**2**). Ellipsoids are plotted at 50 % probability. C15A, C17A and C18A have been omitted for clarity, these formed a minor structure within the crystal with a ratio of the occupancy of the major and minor structures of 0.931:0.069(3). This structure was collected and refined by Adrian C Whitwood.

Table 13: selected bond lengths for ciprofloxacin (**2**).

Atom	Atom	Length/Å	Atom	Atom	Length/Å
C1	C2	1.4891(16)	C1	O2	1.2124(15)
C1	O1	1.3329(15)	C3	O3	1.2700(15)

There are intermolecular interactions between the molecules of (**1**), these interactions are shown in figure 28. Intermolecular hydrogen bonding exists between F1 and H10. The C6 carbon atom in (**1**), which is bonded to the F1 atom is sp^2 hybridised. $C(sp^2)$ -F bonds are weaker than $C(sp^3)$ -F bonds⁹⁰. $C(sp^2)$ -F fluorine atoms cannot enter into as strong hydrogen bonding as $C(sp^3)$ -F fluorine atoms^{90,91} because sp^2 orbitals have greater s-orbital character and therefore are not as expanded as sp^3 orbitals meaning that a lone pair of electrons cannot participate in hydrogen bonding as readily in $C(sp^2)$ -F. The $C(sp^2)$ -F hybridisation explains why hydrogen bonding between H10 and F1 has a relatively long contact distance of 3.101 Å. The shortest intermolecular interaction occurs between the O2 atom of one molecule and the H3 of another, with a contact distance less than half of that of the intermolecular H-F bond, of 1.352 Å.

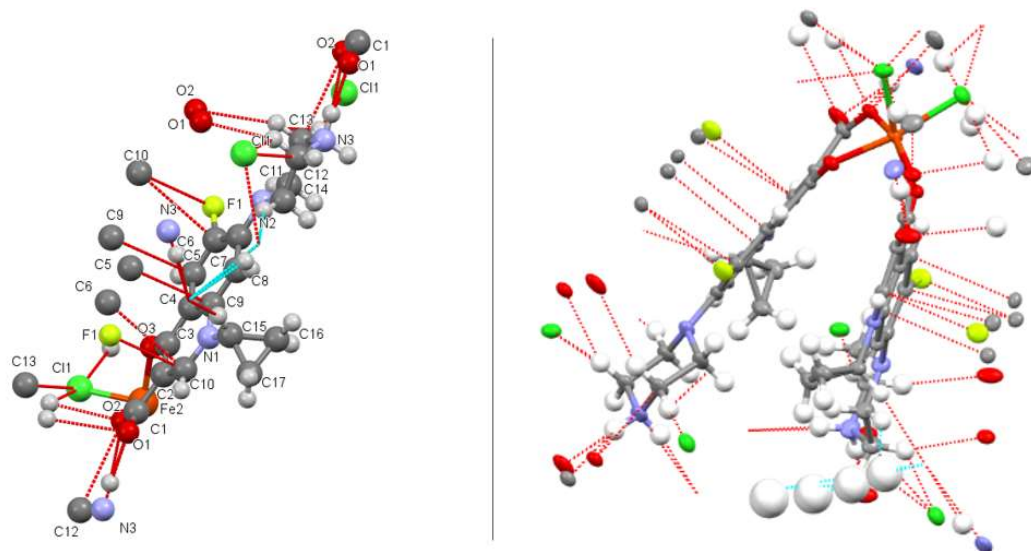


Figure 28: X-ray crystal structure of $[\text{FeCl}(\text{H}_2\text{O})(\text{cfH})]$ (**1**), showing the intermolecular interactions. *Left*: ball and stick asymmetric unit of (**1**) with atom labels showing intermolecular interactions. *Right*: structure of (**1**) with ellipsoids plotted at 50 % probability, showing intermolecular interactions. In both diagrams solvent atoms have been removed for clarity.

The intermolecular interactions described result in packing of the molecules in a stacking formation whereby the molecules of (**1**) flip alternatively allowing for the more hydrophobic piperaziny groups to group together (figure 29).

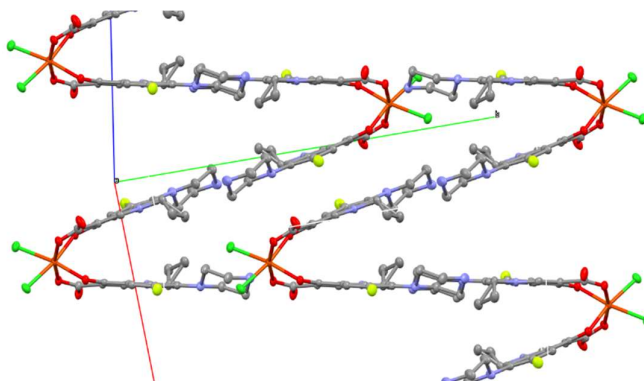
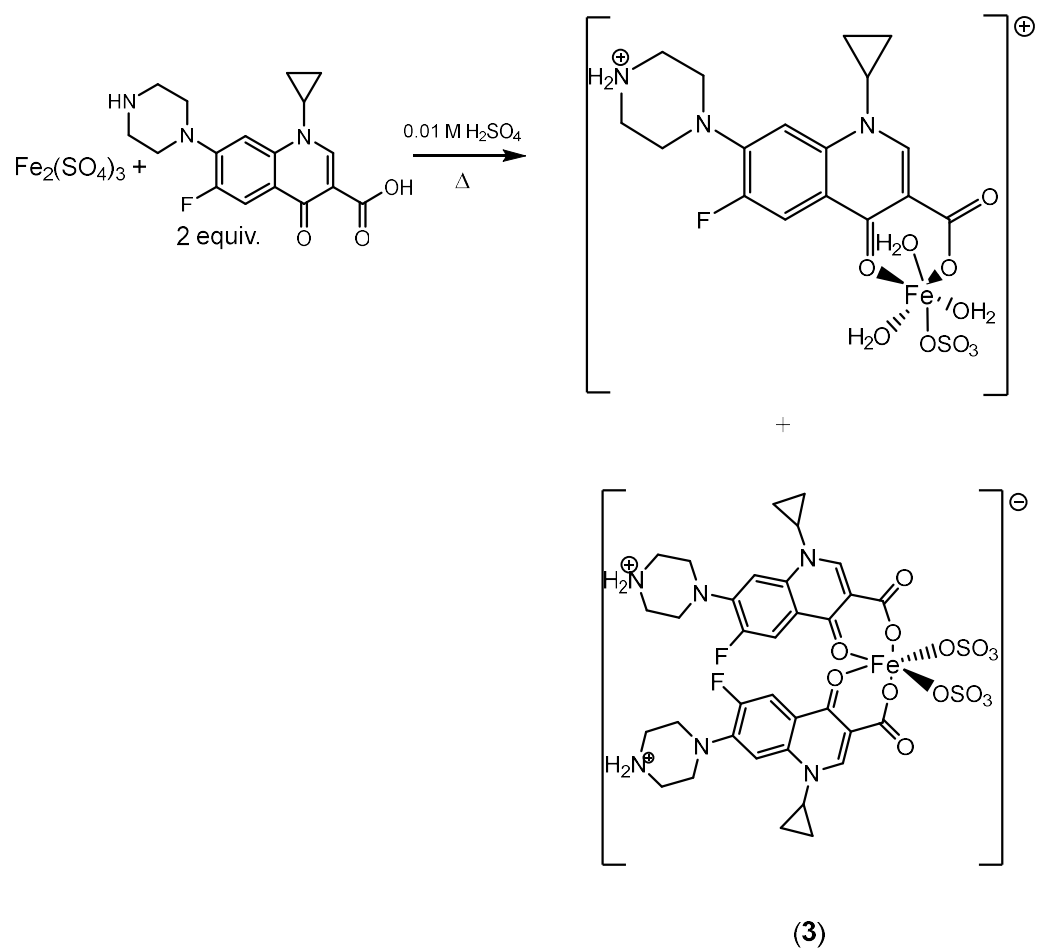


Figure 29: ball and stick packing formation of (**1**).

2.3.3.2 Iron(III) sulfate-ciprofloxacin complex

The chloride ions in the 1:2 iron(III) chloride-ciprofloxacin complex resulted in a mixture of molecules with chloro and aquo ligands present in the structure, therefore an alternate iron source was used: iron(III) sulfate. This time a 1:2 ratio of iron(III) sulfate, $\text{Fe}_2(\text{SO}_4)_3$, and ciprofloxacin reaction was used (to maintain the 1:1 iron(III)-to-ciprofloxacin ratio). Using 0.01 M sulfuric acid (in order to retain the pH 2 condition), the rest of the reaction and crystallisation set up was the same as the successful reaction with iron(III) chloride hexahydrate- solvent vapour diffusion with acetone. The crystals yielded from this reaction were suitable for X-ray crystallography, the X-ray crystallography data for these crystals was collected and refined by Theo Tanner. The crystal structure in figure 30 shows that the product is a 1:1 mixture. The 1:2 iron(III)-ciprofloxacin compound which was present was to be expected based on the results of the iron(III) chloride hexahydrate experiments, however the 1:1 iron(III)-ciprofloxacin compound was also present in the crystal. The formation of the additional 1:1 iron(III)-ciprofloxacin complex is likely due to a discrepancy in the moles of iron(III) sulfate that was added, this is likely because the iron(III) sulfate was yielded from drying iron(III) sulfate hydrate, which had an unknown number of water molecules included. It is possible that there were still water molecules present in the iron(III) sulfate, meaning the stoichiometric calculations were not accurate and in fact tended more towards a 1:3 iron(III)-ciprofloxacin ratio as detailed by the reaction shown in equation 5. As the X-ray crystal data for **(3)** does not indicate the existence of molecules with aquo ligands, the crystal structure is more uniform and therefore the use of iron(III) sulfate could be an improved iron source for this reaction. However, the 1:1 iron(III)-ciprofloxacin complex exists as a cation and the 1:2 iron(III)-ciprofloxacin complex exists as an anion and therefore synthesis of the separate complexes may not be possible as they are co-dependent.

Equation 5



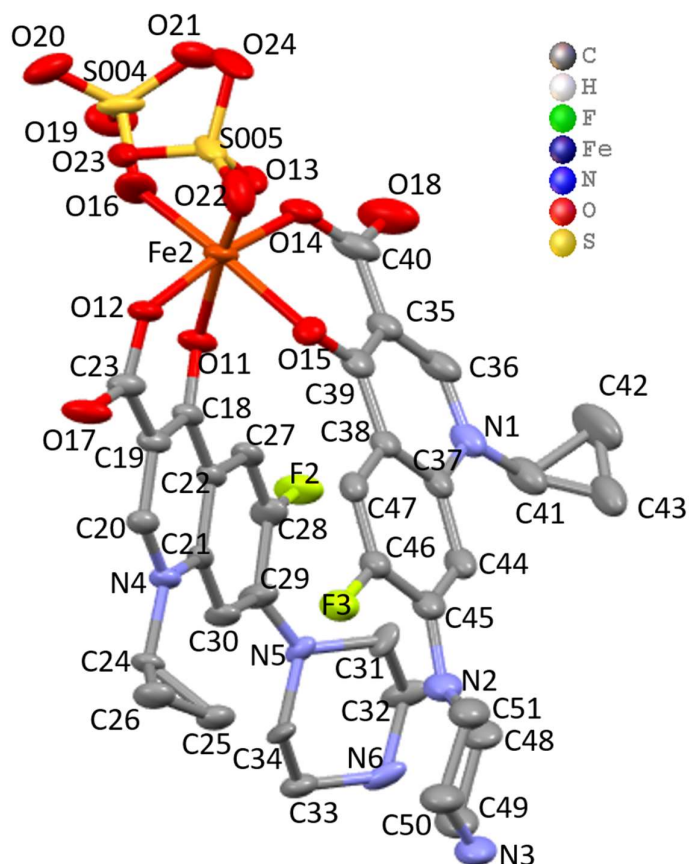


Figure 31: ORTEP representation of the X-ray crystal structure of the 1:2 iron(III)-ciprofloxacin complex found in (**3**), $[\text{Fe}(\text{SO}_4)_2(\text{cfH})_2]$, henceforth referred to as **3i**. Ellipsoids are plotted at 50 % probability. O20 and O19 (occupancy of 0.44(3)), C31A, C32A, C33A and C34A (occupancy of 0.684(6)), and C15A, C16A and C17A (occupancy of 0.361(6)) have been omitted for clarity.

3i has six donor atoms coordinated to the iron(III) centre, each with close to a 90° angles. As expected, the longest bonds in the **3i** complex are the Fe2-O15 and Fe2-O11 bonds, with distances of 2.052(3) Å and 2.037(3) Å, respectively. These bonds are from the coordination of iron(III) to the ketone oxygen in ciprofloxacin, which is the equivalent of the longest bond in (**1**). These particular Fe-O bonds in **3i** are within error of the same bond in (**1**) which is 2.0292(15) Å. The O-M-O bite angles of both the ciprofloxacin ligands would be expected to be equivalent in each of the ciprofloxacin ligands and close to 90° . Both the O11-Fe2-O12 ($85.47(1)^\circ$) and O14-Fe2-O15 ($85.61(1)^\circ$) bond angles are less than 90° and what's more, these angles are not within error of each other. The unexpected bite angles are as a result of distortion caused by the steric and electronic properties of the ligands.

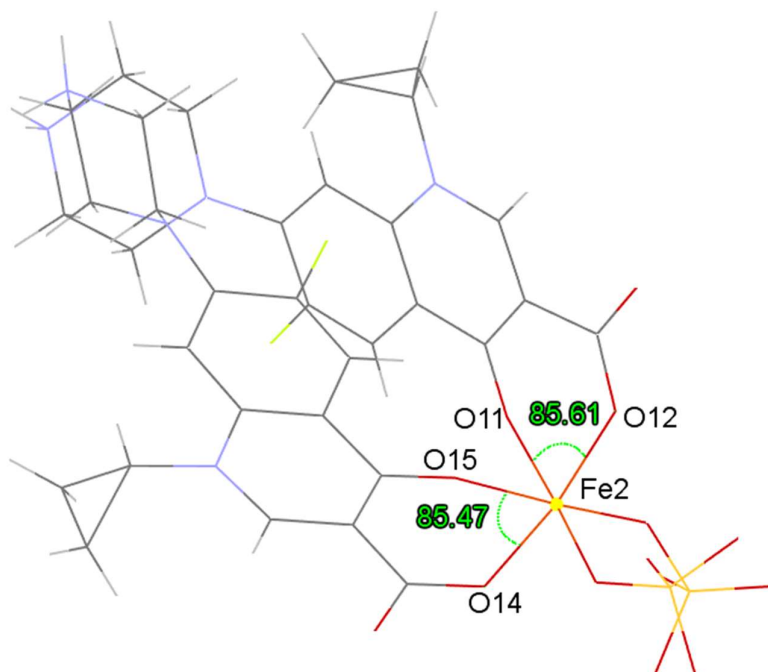


Figure 32: wire frame representation of **3i** with measured bond angles for the O-M-O bite angles for each of the ciprofloxacin ligands. Solvent and hydrogen atoms have been omitted for clarity.

As was seen in the crystal structure of (**1**) the bond length for the coordination of the iron(III) ion to the deprotonated oxygen atom on the carboxylic acid is shorter than that to the ketone. This is again due to the fact that the deprotonated oxygen atom in the carboxylic acid is a negatively charged donor atom, whilst the ketone oxygen atom is neutral and therefore has a greater affinity to coordinate to the iron(III) hard acceptor ion. In **3i** the Fe2-O14 and Fe2-O11 bonds are 1.968(3) Å and 2.037(3) Å, respectively. The Fe2-O14 bond (1.968(3) Å) is of a similar length to that of Wallis *et al.* for their complex: [Fe(cfH)(nta)]₃·5H₂O which was 1.97 Å¹³. The bond length for the equivalent iron(III) oxygen bond in (**1**) is 1.997(16) Å, which lies between the two values for this bond reported in **3i**.

The Fe2-O13 and Fe2-O16 bonds are also amongst the longest bonds in this molecule with lengths of 1.987(4) Å and 1.964(4) Å, respectively. This suggests that these ligands could be quite weakly bonded, but the important distinction between the molecules in (**3**) and the molecules in (**1**) is that we do not see any substitution of ligands such as a substitution of a sulfate for aquo ligands like we do with the chlorine atom in (**1**).

The nitrogen atoms N3 and N6 are protonated and therefore form a cation due compound formation under acidic conditions in 0.1 M sulfuric acid.

There are π - π stacking interactions between the two ciprofloxacin ligands in **3i**. Figure 33 shows that using calculated centroid atoms, the distances between the C18/C19/C20/N4/C21/C22 and the equivalent C35/C36/N1/C37/C38/C39 aromatic rings is 4.258 Å. The distance between these two rings is longer than that of the equivalent rings in (**1**) (3.850 Å), meaning the π - π stacking interaction is weaker. There is also π - π stacking interactions between the C21/C22/C27/C28/C29/C30 and C37/C38/C47/C46/C45/C44 aromatic rings in the two ciprofloxacin ligands. The distance between to calculated centroids for these rings is 4.250 Å, which is comparable to the afore discussed π - π stacking interaction in **3i** (4.258 Å). The distance of 4.250 Å is significantly shorter than that of the distance between the equivalent ciprofloxacin rings in (**1**), which was 5.209 Å. The shorter distance between the C21/C22/C27/C28/C29/C30 and C37/C38/C47/C46/C45/C44 aromatic rings in **3i** suggests that there is a stronger π - π stacking interaction, which is likely due to the steric effects of the other coordinating ligands meaning that the ciprofloxacin ligands are in closer proximity to interact.

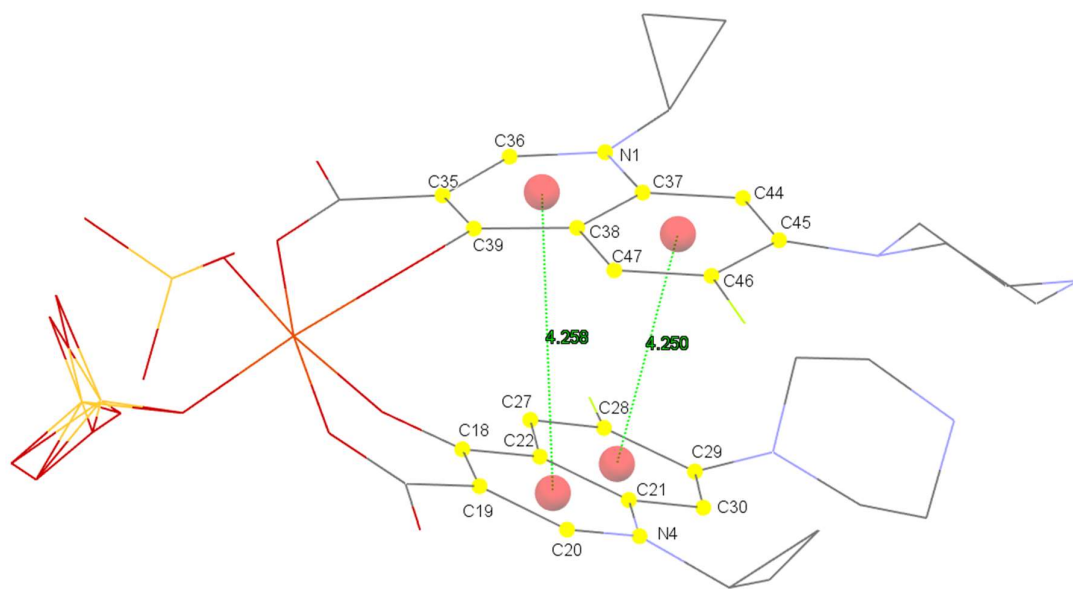


Figure 33: wire frame representation of **3i**, showing the measured distances between calculated centroids in the aromatic rings of the ciprofloxacin ligands. The hydrogen and solvent atoms have been removed for clarity.

In **3ii**, the iron(III) cation also has six coordination sites, however this complex has three aqua ligands, a sulfate ligand and a single bidentate ciprofloxacin ligand, and forms an octahedral complex with distortion.

ligands in **3ii**. The reduced distortion in **3ii** when compared to **3i** and **(1)** highlights the significance of steric factors on the distortion of these complexes.

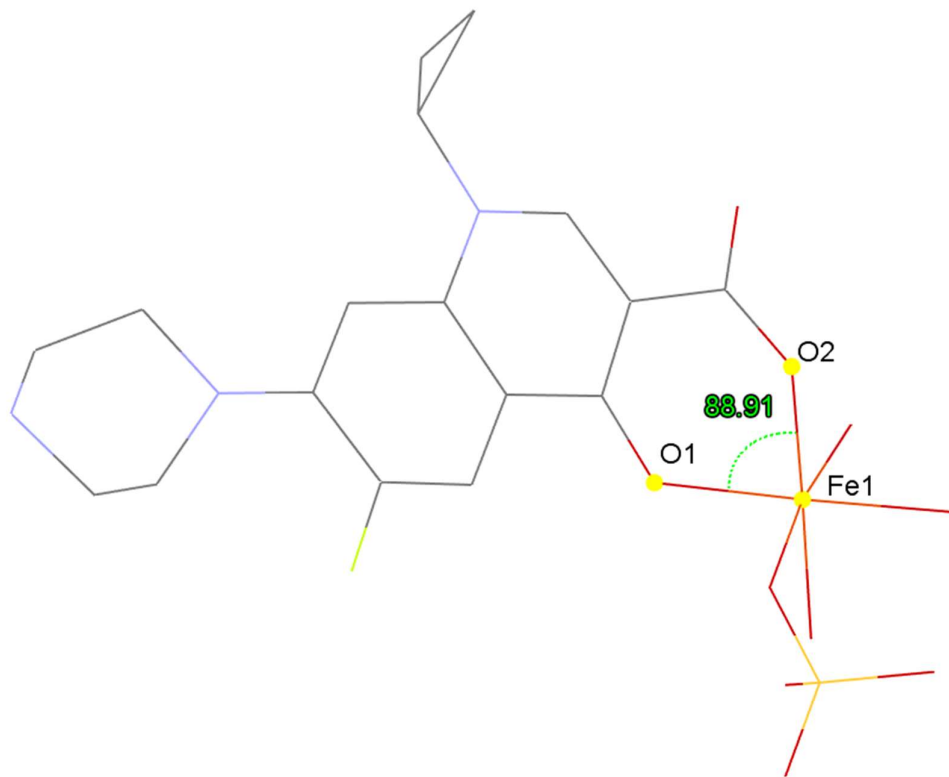


Figure 35: wireframe representation of **3ii** with a measured O-M-O bite angle for the ciprofloxacin ligand. Hydrogen and solvent atoms have been removed for clarity.

The rest of the bond lengths and angles in the ciprofloxacin ligand are consistent with those in the structure of **(2)**.

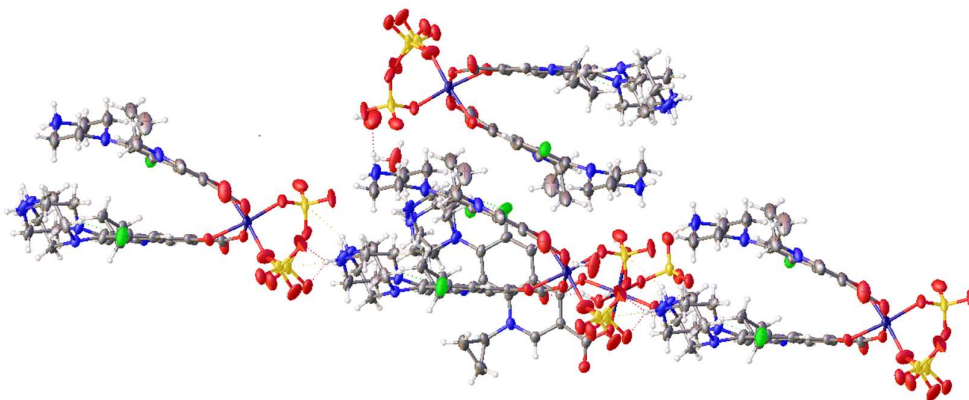
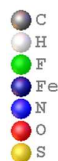


Figure 36: X-ray crystal structure of the 1:1 complex salt of $[\text{Fe}(\text{SO}_4)_2(\text{cfH})_2]^-$ **3i** and $[\text{Fe}(\text{SO}_4)(\text{H}_2\text{O})_3(\text{cfH})]^+$ **3ii**. Ellipsoids plotted at 50 % probability.

Similar to the observations in **(2)**, in **(3)** there are several intermolecular interactions between the complexes **3i** and **3ii** structures. Figure 36 shows the packing and illustrates that the protonated piperazinyl rings in **3i** are interacting with the sulfate groups of the other molecules of **3i** *via* hydrogen bonding.

2.3.3.3 Summary of conclusions from crystallographic information

The X-ray crystallographic structures evidence that two different iron(III)-ciprofloxacin complexes have been synthesised. Across both of the complexes it is evident that the iron(III)-ketone interaction is weaker than the iron(III)-carboxylate interaction, shown by the significantly longer bond lengths between the ciprofloxacin ketone oxygen and the iron(III) ion. Both of the complexes have distorted octahedral geometries, with distortion arising from the steric and electronic effects driven by the ligands. Both complexes also feature π - π stacking interactions between the aromatic groups in the ciprofloxacin ligands. The occasional occupancy of chloro ligands on the Fe(III) ion in the iron(III) chloride-ciprofloxacin complex raises issues in the future applications of this complex as an antimicrobial drug as the complex does not have a uniform structure throughout the crystal structure. However, the iron(III) sulfate-ciprofloxacin complex does appear to have a uniform structure and therefore could be better suited for applications in medicinal chemistry.

2.4 Bismuth-ciprofloxacin complex

Similarly to iron(III), bismuth(III) is a hard metal 3+ ion. Whilst bismuth(III) is not essential for life and has no naturally occurring biological role, it has been administered alongside antibiotics in the treatment of stomach ulcers, although the mechanism of action is largely unknown. Although bismuth can be poisonous, the limited solubility of bismuth salts means that it is possible for them to be administered safely. There were no examples of published X-ray crystal structures of bismuth(III)-ciprofloxacin complexes in a search of the CSD.

The precursor for the bismuth(III)-ciprofloxacin complexes that are described is bismuth oxynitrate. Bismuth oxynitrate is a term used to label a variety of compounds which contain bismuth(III) ions, nitrate ions and oxide ions¹⁰⁶. The synthesis of bismuth oxynitrate was carried out according to a procedure described by B. Lu *et al.*¹⁰⁷. Bismuth oxynitrate exists in a variety of forms. The elemental analysis of the synthesised bismuth oxynitrate compound suggests that there are only trace amounts of hydrogen in the synthesised compound as one run of the sample showed 0 % hydrogen and another measured 0.01 % hydrogen. This suggests that the rest of the compound is made up of bismuth(III), nitrogen and oxygen, which is supported by the absence of carbon in both runs and an average of 3.62 % nitrogen present.

2.4.1 1:4 bismuth(III)-ciprofloxacin

An repeated synthesis of a 1:4 bismuth(III)-ciprofloxacin complex following a procedure reported for the synthesis of a 1:4 bismuth(III)- norfloxacin complex by A. R. Shaikh *et al.*¹⁸, with the structure reported shown in figure 37. The bismuth(III)-norfloxacin complex synthesised by A. R. Shaikh *et al.*¹⁸ was characterised *via* IR which showed characteristic norfloxacin bands as well as Karl-Fischer titration and elemental analysis, which was consistent with a 1:4 bismuth-norfloxacin ratio with two aqua ligands. It is acknowledged here that the structure that has been suggested by A. R. Shaikh *et al.*¹⁸ would also require a counter ion to balance out the charges. Whilst it is not unusual for bismuth(III) to have a high coordination number; the coordination number of bismuth(III) typically ranges between two and nine¹⁰⁸, therefore it is unlikely that all of the suggested bismuth(III)-ligand coordinations would be possible as this would give a coordination number of ten. In the crystal structures of the iron(III)-ciprofloxacin complexes it was found that the metal(III) coordination to the aqua ligands and to the β ketone oxygen atom were the weakest in the complexes and therefore it could be suggested that these coordinations are the most likely to not be present in this compound.

In the repeated synthesis following the procedure reported by A. R. Shaikh *et al.*¹⁸, with ciprofloxacin instead of norfloxacin, X-ray fluorescence (XRF) confirmed the presence of bismuth in the compound and IR confirmed the presence of ciprofloxacin. However, the elemental analysis for this compound was very different from the theoretical calculation. The calculated values for CHN of this reported compound are: C 50.63 %, H 4.78 %, N 11.07 %. However the compound that was synthesised using ciprofloxacin in the procedure outlined A. R. Shaikh *et al.*¹⁸ elemental analysis found: C 35.33 %, H 4.25 %, N 7.10 %, therefore the repeated compound is unlikely to be a 1:4 complex of bismuth(III)-ciprofloxacin.

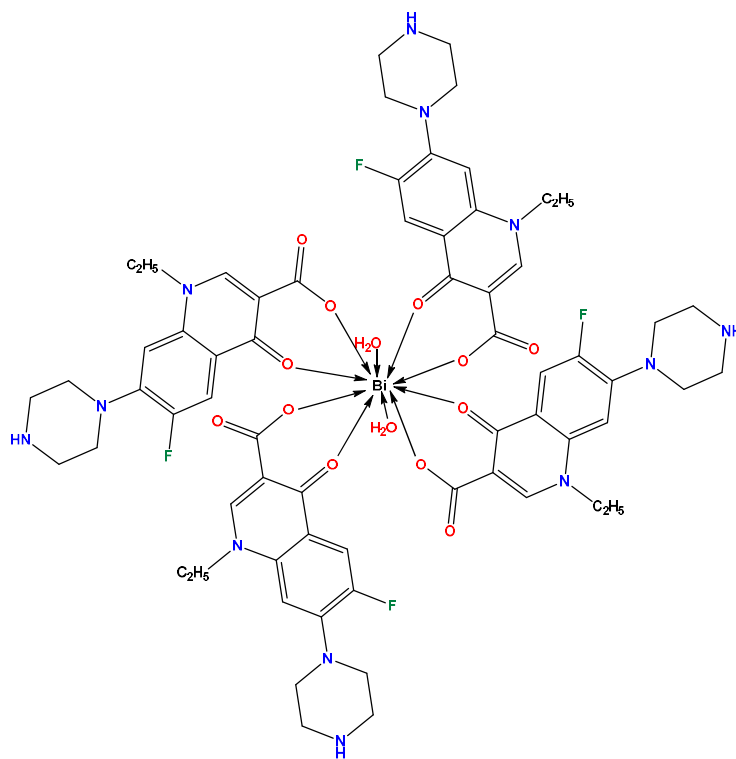


Figure 37: $[\text{Bi}(\text{H}_2\text{O})_2(\text{norfloxacin})_4]$ structure proposed by A. R. Shaikh *et al.*¹⁸, for which an attempt at the synthesis of a bismuth(III)-ciprofloxacin complex was made.

2.4.2 1:3 bismuth(III)-ciprofloxacin

A further attempt at synthesising a bismuth(III)-ciprofloxacin complex was made. The 1:3 bismuth ciprofloxacin complex was synthesised following a procedure from A. R. Shaikh *et al.*¹⁹, in which it is suggested that the structure of this complex is a bismuth(III) ion coordinated to three bidentate ciprofloxacin ligands coordinated through the β ketone and deprotonated carboxylic acid groups, as well as two water ligands, as shown in figure 38. A. R. Shaikh *et al.*¹⁹ characterised the 1:3 bismuth(III)-ciprofloxacin complex using elemental analysis, IR and melting point.

All of the data discussed regarding the repeats of the $[\text{Bi}(\text{H}_2\text{O})_2(\text{cf})_3]$ compound are in triplicate.

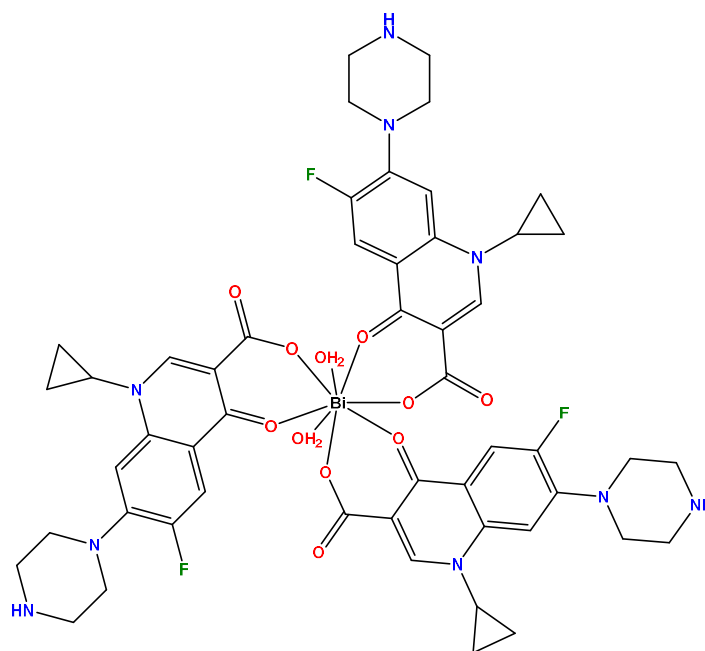


Figure 38: the proposed structure of $[\text{Bi}(\text{H}_2\text{O})_2(\text{cf})_3]$, synthesised by A. R. Shaikh *et al.*¹⁹

In the reported experiment, the melting point for this complex was found to be 322–324 °C, which is in agreement with the value found when repeated; 323–326 °C. The IR for both the reported complex by A. R. Shaikh *et al.*¹⁹ and the repeat that is discussed are in agreement and suggest the presence of ciprofloxacin in the compound as a result of C-F stretching, carbonyl stretching and conjugated alkene stretching peaks. There is also an absence of peaks between 1722–1707 cm^{-1} , which are associated with the carboxylic acid group of uncoordinated ciprofloxacin¹¹⁰. The presence of the water ligands could not be determined in either study as the IR spectra are recorded up to 2000 cm^{-1} and a water O-H stretch would be found at in the frequency range 3700–3100 cm^{-1} . The reported elemental analysis found: C 49.98 %, H 4.99 % and N 10.02 % compared to the calculated values for the formula $[\text{Bi}(\text{H}_2\text{O})_2(\text{cf})_3]$, which were: C 49.56 %, H 4.49 %, N 10.20 %. The repeated synthesis values differ to those found in the synthesis of $[\text{Bi}(\text{H}_2\text{O})_2(\text{cf})_3]$ by A. R. Shaikh *et al.*¹⁹. The CHN results for the repeated synthesis of $[\text{Bi}(\text{H}_2\text{O})_2(\text{cf})_3]$ were found to be: C 48.69%, H 5.64%, N 9.85%. This discrepancy is likely because the repeated sample contained water solvent molecules, which would account for the slightly higher percentage of hydrogen in the repeated synthesis.

Further to the investigation into the structure of the 1:3 bismuth-ciprofloxacin complex by A. R. Shaikh *et al.*¹⁹, in the repeat of their synthesis reported and discussed here, further analysis has been undertaken using NMR and XRF techniques. ¹³C, ¹H and ¹⁹F NMR spectroscopy further confirm the presence of ciprofloxacin in this compound as the spectra recorded for this compound are consistent with that of the free ciprofloxacin ligand. XRF spectroscopy was

employed to confirm the presence of the bismuth ion. Figure 39 shows the results of the XRF analysis, which shows a pattern of peaks which are consistent with the characteristic energy levels in bismuth. The additional peaks that are observed in this spectrum are consistent with that of calcium. The presence of calcium is due to the trace amounts of calcium carbonate on the mounting plate.

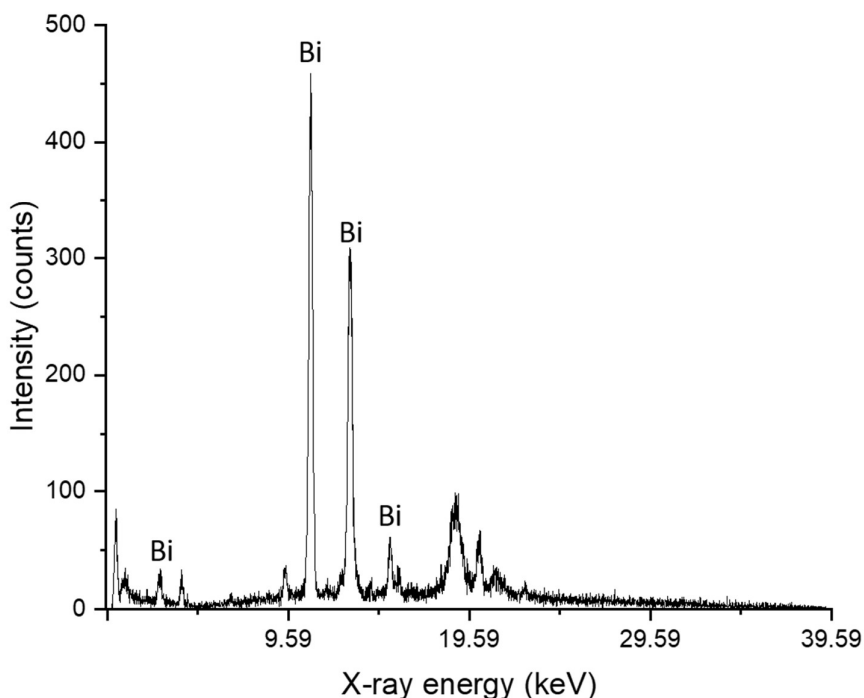


Figure 39: XRF spectrum of the compound $[\text{Bi}(\text{H}_2\text{O})_2(\text{cf})_3]$. This spectrum confirms the presence of bismuth in the product obtained.

Whilst the analysis techniques that have been described can confirm that in this compound there is bismuth and ciprofloxacin present, there is no definitive evidence that the bismuth(III) ions have formed a complex with ciprofloxacin. Without a crystal structure this cannot be confirmed. One of the challenges this compound has presented is its low solubility, because of this, attempts at gaining analysis using mass spectrometry and X-ray crystallography have been unsuccessful.

2.5 Zinc-ciprofloxacin

Zinc is commonly found in biology ¹⁰⁹. Zinc(II) is an intermediate ion in hard-soft acid-base theory, which means that it is not as well suited as a hard metal ion like bismuth(III) or iron(III) to coordination to the hard donor unprotonated oxygen ion in the carboxylic acid group of

ciprofloxacin, however the other coordinating atom in the bidentate ciprofloxacin ligand is the relatively softer oxygen atom in the β ketone, therefore coordination of ciprofloxacin to zinc(II) is still theoretically possible. This is confirmed by the published X-ray crystal structure of a $[\text{Zn}_2(\text{cfH})_2(\text{odpa})]$ complex, which used a 4,4'-oxydiphthalate ligand as well as a ciprofloxacin ligand to form a helical structure ⁷⁹, for which the antimicrobial properties were not tested.

Following the procedure reported by Z. H. Chohan *et al.*¹¹ a zinc(II)-ciprofloxacin complex has been synthesised. The structure of the complex proposed by Z. H. Chohan *et al.*⁴⁰ is of $[\text{Zn}(\text{H}_2\text{O})_2(\text{cf})_2]$, shown in figure 40.

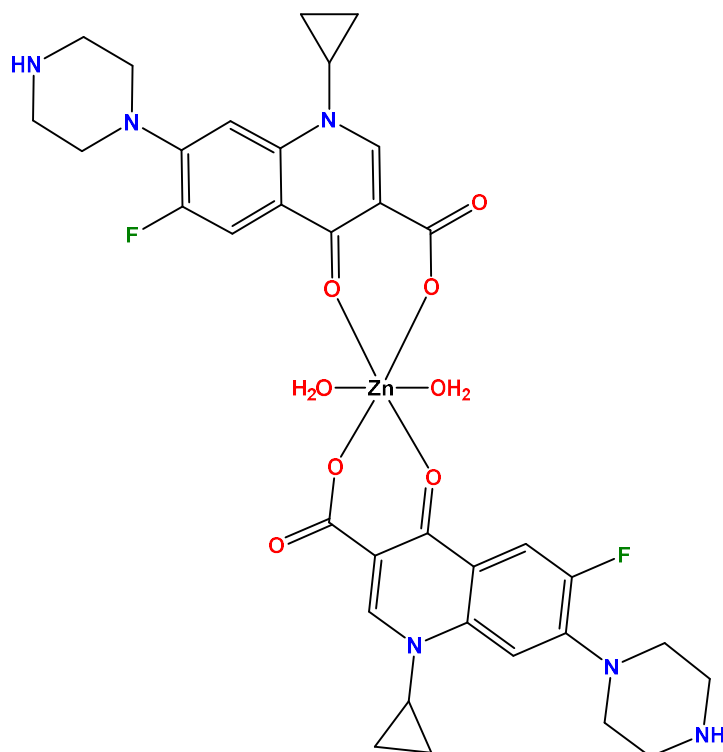


Figure 40: proposed structure of the $[\text{Zn}(\text{H}_2\text{O})_2(\text{cf})_2]$ by Chohan *et al.*⁴⁰.

XRF analysis confirmed that there is zinc present in the compound, the spectrum is shown in figure 41. The labelled peaks in figure 41 are consistent with the characteristic energy levels in zinc, confirming the presence of zinc in the compound. The additional peaks can be attributed

to calcium, from the calcium carbonate present on the mounting plate.

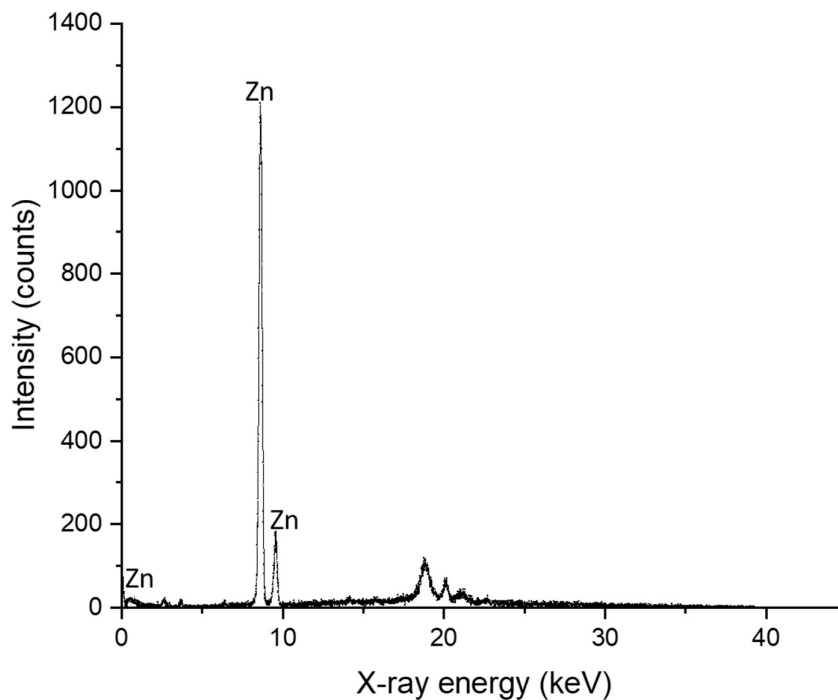


Figure 41: XRF spectrum of the compound synthesised following the procedure reported by Chohan *et al.*⁴⁰

Due to the poor solubility of the complex, solid state NMR (ssNMR) was used to confirm the presence of ciprofloxacin in the complex. Figure 42 shows the proton and carbon decoupled ¹⁹F ssNMR spectrum with a single resonance at -131 ppm showing the presence of a fluorinated compound. The additional peaks observed in the ¹⁹F ssNMR spectrum are spurious signals arising from spinning side bands. Figure 43 shows the proton decoupled ¹³C ssNMR spectrum for the synthesised zinc(II)-ciprofloxacin complex, which shows resonances consistent with ciprofloxacin. Peaks above 180 ppm in the ¹³C ssNMR spectrum for the synthesised zinc(II)-ciprofloxacin complex are spinning side bands.

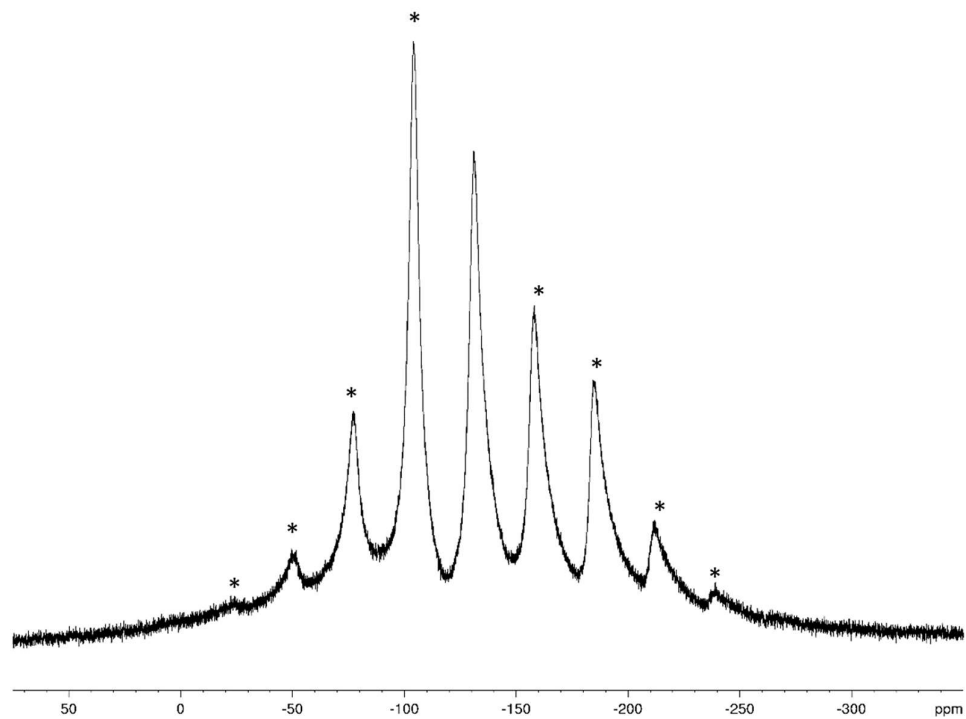


Figure 42: $^{19}\text{F}\{^1\text{H}, ^{13}\text{C}\}$ ssNMR spectrum of the synthesised zinc(II)-ciprofloxacin complex. Asterisks indicate spinning sidebands.

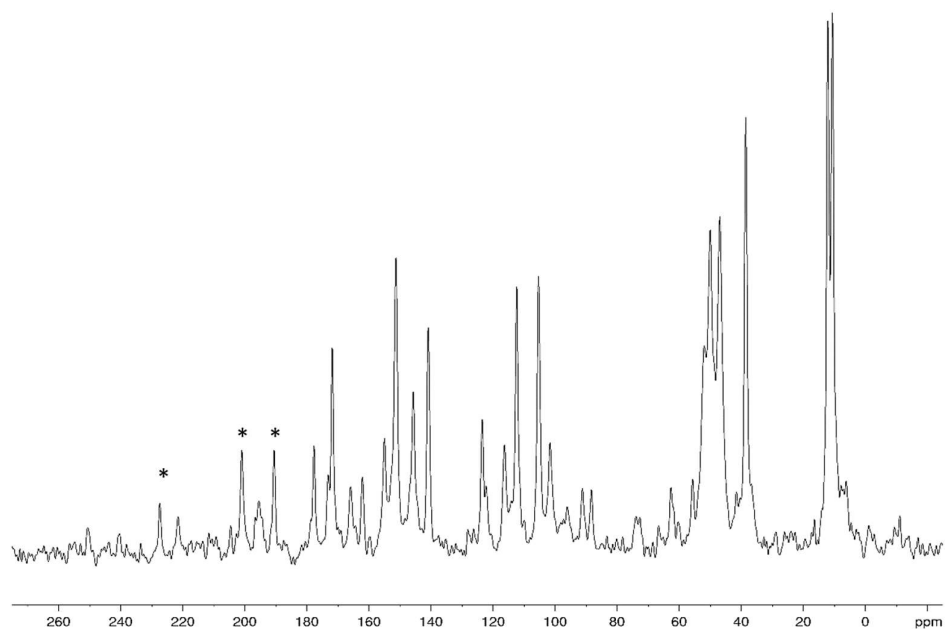


Figure 43: $^{13}\text{C}\{^1\text{H}\}$ ssNMR spectrum of the synthesised zinc(II)-ciprofloxacin complex. Asterisks indicate spinning sidebands.

FTIR confirms the presence of a fluorinated compound, which can only be ciprofloxacin. The FTIR also suggests the coordination of ciprofloxacin to the zinc(II) ion. The characteristic carboxylic acid stretching vibration peaks for uncoordinated ciprofloxacin that are normally found between 1722-1707 cm^{-1} are not observed for this complex and there is an emergence of two peaks; at 1614 and 1379 cm^{-1} which are attributed to the O=C-O asymmetric and symmetric stretching vibrations, respectively¹¹⁰. Furthermore, a peak is observed at 624 cm^{-1} which is typical of an M-O stretching vibration^{111, 112}.

However, the characterisation of the repeat experiment differed significantly from both the reported values and the theoretical values. Both the melting point and the elemental analysis are different to what was expected. The melting point range of the repeated compound is higher than the melting point range of the reported compound (282-284 °C *versus* 218-220 °C⁴⁰ respectively). The elemental analysis also suggests that the repeated synthesis did not yield the expected product. The results of the elemental analysis found: C 47.16 %, H 5.15 % and N 9.54 %. These values are far closer to the calculated values for a structure of the compound shown in figure 44; $[\text{Zn}(\text{H}_2\text{O})_2(\text{cf})(\text{OH})]$. The calculated elemental analysis for $[\text{Zn}(\text{H}_2\text{O})_2(\text{cf})(\text{OH})]$ is: C 45.50 %, H 4.94 % and N 9.36 %.

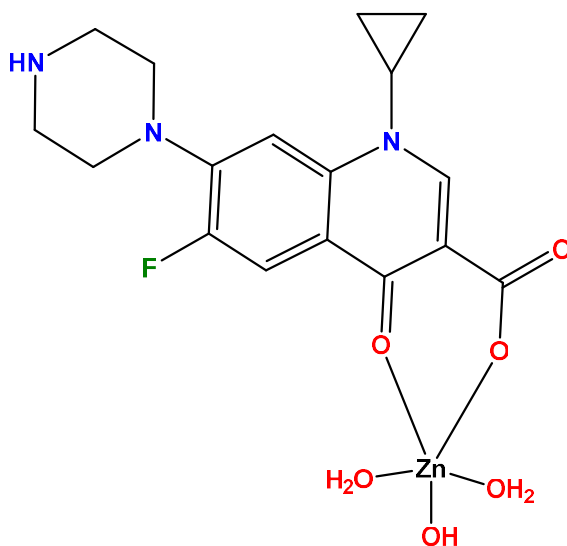


Figure 44: proposed structure of the repeated synthesis of a zinc(II)-ciprofloxacin structure, based on elemental analysis of the compound.

Once again, due to the poor solubility of the compound, attempts at crystallisation have been unsuccessful. Without an X-ray crystal structure, we cannot be certain that the zinc(II) ion is coordinated to the ciprofloxacin ligand, nor how it is coordinated to the ciprofloxacin ligand.

2.2 Other attempts at metallo-FQ complexation

Many other attempts at synthesising metallo-fluoroquinolone complexes were undertaken and are summarised in table 14. The initial efforts to synthesise an iron(III)-ciprofloxacin complex were based on the method described by Saleh MD¹¹³, in which a 1:4 ratio of iron(III) chloride anhydrous and ciprofloxacin were used to create crystals of a 1:2 iron(III)-ciprofloxacin complex. This was unsuccessful in the repeats of this method, but inspired further investigation into the optimisation of the reaction conditions. Experiments with other iron(III) sources found that the iron(III) source has an important role in the formation of the iron(III)-ciprofloxacin complex.

Previous attempts at the complexation of iron(III) and ciprofloxacin had used iron(III) chloride as the iron(III) source, these attempts had been unsuccessful under the same conditions as the successful iron(III) chloride hexahydrate synthesis.

Table 14: summary of unsuccessful attempts at synthesis of metallo-fluoroquinolones.

Reaction M:FQ ratio	Metal source	Fluoroquinolone
1:4	Iron(III) chloride anhydrous	Ciprofloxacin
1:4	Iron(III) acetylacetonate	Ciprofloxacin
1:2, 1:3, 1:4	Iron(III) chloride hexahydrate	Ciprofloxacin
1:1	Iron(III) nitrate nonahydrate	Ciprofloxacin
1:1, 1:2, 1:3, 1:4	Iron(III) chloride hexahydrate	Nalidixic acid
1:1, 1:2, 1:3, 1:4	Gallium(III) nitrate anhydrous	Ciprofloxacin
1:2	Sodium molybdate	Ciprofloxacin
1:2	Sodium tungstate	Ciprofloxacin
1:2	Ammonium vanadate	Ciprofloxacin
1:2	Terbium(III) chloride hexahydrate	Ciprofloxacin

2.3 Conclusions

The complexation of iron(III) and ciprofloxacin is dependent on many factors. Firstly the ratio of iron(III) and ciprofloxacin, the optimum metal-to-ligand ratio at pH 2 is 1:1 however this does not yield a stoichiometric product. The pH plays an important role in the availability of the donor atoms in ciprofloxacin to coordinate to the iron(III) ion, as well as the solubility of the reactants. The literature available on the pKa values of ciprofloxacin species along with an investigation of

the UV/vis absorbance of the reaction solution at different pH values concludes that pH 2 is an ideal pH for complexation. The crystallisation technique is also imperative to the production of good quality crystals for analysis *via* X-ray crystallography, solvent vapor evaporation crystallization was the most favorable technique out of those set up with these reactions. By slowing down the crystallization process, the growth of better quality crystals occurred. Further investigation is required into the gel crystallization technique. Furthermore, the iron(III) source is a critical factor in the iron(III)-ciprofloxacin complexation. Some iron(III) sources did not yield an iron(III)-ciprofloxacin complexes, due to solubility issues or subsequent changes in pH. Iron(III) chloride hexahydrate yielded a 1:2 iron(III)-ciprofloxacin complex, however this complex included chloride anions coordinated to the iron(III) ion, which is not optimal. Iron(III) sulfate as an iron(III) source also yielded iron(III)-ciprofloxacin complexes, including a 1:1 iron(III)-ciprofloxacin complex, which was not observed with the iron(III) chloride hexahydrate iron(III) source. The 1:1 and 1:2 iron(III)-ciprofloxacin sulfate complexes are positively and negatively charged, respectively, meaning that their formation is likely to be codependent.

Other metallo-ciprofloxacin complexes are also feasible, with examples of bismuth(III) and zinc(II) complexes which have been synthesised from literature reported procedures discussed ^{19, 40}.

2.4 Future work

Further investigation into the gel layering crystallisation technique could provide a basis for forming other metallo-fluoroquinolone complexes. Other fluoroquinolones will have their own unique pKa profile and therefore gel layering could be the answer to crystallising the complexes which have so far been unsuccessful attempts. The gel layering crystallisation technique could also yield better quality crystals for more refined structures of the iron(III)-ciprofloxacin complexes.

Crystallisation of zinc(II) and bismuth(III) compounds which have been discussed would allow for a definitive structure of the compounds.

3. Ciprofloxacin Dimers

3.1 Aims and objectives

The overarching aim of this section of work was to synthesise novel dimeric ciprofloxacin compounds with potentially enhanced antimicrobial or anti-tumour properties over ciprofloxacin. This aim is based on literature research into the antimicrobial and anti-tumour properties of fluoroquinolone dimers. The objectives to achieve this aim were to research published examples of fluoroquinolone dimer compounds, to design a synthetic procedure and to characterise the products of the synthesis. The design, synthesis and characterisation of two compounds; an EDTA and a DTPA linked ciprofloxacin dimer was achieved.

3.2 Introduction

The ciprofloxacin dimers that have been synthesised as part of this section of work are comprised of two ciprofloxacin units connected with a linker (figure 45); in this case one used an ethylenediaminetetraacetic acid (EDTA) linker and the other a diethylenetriaminepentaacetic acid (DTPA) linker. The fluoroquinolone dimers were designed to be connected to the linker through the piperazinyl nitrogen. By linking the fluoroquinolones at this position, the ketone and carboxylic acid groups at the other end of the molecule is still able to coordinate to DNA gyrase, a critical part of the fluoroquinolone pharmacophore's antimicrobial mechanism of action. The dimer compound is designed to be able to bridge between the coordination sites in the fluoroquinolone's intracellular target; DNA gyrase, which is a dimer comprised of *gyrA* and *gyrB*⁴⁸⁻⁵¹. By simultaneously targeting both fluoroquinolone target bi sites there could be enhanced antimicrobial effectiveness.

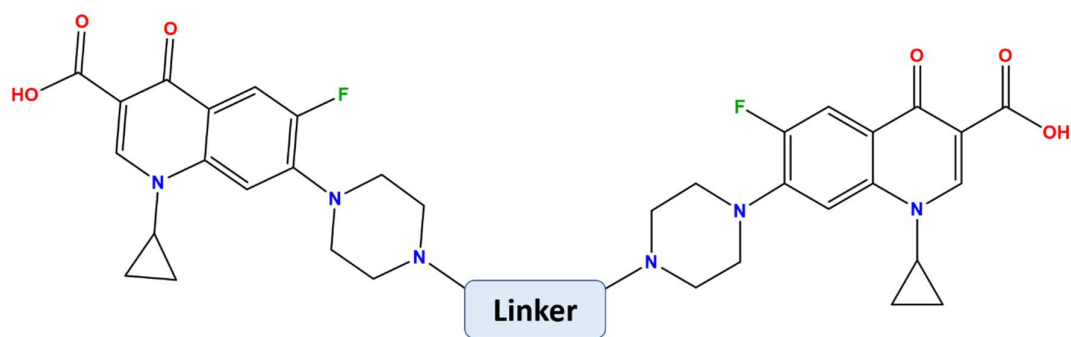


Figure 45: generic structure of dimeric ciprofloxacin compounds comprised of two ciprofloxacin molecules connected by a linker.

Overprescription of fluoroquinolone drugs due to their broad spectrum of antimicrobial activity has resulted in increasing resistance. Bacterial resistance to fluoroquinolones occurs in two

ways; a mutation at the fluoroquinolone binding site in DNA gyrase and mechanisms to reduce accumulation of fluoroquinolones intracellularly¹¹⁴.

Fluoroquinolone resistance arising from mutations in DNA gyrase predominantly occur in the plasmid mediated quinolone resistance (PMQR) gene in *gyrA* in the form of a deletion or insertion mutation at amino acid 83. The mutation in PMQR causes a local conformational change at the 5' terminus in *gyrA* quinolone resistance determining region (QRDR) and as a result a loss of enzyme-fluoroquinolone activity¹¹⁴⁻¹¹⁶. The mutation described in *gyrA* has been shown to give rise to resistance to quinolone drugs but not to unrelated compounds¹¹⁷, therefore making adaptations to ciprofloxacin could overcome resistance occurring through *gyrA* mutations.

Bacterial resistance to fluoroquinolones also occurs through reduced intracellular fluoroquinolone accumulation. Increased active efflux of fluoroquinolone molecules by transmembrane proteins reduces the concentration of fluoroquinolone drugs in bacterial cells. However, even with increased activity of efflux proteins there are still low level concentrations of fluoroquinolone within bacterial cells due to binding to intracellular compounds and pH effects. Only fluoroquinolone zwitterions can be effluxed, but intracellular reactions can yield charged fluoroquinolone molecules in bacterial cells¹¹⁸. Fluoroquinolone dimer compounds possess more electronegative atoms per molecule than a fluoroquinolone molecule and therefore are more likely to form negatively charged ions or coordinate to compounds intracellularly. Therefore a fluoroquinolone dimer complex could accumulate higher intracellular concentrations than traditional fluoroquinolone drug molecules. A further mechanism of reducing intracellular fluoroquinolone accumulation is through the reduced expression of porin proteins. Fluoroquinolone molecules enter bacterial cells *via* passive diffusion through porins. Reduced expression of porins would result in less diffusion of fluoroquinolone drug molecules into bacterial cells¹¹⁴. Whilst porins would also be the primary transport mechanism for fluoroquinolone dimers, one molecule of a fluoroquinolone dimer contains twice the fluoroquinolone pharmacophores as a traditional fluoroquinolone drug and therefore has the potential to have increased antimicrobial properties at lower concentrations than monomeric fluoroquinolone drugs.

Cancer is a multifactorial disease arising from uncontrolled cell growth and is a major public health concern globally¹¹⁹. Because fluoroquinolone drugs target DNA replication enzymes (DNA gyrase) to inhibit cell growth, their anti-tumour properties have been investigated. The intracellular target for fluoroquinolones is type II topoisomerases, both bacterial and human

DNA type II topoisomerases are classified as type II A. In bacteria type II A topoisomerase is DNA gyrase and topoisomerase IV and in humans it is made up of a topoisomerase II α and β dimer¹³² (figure 46).

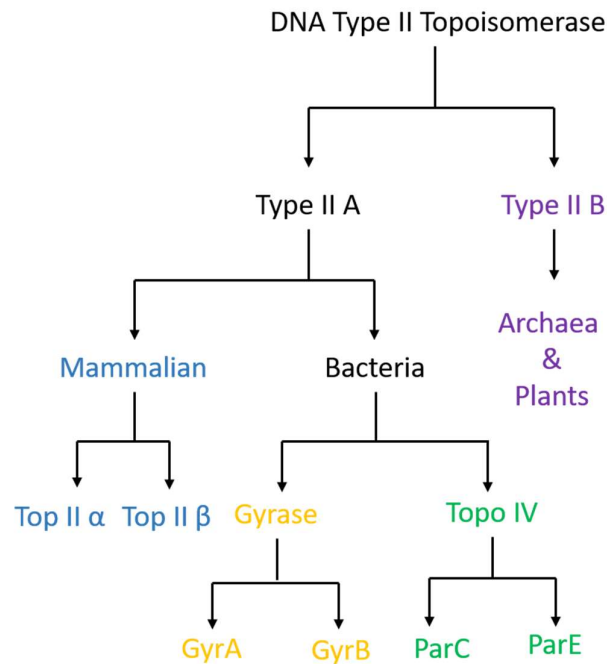


Figure 46: schematic diagram showing the various types of DNA type II topoisomerases¹³².

Mammalian topoisomerase II has similar functions to bacterial topoisomerase II in DNA replication and transcription. Mammalian topoisomerase II is already the intracellular target for the anti-tumour drugs doxorubicin and mitoxantrone, shown in figure 47. Doxorubicin and mitoxantrone are examples of topoisomerase II poisons because they cause damage to the topoisomerase II-DNA complex. Other anti-tumour drugs which target topoisomerase II do so *via* catalytic inhibition¹²¹.

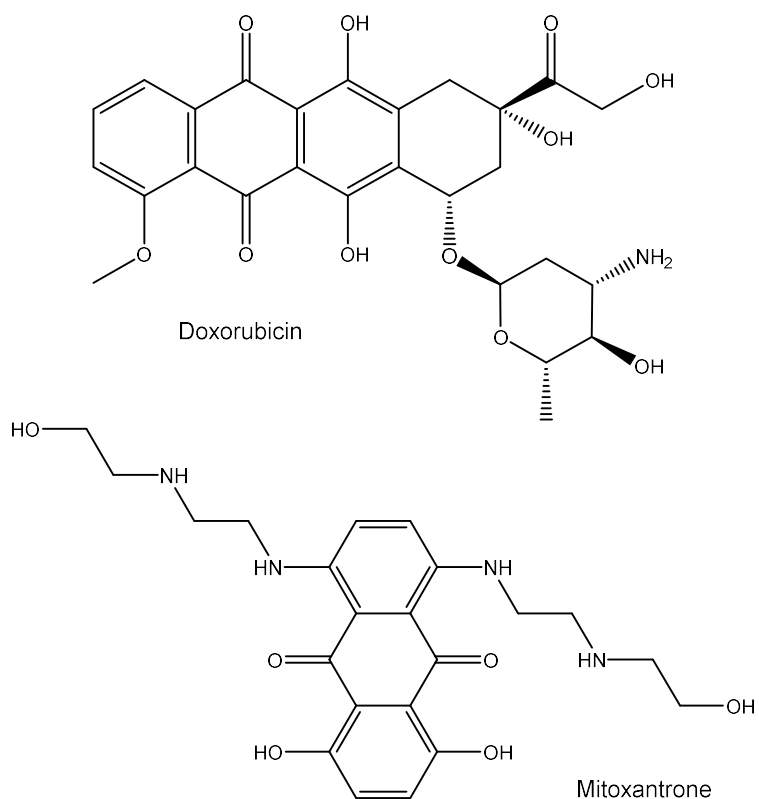


Figure 47: structures of two anti-tumour drugs which target mammalian topoisomerase II. *Top*: doxorubicin. *Bottom*: mitoxantrone.

Ciprofloxacin has demonstrated anti-tumour properties against bladder and prostate cancerous cells^{110, 122,133}. Often, complications arising from cancer treatments are bacterial infections as a result of a weakened immune system; a side-effect of anti-tumour treatments. As such, an antimicrobial anti-tumour drug could be a significant advancement in anti-tumour therapy. Furthermore, fluoroquinolone drugs tend to have significantly milder side-effects relative to current anti-tumour drugs.

Dimer fluoroquinolone complexes with modifications at either the carboxylic or piperazinyl groups may display greater anti-tumour properties as they have reduced zwitterionic character¹²³, which improves the cellular internalisation efficiency by increasing surface-cell interactions¹²⁰. There are a few literature examples of fluoroquinolone dimer compounds which have been shown to have increased anti-tumour activity over the fluoroquinolone monomers, these structures are shown in figure 48⁶².

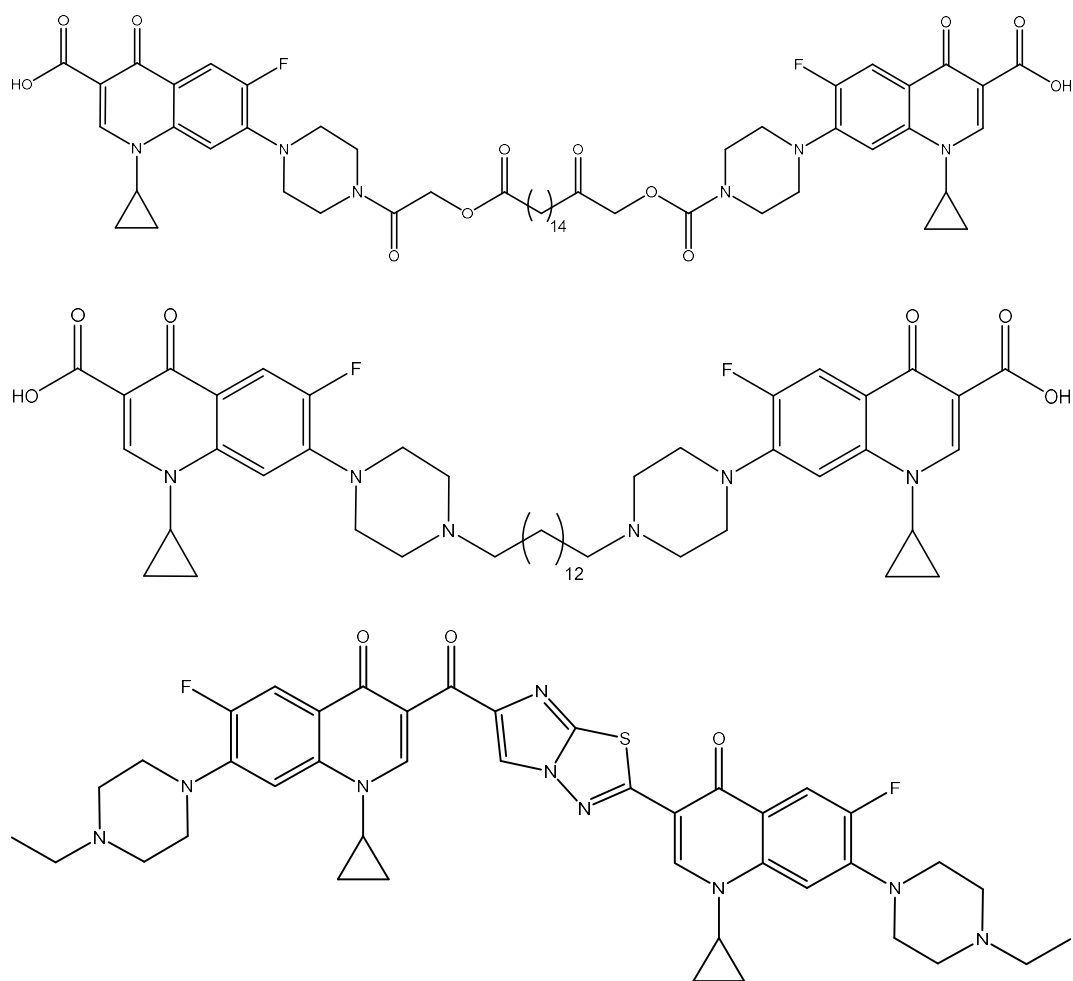


Figure 48: reported structures of fluoroquinolone dimers with increased anti-tumour properties in comparison to their fluoroquinolone monomers. *Top*: ciprofloxacin dimer with $\text{CH}_2\text{OCO}(\text{CH}_2)_{14}\text{COOCH}_2$ linker⁶². *Middle*: ciprofloxacin dimer with $(\text{CH}_2)_{14}$ linker⁶². *Bottom*: modified (ethyl group added to piperazinyl group) ciprofloxacin dimer with linker in the C_3 position⁶³.

A literature search for “fluoroquinolone dimer” using SciFinder¹²⁴ returned 80 published materials. Of these 80 results, it was found that only four of the papers contained structures of fluoroquinolone dimers linked at the R_2 position shown in figure 49. Table 15 summarises the currently published fluoroquinolone dimer molecules and whether they possess antimicrobial or anti-tumour properties.

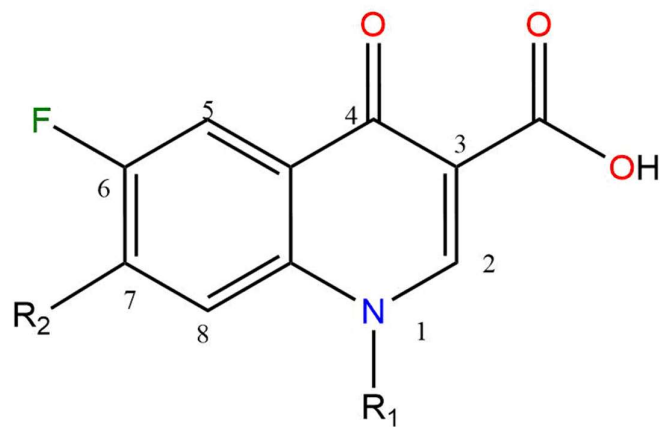


Figure 49: fluoroquinolone pharmacophore, for fluoroquinolone dimer linker position reference.

Table 15: summary of current literature on fluoroquinolone dimer molecules and their antimicrobial/ anti-tumour properties.

Fluoroquinolone	Linker	Antimicrobial	Anti-tumour	Reference
Ciprofloxacin	(CH ₂) ₈	<	<	62
Ciprofloxacin	(CH ₂) ₁₀	=	<	62
Ciprofloxacin	(CH ₂) ₁₂	=	<	62
Ciprofloxacin	(CH ₂) ₁₃	=	<	62
Ciprofloxacin	(CH ₂) ₁₄	<	>	62
Ciprofloxacin	(CH ₂) ₁₆	<	<	62
Ciprofloxacin	CH ₂ OCO(CH ₂) ₈ COOCH ₂	<	<	62
Ciprofloxacin	CH ₂ OCO(CH ₂) ₁₀ COOCH ₂	=	=	62
Ciprofloxacin	CH ₂ OCO(CH ₂) ₁₂ COOCH ₂	=	=	62
Ciprofloxacin	CH ₂ OCO(CH ₂) ₁₃ COOCH ₂	=	=	62
Ciprofloxacin	CH ₂ OCO(CH ₂) ₁₄ COOCH ₂	=	>	62
Ciprofloxacin	CH ₂ OCO(CH ₂) ₁₆ COOCH ₂	<	=	62
Gatifloxacin	CH ₂ CH ₂	NT	NT	125
Ciprofloxacin	CH ₂ CHCHCH ₂	>	NT	54, 56
Ciprofloxacin	<i>m</i> -(CH ₂) ₂ (C ₆ H ₄)	<	NT	54, 56
Ciprofloxacin	<i>p</i> -(CH ₂) ₂ (C ₆ H ₄)	=	NT	54, 56
Ciprofloxacin	CH ₂ (2,6-C ₅ H ₃ N) CH ₂	=	NT	54, 56
Levofloxacin	(CH ₂) ₅	<	<	62
Levofloxacin	(CH ₂) ₆	=	=	62
Levofloxacin	(CH ₂) ₈	=	=	62
Levofloxacin	(CH ₂) ₉	=	=	62
Levofloxacin	(CH ₂) ₁₀	=	=	62
Levofloxacin	(CH ₂) ₁₂	<	<	62
Norfloxacin	CH ₂ CHCHCH ₂	=	NT	54, 56
Norfloxacin	<i>p</i> -(CH ₂) ₂ (C ₆ H ₄)	<	NT	54, 56

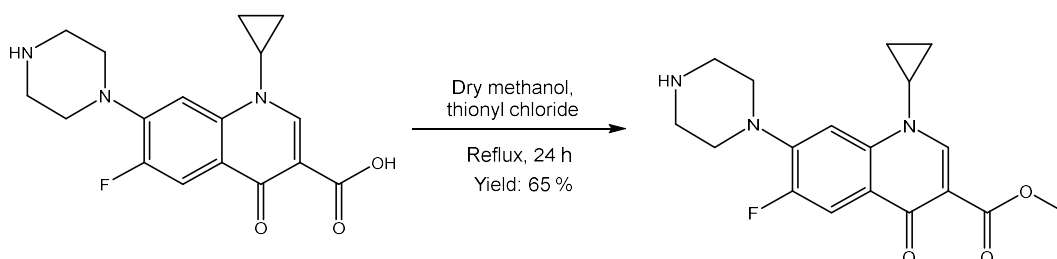
NT: not tested, > : greater activity than fluoroquinolone monomer, = : activity is the same as fluoroquinolone monomer, < : activity is lower than fluoroquinolone monomer, *m*- : meta, *p*- : para.

The results of the literature search highlight that there is potential for further research to be undertaken into fluoroquinolone dimer compounds and their antibiotic/ anti-tumour properties.

3.3 Ciprofloxacin methyl ester

The fluoroquinolone starting reagent for the synthesis of both the EDTA-ciprofloxacin and DTPA-ciprofloxacin dimers is ciprofloxacin methyl ester. Ciprofloxacin methyl ester is used in the dimer synthesis in order to protect the carboxylic acid group in ciprofloxacin, to selectively bond the linker compound to the ciprofloxacin molecules to yield the dimer compound. The synthesis for ciprofloxacin methyl ester was completed according to scheme 1.

Scheme 1



Evidence for the successful synthesis of ciprofloxacin methyl ester is best observed in the ^1H NMR, which shows the addition of a peak associated with the added methyl group in comparison to the ciprofloxacin ^1H NMR spectrum. This is similarly observed in the reported literature synthesis of ciprofloxacin methyl ester, in which the same NMR shifts are reported across ^1H , ^{13}C and ^{19}F NMR. Furthermore, the literature procedure followed reported a positive ESI mass spec peak of m/z 346, which was also observed with this complex and attributed to being $\text{C}_{18}\text{H}_{21}\text{FN}_3\text{O}_3$. The FTIR and melting point values for the synthesised ciprofloxacin methyl ester compound are also consistent with the literature values, meaning that the synthesised compound was suitable to be used as a starting material in the synthesis of ciprofloxacin dimer compounds¹²⁶.

3.4 EDTA-ciprofloxacin dimer

An EDTA linker was chosen as EDTA has been shown to demonstrate broad-spectrum antimicrobial properties and therefore could further enhance the antimicrobial properties of the compound^{127, 128}. EDTA's antimicrobial properties arise from its ability to chelate inorganic components that bacterial cells rely on for survival¹²⁹. EDTA's chelating abilities also present an opportunity to create metallo-dimer complexes, with potentially up to three chelation sites in the dimeric compound, to continue from the research on metallo-fluoroquinolone complexes.

A structure search for the proposed EDTA-linked ciprofloxacin dimer was undertaken using SciFinder¹²⁴, which returned one pre-existing publication of the structure. The single search result was an international patent for “dual-sensitizer-containing luminescent compounds, conjugates, and uses thereof” whereby the EDTA-ciprofloxacin dimer was synthesised by reacting a two fold excess of ciprofloxacin with EDTA, for use as a lanthanide chelating probe for use in biological assays¹³⁰. It is suggested in the afore mentioned patent that solvation of the EDTA-ciprofloxacin dimer in either water or methanol affects the intramolecular interactions of the molecule as shown in figure 50. Nowhere in the patent describe is any mention of potential antibiotic, antimicrobial or anti-tumour properties.

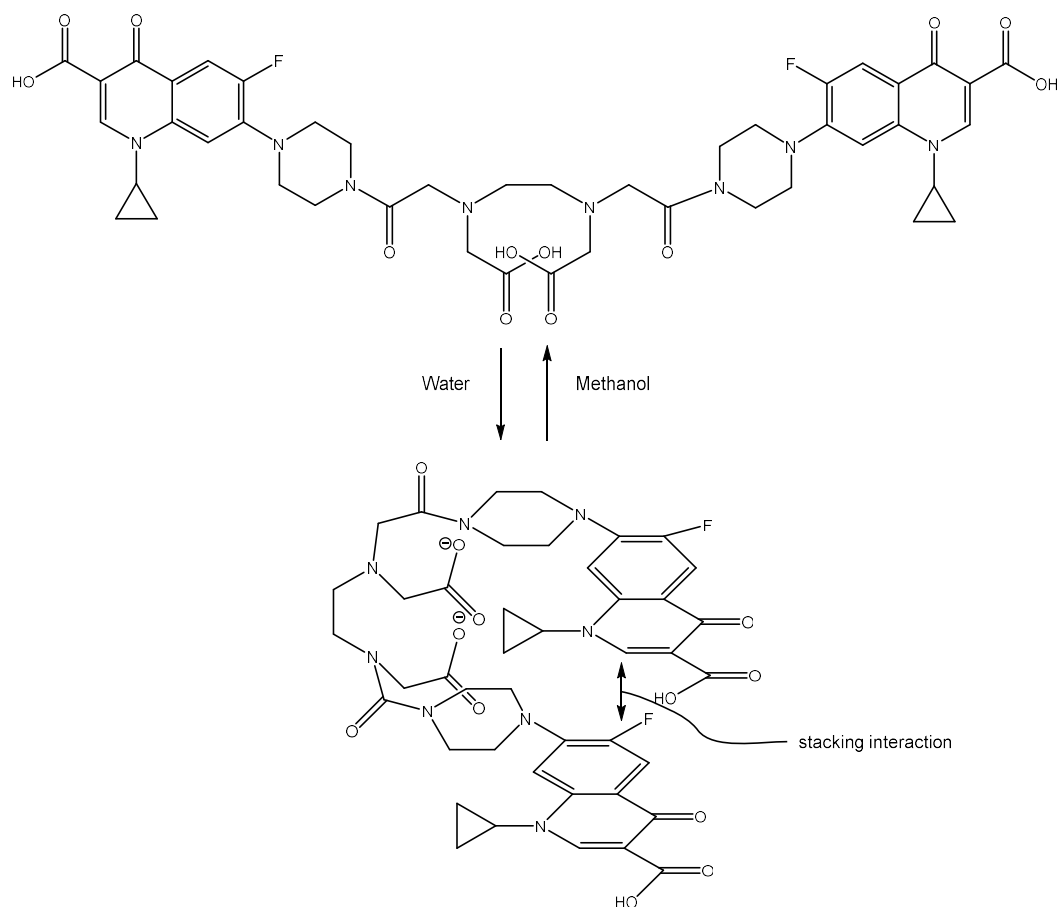


Figure 50: proposed changes in stacking of EDTA-ciprofloxacin molecules as a result of different solvents¹³⁰.

The overall synthetic route taken to form the EDTA-ciprofloxacin dimer is shown in figure 51 and the individual steps are then described in further detail.

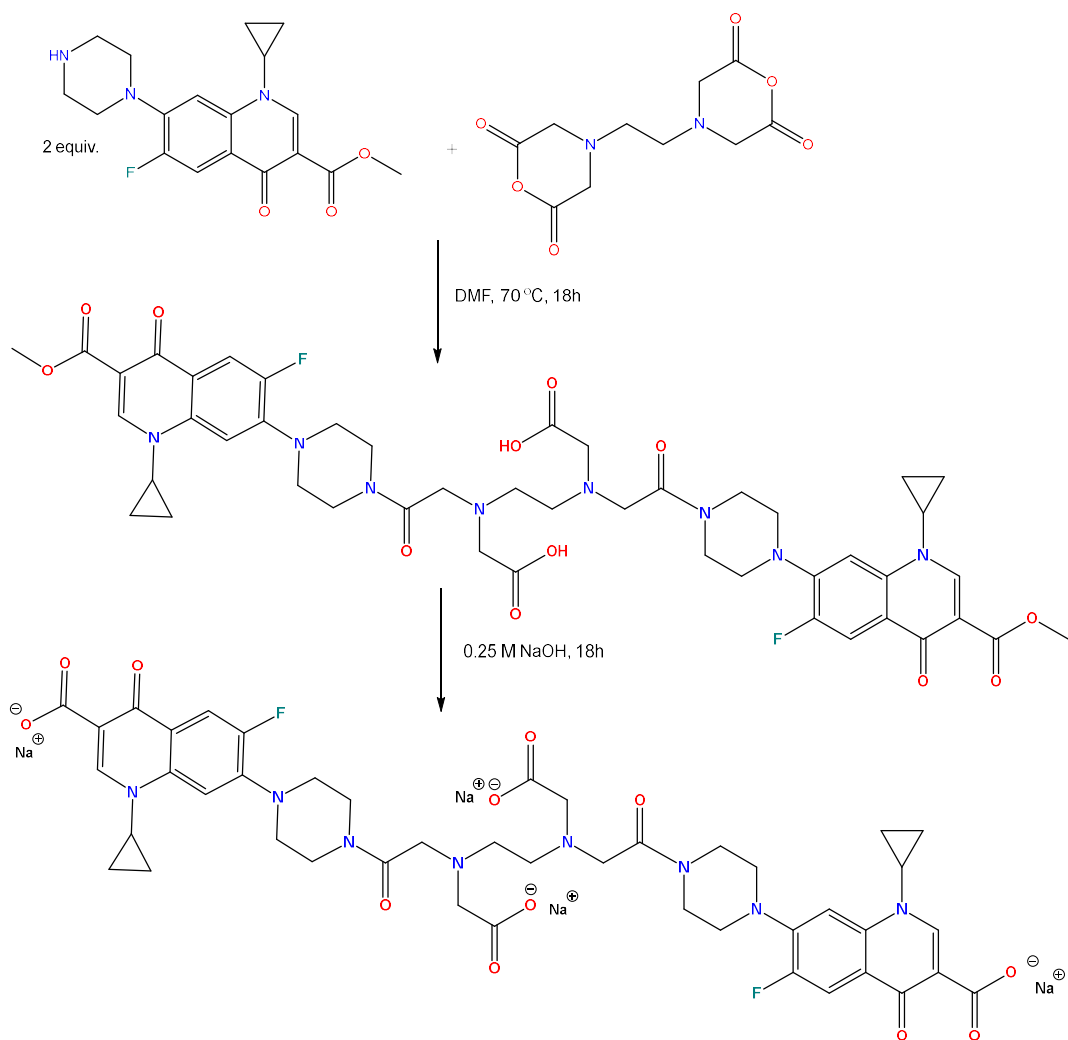


Figure 51: reaction scheme for the synthesis of the ciprofloxacin EDTA dimer sodium salt.

The sodium salt of the product of the synthesis outlined in figure 53 is very hygroscopic, as shown by the water molecules included in the formula determined by elemental analysis ($C_{44}H_{44}F_2N_8O_{12}Na_4 \cdot 7H_2O$). It is unsurprising that the EDTA-ciprofloxacin dimer is hygroscopic given that it contains four carboxylate groups.

In the first stage of the synthesis of the EDTA-ciprofloxacin dimer, ciprofloxacin methyl-ester is reacted with EDTA dianhydride. It is important that it is EDTA dianhydride in order to selectively add the fluoroquinolone to either end of the EDTA molecule. The methyl protecting groups in the EDTA-ciprofloxacin methyl ester compound are then removed using sodium hydroxide, yielding an EDTA-ciprofloxacin methyl ester sodium salt, as summarised in figure 51.

High performance liquid chromatography (HPLC) of the EDTA-ciprofloxacin dimer sodium salt showed significant changes in the retention time in comparison to ciprofloxacin (figure 52). A longer retention time for the EDTA-ciprofloxacin dimer is what would be expected due to the introduction of more polar groups through the addition of the EDTA linker and also because the dimer is a significantly larger molecule than ciprofloxacin.

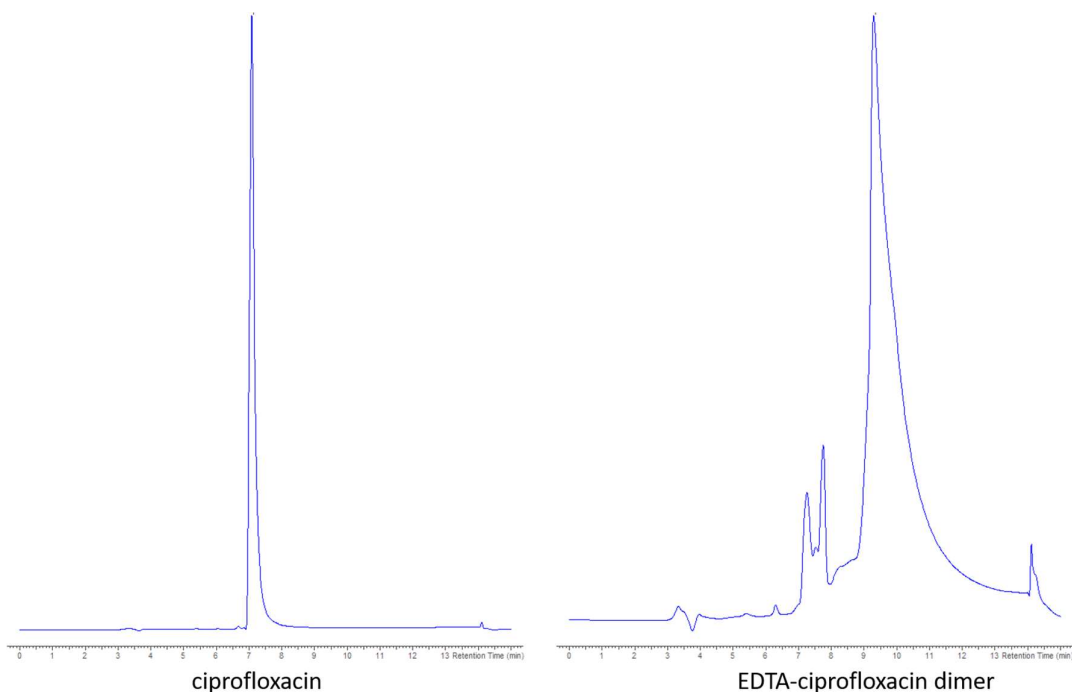


Figure 52: HPLC graphs for ciprofloxacin (*left*) and EDTA-ciprofloxacin dimer (*right*).

The NMR spectra for the EDTA-ciprofloxacin compound indicate that the structure has C_2 symmetry. The symmetry of the EDTA-ciprofloxacin compound is demonstrated by the single peak found in the hydrogen-uncoupled fluorine NMR spectrum, suggesting that the two fluorine atoms found in the proposed structure of the EDTA-ciprofloxacin structure have equivalent chemical environments resulting in a single resonance at -124.23 ppm (figure 53).

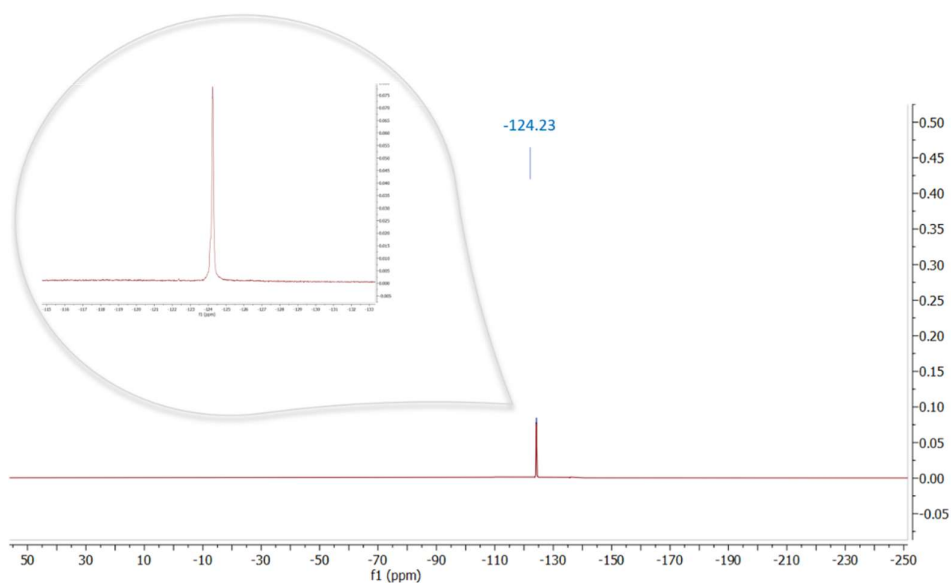


Figure 53: $^{19}\text{F}\{^1\text{H}\}$ NMR of EDTA-ciprofloxacin sodium salt, showing a single peak at -124.23 ppm with the zoomed in image of the peak in the top left.

The single peak in the $^{19}\text{F}\{^1\text{H}\}$ NMR appears at -124.23 ppm which is similar to the chemical shift obtained for the ciprofloxacin methyl ester reagent used (-123.42 ppm), with the slight differences being accounted for by the different solvents used to record the spectra as a result of the different solubilities of the compounds. The spectra $^{19}\text{F}\{^1\text{H}\}$ NMR spectra for the EDTA-ciprofloxacin dimer sodium salt and ciprofloxacin methyl ester are shown in figure 54.

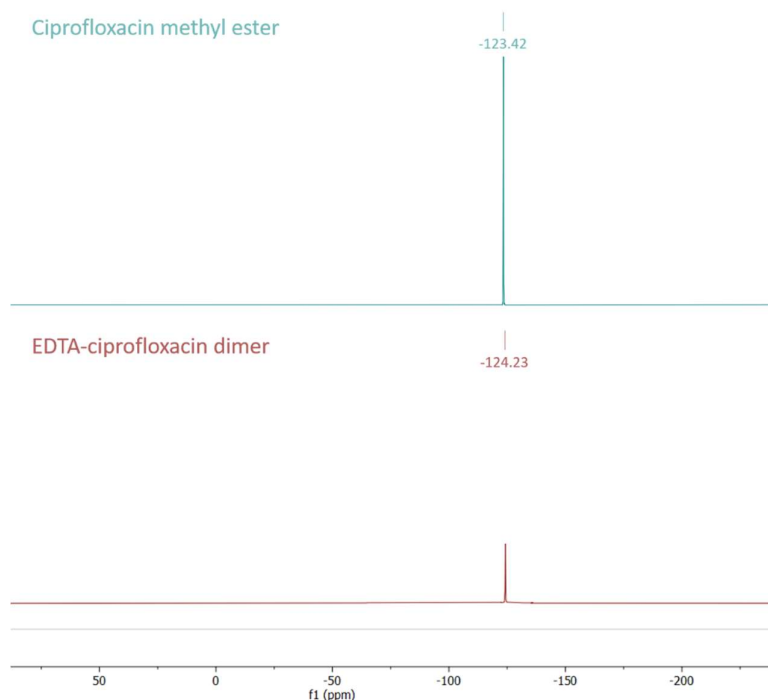


Figure 54: $^{19}\text{F}\{^1\text{H}\}$ NMR spectra for ciprofloxacin methyl ester (*top*) in chloroform- d , and the EDTA-ciprofloxacin dimer sodium salt (*bottom*) in DMSO- d_6 /sodium hydroxide.

Because of the poor solubility of the EDTA-ciprofloxacin dimer compound, the NMR spectra for this compound have been recorded in DMSO- d_6 with dilute sodium hydroxide added. An NMR of sodium hydroxide in DMSO- d_6 is shown in figure 55 in order to confirm that the signal at 2.54 ppm is due to the hydroxide ions in solution.

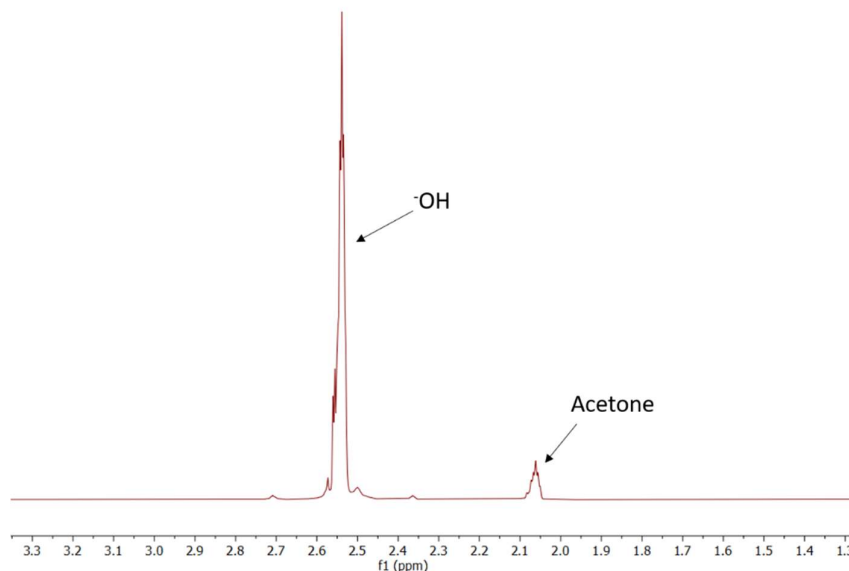


Figure 55: ^1H NMR of sodium hydroxide and acetone in DMSO, with the corresponding peaks labelled.

A ^1H - ^1H correlation spectrum (COSY) was recorded in order to assist in assigning the signals in the ^1H NMR spectrum (figure 60). The chemical shift assignments for the ^1H NMR spectrum and the coupling found in the ^1H - ^1H COSY spectrum for the EDTA-ciprofloxacin dimer sodium salt are summarised in table 19. The COSY confirmed the assignment of the signals at 0.91 and 1.17 ppm being attributable to the 4 cyclopropane protons labelled as 75 and 76 (figure 56) due to the coupling of both of these signals to the signal attributed to the single proton labelled 74 (3.40 ppm) in the cyclopropane ring. However, the COSY did not allow for differentiation between the signals at 0.91 and 1.17 ppm and therefore the protons labelled 75 and 76. The COSY spectrum also confirmed the assignment of the signal at 3.15 ppm to be attributable to the four equivalent protons labelled 78 and 79, and the signal at 3.57 ppm to be attributable to the four equivalent protons labelled 80 and 81. The equivalency of the protons labelled 78/79 and 80/81 shown by the single peaks in the ^1H and COSY NMR spectra further demonstrates the symmetry present

in the EDTA-ciprofloxacin dimer compound. The double doublet attributed to the proton labelled 5 in figure 56 does not show coupling in the COSY spectrum because it is split by fluorine.

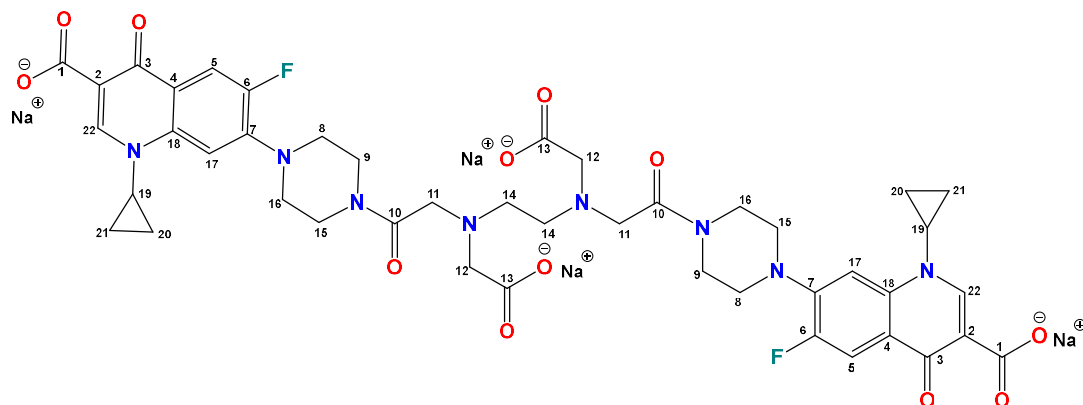


Figure 56: numbered structure of the EDTA-ciprofloxacin dimer sodium salt.

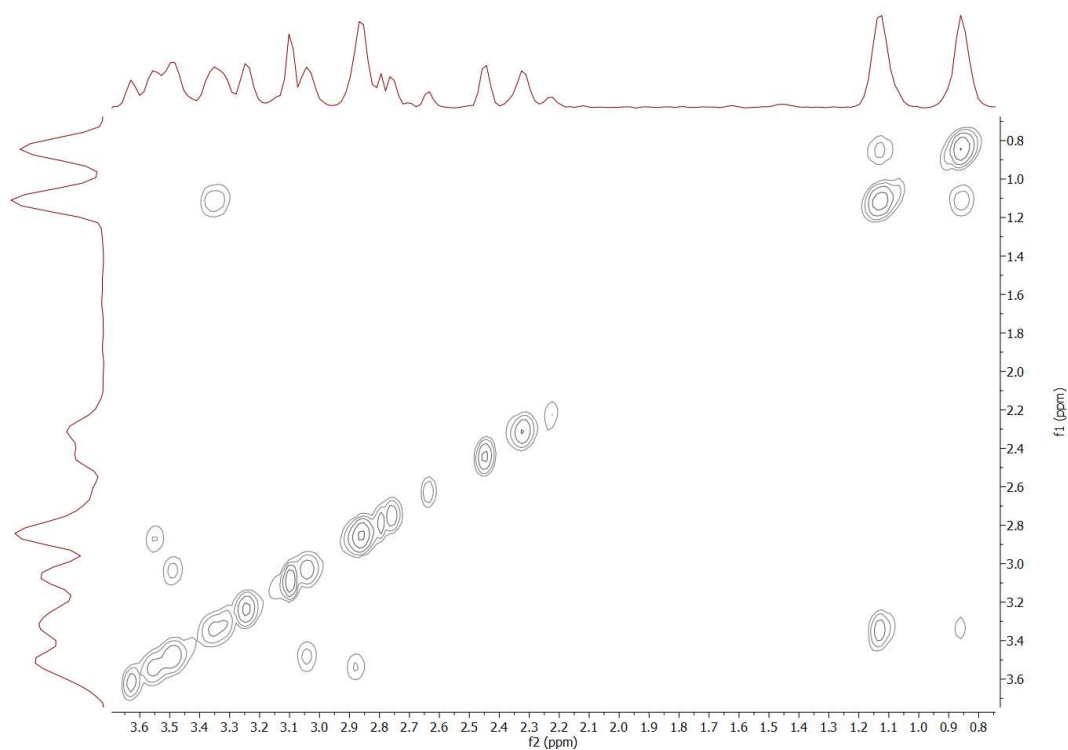


Figure 57: ¹H-¹H COSY spectrum for the EDTA-ciprofloxacin dimer sodium salt in sodium hydroxide and DMSO-*d*₆.

Table 16: summary of the EDTA-ciprofloxacin dimer sodium salt ^1H NMR chemical shifts and associated data (integration and multiplicity) as well as any ^1H - ^1H coupling observed in the COSY NMR spectrum recorded in sodium hydroxide and $\text{DMSO-}d_6$.

Label	^1H Chemical shift / ppm	Integration	Multiplicity	Type	^1H - ^1H coupling / ppm	Coupling constants/ Hz
5	7.59	1	dd	CH	-	$^3J_{\text{H,F}} = 13.3, 2.6$
8	3.57	4	d	CH_2	3.15	$^3J_{\text{H,H}} = 23.1$
9	3.15	4	d	CH_2	3.57	$^3J_{\text{H,H}} = 2.9$
14	2.92	4	s	CH_2	-	-
15	3.15	4	d	CH_2	3.57	$^3J_{\text{H,H}} = 2.9$
16	3.57	4	d	CH_2	3.15	$^3J_{\text{H,H}} = 23.1$
17	7.37-7.19	1	m	CH	-	-
19	3.40	1	m	CH	0.91, 1.17	-
20	0.91, 1.17	2	m	CH_2	0.91, 1.17, 3.40	$^1J_{\text{H,H}} = 6.0$
21	0.91, 1.17	2	m	CH_2	0.91, 1.17, 3.40	$^1J_{\text{H,H}} = 6.0$
22	8.35	1	s	CH	-	-

The EDTA-ciprofloxacin dimer sodium salt was also characterised by its melting point which was found to be 195-196 °C, mass spectrometry and FTIR. ESI negative mode mass spectrometry found two peaks for the EDTA-ciprofloxacin dimer. A peak at m/z 917.3258 is attributed to the protonated compound rather than the sodium salt, and a peak at m/z 939.3080 is attributed to the singly deprotonated sodium salt. The FTIR for the EDTA-ciprofloxacin compound shows the same characteristic peaks as the FTIR of ciprofloxacin.

The EDTA-ciprofloxacin dimer sodium salt has several donor atoms which could in theory coordinate to a metal ion. A Job's plot to analyse the possible coordination of the EDTA-ciprofloxacin dimer sodium salt to iron(III) was attempted, however over a range of molar fractions of the EDTA-ciprofloxacin dimer sodium salt there was no absorbance in the UV spectra that would be consistent with coordination to a metal ion. This problem arose because of the

poor solubility of the EDTA-ciprofloxacin dimer sodium salt- as it has only been found to be soluble in weakly basic conditions it is likely that an iron(III)-hydroxide species formed, the complexation of which outcompeted the formation of an EDTA-ciprofloxacin dimer-iron(III) complex. Further investigation into the coordination of the EDTA-ciprofloxacin dimer sodium salt to metal ions could yield interesting complexes with medicinal and bioinorganic properties.

3.5 DTPA-ciprofloxacin dimer

DTPA is a commercial chelator and as such has demonstrated antimicrobial properties through the chelation of iron, an essential ion for bacteria¹²². A dimer which incorporated DTPA as a linker molecule could therefore have enhanced antimicrobial properties.

A structure search for an EDTA linked ciprofloxacin dimer using SciFinder¹²⁴ found one result; a patent previously discussed in the EDTA-ciprofloxacin dimer section¹³⁰. Similarly to the EDTA-ciprofloxacin dimer, within this patent it suggests that the solvent affects to stacking of the DTPA-ciprofloxacin molecule as summarised in figure 58. The proposed application of the DTPA-ciprofloxacin molecule in this patent is as a lanthanide chelating probe for use in biological assays and indeed the potential antimicrobial, antibacterial or anti-tumour applications have not been suggested within this patent¹³⁰.

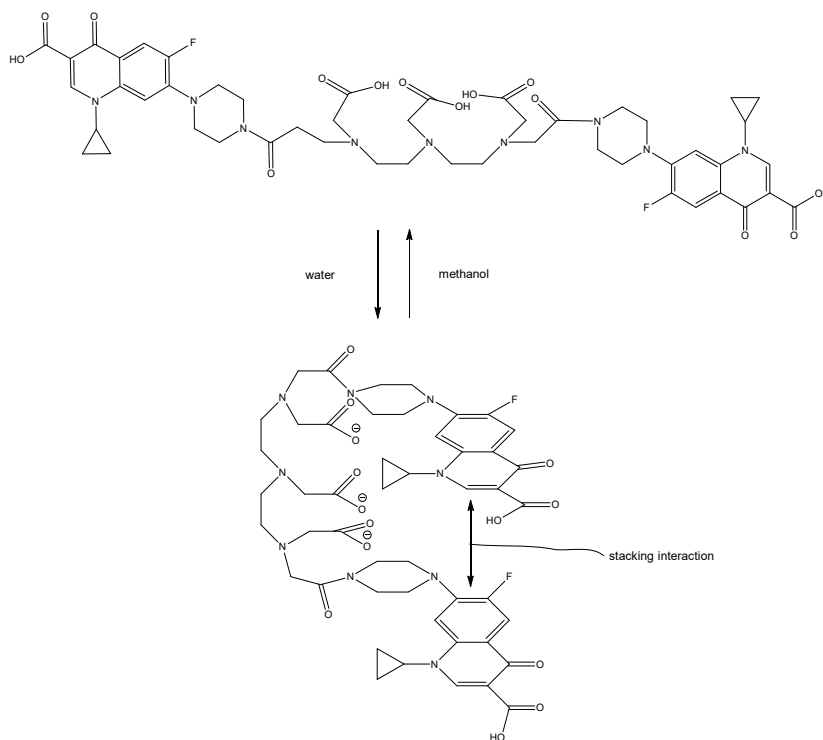


Figure 58: DTPA-ciprofloxacin dimer stacking interaction as a result of different solvents⁸¹.

The synthesis of the DTPA-ciprofloxacin dimer sodium salt is summarised in figure 59. The synthesis of the DTPA-ciprofloxacin methyl ester dimer used ciprofloxacin methyl ester (synthesis summarised in equation 6) and DTPA dianhydride. It is important that the DTPA is the dianhydride in order to yield the desired structural isomer. The DTPA-ciprofloxacin methyl ester dimer was then deprotected using sodium hydroxide in order to yield the DTPA-ciprofloxacin dimer sodium salt.

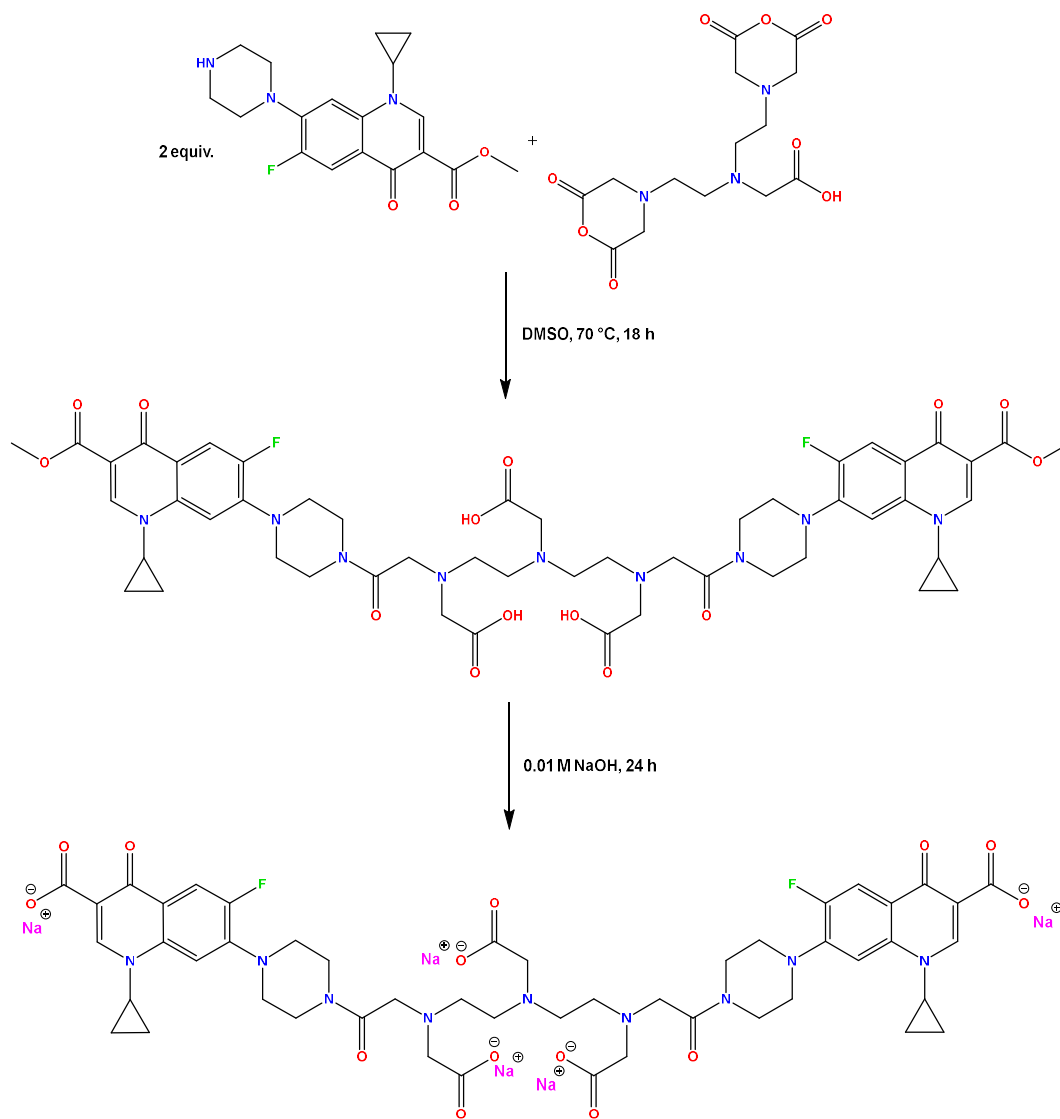


Figure 59: reaction scheme for the synthesis of the ciprofloxacin DTPA dimer sodium salt.

Elemental analysis suggests the formula of the DTPA-ciprofloxacin dimer to be a sodium salt with traces of sodium chloride and water; $C_{48}H_{50}F_2N_9O_{14}Na_5 \cdot 2NaCl \cdot 3H_2O$. The sodium chloride salt impurity arises from the sodium hydroxide added to deprotect the DTPA-ciprofloxacin methyl ester dimer and the hydrochloric acid which was added to adjust the pH. Most of the

sodium chloride salt was removed by washing the precipitate with water, but after three washes there is evidently still sodium chloride present. The water molecules in the product are unsurprising as the DTPA-ciprofloxacin dimer is hygroscopic.

^{19}F NMR spectroscopy indicates that the DTPA-ciprofloxacin dimer sodium salt has C_2 symmetry as observed in the EDTA-ciprofloxacin dimer because there is only a single resonance associated with the two fluorine atoms in the molecule, suggesting that they are in equivalent chemical environments. The $^{19}\text{F}\{^1\text{H}\}$ NMR spectrum of the DTPA-ciprofloxacin dimer sodium salt is shown in figure 60.

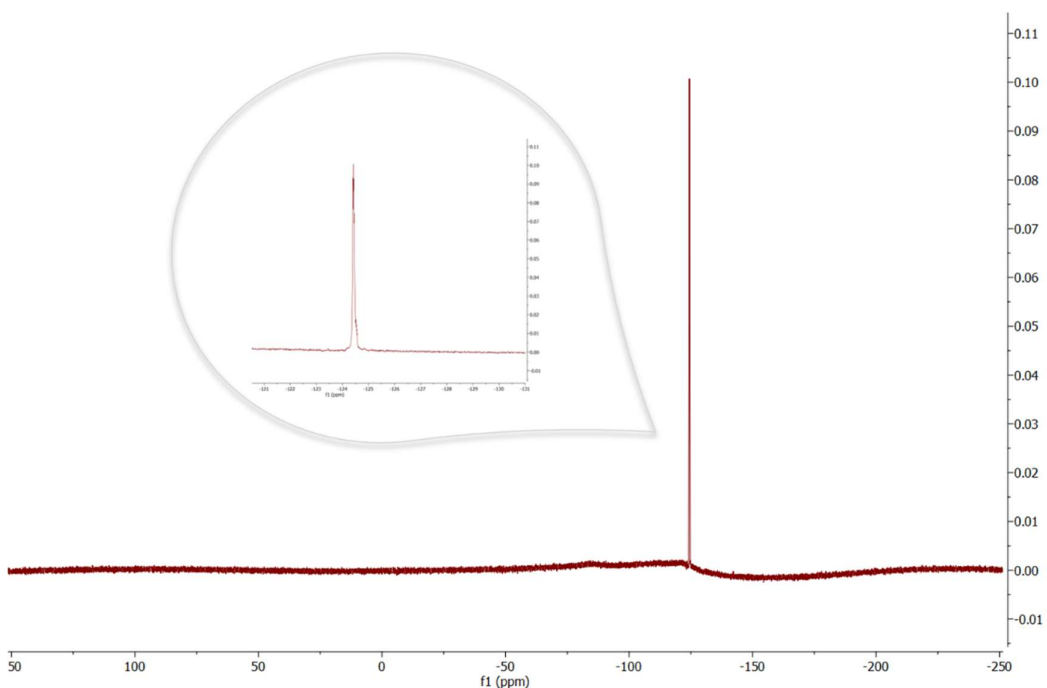


Figure 60: $^{19}\text{F}\{^1\text{H}\}$ NMR spectrum of the DTPA-ciprofloxacin dimer sodium salt with an expanded image showing that there is only a singlet peak.

The $^{19}\text{F}\{^1\text{H}\}$ NMR spectrum of the DTPA-ciprofloxacin dimer sodium salt also shows that the chemical shift of the DTPA-ciprofloxacin dimer sodium salt fluorine atoms is the same as the EDTA-ciprofloxacin dimer sodium salt fluorine atoms (figure 61).

EDTA-ciprofloxacin dimer



DTPA-ciprofloxacin dimer

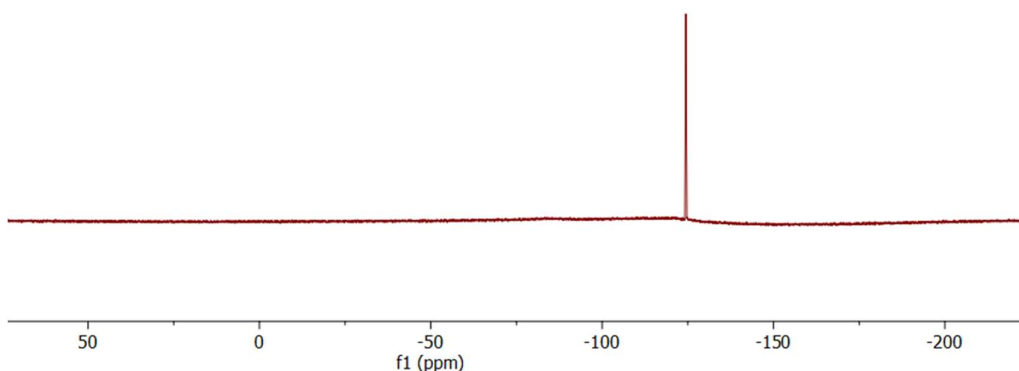


Figure 61: stacked $^{19}\text{F}\{^1\text{H}\}$ NMR spectra of the EDTA-ciprofloxacin dimer sodium salt (*top*) and the DTPA-ciprofloxacin dimer sodium salt (*bottom*) showing that they contain a single peak at -124.23 ppm.

A ^1H - ^1H correlation spectrum (COSY) was recorded in order to assist in assigning the signals in the ^1H NMR spectrum (figure 66). The chemical shift assignments for the ^1H NMR spectrum and the coupling found in the ^1H - ^1H COSY spectrum for the EDTA-ciprofloxacin dimer sodium salt are summarised in table 17.

Using the COSY spectrum, the signals at 2.93 and 3.44 ppm were confirmed to be attributed to the two sets of equivalent protons in the piperazinyl groups labelled 128, 129, 148 and 149 in figure 62. The single resonance assigned to protons 128 and 148 at 2.93 ppm further confirms the symmetry of the DTPA-ciprofloxacin dimer molecule, similarly with the single resonance at 3.44 ppm which is attributed to the equivalent protons labelled 129 and 149. The COSY spectrum further confirms the assignment of the peaks at 2.93 and 3.44 ppm to be the piperazinyl protons as these signals couple to one another. The COSY confirmed the assignment of the signals at 1.09 and 1.14 ppm being attributable to the 4 cyclopropane protons labelled as 144 and 145 due to the coupling of both of these signals to the signal attributed to the single proton labelled 143

(3.73 ppm) in the cyclopropane ring. However, the COSY did not allow for differentiation between the signals at 1.09 and 1.14 ppm and the protons labelled 144 and 145.

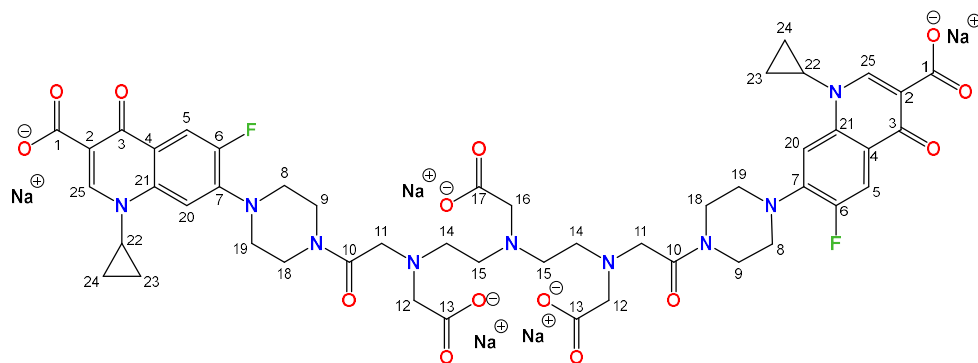


Figure 62: numbered structure of the DTPA-ciprofloxacin dimer sodium salt.

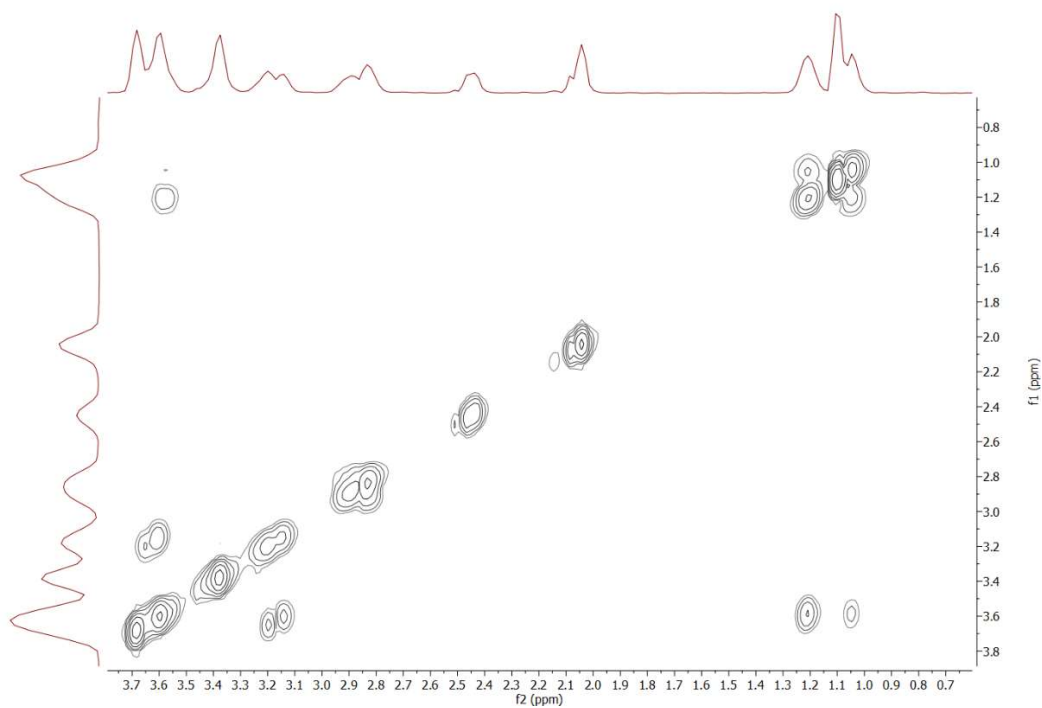


Figure 63: COSY spectrum of the DTPA-ciprofloxacin dimer sodium salt in DMSO- d_6 and sodium hydroxide.

Table 17: summary of the DTPA-ciprofloxacin dimer sodium salt ^1H NMR chemical shifts and associated data (integration and multiplicity) as well as any ^1H - ^1H coupling observed in the COSY NMR spectrum recorded in $\text{DMSO-}d_6$ and sodium hydroxide.

Label	^1H Chemical shift/ ppm	Integration	Multiplicity	Type	^1H - ^1H coupling / ppm	Coupling constants/ Hz
8	2.94	4	d	CH_2	3.44	$^3J_{\text{H,H}} = 8.1$
9	3.45	4	dd	CH_2	2.94, 3.65	$^3J_{\text{H,H}} = 14.7,$ 6.8
11	3.65	2	d	CH_2	3.45	$^3J_{\text{H,H}} = 5.1$
12	2.10	2	s	CH_2	-	-
14	2.86	2	s	CH_2	-	-
18	3.45	4	dd	CH_2	2.94, 3.65	$^3J_{\text{H,H}} = 14.7,$ 6.8
19	2.94	4	d	CH_2	3.45	$^3J_{\text{H,H}} = 8.1$
22	3.72	1	m	CH	1.10, 1.27	$^3J_{\text{H,H}} = 3.6$
23	1.10, 1.27	2	m	CH_2	1.10, 1.27, 3.72	-
24	1.10, 1.27	2	m	CH_2	1.10, 1.27, 3.72	-
25	7.81-7.69	1	m	CH	-	-

The melting point for the DTPA-ciprofloxacin dimer sodium salt (205-206 °C) is higher than the melting point for the EDTA-ciprofloxacin dimer sodium salt (195-196 °C), which is what would

be expected because of the additional acid groups in the DTPA linker compared to the EDTA linker, which means that there are more electronegative atoms capable of intermolecular interactions. Additionally, the DTPA-ciprofloxacin dimer is larger in general than the EDTA-ciprofloxacin dimer, again meaning that there are more intermolecular interactions in the DTPA-dimer than the EDTA-dimer and thus the DTPA-dimer has a higher melting point.

Attempts at gaining mass spectrometry data for the DTPA-ciprofloxacin dimer were unsuccessful because of the poor solubility of the DTPA-ciprofloxacin dimer. However, negative ESI mass spectrometry of the DTPA-ciprofloxacin methyl ester dimer which is much more soluble found a peak at m/z 1046.4034 in methanol, which corresponds to $C_{50}H_{58}F_2N_9O_{14}$ (m/z 1046.4077, 0.7 ppm error).

The FTIR spectrum for the DTPA-ciprofloxacin dimer sodium salt is consistent with what would be expected of a ciprofloxacin containing compound, with many of the peaks being attributable to both ciprofloxacin and the DTPA linker, such as the C-H stretching at 2982 cm^{-1} , C=O stretching at 1709 cm^{-1} and the O-H bending at 1408 cm^{-1} from a carboxylic acid group. The presence of the O-H bending peak also signifies that some of the molecules in the compound contain carboxylic acid groups rather than the salt forming carboxylate groups.

The characterisation data presented shows that a DTPA-ciprofloxacin dimer has been synthesised. The synthesis of a DTPA-linked ciprofloxacin dimer provides a foundation for further research into the biological applications, such as for antimicrobial or anti-tumour agents, of linked ciprofloxacin dimers.

3.6 Conclusions

Two dimeric ciprofloxacin molecules have been designed, synthesised and characterised. The synthetic routes to form both an EDTA and a DTPA linked ciprofloxacin dimer have been outlined. Techniques used to characterise the EDTA and DTPA-ciprofloxacin dimers include melting point, FTIR, ^1H NMR, ^{13}C NMR, ^{19}F NMR, ^1H - ^1H COSY NMR, HPLC and mass spectrometry. Characterisation of both the EDTA and DTPA ciprofloxacin dimers show that both are hygroscopic and should be handled/ stored as such. Furthermore, based on fluorine NMR spectroscopic investigations it has been demonstrated that both the EDTA and DTPA ciprofloxacin dimers exhibit C_2 symmetry. Further investigation into the applications of both the synthetic routes to form a ciprofloxacin dimer and the properties of the ciprofloxacin dimers yielded is required.

3.7 Future Work

Now that there is a synthetic route to create EDTA and DTPA linked ciprofloxacin dimers, these compounds should have their antimicrobial and anti-tumour activities examined in order to determine the applications of these compounds in medicines and bioinorganic chemistry.

Furthermore, the synthesise outlined could be applied to create other dimeric fluoroquinolone compounds, both with different fluoroquinolone and with linker molecules.

Further investigation into the coordination of the described ciprofloxacin dimer complexes to metal ions should be undertaken. In order to do this, the solubility issues of the dimeric compounds have to be addressed. Coordination of the dimeric ciprofloxacin compounds could further enhance their antimicrobial properties based on the same reasoning as metallo-ciprofloxacin complexes.

Beyond the scope of this project, the development of a synthesis for asymmetric fluoroquinolone dimers could have further increased antimicrobial and/or anti-tumour activity over the respective fluoroquinolone compounds⁵⁶. If there is resistance to one of the fluoroquinolone pharmacophores in the molecule the compound may still show antimicrobial/anti-tumour activity through the other fluoroquinolone pharmacophore which the target cells may not be resistant to.

4. Overall summary, conclusions and future work

There is a need for innovation to produce new antimicrobial agents in order to combat the rise in antimicrobial resistance. Ciprofloxacin is a frequently prescribed fluoroquinolone antibiotic drug, however, increasing antimicrobial resistance is compromising its efficacy. Presented is an investigation into two approaches to modify the structure of ciprofloxacin in order to promote its antimicrobial activity. The two approaches presented are the formation of metallo-ciprofloxacin complexes and the synthesis of linked dimeric ciprofloxacin molecules.

4.1 Metallo-ciprofloxacin complexes

Coordination of ciprofloxacin to metal ions may enhance the antimicrobial properties of ciprofloxacin through the additional biological effects of the metal ions whether that be *in vivo* transportation for biologically available metal ions or antimicrobial properties. There are literature examples of metallo-fluoroquinolone complexes which have had increased antimicrobial properties over the respective fluoroquinolone on its own.

Preliminary experiments investigated the pH dependence of the complexation of iron(III) and found that pH 2 is a preferential to pH 3 and that a iron(III)-to-ciprofloxacin ratio of 1:1 is optimum for iron(III)-ciprofloxacin complexation. Various crystallisation techniques were used, with the most successful being vapour diffusion. Presented are three novel fluoroquinolone complexes: a 1:2 iron(III)-ciprofloxacin complex, a 1:1 and 1:2 iron(III)-ciprofloxacin salt and a 1:1 zinc(II)-ciprofloxacin complex. These complexes have been characterised using a range of techniques including X-ray crystallography, XRF, FTIR, melting point and elemental analysis.

The antimicrobial properties of both the iron(III)-ciprofloxacin complexes as well as the zinc(II) and bismuth(III)-ciprofloxacin complexes should be investigated in order to evaluate their effectiveness as antimicrobial agents. To gain further structural information for the zinc(II) and bismuth(III) complexes that have been synthesised, good quality crystals should be grown in order to obtain crystallographic information. Furthermore, gel crystallisation techniques could lead to better crystals of metallo-fluoroquinolone complexes. Future work into metallo-fluoroquinolone complexes should employ similar preliminary experiments in order to determine reaction conditions such as the ratio and pH required to form other metallo-ciprofloxacin complexes.

4.2 Linked dimeric ciprofloxacin compounds

The fluoroquinolone intracellular target molecule; DNA gyrase, exists as a dimer. A linked fluoroquinolone dimer drug could bridge between the two binding sites in DNA gyrase. The few literature examples which are discussed suggest that dimeric fluoroquinolone compounds could have enhanced antimicrobial properties and may even possess anti-tumour properties.

As part of the research that has been presented, two linked ciprofloxacin dimers have been synthesised; an EDTA-ciprofloxacin dimer and a DTPA-ciprofloxacin dimer. The EDTA and DTPA linkers were chosen because they have been found to possess antimicrobial properties on their own due to their ability to chelate iron(III), an essential ion for bacteria. The synthetic route to form both the EDTA- and DTPA-ciprofloxacin dimers have been summarised as well as the characterisations for each compound. The dimer compounds which have been synthesised have been characterised using NMR, mass spectrometry, elemental analysis, HPLC, FTIR and melting point. The elemental analysis found that both the EDTA and DTPA-ciprofloxacin dimers were isolated as sodium salts. NMR spectroscopy confirmed that both the compounds have C_2 symmetry.

The next steps in researching linked ciprofloxacin compounds should be to test the antimicrobial and anti-tumour properties of the EDTA and DTPA-ciprofloxacin dimer sodium salt compounds, now that these compounds have been isolated and characterised. An investigation into the biological properties of asymmetric linked fluoroquinolone dimer compounds could find further improved antimicrobial or anti-tumour properties because if resistance occurs against one of the fluoroquinolone pharmacophores in the compound, the other fluoroquinolone in the compound could still be effective.

5. Experimental

5.1 General Remarks

5.1.1 Materials

All chemicals were obtained from commercial suppliers: Alfa Aesar, Acros, Merck and Sigma Aldrich.

5.1.2 Instruments

^1H , ^{13}C and COSY NMR spectra recorded on a Jeol ECS 400 at 400 MHz for ^1H and 100 MHz for ^{13}C at ambient temperature, unless otherwise stated. ^{13}C and ^{19}F solid state NMR spectra recorded on a Bruker AVIIIHD 400 MHz at ambient temperature by Mr. C. Goult. NMR data is reported as following: chemical shift (multiplicity, coupling constants, assignment, number of protons). Chemical shifts are reported relative to residual solvent peaks to the nearest 0.01 ppm for ^1H spectra and 0.1 ppm for ^{13}C spectra. Multiplicity is reported as s=singlet, d=doublet, t=triplet, q=quartet, m=multiplet, br=broad. Coupling constants (J) are given in Hz and quoted to the nearest 0.5 Hz. All NMR spectra have been processed using MestReNova analysis software.

High resolution ESI mass spectra were recorded on a Bruker microTOF electrospray mass spectrometer by Mr. K. Heaton.

Thin layer chromatography (TLC) used Merck silica gel 60 F253 aluminium-backed plates using specified solvent systems and visualised under an ultraviolet lamp.

X-ray crystals structures were obtained from an Oxford Diffraction SuperNova equipped with a 4-circle goniometer and dual copper and molybdenum micro-focus X-ray sources, samples were run by Dr Adrian Whitwood and images viewed on Crystal Maker software.

pH values were measured using a Mettler Toledo InLab pH electrode at ambient temperature, unless otherwise stated.

Fourier transform infrared (FT-IR) spectroscopy was obtained on a PerkinElmer Spectrum Two FT-IR spectrometer. Spectra are reported as: absorption cm^{-1} (appearance, group, compound class). Appearance is reported as: s=strong, m=medium, w=weak, br=broad.

Melting points were measured using Stuart Scientific Melting Point Apparatus SMP3.

5.2 Methods

5.2.1 Job's Plot

pH 2

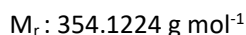
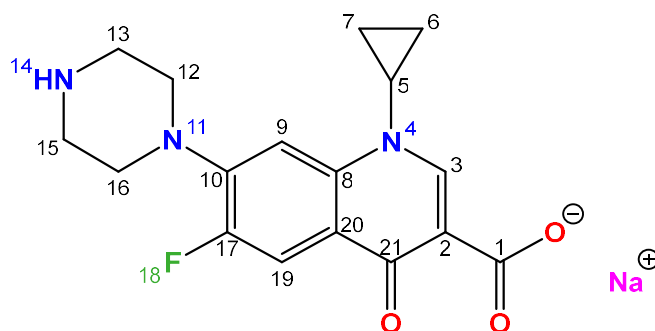
A stock solution of ciprofloxacin ($1.81 \times 10^{-3} \text{ mol dm}^{-3}$) was made up from ciprofloxacin ($\text{C}_{17}\text{H}_{18}\text{FN}_3\text{O}_3$, 15 mg, 0.045 mmol) in hydrochloric acid (25 mL, 0.1 M). A stock solution of iron(III) ($1.81 \times 10^{-3} \text{ mol dm}^{-3}$) was made up from iron(III) trichloride (FeCl_3 , 6.0 mg, 0.037 mmol) in hydrochloric acid (25 mL, 0.1 M). The stock solutions were used to make samples of varying molar ratio of iron and ciprofloxacin between 0.00 and 1.00 in 0.1 increments. UV-vis spectroscopy was used to analyse the samples.

pH 3

Hydrochloric acid (1 M) was added dropwise to deionised water (20 mL), whilst measuring the pH using a pH probe. Hydrochloric acid (0.5 mL, 1 M) was added to deionised water (20 mL) to make a pH 3 solution. This solution was used to make separate equimolar stock solutions ($1.81 \times 10^{-3} \text{ mol dm}^{-3}$) of ciprofloxacin and iron(III) trichloride. The stock solutions were used to make samples of varying molar ratio of iron(III) and ciprofloxacin between 0.00 and 1.00 in 0.1 increments. UV-vis spectroscopy was used to analyse the samples.

5.2.2 Metallo-fluoroquinolone precursors

5.2.2.1 Ciprofloxacin Sodium Salt



Ciprofloxacin (680 mg, 2.1 mmol) was added to deionised water (3 mL). A solution of sodium hydroxide pellets (NaOH , 80 mg, 2.0 mmol) in deionised water (0.3 mL) was added to the ciprofloxacin solution and stirred for 30 minutes, a white precipitate formed. The solution was

filtered into a round bottomed flask and concentrated, leaving a crystalline yellow precipitate (**1-21**, 553.4 mg, 1.6 mmol, 94 % yield).

m.p.: 321-323 °C (lit¹³¹: 325 °C).

IR 2926 cm⁻¹ (m, C-H stretching, alkane), 1628 cm⁻¹ (m, O=C-O asymmetric stretching), 1625 cm⁻¹ (m, C=C stretching, conjugated alkene), 1370 cm⁻¹ (m, O=C-O symmetric stretching), 1263 cm⁻¹ (s, C-F stretching), 882 cm⁻¹ (s, C=C bending, alkene).

¹H NMR (400 MHz, D₂O) δ_H 8.32 (s, 1H, C=H**3**), 7.59 (d, ³J_{H,F} = 13.5 Hz, Ar-H**19**, 1H), 7.30 (d, ⁴J_{H,F} = 7.3 Hz, Ar-H**9**, 1H), 3.38 (tt, ³J_{H,H} = 7.4, 4.0 Hz, H**5**, 1H), 3.05 (t, ³J_{H,H} = 6.4 Hz, H**12/16**, 4H), 2.88 (t, ³J_{H,H} = 6.4 Hz, H**13/15**, 4H), 1.18 (m, H**6/7**, 2H), 0.96 – 0.87 (m, H**6/7**, 2H).

¹³C NMR (101 MHz, D₂O) δ_C 175.4 (s, C**21**), 172.5 (s, C1-OOH), 154.4 (d, ¹J_{C,F} = 209.6 Hz, C**17**), 151.9 (s, C**3**), 144.4 (d, ²J_{C,F} = 10.6 Hz, C**10**), 138.4 (s, C**9**), 122.0 (d, ³J_{C,F} = 7.3 Hz, C**20**), 111.3 (d, ²J_{C,F} = 22.9, 12.3 Hz, C**19**), 106.4 (s, C**8**), 50.6 (s, C**12/16**), 43.7 (s, C**13/15**), 34.7 (s, C**5**), 7.4 (s, C**6/7**).

¹⁹F NMR {¹H}(376 MHz, D₂O) δ -124.26 (s, F**18**).

MS (ESI+, CH₃OH): found *m/z* 354.1231 (calc. for C₁₇H₁₈FN₃NaO₃ = *m/z* 354.1224, 1.4 ppm error).

Data consistent with literature values¹³¹

5.2.2.2 Bismuth Oxynitrate (BiONO₃, M_r: 286.9834 g mol⁻¹) Bismuth(III) nitrate pentahydrate (Bi(NO₃)₃·5H₂O, 1.20 g, 2.5 mmol) was added to deionised water (15 mL) with vigorous stirring for 30 minutes, followed by sonication for 15 minutes. The pH was adjusted to 7 using ammonia solution and the mixture was then sonicated for a further 15 minutes. The solution was heated at 180 °C for 30 minutes. The solution was vacuum filtered, and the precipitate washed three times with deionised water and left to dry. The product was a white powder (0.7048 g, 2.6 mmol, 81 % yield).

The product had poor solubility, limiting characterisation techniques to IR and melting point.

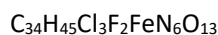
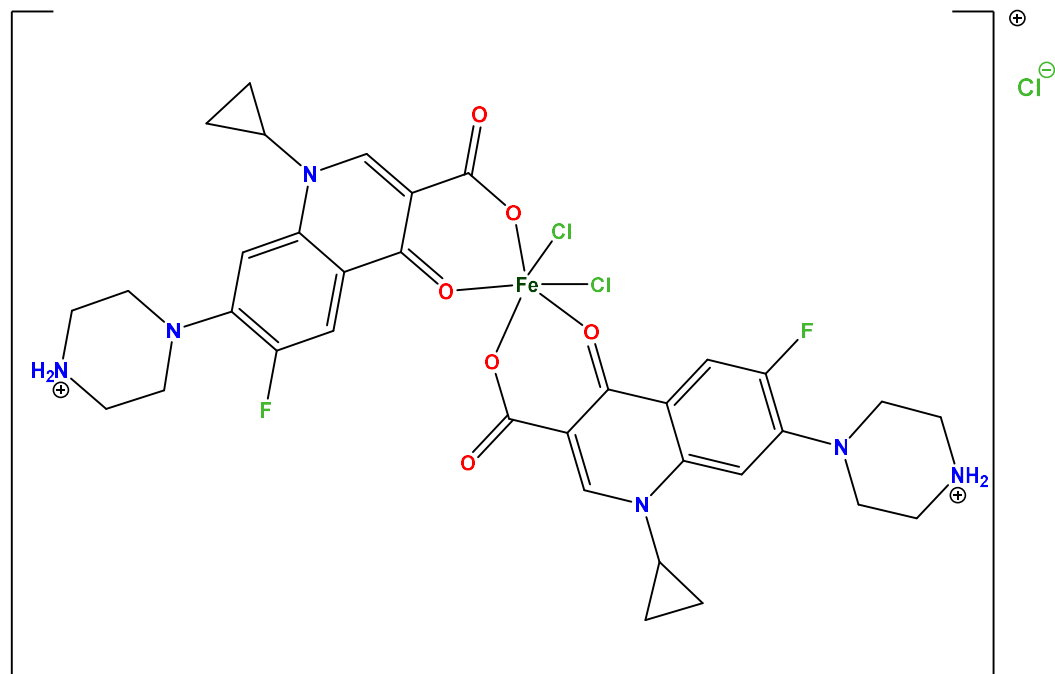
m.p.: >400 °C (limit of the machine).

IR 1511 cm⁻¹ (w, N-O symmetric stretching), 1322 cm⁻¹ (s, N-O asymmetric stretching).

CHN C: 0.00 %, H: 0.01 %, N: 3.62 % (theoretical: C=0.00 %, H=0.00 %, N=4.88 %).

5.2.3 Metallo-fluoroquinolone synthesis

5.2.3.1 1:2 Iron(III) chloride-ciprofloxacin

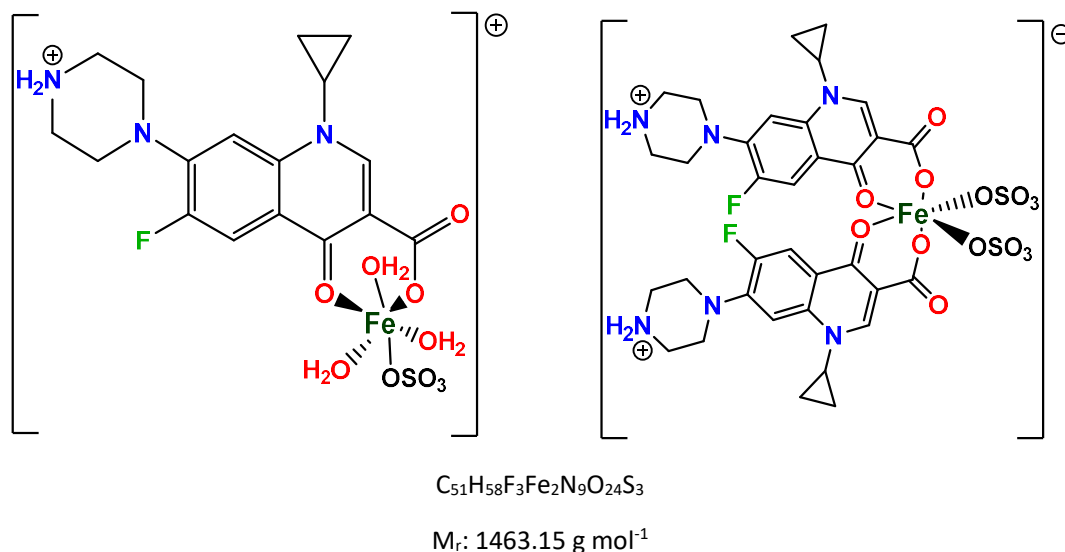


Ciprofloxacin ($\text{C}_{17}\text{H}_{18}\text{FN}_3\text{O}_3$, 25 mg, 0.1 mmol) was dissolved in hydrochloric acid (0.8 mL, 0.1 M) at 50 °C. Iron(III) chloride hexahydrate ($\text{FeCl}_3 \cdot 6\text{H}_2\text{O}$, 21 mg, 0.1 mmol) was added to the ciprofloxacin solution, and stirred at room temperature for four hours. The solution was then divided into 0.5 mL aliquots and set up for vapour diffusion crystallisation with acetone and left undisturbed for one week (see section 2.3 crystallisation methods). After one week, small red square-shaped crystals formed (8.2 mg, 8.7×10^{-3} mmol, 23 %).

m.p: 220-221 °C.

IR: 1610 cm^{-1} (m, O=C-O asymmetric stretching), 1454 cm^{-1} (m, C-H bending, alkane), 1376 cm^{-1} (m, O=C-O symmetric stretching), 1269 cm^{-1} (s, C-F stretching), 506 cm^{-1} (m, Fe(III)-O stretching).

6.2.3.2 Iron(III) sulfate-ciprofloxacin



Ciprofloxacin ($C_{17}H_{18}FN_3O_3$, 50 mg, 0.2 mmol) was dissolved in sulfuric acid (0.8 mL, 0.01 M) at 37 °C. Iron(III) sulfate ($Fe_2(SO_4)_3$, 30 mg, 0.08 mmol) was added to the ciprofloxacin solution, and stirred at room temperature for three hours. The solution was then divided into 0.5 mL aliquots and set up for vapour diffusion crystallisation with acetone and left undisturbed for one week (see section 5.2.5 crystallisation methods). After one week, small red square-shaped crystals formed.

m.p: 352-356 °C.

IR: 1610 cm^{-1} (m, O=C-O asymmetric stretching), 1465 cm^{-1} (m, O=C-O symmetric stretching), 1385 cm^{-1} (m, S=O asymmetric stretching), 1270 cm^{-1} (s, C-F stretching), 599 cm^{-1} (m, Fe(III)-O stretching), 1183 cm^{-1} (m, S=O symmetric stretching).

5.2.3.3 1:3 Bismuth(III)- ciprofloxacin: $[Bi(ciprofloxacin)_3(H_2O)_2]$

Bismuth oxynitrate ($BiONO_3$, 50 mg, 0.02 mmol) was dissolved in hydrochloric acid (1 mL, 0.1 M). Separately, ciprofloxacin ($C_{17}H_{18}FN_3O_3$, 290 mg, 0.88 mmol) was dissolved in hydrochloric acid (1.5 mL, 0.1 M). The two solutions were combined, producing a white precipitate. The resulting solution was filtered into a round bottomed flask and the filtrate was heated to 85 °C for six hours. Three drops of ammonia solution were added every hour in order to maintain the basicity of the solution. The solution was left to cool and then vacuum filtered to give a white powder (89.7 mg, 0.07 mmol, 17 % yield, $BiC_{51}H_{55}F_3N_9O_{11}$, $M_r: 1235.38 \text{ g mol}^{-1}$).

m.p: 323-326 °C (lit¹⁹: 322-324 °C).

IR: 1616 cm^{-1} (m, C=C stretching, conjugated alkene), 1610 cm^{-1} (m, O=C-O asymmetric stretching), 1358 cm^{-1} (m, O=C-O symmetric stretching), 1291 cm^{-1} (s, C-F stretching), 538 cm^{-1} (m, Bi(III)-O stretching).

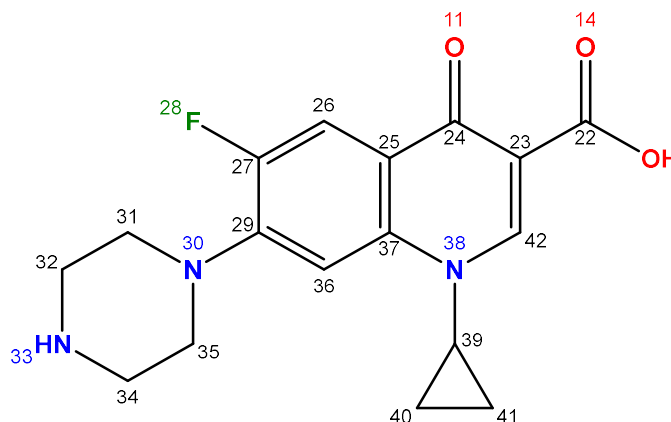


Figure 64: numbered ciprofloxacin structure for the assignment of NMR peaks in $[\text{Bi}(\text{ciprofloxacin})_3(\text{H}_2\text{O})]$.

^1H NMR (400 MHz, DMSO-d_6) δ_{H} 8.66 (s, C=CH**42**, 23,1H), 7.90 (d, $^3J_{\text{H,F}} = 13.4$ Hz, Ar-H**36**, 1H), 7.54 (d, $^4J_{\text{H,F}} = 7.6$ Hz, Ar-H**26**, 1H), 3.83 (tt, $^3J_{\text{H,H}} = 7.4, 4.0$ Hz, H**39**, 2H), 3.32 (s, H**31/35**, 2H), 3.23 (dd, $^3J_{\text{H,H}} = 6.1, 3.5$ Hz, H**32/34**, 4H), 2.93 – 2.86 (m, H**40/41**, 2H), 1.35 – 1.13 (m, H**40/41**, 4H).

^{13}C NMR (101 MHz, DMSO-d_6) δ_{C} 176.8 (s, C=O, **C24**), 166.0 (s, COO^- , **C22**), 148.0 (s, C=C, **C42**), 139.3 (s, C=C**36**), 106.2 (s, C=C**37**), 50.7 (s, **C31/35**), 45.4 (s, **C32/34**), 35.9 (s, **C39**), 7.6 (s, **C40/41**).

^{19}F NMR $\{^1\text{H}\}$ (376 MHz, DMSO-d_6) δ_{F} -121.36 (dd, $J = 13.7, 7.5$ Hz, **F28**).

CHN C: 48.69%, H: 5.64%, N: 9.85% (theoretical: C=49.56 %, H=4.49 %, N=10.20 %).

Data consistent with literature values¹⁹

5.2.3.4 zinc(II)- ciprofloxacin: $\text{Zn}(\text{ciprofloxacin})(\text{OH})(\text{H}_2\text{O})_2$ $\text{ZnC}_{34}\text{H}_{38}\text{F}_2\text{N}_6\text{O}_8$ (M_r : 762.0888 g mol⁻¹) Ciprofloxacin ($\text{C}_{17}\text{H}_{18}\text{FN}_3\text{O}_3$, 0.10 g, 0.3 mmol) sodium salt was added to a warmed solution of hydrochloric acid (1 mL, 0.1 M). A solution of anhydrous zinc(II) chloride (ZnCl_2 , 20 mg, 0.2 mmol) in deionised water (2 mL) was added to the ciprofloxacin solution. The new solution was refluxed for one hour and then cooled to room temperature. Methanol (1 mL) was added and left at room temperature for 24 hours. The resulting solution was filtered and washed with ethanol and then ether and left to dry, to give a white powder (89.8 mg, 0.1 mmol, 80 % yield).

See figure 64 for atom labels

m.p: 282- 284 °C.

IR: 3410 cm^{-1} (s, O-H stretching, water), 1614 cm^{-1} (m, O=C-O asymmetric stretching), 1379 cm^{-1} (m, O=C-O symmetric stretching), 1253 cm^{-1} (s, C-F stretching), 624 cm^{-1} (m, Zn(II)-O stretching).

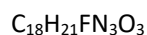
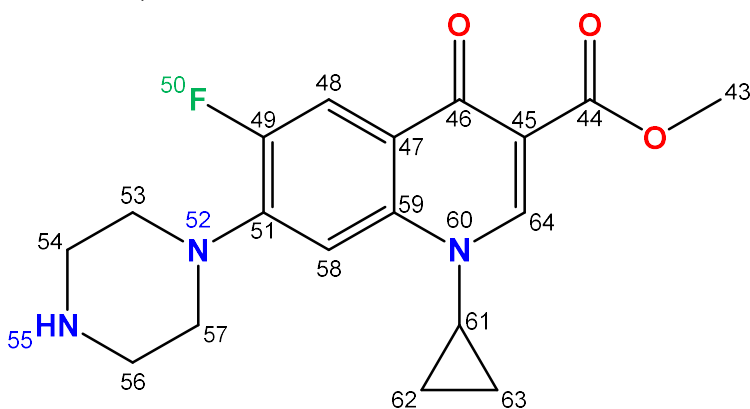
^{13}C ssNMR: $\{^1\text{H}\}$ (5 kHz) δ_{C} 171(s, C=O, **C24**), 165(s, COO⁻, **C22**), 152(s, **C27**), 146(s, CH, **C42**), 143 (s, CH, **C36**), 124(s, **C25**), 115(s, CH, **C26**), 110(s, **C37**), 50(s, CH₂, **C31/35**), 47(m, CH₂, **C32/34**), 39(m, CH, **C39**), 12(m, CH₂, **C40/41**).

^{19}F ssNMR: $\{^1\text{H}\}$ (10 kHz) δ_{F} -131(s, **F28**).

CHN: C: 47.16 %, H: 5.15 %, N: 9.54 % (theoretical: C=45.50 %, H=4.94 % and N=9.36 %).

5.2.4 Dimer complex synthesise

5.2.4.1 Ciprofloxacin methyl ester



M_r : 346.1561 g mol^{-1}

The reaction was carried out under the exclusion of air and moisture. A solution of ciprofloxacin ($\text{C}_{17}\text{H}_{18}\text{FN}_3\text{O}_3$, 1.50 g, 4.5 mmol) in dry methanol (50 mL) was stirred for 30 minutes in an ice/water bath. Thionyl chloride (6.5 mL, 89.6 mmol) was added dropwise to the ciprofloxacin solution, causing an instant white to yellow colour change and resulting in a clear yellow solution. The resulting solution was refluxed for 24 hours and allowed to cool to room temperature before the solvent and residual thionyl chloride was removed. An aqueous potassium carbonate solution (50 mL, 5% w/v) was added to the residue and extracted with DCM (3 x 20 mL). The organic extract was washed with deionised water (2 x 10 mL). An aqueous potassium carbonate solution (50 mL, 5% w/v) was added to the resulting aqueous fractions and the combined fractions were re-extracted with DCM (3 x 20 mL) and washed with deionised water (2 x 10 mL). The collective organic fractions were dried over MgSO_4 and the solvent was

removed *via* rotary evaporation to give a white powder. The resulting powder was recrystallised from hot MeCN to give a white powder (**43-64**, 1.01 g, 2.9 mmol, 65% yield).

m.p.: 226-228 °C (lit¹²⁶ = 227 – 228 °C).

IR: 2951 cm⁻¹ (w, C-H stretching, alkane), 1721 cm⁻¹ (s, C=O stretching, ester), 1618 cm⁻¹ (s, C-O stretching, ester), 1478 cm⁻¹ (s, C-O stretching, ester), 1256 cm⁻¹ (s, C-F stretching), 893 cm⁻¹ (s, C=C bending, alkene).

¹H NMR (400 MHz, Chloroform-*d*) δ_H 8.48 (s, **H64**, 1H), 7.94 (d, **H48**, ³J_{H,F} = 13.4 Hz, 1H), 7.22 (d, ⁴J_{H,F} = 7.2 Hz, **H58**, 1H), 3.87 (s, **H43**, 3H), 3.42 (tt, ³J_{H,H} = 7.3, 3.9 Hz, **H61**, 1H), 3.24 – 3.18 (m, **H53/57**, 4H), 3.08 (d, ³J_{H,H} = 5.1 Hz, **H54/56**, 4H), 2.34 (s, **H55**, 1H), 1.29 (t, ¹J = 6.7 Hz, **H62/63**, 2H), 1.12 (d, ¹J = 4.6 Hz, **H62/63**, 2H).

¹³C NMR (101 MHz, Chloroform-*d*) δ_C 173.3 (s, C=O, **C46**), 166.64 (s, C=O, **C44**), 153.6 (d, ¹J_{C,F} = 250 Hz, **C49**), 148.5 (s, **C64**), 145.2 (d, ²J_{C,F} = 11.1 Hz, **C58**), 138.2 (s, **C45**), 123.2 (d, ³J_{C,F} = 6.1 Hz, **C47**), 113.4 (d, ³J_{C,F} = 23.1 Hz, **C48**), 110.2 (s, **C59**), 104.9 (d, ³J_{C,F} = 3.0 Hz, **C58**), 52.2 (s, **C53/57**), 46.1 (s, **C54/56**), 34.7 (s, **C61**), 8.3 (s, **C62/63**).

¹⁹F NMR {¹H}(376 MHz, Chloroform-*d*) δ_F -123.42 (s, **F50**).

MS (ESI +, CH₃OH) found *m/z* 346.1561 (calc. for C₁₈H₂₁FN₃O₃ = *m/z* 346.1561, 0.2 ppm error).

CHN C: 61.78%, H: 5.75 %, N: 11.9 % (theoretical: C=62.61 %, H=5.84 %, N=12.17 %).

Data consistent with literature values¹²⁶

5.2.4.2 Synthesis of EDTA-ciprofloxacin methyl ester dimer

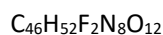
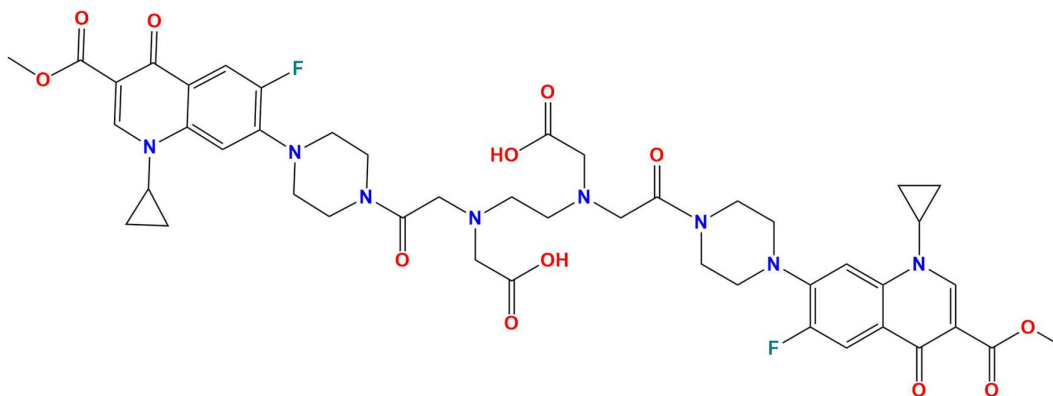


Figure 65: structure of 2-({2-[(carboxymethyl)(2-{4-[1-cyclopropyl-6-fluoro-3-(methoxycarbonyl)-4-oxo-1,4-dihydroquinolin-7-yl]piperazin-1-yl}-2-oxoethyl)amino]ethyl}{2-{4-[1-cyclopropyl-6-fluoro-3-(methoxycarbonyl)-4-oxo-1,4-dihydroquinolin-7-yl]piperazin-1-yl}-2-oxoethyl)amino)acetic acid, referred to as [EDTA(ciprofloxacin methyl ester)₂].

The reaction was carried out under the exclusion of air and moisture. Methyl-protected ciprofloxacin ($\text{C}_{18}\text{H}_{20}\text{FN}_3\text{O}_3$, 335 mg, 0.97 mmol) and EDTA dianhydride ($\text{C}_{10}\text{H}_{12}\text{N}_2\text{O}_6$, 125 mg, 0.49 mmol) were added to dry DMF (5 mL) and stirred under nitrogen at 70 °C for 18 hours. The solvent was removed, and the resulting precipitate was first triturated with methanol (1.25 mL) and acetone (12.5 mL), then triturated a further four times with acetone, the final time the solvent was removed via rotary evaporation. A dry off-white powder was produced (310 mg, 0.33 mmol, 68 % yield). The product was only found to be soluble in aqueous sodium hydroxide, which hydrolysed at the terminal methyl ester groups, forming the [EDTA(ciprofloxacin)₂] compound, characterisation of which can be found in section 5.2.4.3.

5.2.4.3 EDTA-ciprofloxacin dimer [EDTA(ciprofloxacin)₂]

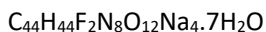
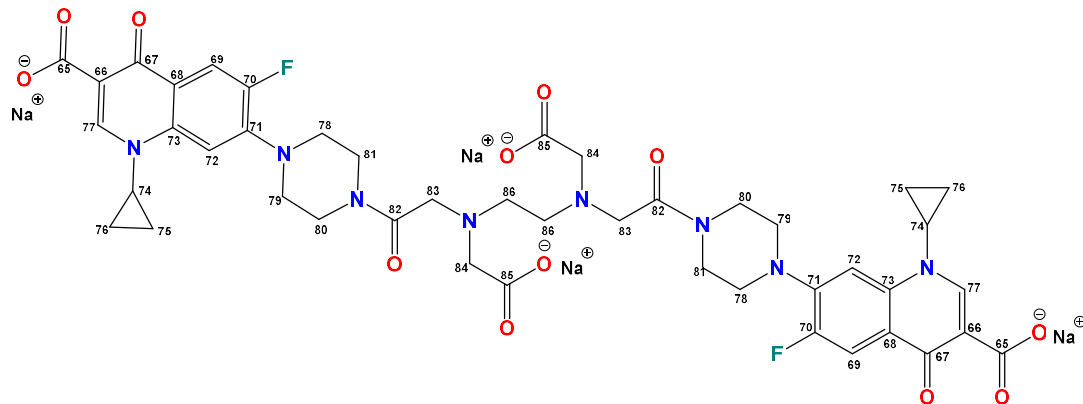


Figure 66: numbering scheme used for the NMR assignment of 7-[4-(2-[[2-({2-[4-(3-carboxy-1-cyclopropyl-6-fluoro-4-oxo-1,4-dihydroquinolin-7-yl)]piperazin-1-yl]-2-oxoethyl}(carboxymethyl)amino)ethyl(carboxymethyl)amino)acetyl]piperazin-1-yl]-1-cyclopropyl-6-fluoro-4-oxo-1,4-dihydroquinoline-3-carboxylic acid, formed in an NMR tube with DMSO-d⁶ and sodium hydroxide, referred to as [EDTA(ciprofloxacin)₂]. Spectra described below.

[EDTA(ciprofloxacin methyl ester)₂] (C₄₆H₅₂F₂N₈O₁₂, 194 mg, 0.2 mmol) was stirred in a sodium hydroxide solution (5 mL, 0.25 M) for 18 hours, resulting in a clear, colourless solution. Hydrochloric acid (1 M) was added dropwise to the solution, until indicator paper showed the solution had been neutralised. A precipitate formed, which was vacuum filtered and washed with deionised water to give a yellow precipitate (**65-86**, 148 mg, 0.1 mmol, 50% yield).

m.p.: 195-196 °C.

IR: 3017 cm⁻¹ (w, C-H stretching, alkene), 2854 cm⁻¹ (w, C-H stretching, alkane), 1723 cm⁻¹ (w, C-H bending, aromatic), 1626 cm⁻¹ (m, O=C-O asymmetric stretching), 1453 cm⁻¹ (m, C-H bending, alkane), 1335 cm⁻¹ (m, O=C-O symmetric stretching), 1245 cm⁻¹ (s, C-F stretching), 1025 cm⁻¹ (m, C-N stretching, amine), 885 cm⁻¹ (s, C=C bending, alkene).

¹H NMR (400 MHz, D₂O/ NaOD) δ_H 8.35 (s, C=C-H**77**, 1H), 7.59 (dd, ³J_{H,F} = 13.3, 2.6 Hz, Ar-H**69**, 1H), 7.37 – 7.19 (m, Ar-H**72**, 1H), 3.57 (d, ³J_{H,H} = 23.1 Hz, piperazine H**78/79**, 4H), 3.40 (m, cyclopropyl H**74**, 1H), 3.15 (d, ³J_{H,H} = 2.9 Hz, piperazine H**80/81**, 4H), 2.92 (s, H**86**, 4H), 1.17 (m, ¹J_{H,H} = 6.0 Hz, cyclopropyl H**75/76**, 2H), 0.91 (m, cyclopropyl H**75/76**, 2H).

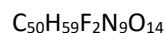
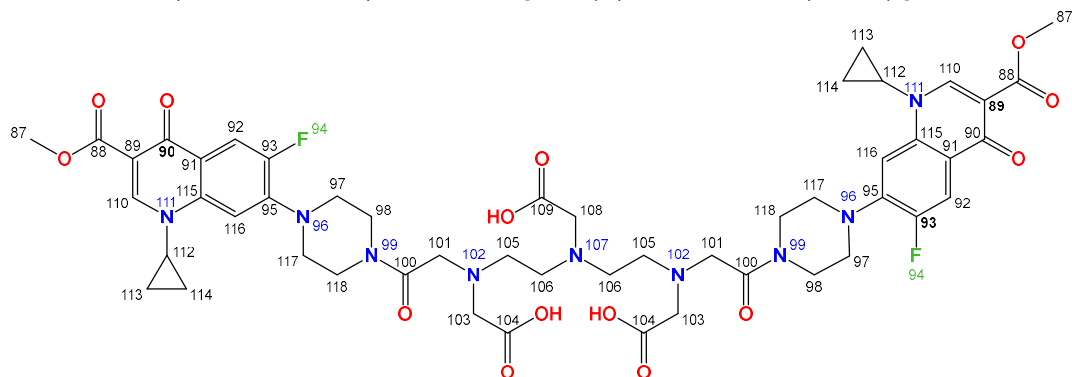
^{13}C NMR (101 MHz, D_2O) δ_{C} 175.07 (s, C67), 172.1 (s, C=O, C67), 171.4 (s, COOH, C65), 151.19 (s, C77), 143.2 (d, $^2J_{\text{C,F}}$ = 10.6 Hz, C71), 138.07 (s, C72), 121.76 (d, $^3J_{\text{C,F}}$ = 7.0 Hz, C68), 105.7 (s, C73), 51.8 (s, C78/79), 34.6 (s, C80/81), 27.24 (s, C74), 7.3 (s, C75/76).

^{19}F NMR $\{^1\text{H}\}$ (400 MHz, DMSO-d_6) δ_{F} -124.23 (s, CF).

MS (ESI-, NaOH) found m/z 917.3258 (calc. for $\text{C}_{44}\text{H}_{47}\text{F}_2\text{N}_8\text{O}_{12}$ = m/z 917.3287, 2.9 ppm error), m/z 939.3080 ($\text{C}_{44}\text{H}_{46}\text{F}_2\text{N}_8\text{NaO}_{12}$ = m/z 393.3106, 1.6 ppm error).

CHN C: 46.88 %, H: 5.07 %, N: 9.52 % (theoretical: C=46.65 %, H=5.16 %, N=9.89 %.)

5.2.4.4 DTPA-ciprofloxacin methyl ester dimer [DTPA(ciprofloxacin methyl ester) $_2$]

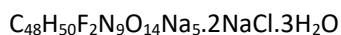
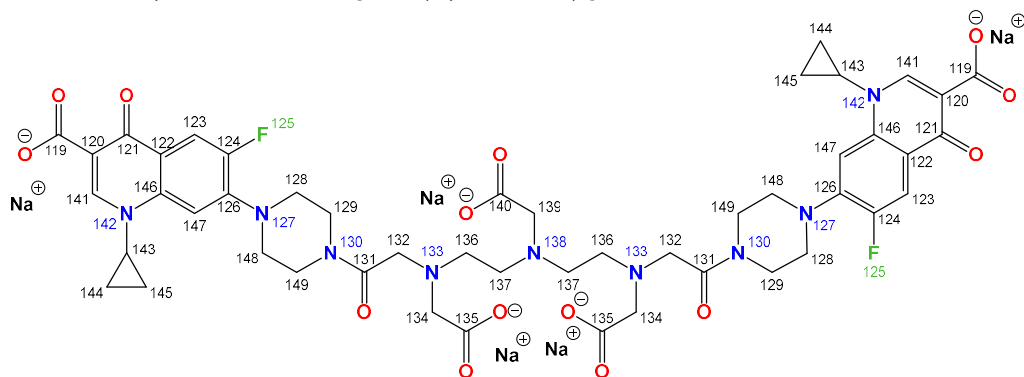


M_r : 1047.41 g mol^{-1}

The reaction was carried out under the exclusion of air and moisture. DTPA dianhydride ($\text{C}_{14}\text{H}_{19}\text{N}_3\text{O}_8$, 0.03 g, 0.1 mmol) was added to a solution of ciprofloxacin methyl-ester ($\text{C}_{18}\text{H}_{21}\text{FN}_3\text{O}_3$, 0.0600 g, 0.2 mmol) in dry DMSO (5 mL). The resulting solution was stirred under nitrogen for 18 hours at 70 °C. Acetone (45 mL) was added to the reaction solution and sonicated then centrifuged before the solvent was removed, this was repeated five times. On the final addition of acetone, the solvent was removed *via* rotary evaporation, leaving an off-white precipitate (**87-118**, 16 mg, 0.05 mmol, 56 % yield).

MS (ESI-, CH_3OH) found m/z 1046.4034 (calc. for $\text{C}_{50}\text{H}_{58}\text{F}_2\text{N}_9\text{O}_{14}$ = m/z 1046.4077, 0.7 ppm error).

5.2.4.5 DTPA-ciprofloxacin dimer [EDTA(ciprofloxacin)₂]



$$M_r: 1246.80 \text{ g mol}^{-1}$$

[EDTA(ciprofloxacin methyl ester)₂] (C₅₀H₅₉F₂N₉O₁₄, 16 mg, 0.05 mmol) was dissolved in sodium hydroxide (NaOH, 0.01 M, 10 mL, 0.09 mmol) and stirred for 24 hours at room temperature. After 24 hours hydrochloric acid (HCl, 0.1 M) was added dropwise until the basic solution was neutralised, determined with universal indicator paper. During the neutralisation a pale blue precipitate formed. The precipitate was isolated *via* rotary evaporation. The precipitate was triturated with acetone three times before being isolated *via* rotary evaporation, giving a yellow precipitate (**119-149**, 10 mg, 0.01 mmol, 22 % yield).

m.p.: 205-206 °C.

IR: 3381 cm⁻¹ (m, N-H stretching, amine), 2982 cm⁻¹ (m, C-H stretching, alkane), 1659 cm⁻¹ (m, C=C stretching, alkene), 1616 cm⁻¹ (m, O=C-O asymmetric stretching), 1387 cm⁻¹ (m, O=C-O symmetric stretching), 1273 cm⁻¹ (s, C-F stretching).

¹H NMR (400 MHz, DMSO-*d*₆ / NaOD) δ_H 7.81 – 7.69 (m, C=CH**141**, 1H), 3.72 (m, ³J_{H,H} = 3.6 Hz, cyclopropyl H**143**, 1H), 3.65 (d, ³J_{H,H} = 5.1 Hz, H**132**, 2H), 3.45 (dd, ³J_{H,H} = 14.7, 6.8 Hz, piperazine H**129/149**, 4H), 2.94 (d, ³J_{H,H} = 8.1 Hz, piperazine H**128/148**, 4H), 2.86 (s, H**136**, 2H), 2.10 (s, H**134**, 2H), 1.27 (m, cyclopropyl H**144/145**, 2H), 1.10 (m, cyclopropyl H**144/145**, 2H).

¹³C NMR (101 MHz, DMSO-*d*₆ / NaOD) δ_C 173.2 (s, C**121**), 173.1 (s, C**119**), 166.8 (d, ¹J_{C,F} = 374.7 Hz, C**124**), 143.6 (d, ²J_{C,F} = 9.8 Hz, C**126**), 138.0 (s, C**147**), 109.4 (s, C**146**), 51.3 (s, C**128/148**), 34.8 (s, C**129/149**), 32.2 (s, C**143**), 7.6 (s, C**144/145**).

¹⁹F NMR {¹H}(376 MHz, DMSO-*d*₆) δ_F -124.31 – -124.64 (m, F**125**).

MS product was not soluble enough to get a spectrum

CHN C: 44.64 %, H: 4.52 %, N: 9.23 % (theoretical: C = 44.3186 %, H = 4.3391 %, N = 9.6907 %.)

5.2.5 Crystallisation Methods

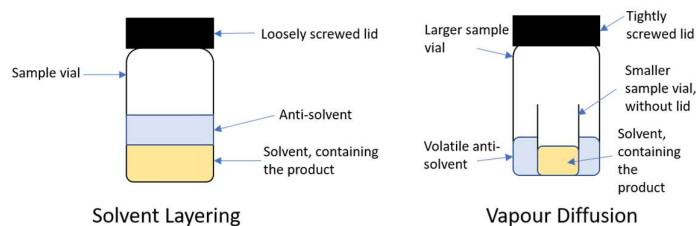


Figure 67: diagrams of crystallisation methods described in this section.

5.2.5.1 Solvent layering

The solution containing the product was divided into aliquots and an equal volume of an anti-solvent (which the product is not soluble in) was added to the aliquots (figure 67). As the original solvent evaporates off, the product 'crashes out' in the anti-solvent.

5.2.5.2 Vapour diffusion

The solution containing the product was divided into aliquots in small vials. An equivalent volume of a volatile anti-solvent (which the product is not soluble in) was added to a larger vial (figure 67). The smaller vial with the product solution was placed inside the larger vial with the anti-solvent in. The large sample vial was then sealed, allowing the anti-solvent vapour to diffuse into the smaller with the product, causing the product to 'crash out' at a slower rate than in solvent layering.

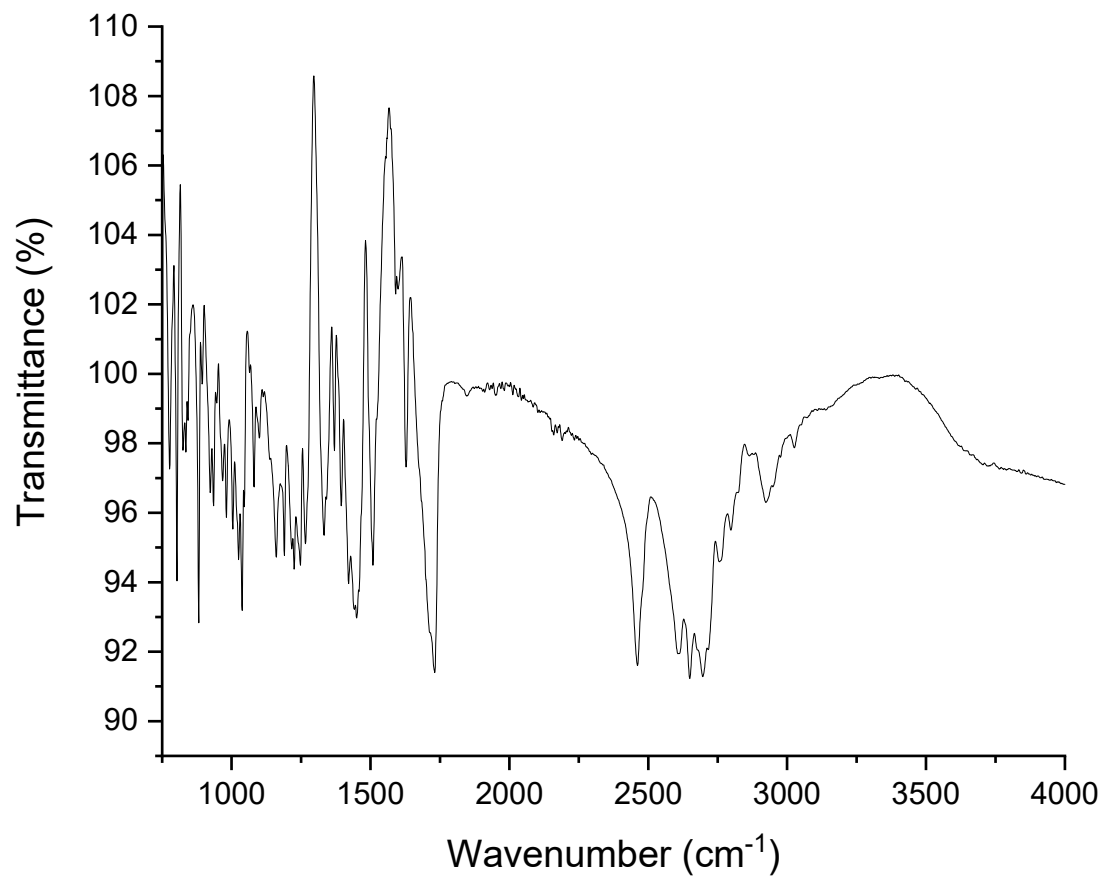
Abbreviations

ATP	Adenosine triphosphate
btc	Trimesic acid
Cf-	Ciprofloxacin
cfA	7-(4-(decanoyl)piperazin-1-yl)-ciprofloxacin
cfH	Protonated ciprofloxacin
CHN	Elemental analysis of carbon, hydrogen and nitrogen
COSY	¹ H ¹ H correlation spectrum
CSD	Cambridge structural database
cym	Cymene
DMSO	Dimethyl sulfoxide
DTPA	Diethylenetriamine pentaacetate
EDTA	Ethylenediaminetetraacetic acid
FTIR	Fourier transform infrared spectroscopy
HPLC	High performance liquid chromatography
IR	Infrared radiation
m.p.	Melting point
MIC	Minimum inhibitory concentration
MS	Mass spectrometry
NMR	Nuclear magnetic resonance
nta	nitrilotricetato
oba	2-(oxalyl-amino)-benzoic acid
odpa	Octadecylphosphonic acid
Ox	Oxalate
phen	Phenethylamine
PMQR	Plasmid mediated quinolone resistance
scXRD	Single crystal X-ray diffraction
ssNMR	Solid state nuclear magnetic resonance
XRF	X-ray fluorescence

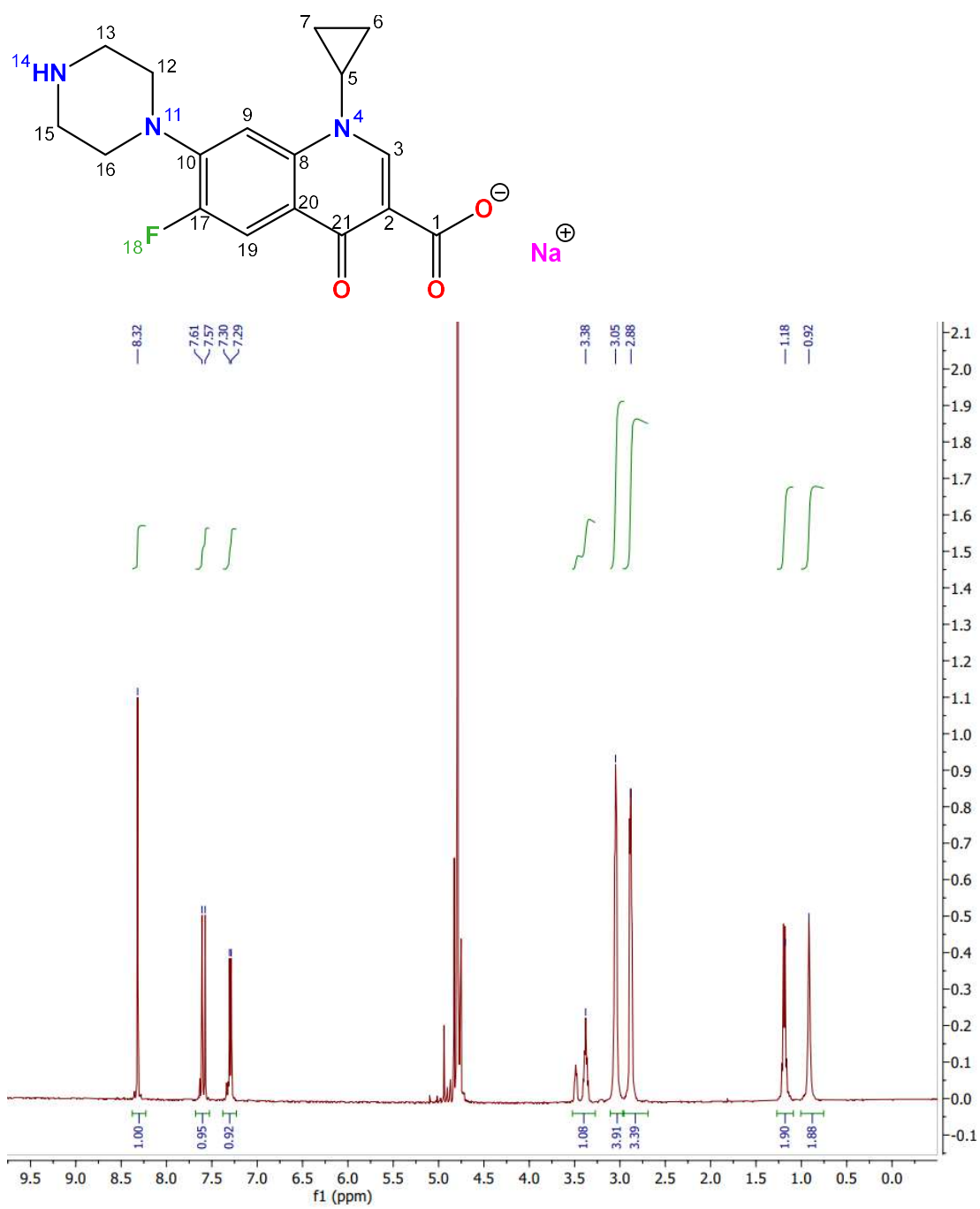
6. Appendices

6.1 Ciprofloxacin sodium salt

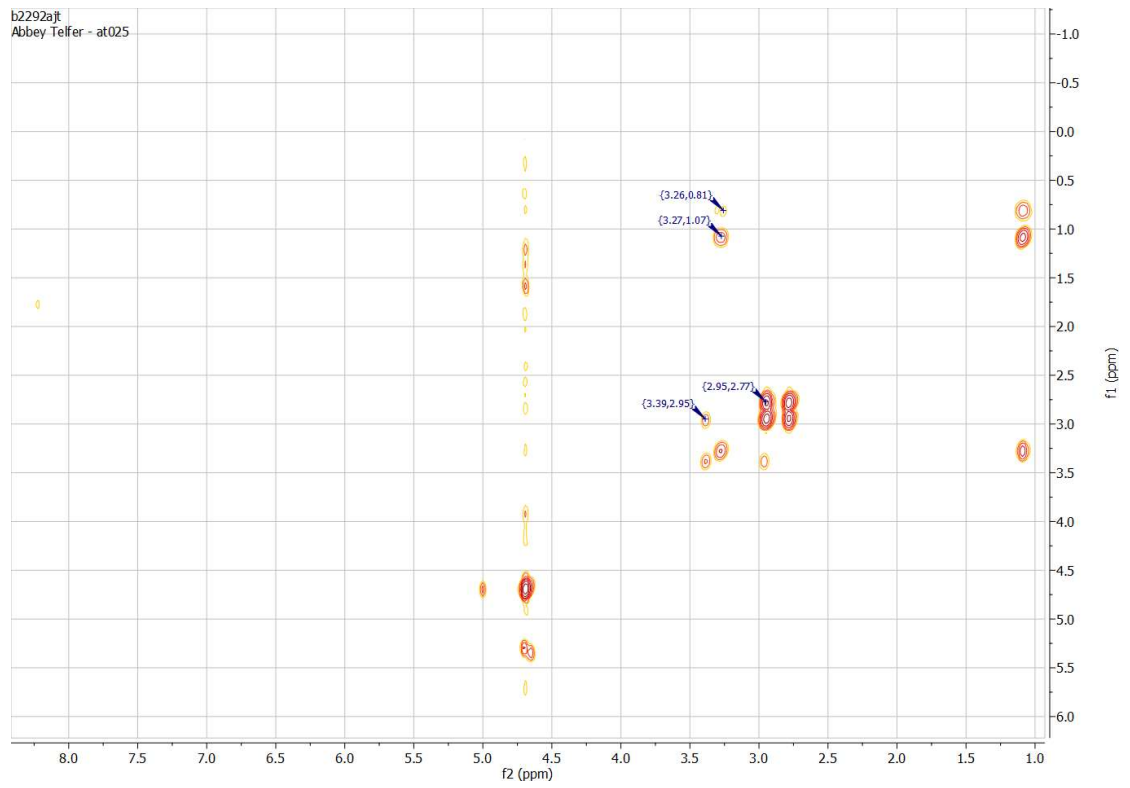
6.1.1 FTIR



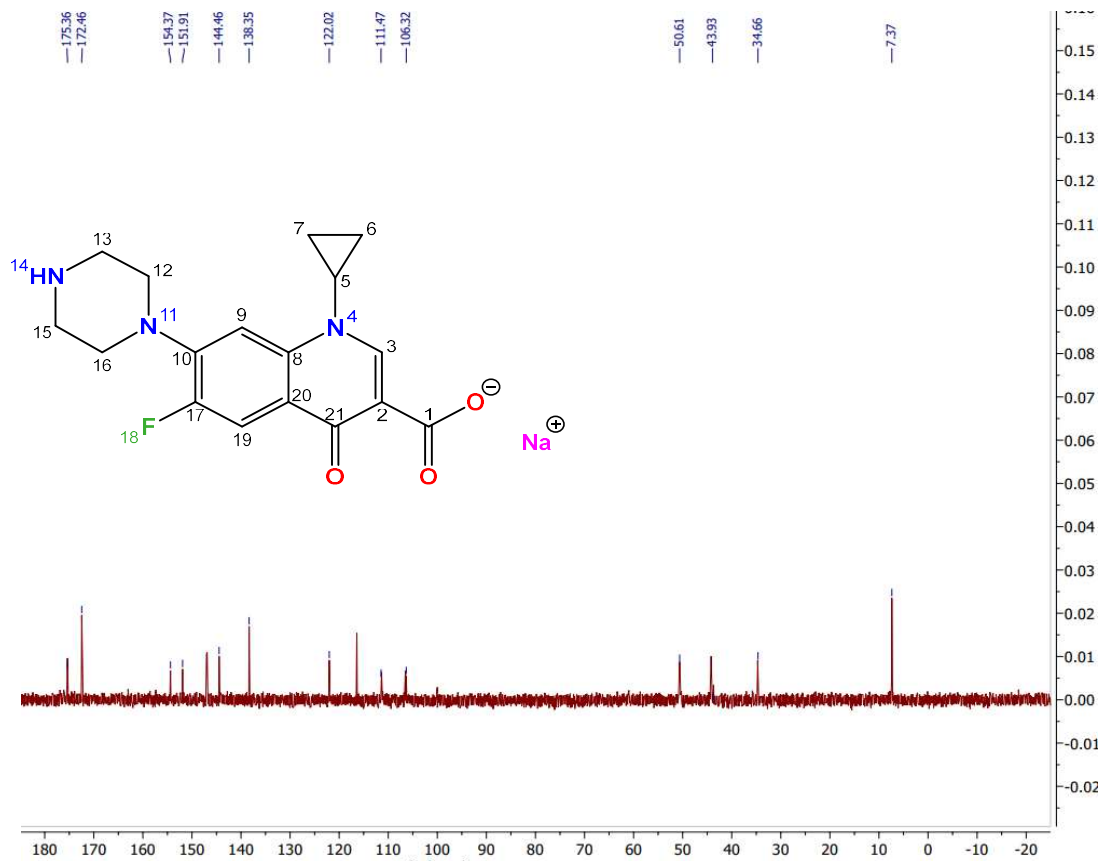
6.1.2 ^1H NMR



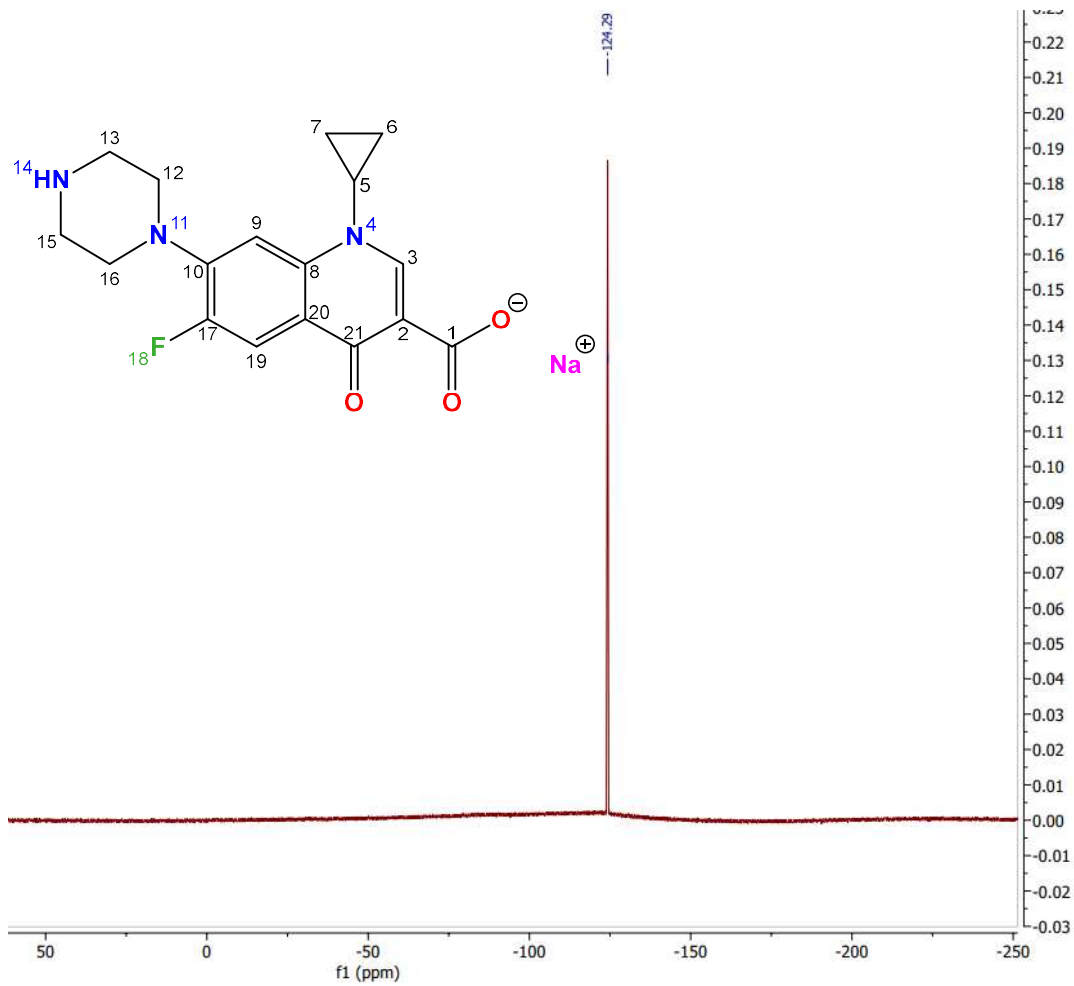
6.1.3 COSY



6.1.4 ^{13}C NMR



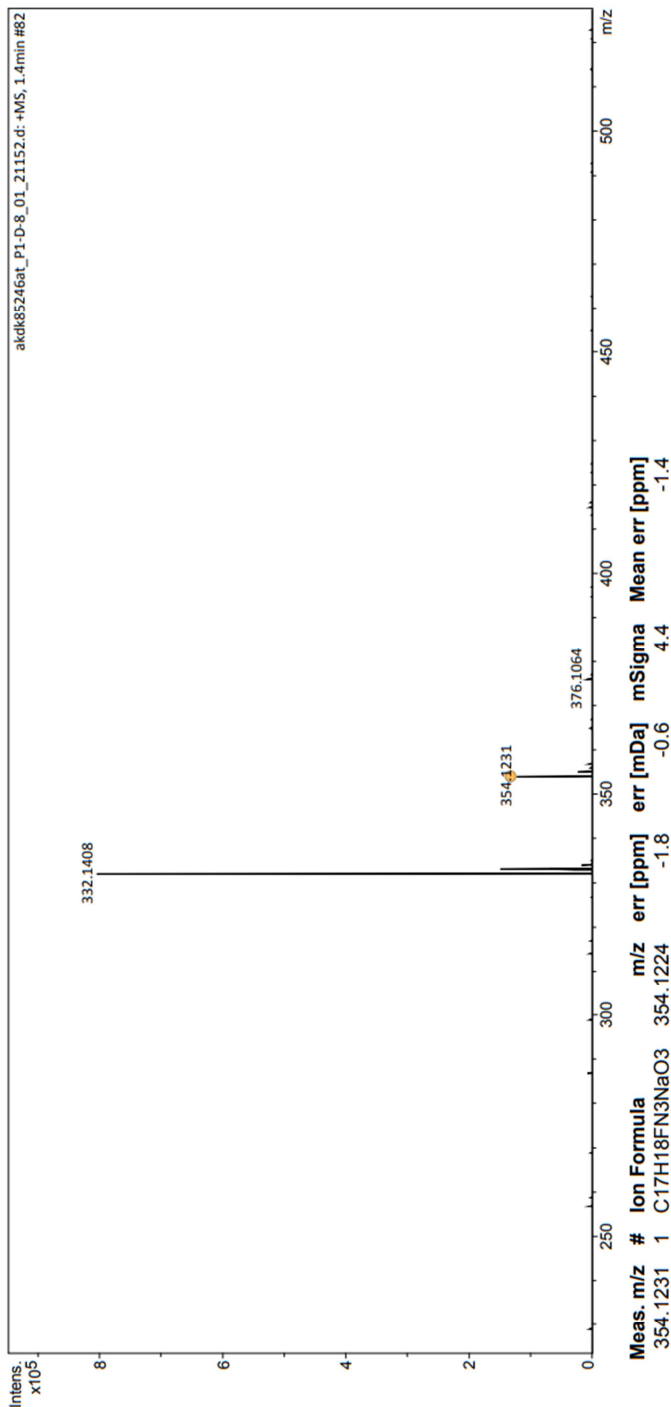
6.1.5 ^{19}F NMR



6.1.6 mass spectrometry

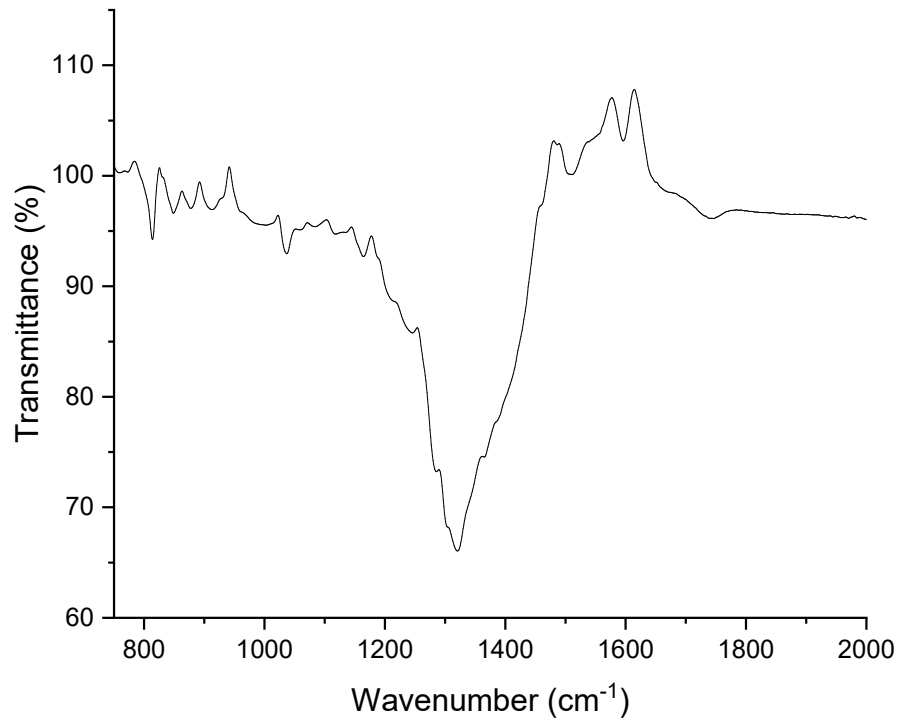
Analysis Filename akdk85246at_P1-D-8_01_21152.d
 Method ESI_low mass_2c1s.m
 Submission Name akdk85246at

Acquisition Date 18/09/2020 12:59:27
 Instrument compact
 ESI Positive



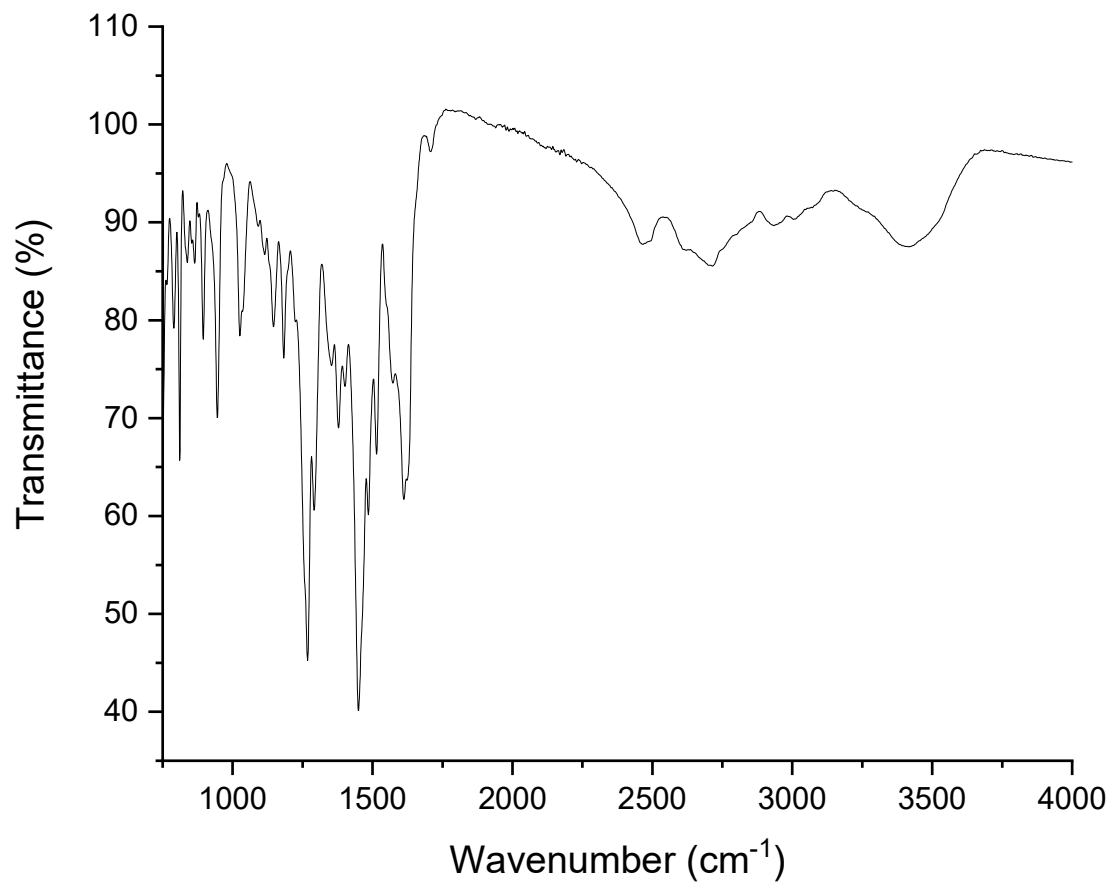
6.2 Bismuth oxynitrate

6.2.1 FTIR



6.3 1:2 iron(III)-ciprofloxacin

6.3.1 FTIR



6.3.2 X-ray crystal structure data and refinement

Crystal data and structure refinement	(1)	(2)	(3)
<i>Empirical formula</i>	C ₃₄ H _{44.84} Cl _{2.98} F ₂ FeN ₆ O _{12.74}	C ₁₇ H ₁₉ FN ₄ O ₆	C ₅₁ H ₅₈ F ₃ Fe ₂ N ₉ O ₂₄ S ₃
<i>Formula weight</i>	941.06	394.36	1445.94
<i>Temperature/K</i>	110.00(10)	110.05(10)	110.00(10)
<i>Crystal system</i>	monoclinic	triclinic	triclinic
<i>Space group</i>	I2/a	P-1	P-1
<i>a/Å</i>	15.0765(4)	6.5649(3)	13.8361(5)
<i>b/Å</i>	20.9070(5)	10.5826(5)	15.3995(4)
<i>c/Å</i>	17.9328(5)	12.5989(6)	17.2045(8)
<i>α/°</i>	90	73.023(4)	67.583(3)
<i>β/°</i>	112.582(3)	87.216(3)	79.960(4)
<i>γ/°</i>	90	85.734(4)	89.311(3)
<i>Volume/Å³</i>	5219.1(3)	834.51(7)	3330.9(2)
<i>Z</i>	4	2	2
<i>ρ_{calc} g/cm³</i>	1.198	1.569	1.442
<i>μ/mm¹</i>	4.263	1.092	5.157
<i>F(000)</i>	1950.0	412.0	1492.0
<i>Crystal size/mm³</i>	0.198 × 0.168 × 0.133	0.137 × 0.089 × 0.06	0.152 × 0.084 × 0.076
<i>Radiation</i>	Cu Kα (λ = 1.54184)	CuKα (λ = 1.54184)	CuKα (λ = 1.54184)
<i>2θ range for data collection/°</i>	7.63 to 134.134	7.34 to 134.156	7.794 to 142.248
<i>Index ranges</i>	-18 ≤ h ≤ 11, -24 ≤ k ≤ 24, -21 ≤ l ≤ 21	-7 ≤ h ≤ 7, -11 ≤ k ≤ 12, -15 ≤ l ≤ 15	-16 ≤ h ≤ 14, -18 ≤ k ≤ 13, -20 ≤ l ≤ 20
<i>Reflections collected</i>	9384	11424	23793
<i>Independent reflections</i>	4648 [R _{int} = 0.0172, R _{sigma} = 0.0234]	2983 [R _{int} = 0.0190, R _{sigma} = 0.0156]	12608 [R _{int} = 0.0319, R _{sigma} = 0.0485]
<i>Data/restraints/parameters</i>	4648/0/321	2983/0/344	12608/0/976

<i>Goodness-of-fit on F^2</i>	1.065	1.055	1.028
<i>Final R indexes [$I \geq 2\sigma(I)$]</i>	$R_1 = 0.0468, wR_2 = 0.1442$	$R_1 = 0.0306, wR_2 = 0.0854$	$R_1 = 0.0501, wR_2 = 0.1175$
<i>Final R indexes [all data]</i>	$R_1 = 0.0494, wR_2 = 0.1477$	$R_1 = 0.0342, wR_2 = 0.0888$	$R_1 = 0.0675, wR_2 = 0.1277$
<i>Largest diff. peak/hole / $e \text{ \AA}^{-3}$</i>	0.74/-0.38	0.25/-0.20	0.42/-0.58

6.3.3 X-ray crystal structure bond lengths

Atom	Atom	Length/Å	Atom	Atom	Length/Å
C1	C2	1.489(3)	C11	N2	1.473(3)
C1	O1	1.275(3)	C12	N3	1.485(3)
C1	O2	1.246(3)	C13	C14	1.527(3)
C2	C3	1.419(3)	C13	N3	1.488(3)
C2	C10	1.378(3)	C14	N2	1.467(3)
C3	C4	1.446(3)	C15	C16	1.497(3)
C3	O3	1.279(3)	C15	C17	1.492(3)
C4	C5	1.404(3)	C15	N1	1.457(3)
C4	C9	1.404(3)	C16	C17	1.507(4)
C5	C6	1.368(3)	Cl1	Fe2	2.293(3)
C6	C7	1.421(3)	Fe2	O1 ¹	1.997(16)
C6	F1	1.352(2)	Fe2	O1	1.997(16)
C7	C8	1.396(3)	Fe2	O3	2.029(15)
C7	N2	1.395(3)	Fe2	O3 ¹	2.029(15)
C8	C9	1.400(3)	Fe2	O4	2.028(5)
C9	N1	1.398(3)	Fe2	O4 ¹	2.028(5)
C10	N1	1.341(3)	Cl3	Cl3 ¹	1.431(17)
C11	C12	1.517(3)			

¹3/2-X,+Y,1-Z

6.3.4 X-ray crystal structure bond angles

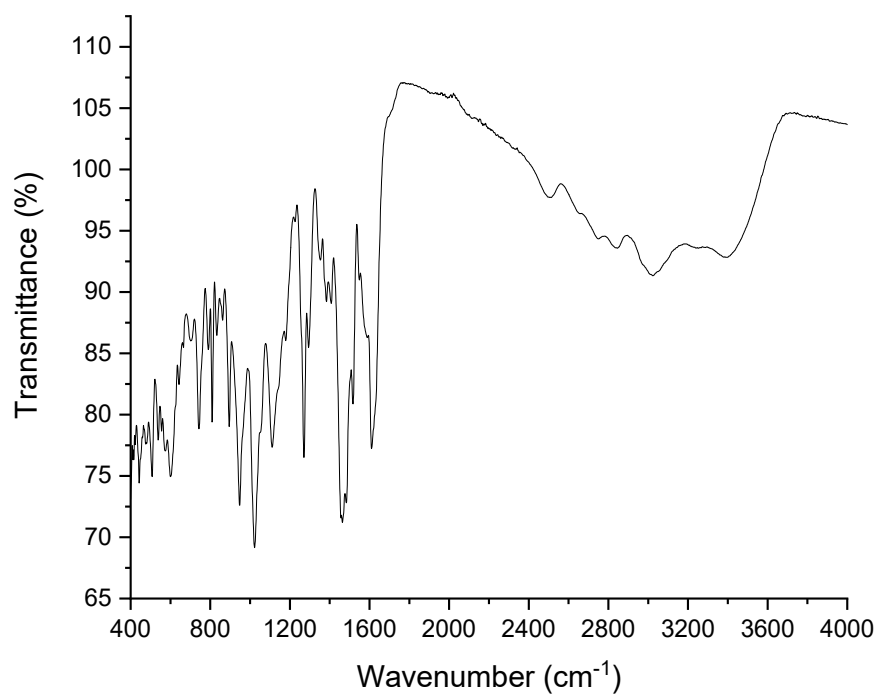
Atom	Atom	Atom	Angle/°	Atom	Atom	Atom	Angle/°
O1	C1	C2	119.20(19)	O1	Fe2	Cl1	96.65(8)
O2	C1	C2	118.70(2)	O1 ¹	Fe2	Cl1 ¹	96.65(8)
O2	C1	O1	122.10(2)	O1 ¹	Fe2	Cl1	94.27(8)
C3	C2	C1	122.92(19)	O1 ¹	Fe2	Cl1	94.27(8)
C10	C2	C1	117.86(19)	O1	Fe2	O1 ¹	166.31(9)
C10	C2	C3	119.21(19)	O1 ¹	Fe2	O3	85.48(6)
C2	C3	C4	116.74(19)	O1 ¹	Fe2	O3 ¹	84.99(6)
O3	C3	C2	124.27(19)	O1	Fe2	O3	84.99(6)
O3	C3	C4	118.99(19)	O1	Fe2	O3 ¹	85.48(6)
C5	C4	C3	120.40(2)	O1 ¹	Fe2	O4 ¹	97.03(16)
C9	C4	C3	120.97(19)	O1 ¹	Fe2	O4	92.04(15)
C9	C4	C5	118.60(19)	O1	Fe2	O4	97.03(16)
C6	C5	C4	119.50(2)	O1	Fe2	O4 ¹	92.04(15)
C5	C6	C7	123.40(2)	O3	Fe2	Cl1 ¹	171.08(9)
F1	C6	C5	117.60(2)	O3 ¹	Fe2	Cl1	171.08(9)
F1	C6	C7	118.98(19)	O3 ¹	Fe2	Cl1 ¹	97.20(9)
C8	C7	C6	116.34(19)	O3	Fe2	Cl1	97.20(9)
N2	C7	C6	120.80(2)	O3 ¹	Fe2	O3	91.61(9)
N2	C7	C8	122.70(2)	O4	Fe2	Cl1 ¹	85.50(2)
C7	C8	C9	121.10(2)	O4 ¹	Fe2	Cl1 ¹	11.50(16)
C8	C9	C4	120.92(19)	O4	Fe2	O3	85.78(17)
N1	C9	C4	118.78(18)	O4 ¹	Fe2	O3 ¹	85.78(18)
N1	C9	C8	120.29(19)	O4 ¹	Fe2	O3	176.20(16)

N1	C10	C2	123.96(19)	O4	Fe2	O3 ¹	176.20(16)
N2	C11	C12	109.90(2)	O4 ¹	Fe2	O4	97.00(3)
N3	C12	C11	109.50(2)	C9	N1	C15	120.13(17)
N3	C13	C14	110.80(2)	C10	N1	C9	119.94(18)
N2	C14	C13	111.10(2)	C10	N1	C15	119.78(18)
C17	C15	C16	60.56(17)	C7	N2	C11	117.80(18)
N1	C15	C16	118.20(2)	C7	N2	C14	115.94(19)
N1	C15	C17	118.55(19)	C14	N2	C11	111.36(19)
C15	C16	C17	59.57(16)	C12	N3	C13	110.77(19)
C15	C17	C16	59.87(16)	C1	O1	Fe2	128.29(14)
Cl1 ¹	Fe2	Cl1	74.04(16)	C3	O3	Fe2	121.86(13)

¹ 3/2-X,+Y,1-Z

6.4 1:1/1:2 Iron(III)-ciprofloxacin salt

6.4.1 FTIR



6.4.2 X-ray crystal structure bond lengths

Atom	Atom	Length/Å	Atom	Atom	Length/Å
Fe1	O1	1.9620 (19)	C4	C5	1.407 (4)
Fe1	O2	1.955 (2)	C13	C12	1.392 (5)
Fe1	O6	2.021 (2)	C5	C10	1.402 (4)
Fe1	O3	1.977 (2)	N2	C45	1.397 (4)
Fe1	O4	2.050 (2)	N2	C48	1.455 (5)
Fe1	O5	2.055 (2)	N2	C51	1.460 (5)
Fe2	O12	1.968 (2)	C6	C2	1.493 (4)
Fe2	O11	2.036 (2)	C10	C11	1.353 (4)
Fe2	O15	2.050 (2)	C30	C29	1.389 (4)
Fe2	O13	1.984 (2)	C12	C11	1.427 (4)
Fe2	O14	1.967 (2)	C3	C2	1.383 (4)
Fe2	O16	1.963 (3)	C27	C28	1.350 (4)
S003	O3	1.514 (2)	C24	C26	1.487 (4)
S003	O9	1.468 (2)	C24	C25	1.500 (4)
S003	O10	1.457 (3)	N3	C50	1.492 (5)
S003	O8	1.458 (3)	N3	C49	1.497 (6)
S004	O13	1.492 (2)	C28	C29	1.430 (4)
S004	O23	1.463 (2)	N5A	C29	1.437 (6)
S004	O22	1.460 (3)	N5A	C31A	1.466 (7)
S004	O24	1.477 (2)	N5A	C34A	1.458 (7)
S005	O16	1.514 (4)	C38	C47	1.408 (5)
S005	O21A	1.304 (17)	C38	C37	1.408 (4)
S005	O19A	1.461 (6)	C38	C39	1.445 (4)
S005	O20A	1.457 (8)	C46	C47	1.354 (4)
F3	C46	1.359 (4)	C46	C45	1.411 (5)
F2	C28	1.353 (4)	C37	C44	1.408 (5)
O1	C1	1.291 (3)	C39	C35	1.417 (5)

O12	C23	1.285 (3)	C7	C9	1.501 (5)
O2	C6	1.290 (4)	C7	C8	1.491 (5)
O11	C18	1.285 (3)	C45	C44	1.385 (5)
O15	C39	1.279 (4)	C26	C25	1.495 (5)
O7	C6	1.234 (4)	C29	N5	1.313 (12)
F1	C11	1.358 (4)	C35	C36	1.375 (5)
O14	C40	1.280 (5)	C35	C40	1.497 (5)
O17	C23	1.236 (4)	C48	C49	1.532 (5)
N4	C21	1.392 (4)	C9	C8	1.495 (6)
N4	C20	1.339 (4)	C51	C50	1.518 (5)
N4	C24	1.464 (3)	C41	C43	1.487 (7)
N7	C4	1.395 (4)	C41	C42	1.480 (5)
N7	C3	1.337 (4)	C43	C42	1.471 (8)
N7	C7	1.459 (4)	C31A	C32A	1.519 (8)
N8	C12	1.377 (4)	C31	C32	1.522 (14)
N8	C14	1.496 (7)	C31	N5	1.474 (15)
N8	C17	1.462 (7)	C32A	N6	1.504 (9)
N8	C14A	1.451 (10)	C14	C15	1.521 (8)
N8	C17A	1.376 (9)	C17	C16	1.532 (8)
O16	S0	1.539 (6)	C14A	C15A	1.478 (14)
N1	C37	1.388 (4)	C15	N9	1.485 (8)
N1	C36	1.354 (5)	C16	N9	1.474 (8)
N1	C41	1.462 (4)	C16A	C17A	1.497 (11)
C18	C22	1.428 (4)	C16A	N9A	1.488 (13)
C18	C19	1.418 (4)	C34A	C33A	1.466 (9)
C1	C5	1.442 (4)	N9A	C15A	1.498 (15)
C1	C2	1.409 (4)	N6	C33A	1.500 (9)
O18	C40	1.253 (5)	N6A	C33	1.448 (15)
C22	C21	1.411 (4)	N6A	C32	1.478 (14)

C22	C27	1.412 (4)	C33	C34	1.504 (15)
C21	C30	1.392 (4)	C34	N5	1.459 (16)
C19	C20	1.380 (4)	O19	S0	1.454 (9)
C19	C23	1.496 (4)	O20	S0	1.505 (11)
C4	C13	1.396 (4)	O21	S0	1.69 (3)

6.4.3 X-ray crystal structure bond angles

A	B	C	D	Angle/°	A	B	C	D	Angle/°
Fe1	O1	C1	C5	162.15 (19)	C30	C29	N5	C34	23.3 (13)
Fe1	O1	C1	C2	-20.1 (4)	C12	N8	C14	C15	-117.7 (5)
Fe1	O2	C6	O7	-171.9 (2)	C12	N8	C17	C16	118.8 (5)
Fe1	O2	C6	C2	6.9 (4)	C12	N8	C14AC15A		-141.3 (7)
Fe2	O12	C23	O17	168.3 (2)	C12	N8	C17AC16A		142.3 (5)
Fe2	O12	C23	C19	-12.4 (4)	C3	N7	C4	C13	175.2 (3)
Fe2	O11	C18	C22	-148.4 (2)	C3	N7	C4	C5	-3.4 (4)
Fe2	O11	C18	C19	32.3 (4)	C3	N7	C7	C9	108.7 (4)
Fe2	O15	C39	C38	-145.5 (2)	C3	N7	C7	C8	39.2 (5)
Fe2	O15	C39	C35	31.8 (4)	C27	C22	C21	N4	179.7 (3)
Fe2	O14	C40	O18	160.1 (3)	C27	C22	C21	C30	-1.1 (4)
Fe2	O14	C40	C35	-21.2 (5)	C27	C28	C29	C30	0.2 (6)
Fe2	O16	S0	O19	78.1 (13)	C27	C28	C29	N5A	168.4 (4)
Fe2	O16	S0	O20	-161.6 (12)	C27	C28	C29	N5	-159.4 (7)
Fe2	O16	S0	O21	-47.0 (14)	C24	N4	C21	C22	175.4 (3)
F3	C46	C47	C38	-175.7 (3)	C24	N4	C21	C30	-3.7 (4)
F3	C46	C45	N2	1.2 (5)	C24	N4	C20	C19	-176.8 (3)
F3	C46	C45	C44	176.0 (3)	C2	C1	C5	C4	0.6 (4)
F2	C28	C29	C30	-175.9 (3)	C2	C1	C5	C10	-179.5 (3)
F2	C28	C29	N5A	-7.7 (6)	C28	C29	N5	C31	37.1 (13)
F2	C28	C29	N5	24.5 (8)	C28	C29	N5	C34	-177.9 (8)
O1	C1	C5	C4	178.5 (3)	N5A	C31AC32A	N6		-60.0 (6)
O1	C1	C5	C10	-1.6 (4)	N5A	C34AC33A	N6		57.6 (7)
O1	C1	C2	C6	0.3 (5)	C38	C37	C44	C45	1.5 (5)
O1	C1	C2	C3	-179.2 (3)	C38	C39	C35	C36	-5.7 (5)
O2	C6	C2	C1	6.8 (4)	C38	C39	C35	C40	174.3 (3)
O2	C6	C2	C3	-173.8 (3)	C46	C45	C44	C37	-0.7 (5)

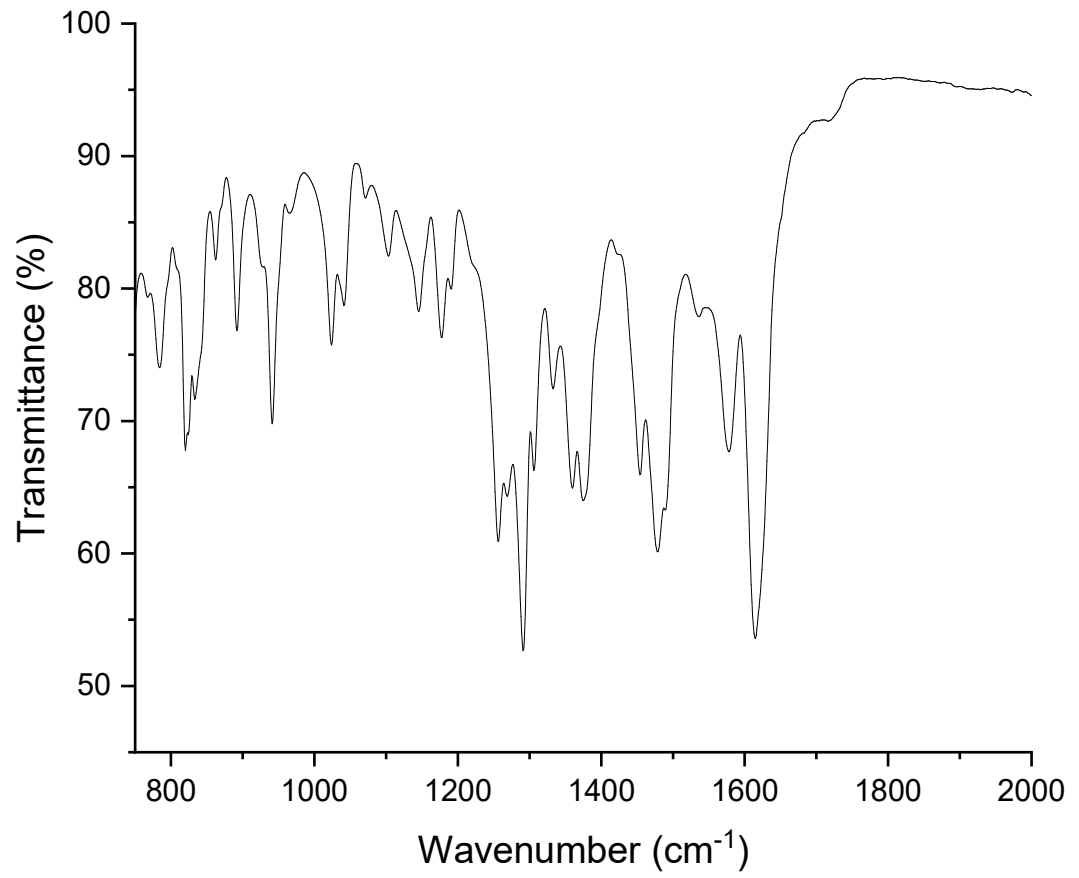
O11	C18	C22	C21	-178.0(3)	C47	C38	C37	N1	179.2(3)
O11	C18	C22	C27	2.3(4)	C47	C38	C37	C44	-1.1(5)
O11	C18	C19	C20	176.6(3)	C47	C38	C39	O15	4.8(5)
O11	C18	C19	C23	-1.1(5)	C47	C38	C39	C35	-172.7(3)
O15	C39	C35	C36	177.0(3)	C47	C46	C45	N2	-175.4(3)
O15	C39	C35	C40	-3.0(5)	C47	C46	C45	C44	-0.5(5)
O7	C6	C2	C1	-174.3(3)	C37	N1	C36	C35	4.0(5)
O7	C6	C2	C3	5.1(4)	C37	N1	C41	C43	-66.4(5)
O23	S004	O13	Fe2	-21.3(3)	C37	N1	C41	C42	-134.9(5)
N4	C21	C30	C29	-179.8(3)	C37	C38	C47	C46	-0.1(5)
N4	C24	C26	C25	-107.9(3)	C37	C38	C39	O15	179.7(3)
N4	C24	C25	C26	109.5(3)	C37	C38	C39	C35	2.3(5)
O9	S003	O3	Fe1	36.7(2)	C39	C38	C47	C46	175.1(3)
N7	C4	C13	C12	178.7(3)	C39	C38	C37	N1	4.2(5)
N7	C4	C5	C1	1.8(4)	C39	C38	C37	C44	-176.1(3)
N7	C4	C5	C10	-178.1(3)	C39	C35	C36	N1	2.8(6)
N7	C3	C2	C1	-0.3(5)	C39	C35	C40	O14	-4.5(5)
N7	C3	C2	C6	-179.8(3)	C39	C35	C40	O18	174.2(4)
N7	C7	C9	C8	-110.1(3)	O19A	S005	O16	Fe2	109.3(8)
N7	C7	C8	C9	106.9(4)	C7	N7	C4	C13	-4.0(4)
O10	S003	O3	Fe1	157.56(19)	C7	N7	C4	C5	177.4(3)
O8	S003	O3	Fe1	-82.2(2)	C7	N7	C3	C2	-178.1(3)
O22	S004	O13	Fe2	101.0(2)	C45	N2	C48	C49	-155.5(4)
N8	C12	C11	F1	1.7(5)	C45	N2	C51	C50	152.7(3)
N8	C12	C11	C10	-177.2(3)	C45	C46	C47	C38	0.9(5)
N8	C14	C15	N9	-59.6(6)	C29	N5A	C31A	C32A	-86.1(6)
N8	C17	C16	N9	59.3(7)	C29	N5A	C34A	C33A	86.6(6)
N8	C14A	C15A	N9A	-50.6(11)	C36	N1	C37	C38	-7.3(5)
O24	S004	O13	Fe2	-139.0(2)	C36	N1	C37	C44	173.0(3)

O21AS005	O16	Fe2	-7.4 (13)	C36	N1	C41	C43	117.7 (4)	
N1	C37	C44	C45	-178.8 (3)	C36	N1	C41	C42	49.3 (6)
N1	C41	C43	C42	-106.7 (4)	C36	C35	C40	O14	175.5 (3)
N1	C41	C42	C43	108.9 (5)	C36	C35	C40	O18	-5.8 (6)
C18	C22	C21	N4	0.0 (4)	C40	C35	C36	N1	-177.1 (3)
C18	C22	C21	C30	179.2 (3)	O20AS005	O16	Fe2	-130.5 (8)	
C18	C22	C27	C28	-179.5 (3)	C48	N2	C45	C46	163.9 (3)
C18	C19	C20	N4	2.8 (5)	C48	N2	C45	C44	-10.6 (6)
C18	C19	C23	O12	-10.8 (5)	C48	N2	C51	C50	-63.8 (4)
C18	C19	C23	O17	168.6 (3)	C51	N2	C45	C46	-55.7 (5)
C1	C5	C10	C11	179.0 (3)	C51	N2	C45	C44	129.8 (4)
C22	C18	C19	C20	-2.7 (4)	C51	N2	C48	C49	61.3 (4)
C22	C18	C19	C23	179.6 (3)	C50	N3	C49	C48	54.2 (5)
C22	C21	C30	C29	1.0 (5)	C41	N1	C37	C38	176.9 (3)
C22	C27	C28	F2	175.7 (3)	C41	N1	C37	C44	-2.8 (5)
C22	C27	C28	C29	-0.4 (5)	C41	N1	C36	C35	179.9 (4)
C21	N4	C20	C19	-1.4 (5)	C49	N3	C50	C51	-55.0 (5)
C21	N4	C24	C26	146.2 (3)	C31A	N5A	C29	C30	-1.3 (7)
C21	N4	C24	C25	76.3 (4)	C31A	N5A	C29	C28	-168.7 (4)
C21	C22	C27	C28	0.8 (5)	C31A	N5A	C34A	C33A	-58.8 (6)
C21	C30	C29	C28	-0.5 (5)	C31A	C32A	N6	C33A	59.2 (7)
C21	C30	C29	N5A	-168.5 (4)	C32A	N6	C33A	C34A	-58.6 (7)
C21	C30	C29	N5	159.5 (7)	C14	N8	C12	C13	17.4 (6)
C19	C18	C22	C21	1.4 (4)	C14	N8	C12	C11	-163.3 (4)
C19	C18	C22	C27	-178.3 (3)	C14	N8	C17	C16	-60.9 (6)
C4	N7	C3	C2	2.8 (4)	C14	C15	N9	C16	57.5 (7)
C4	N7	C7	C9	-72.2 (4)	C17	N8	C12	C13	-162.3 (4)
C4	N7	C7	C8	-141.7 (3)	C17	N8	C12	C11	17.1 (6)
C4	C13	C12	N8	179.5 (3)	C17	N8	C14	C15	62.1 (6)

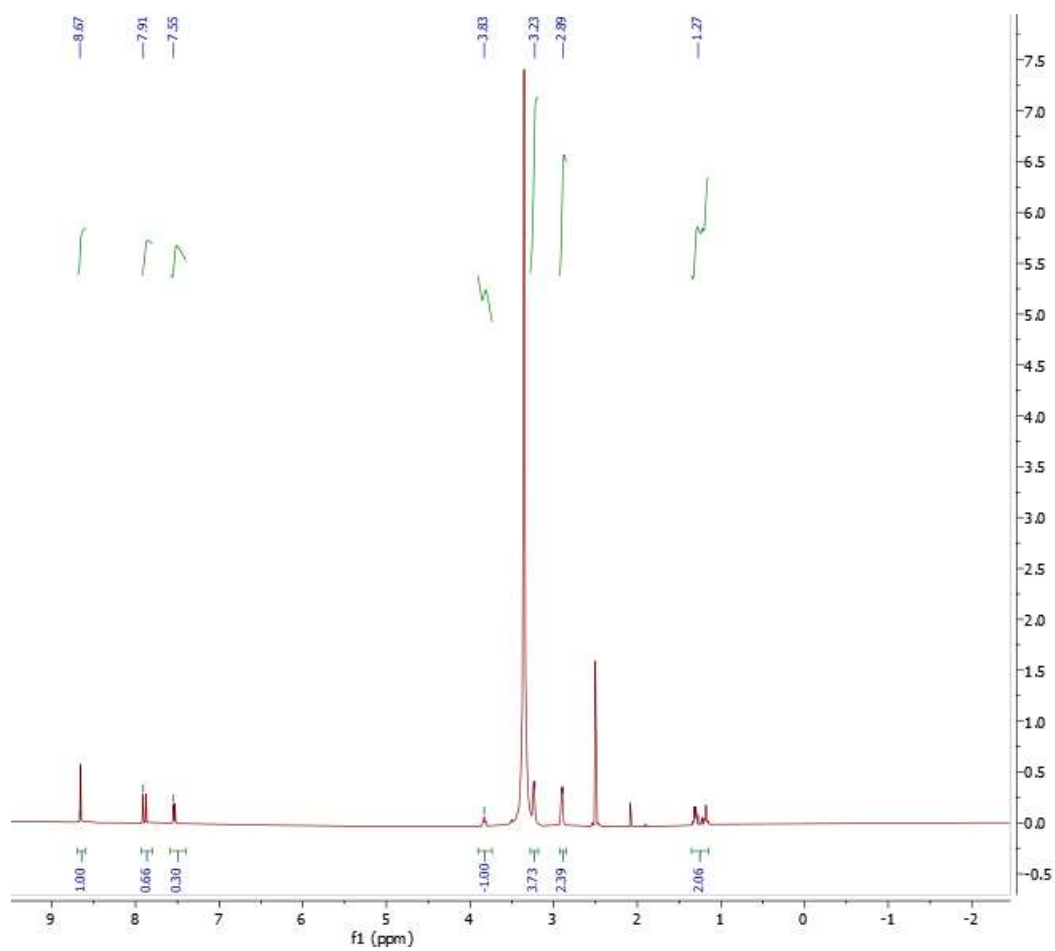
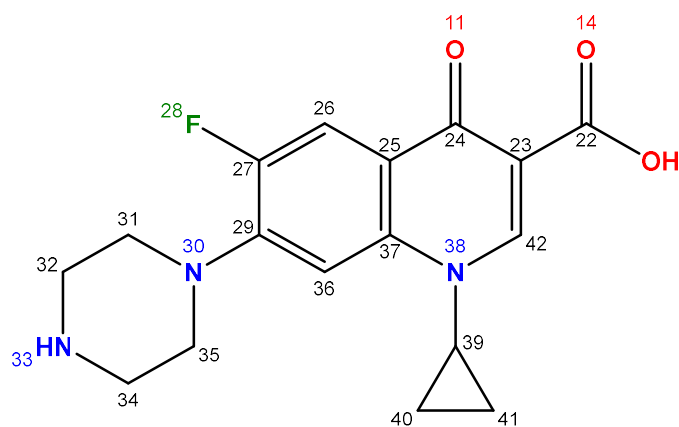
C4	C13	C12	C11	0.1 (4)	C17	C16	N9	C15	-57.4 (8)
C4	C5	C10	C11	-1.1 (4)	C14A	N8	C12	C13	-17.1 (7)
C20	N4	C21	C22	-0.1 (4)	C14A	N8	C12	C11	162.3 (6)
C20	N4	C21	C30	-179.2 (3)	C14A	N8	C17A	C16A	-55.2 (9)
C20	N4	C24	C26	-38.4 (4)	C16A	N9A	C15A	C14A	51.0 (11)
C20	N4	C24	C25	-108.2 (3)	C17A	N8	C12	C13	145.2 (6)
C20	C19	C23	O12	171.5 (3)	C17A	N8	C12	C11	-35.4 (7)
C20	C19	C23	O17	-9.2 (5)	C17A	N8	C14A	C15A	55.2 (10)
C13	C4	C5	C1	-176.8 (3)	C17A	C16A	N9A	C15A	-51.6 (10)
C13	C4	C5	C10	3.3 (4)	C34A	N5A	C29	C30	-143.8 (5)
C13	C12	C11	F1	-178.9 (3)	C34A	N5A	C29	C28	48.8 (7)
C13	C12	C11	C10	2.2 (5)	C34A	N5A	C31A	C32A	60.0 (6)
C5	C1	C2	C6	178.1 (3)	N9A	C16A	C17A	N8	52.6 (9)
C5	C1	C2	C3	-1.3 (4)	N6A	C33	C34	N5	55.9 (13)
C5	C4	C13	C12	-2.8 (4)	C33	N6A	C32	C31	52.9 (13)
C5	C10	C11	F1	179.4 (3)	C33	C34	N5	C29	153.8 (10)
C5	C10	C11	C12	-1.7 (5)	C33	C34	N5	C31	-57.3 (14)
N2	C45	C44	C37	173.9 (3)	C32	C31	N5	C29	-157.4 (10)
N2	C48	C49	N3	-56.0 (5)	C32	C31	N5	C34	56.5 (12)
N2	C51	C50	N3	59.1 (4)	C32	N6A	C33	C34	-54.4 (13)
C23	C19	C20	N4	-179.3 (3)	N5	C31	C32	N6A	-53.1 (13)
C30	C29	N5	C31	-121.7 (10)					

6.5 1:3 bismuth(III)-ciprofloxacin

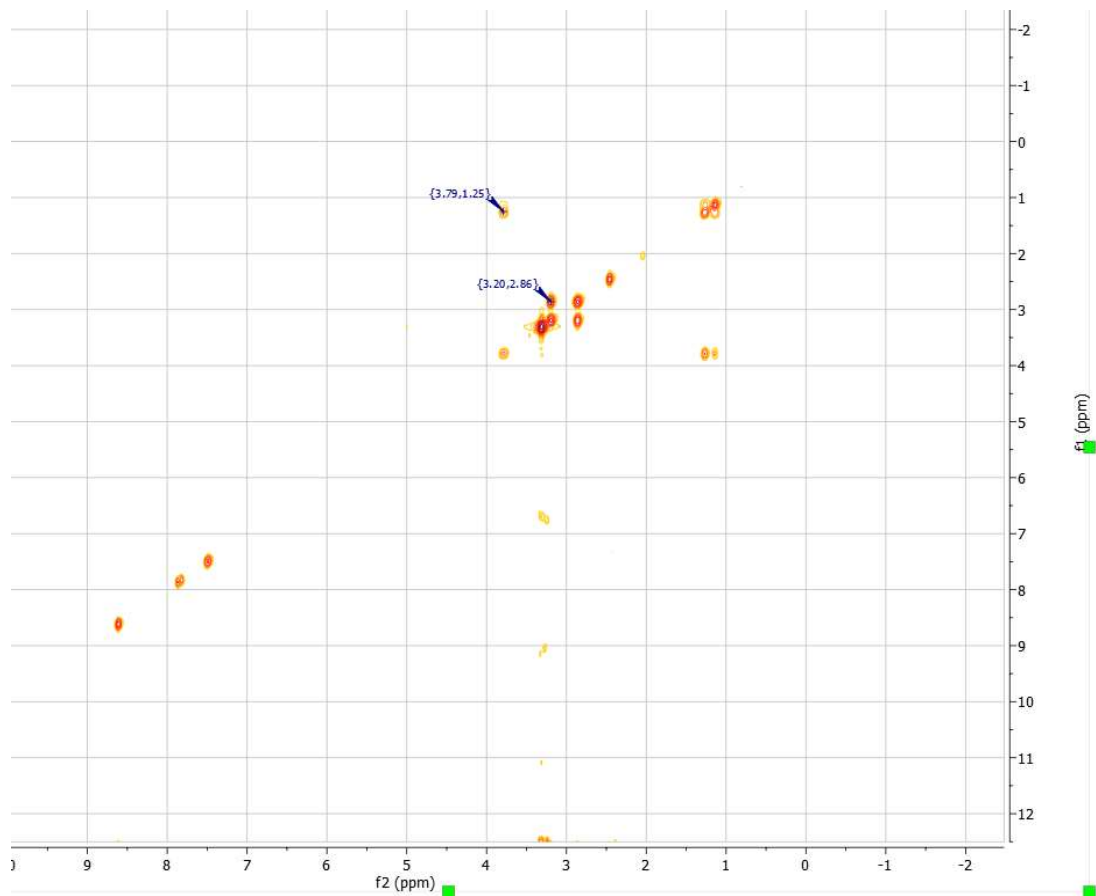
6.5.1 FTIR



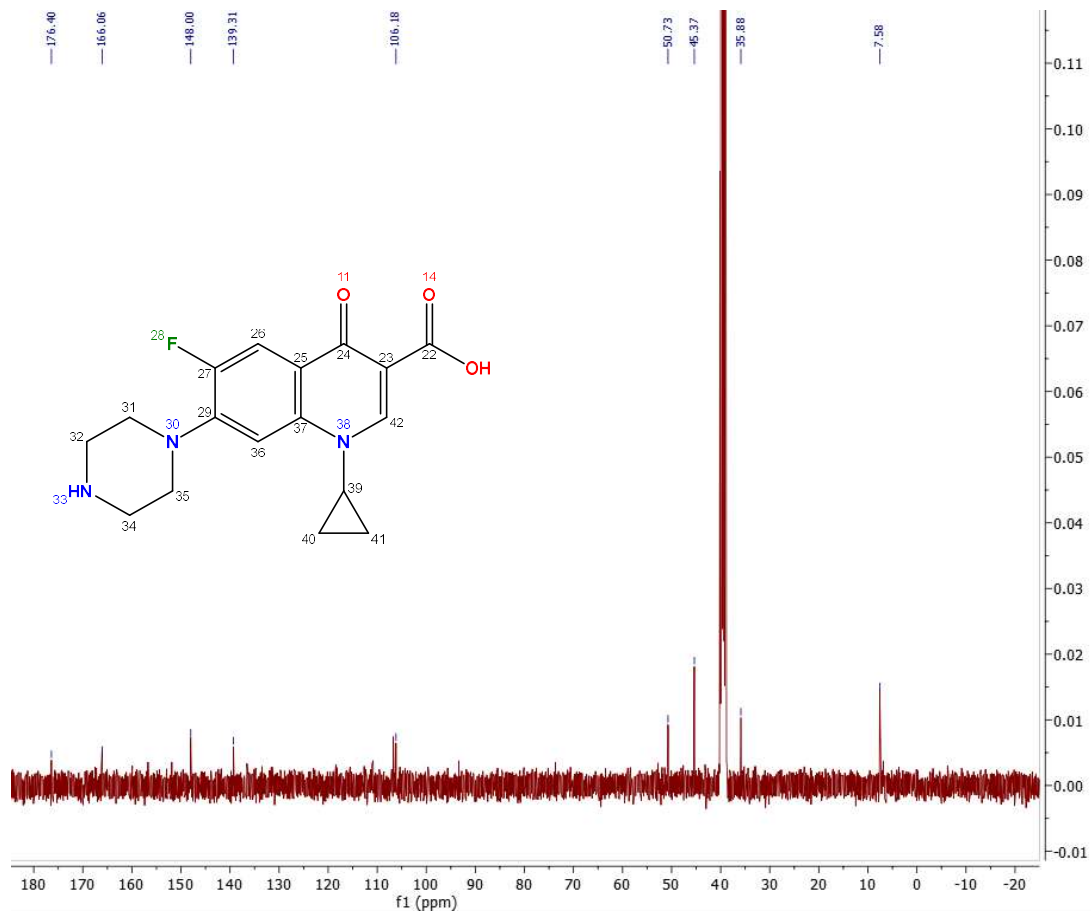
6.5.2 ^1H NMR



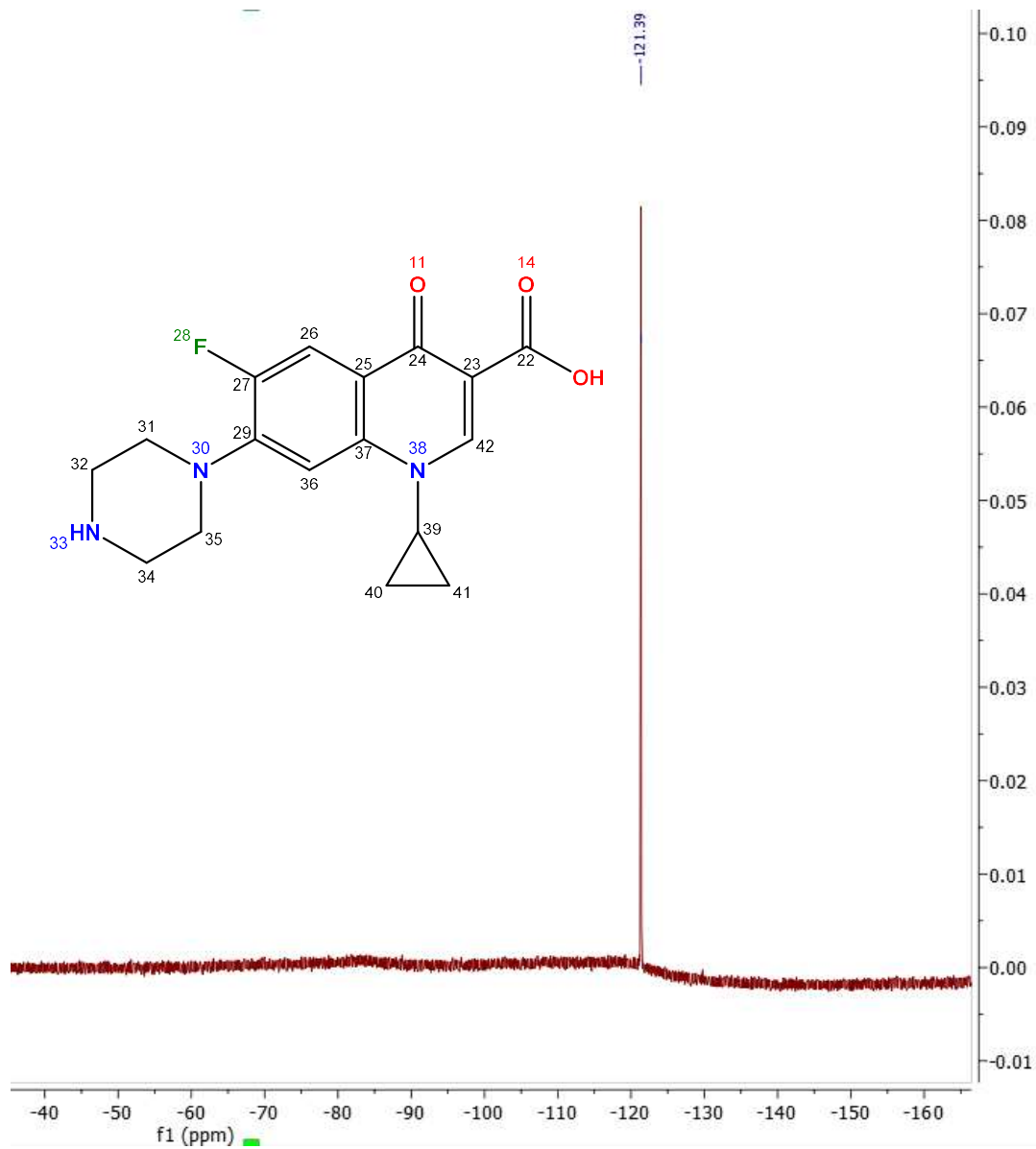
6.5.3 COSY



6.5.4 ^{13}C NMR

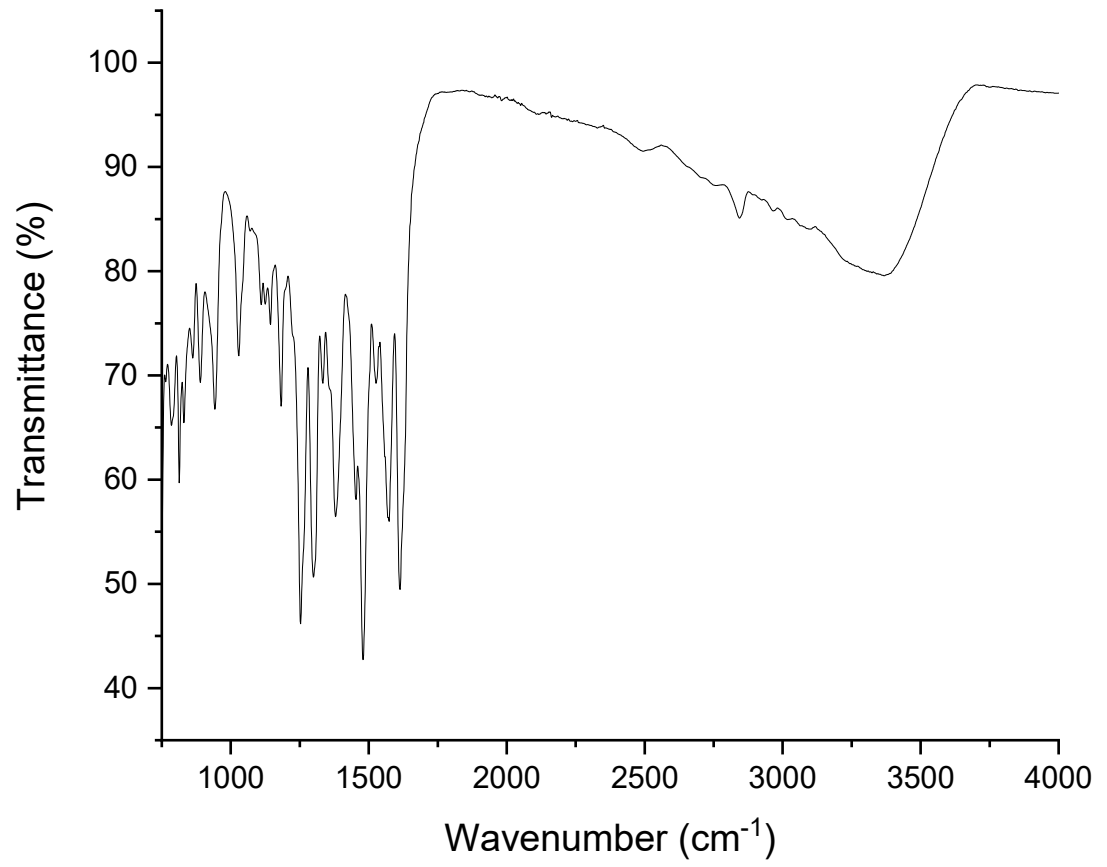


6.5.5 ^{19}F NMR

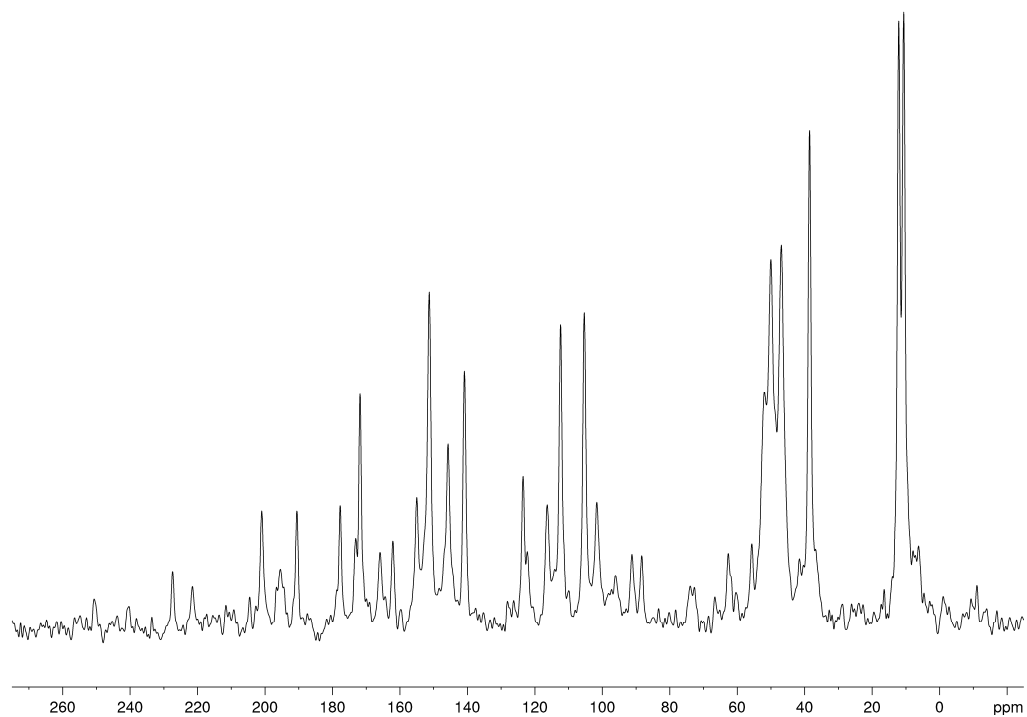


6.6 1:2 zinc(II)-ciprofloxacin

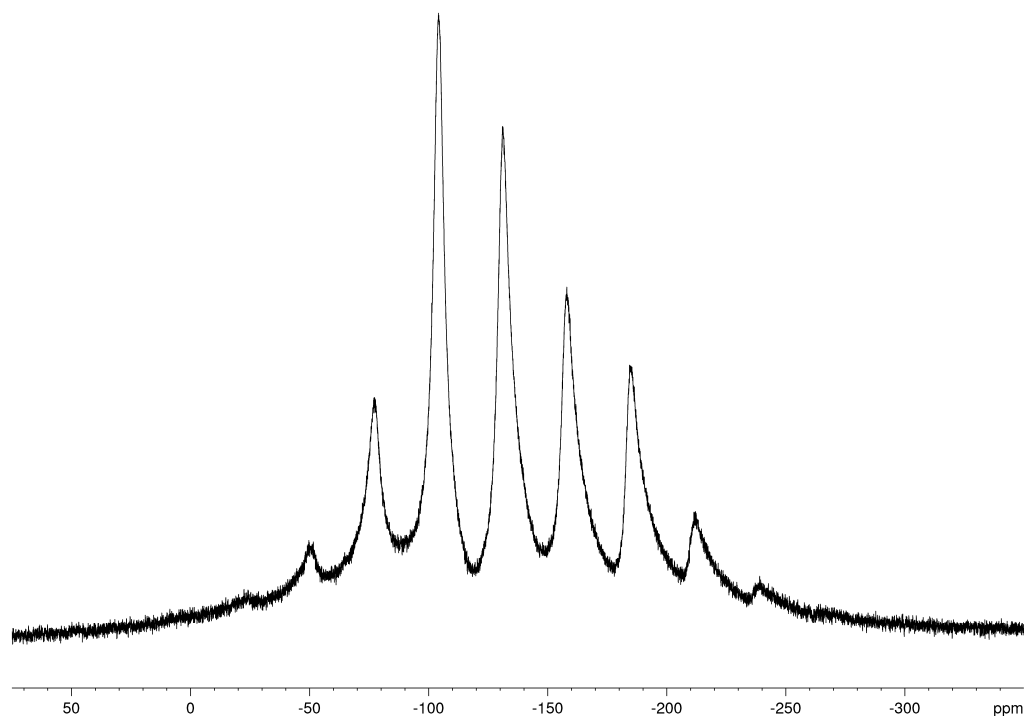
6.6.1 FTIR



6.6.2 ^{13}C ssNMR

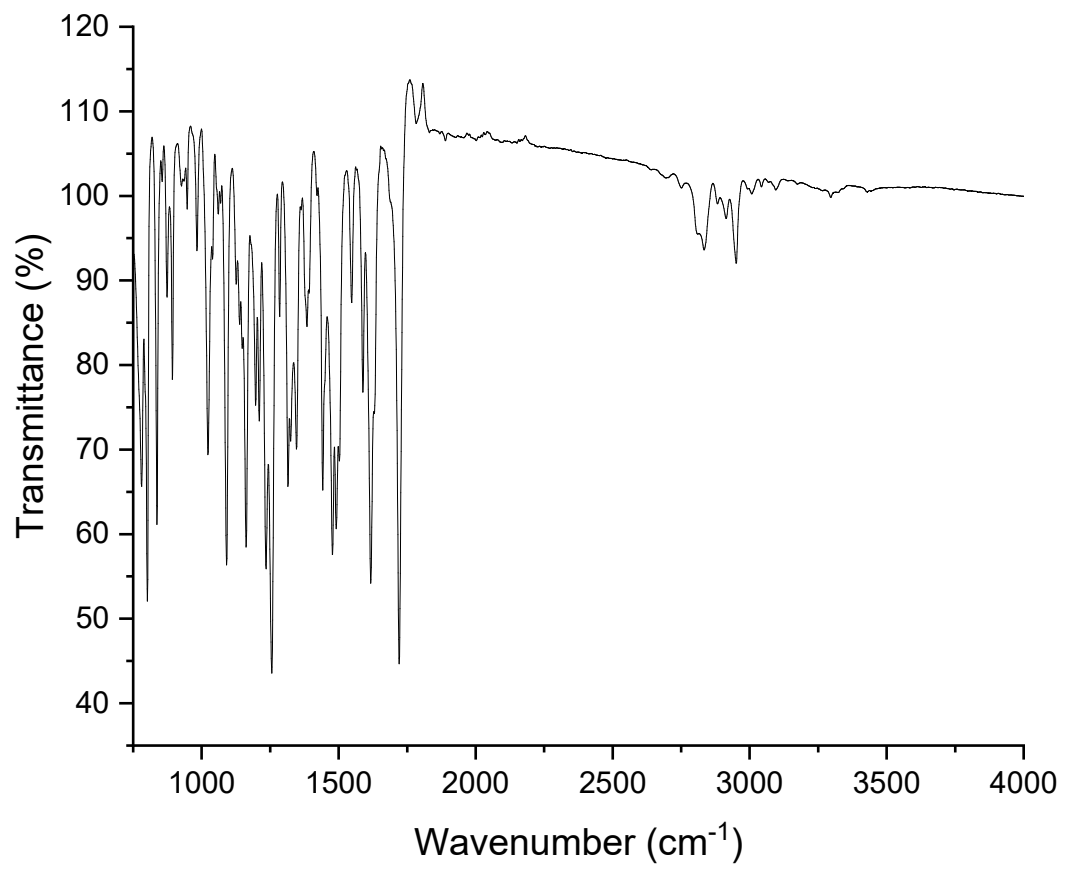


6.6.3 ^{19}F ssNMR

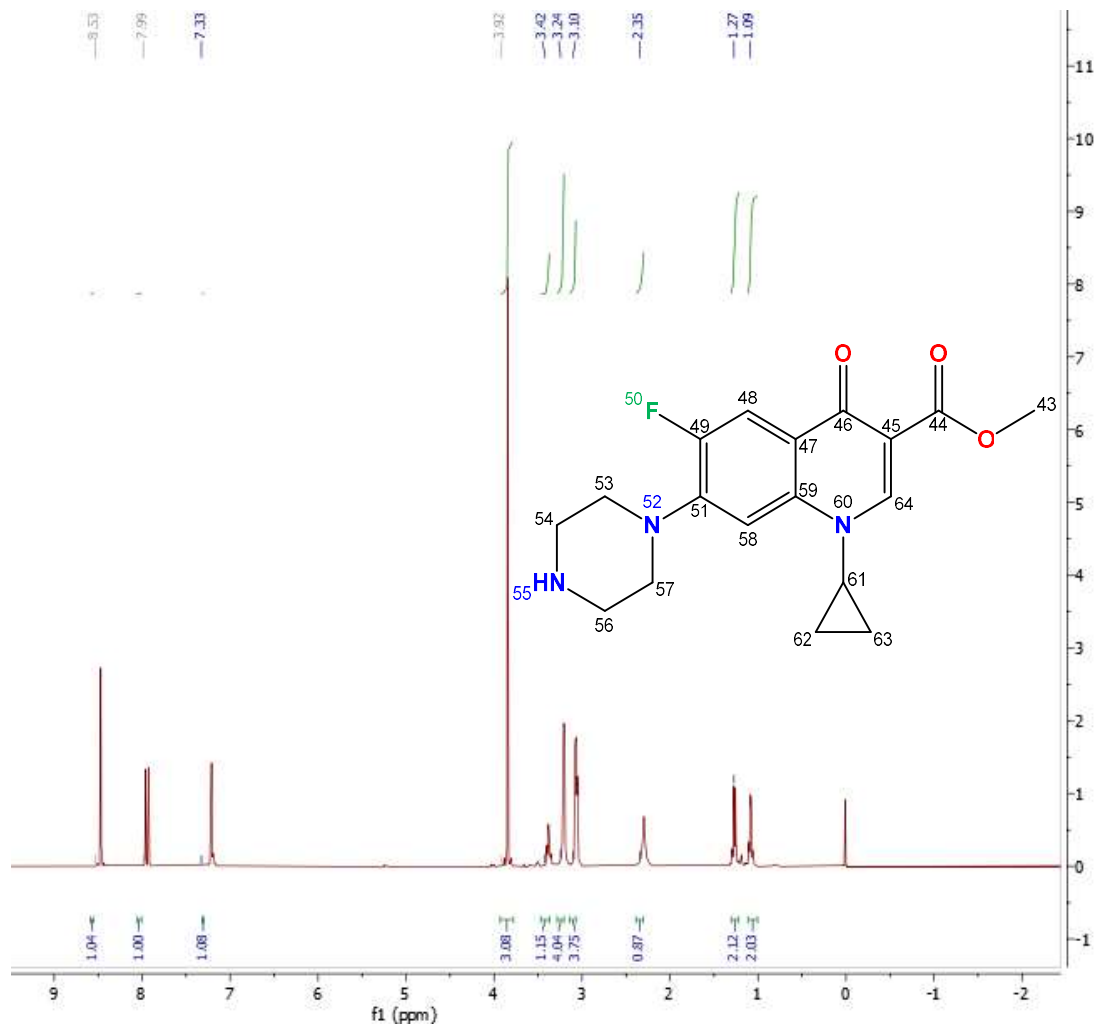


6.7 Ciprofloxacin methyl ester

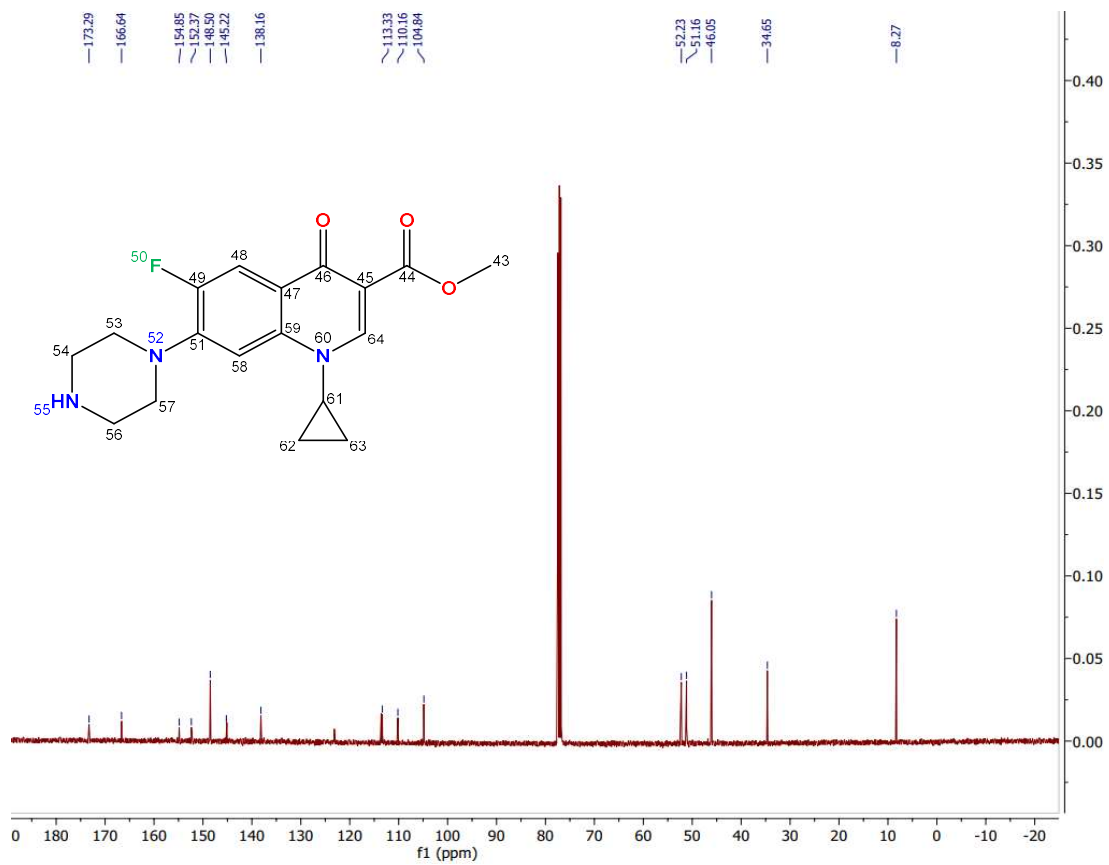
6.7.1 FTIR



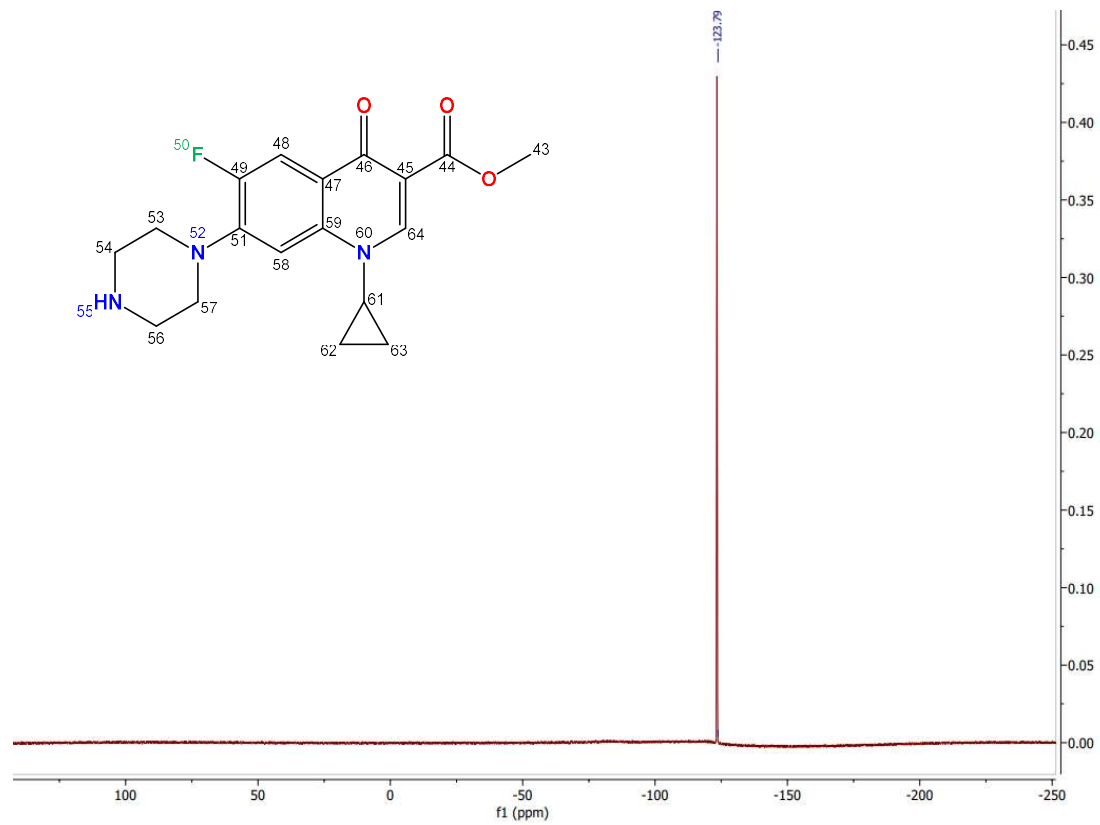
6.7.2 ^1H NMR



6.7.3 ^{13}C NMR



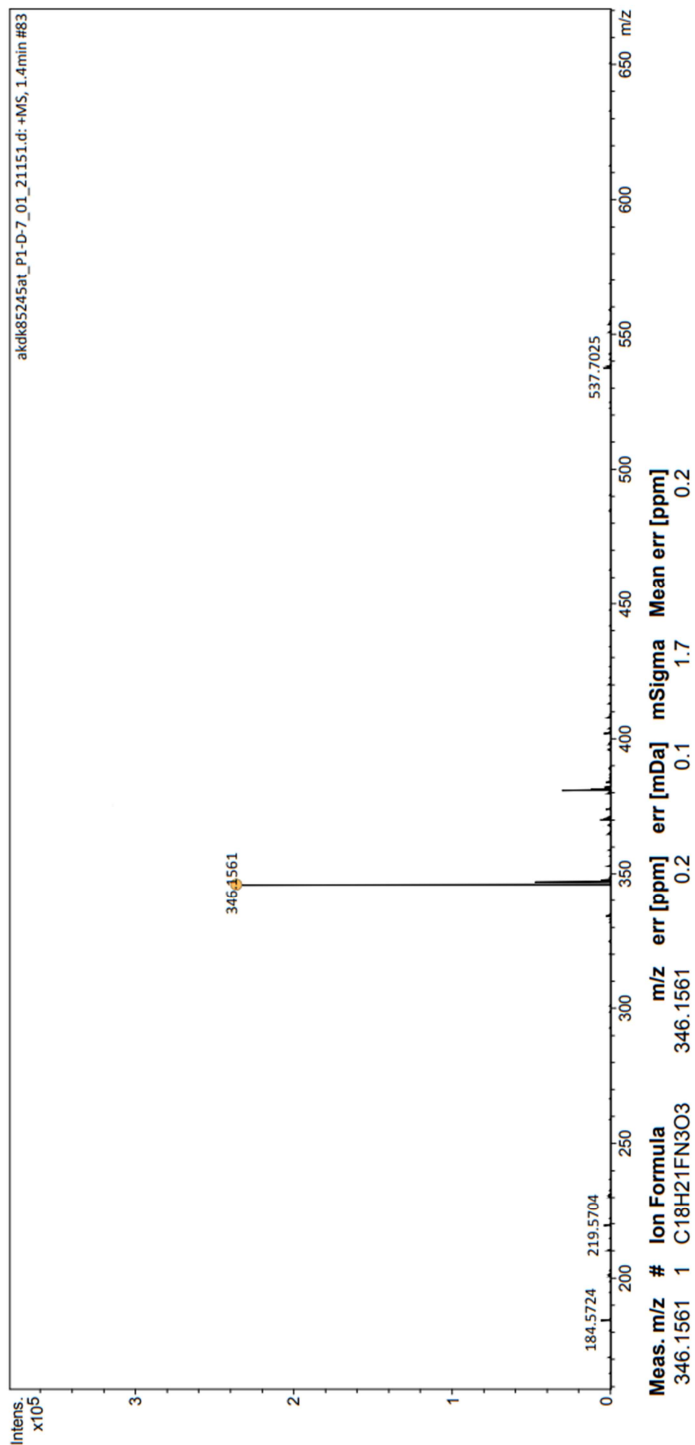
6.7.4 ^{19}F NMR



6.7.5 mass spectrometry

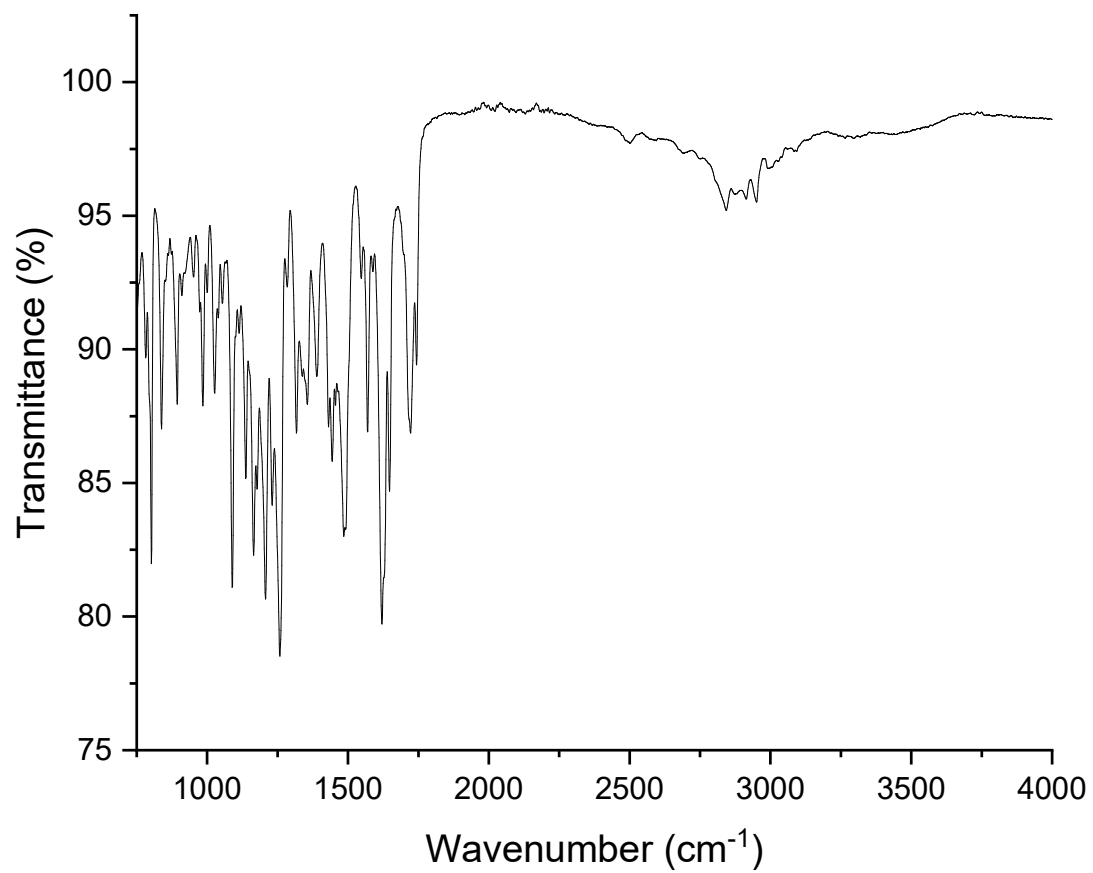
Analysis Information

Analysis Filename akdk85245at_P1-D-7_01_21151.d Acquisition Date 18/09/2020 12:56:28
Method ESI_low mass_2c1s.m Instrument compact
Submission Name akdk85245at Positive

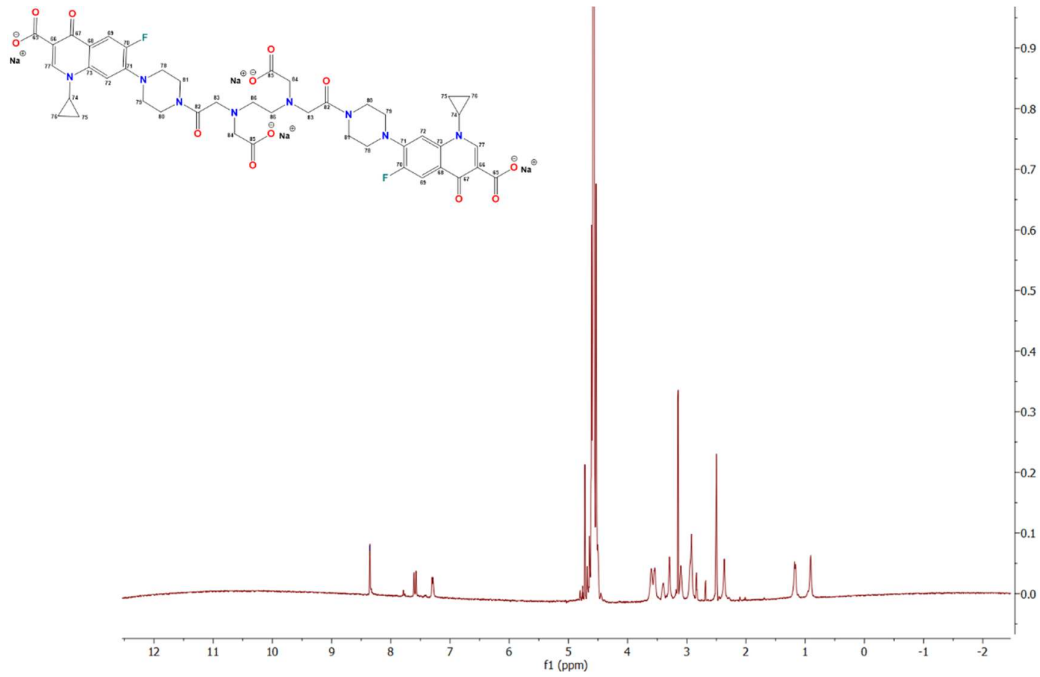


6.8 EDTA-ciprofloxacin dimer sodium salt

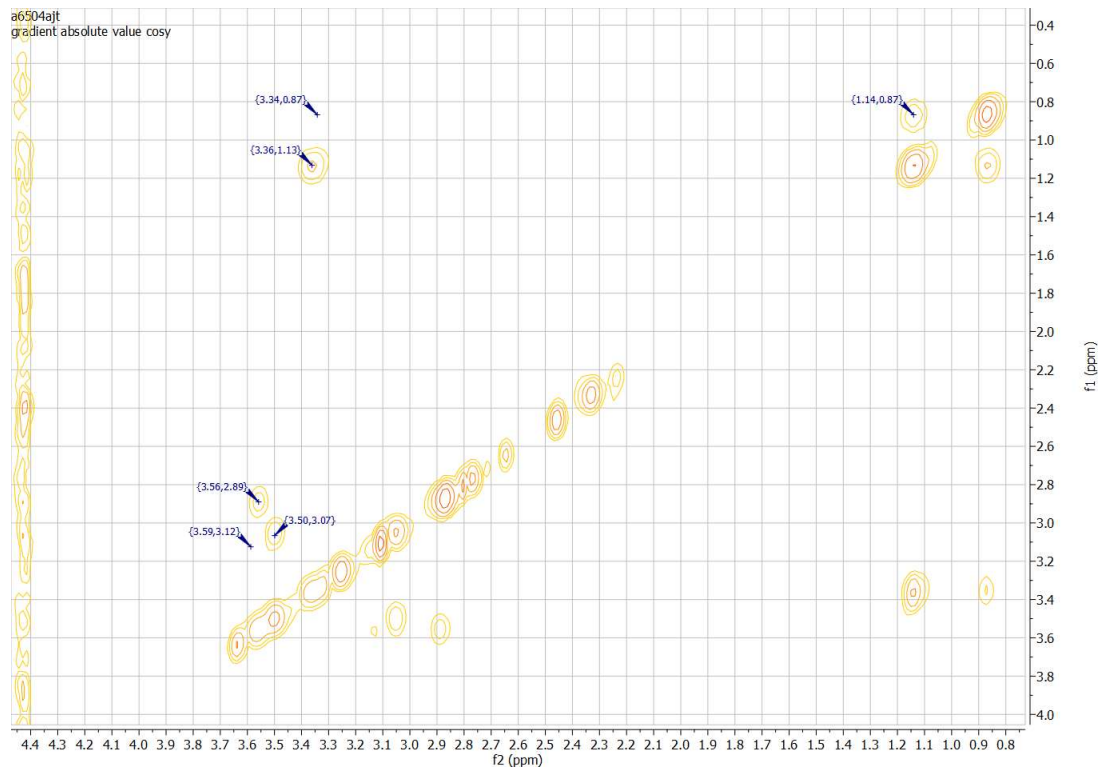
6.8.1 FTIR



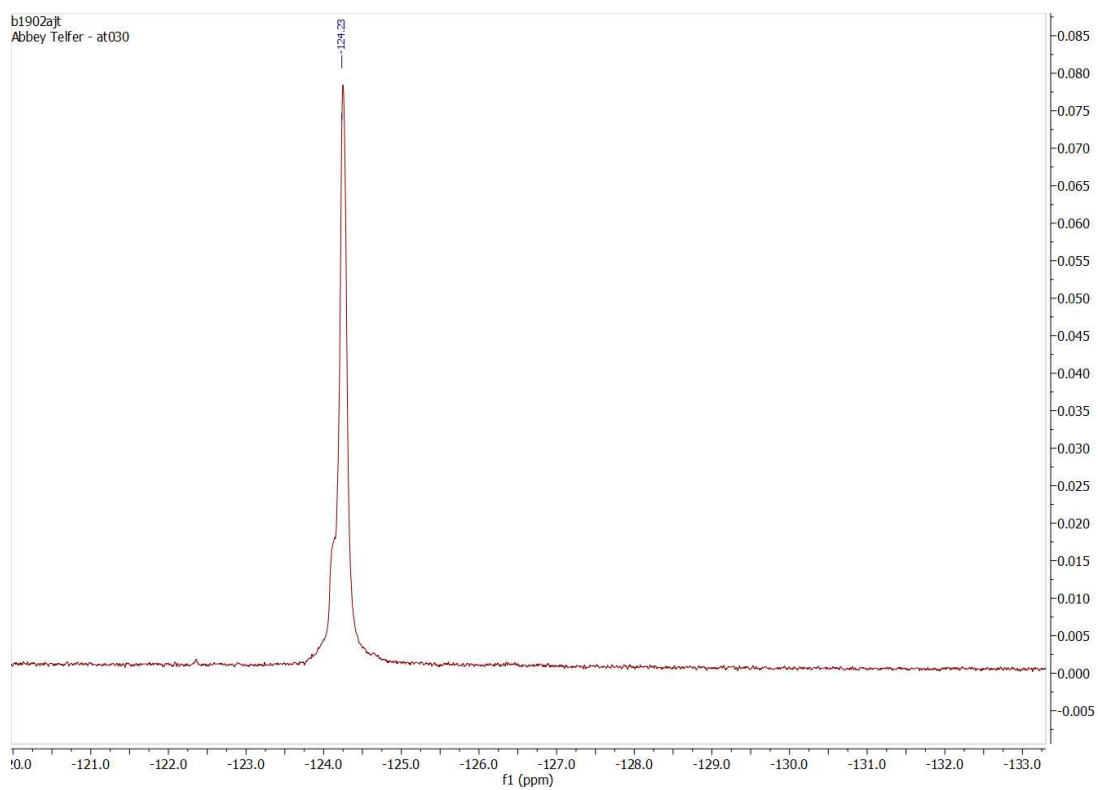
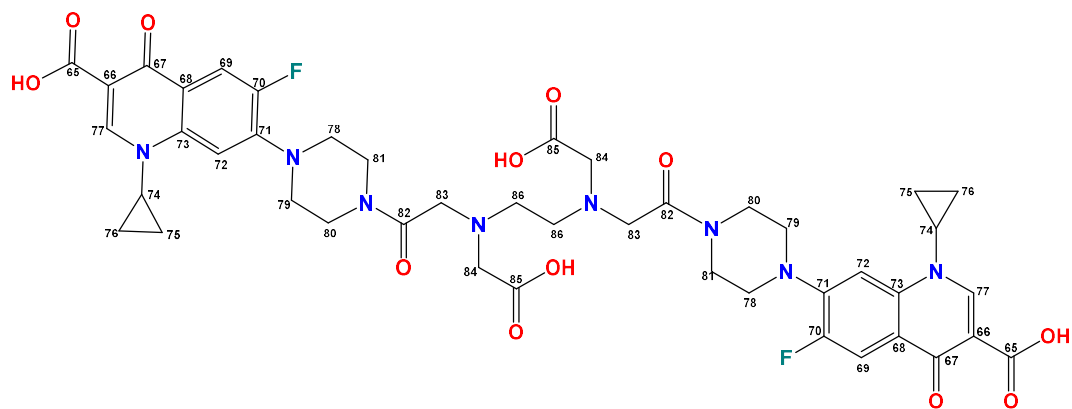
6.8.4 ^1H NMR



6.8.3 COSY

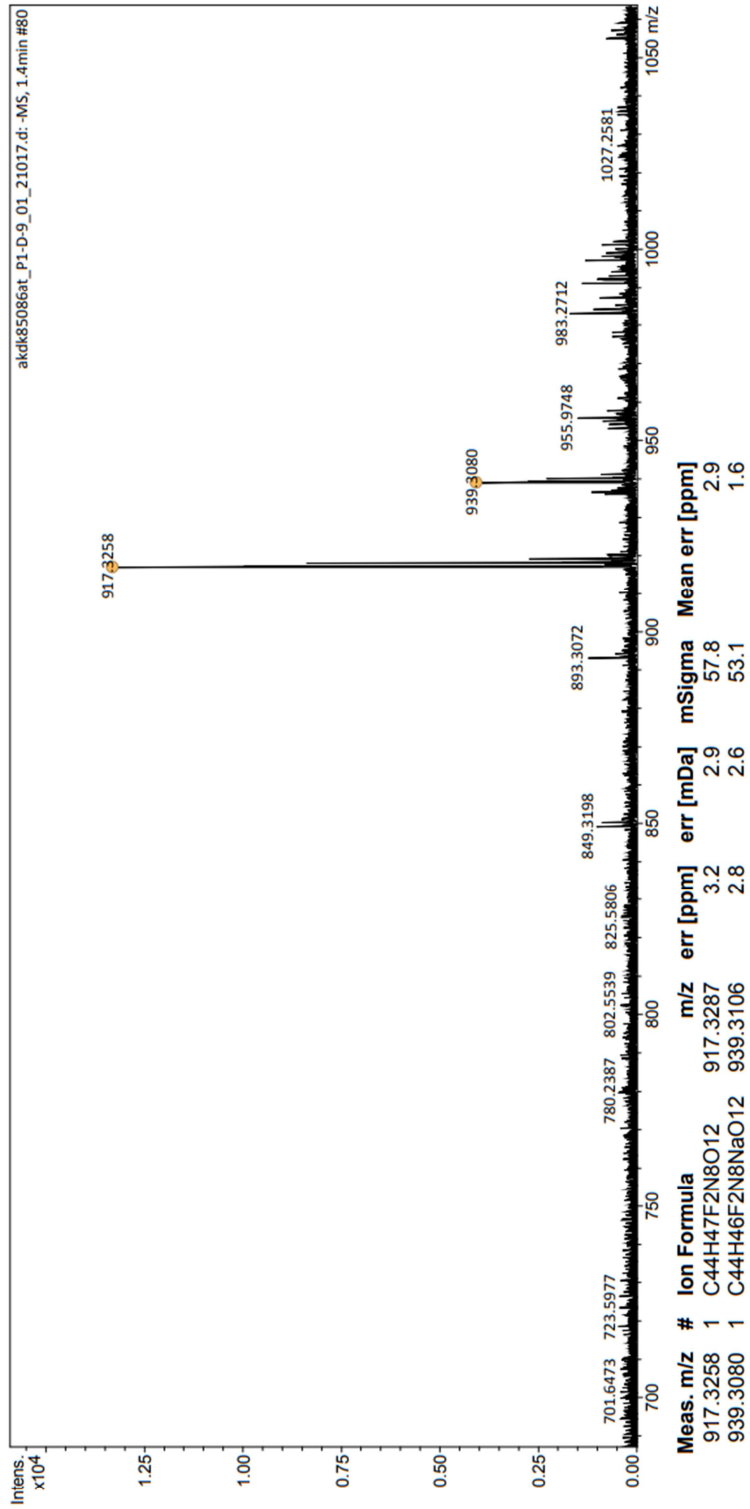


6.8.4 ^{19}F NMR



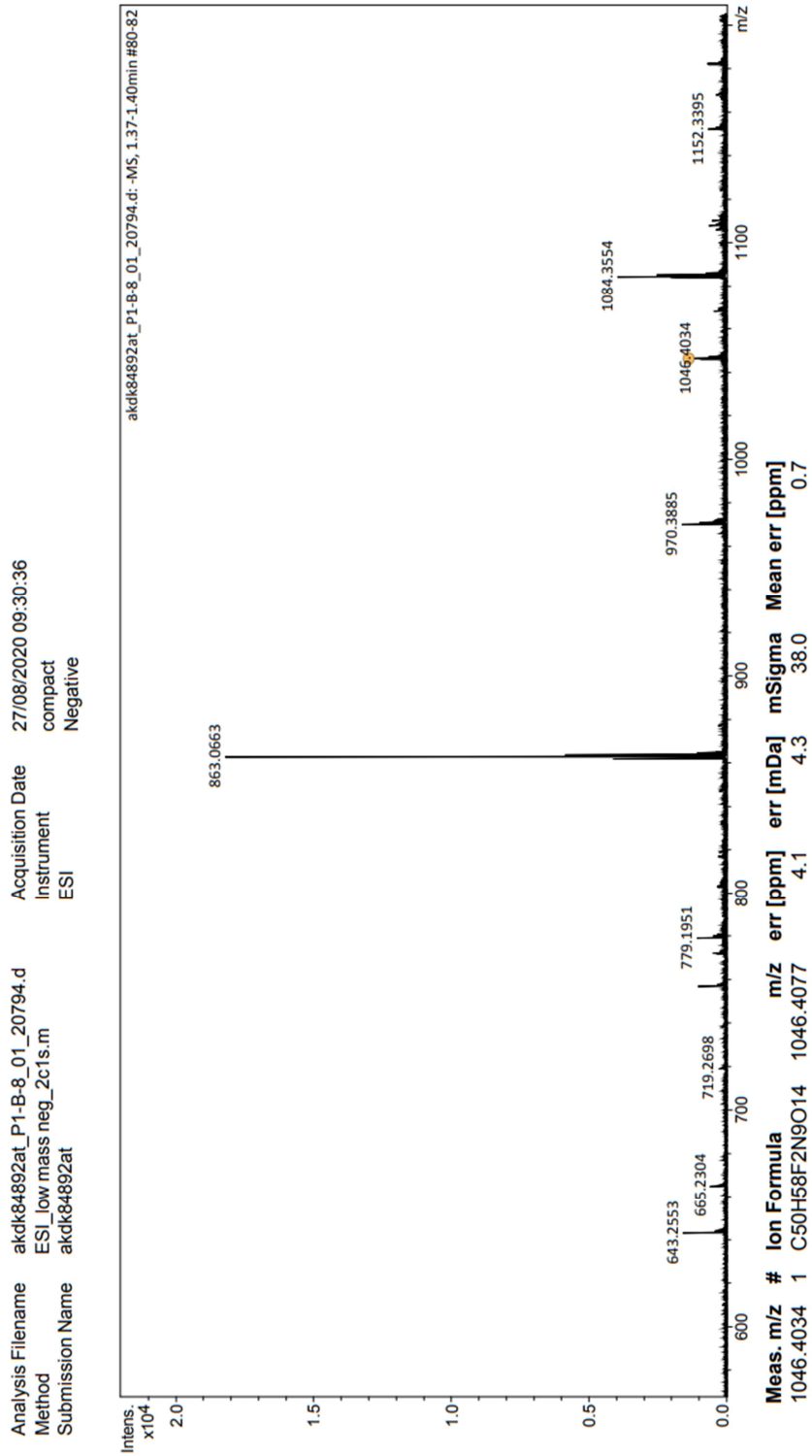
6.8.4 mass spectrometry

Analysis Filename akdk85086at_P1-D-9_01_21017.d
 Method ESI_low mass neg_2c1s.m
 Submission Name akdk85086at
 Acquisition Date 09/09/2020 12:16:53
 Instrument compact
 ESI Negative



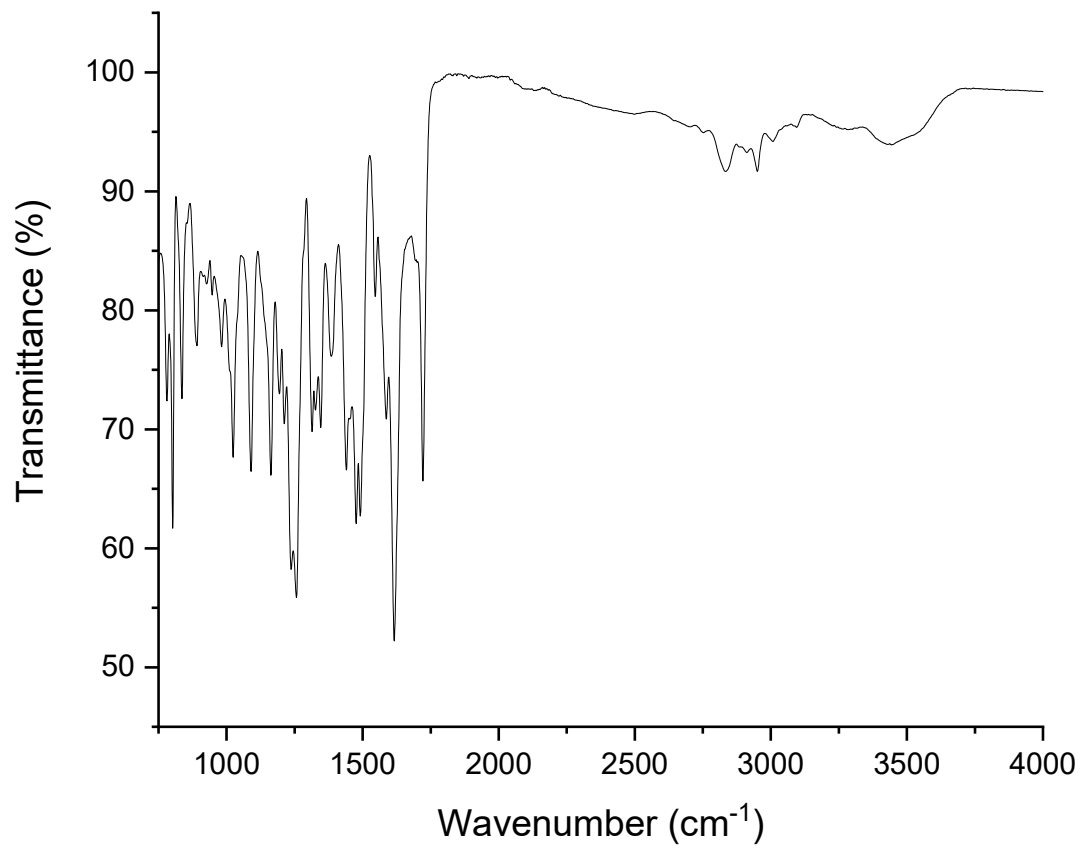
6.9 DTPA-ciprofloxacin methyl ester dimer

6.9.1 mass spectrometry

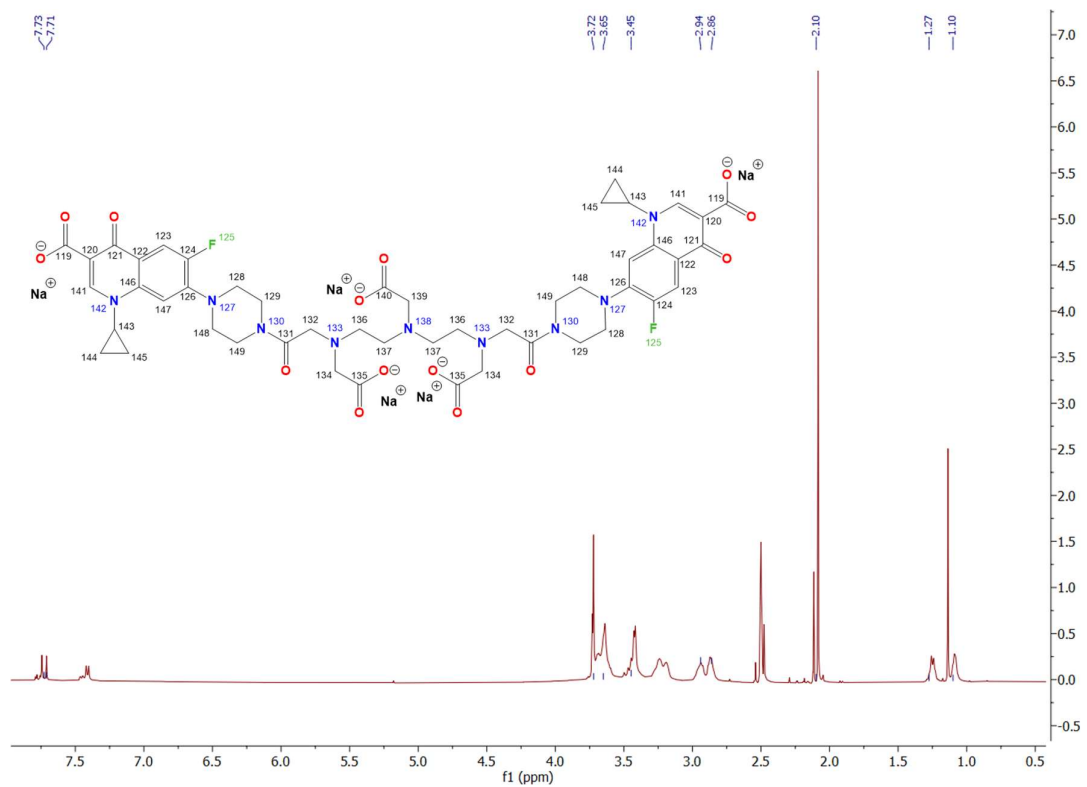


6.10 DTPA-ciprofloxacin dimer sodium salt

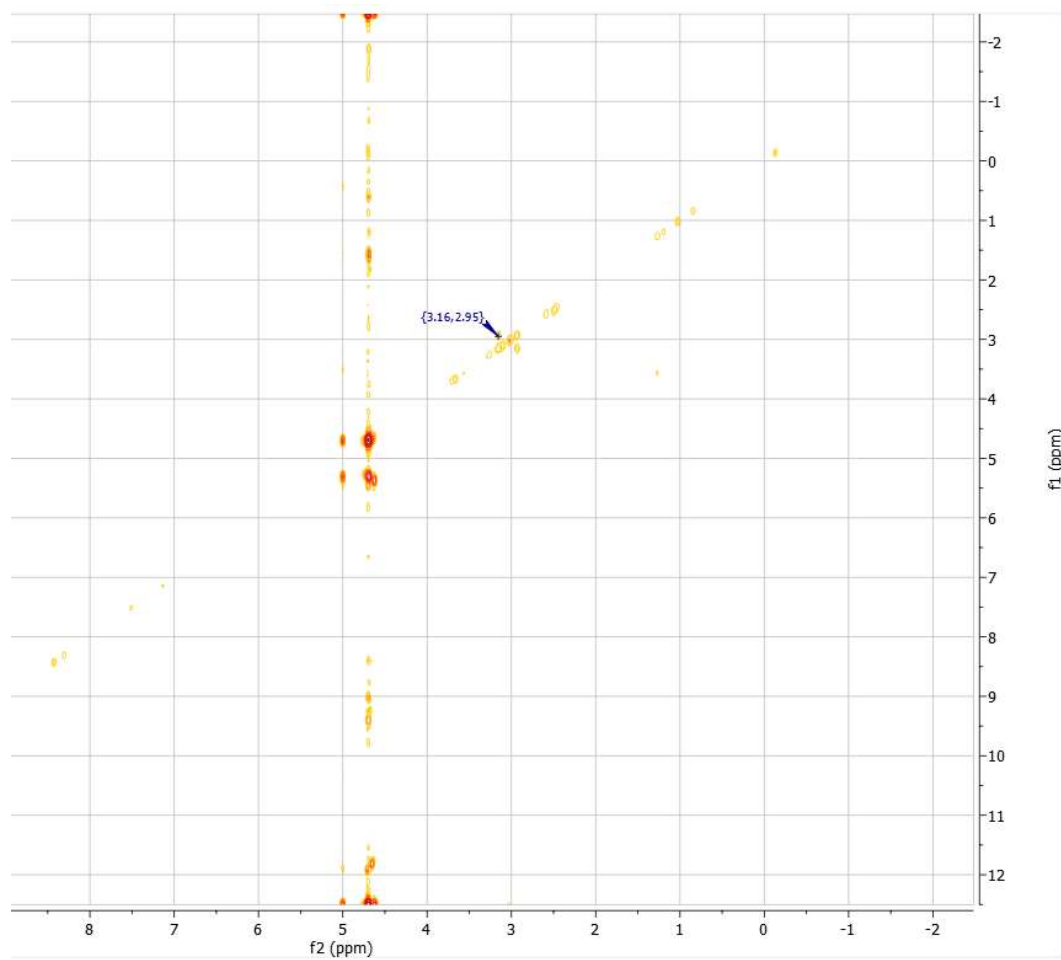
6.10.1 FTIR



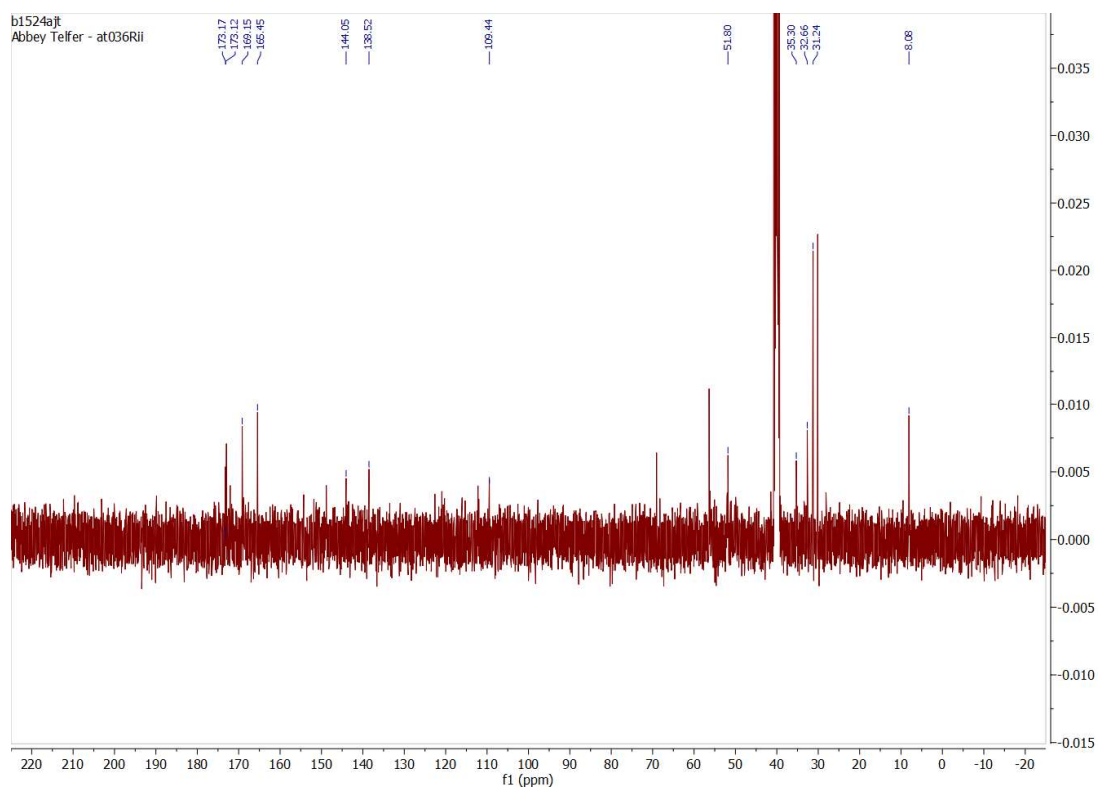
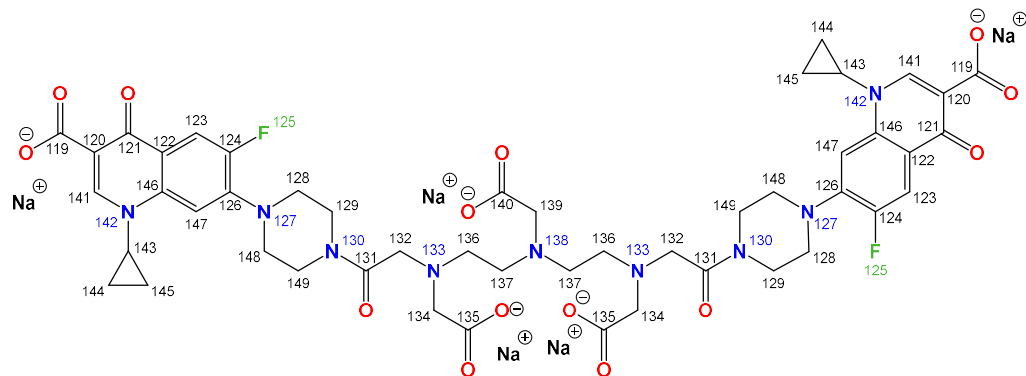
6.10.2 ^1H NMR



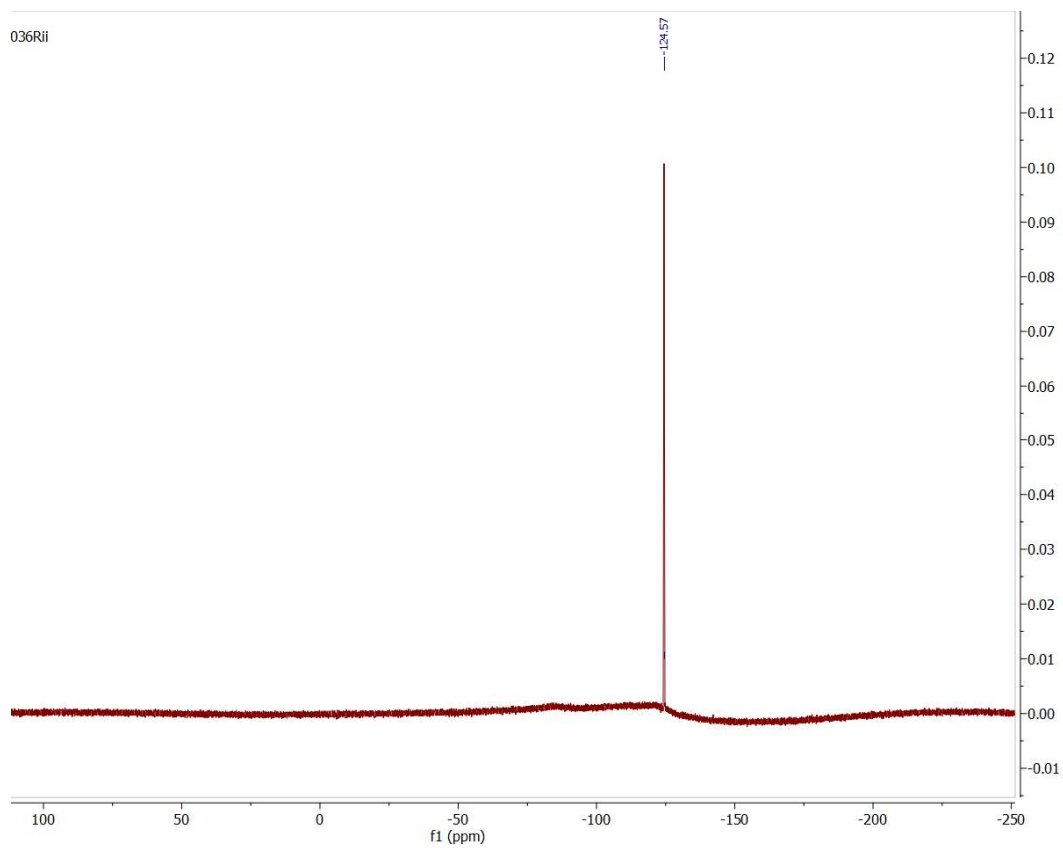
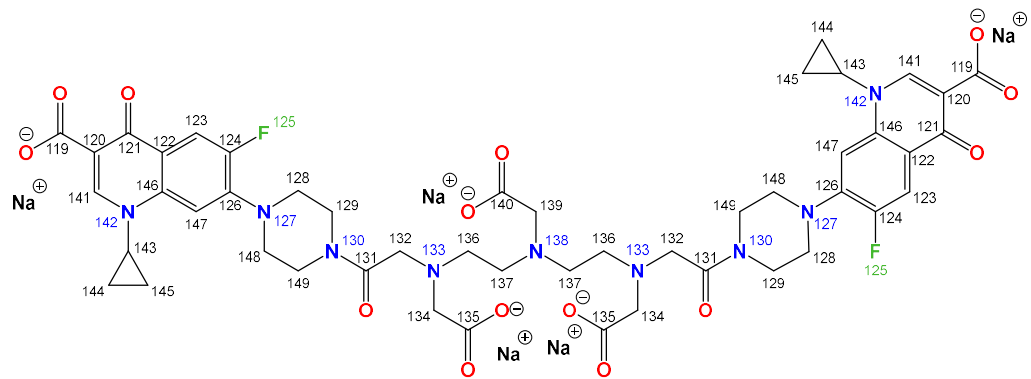
6.10.3 COSY



6.10.4 ^{13}C NMR



6.10.5 ^{19}F NMR



References

- 1 The European Centre for Disease Prevention and Control, *Surveillance of antimicrobial resistance in Europe*, Stockholm, 2018.
- 2 O. Guneyssel, O. Onur, M. Erdede and A. Denizbasi, *J. Emerg. Med.*, 2009, **36**, 338–341.
- 3 P. C. Sharma, A. Jain and S. Jain, *Acta Pol. Pharm.*, 2009, **66**, 587–604..
- 4 Kyorin Pharmaceutical Co Ltd. Substituted quinolinecarboxylic acid. GB:2030562, 1980.
- 5 P. C. Appelbaum and P. A. Hunter, *Int. J. Antimicrob. Agents*, 2000, **16**, 5–15.
- 6 C. M. Oliphant and G. M. Green, *Am. Fam. Physician*, 2002, **65**, 455–464.
- 7 D. E. King, R. Malone and S. H. Lilley, *Am. Fam. Physician*, 2000, **61**, 2741–2748.
- 8 World Health Organisation, ANTIMICROBIAL RESISTANCE Global Report on Surveillance, 2014.
- 9 K. Drlica, *Curr. Opin. Microbiol.*, 1999, **2**, 504–508. Drlica K.
- 10 S. M. Opal and A. Pop-Vicas, in Mandell, Douglas, and Bennett's *Principles and Practice of Infectious Diseases* (Eighth Edition), eds. J. E. Bennett, R. Dolin and M. J. Blaser, Philadelphia, 2015, pp. 235–251.e3.
- 11 J. M. Domagala, *J. Antimicrob. Chemother.*, 1994, **33**, 685–706.
- 12 G. S. Tillotson, *J. Med. Microbiol.*, 1996, **44**, 320–324.
- 13 S. C. Wallis, L. R. Gahan, B. G. Charles and T. W. Hambley, *Polyhedron*, 1995, **14**, 2835–2840.
- 14 P. Djurdjevic, I. Jakovljevic, L. Joksovic, N. Ivanovic and M. Jelkic-Stankov, *Molecules*, 2014, **19**, 12194–12223.

- 15 S. A. Sadeek, W. H. El-Shwiniy and M. S. El-Attar, *Spectrochim. Acta A Mol. Biomol. Spectrosc.*, 2011, **84**, 99–110.
- 16 V. Uivarosi, *Molecules*, 2013, **18**, 11153–11197.
- 17 F. Gao, P. Yang, J. Xie and H. Wang, *J. Inorg. Biochem.*, 1995, **60**, 61–67.
- 18 A. R. Shaikh, R. Giridhar, F. Megraud and M. R. Yadav, *Acta Pharm.*, 2009, **59**, 259–271.
- 19 A. R. Shaikh, R. Giridhar and M. R. Yadav, *Int. J. Pharm.*, 2007, **332**, 24–30.
- 20 I. Turel, I. Leban, G. Klintschar, N. Bukovec and S. Zalar, *J. Inorg. Biochem.*, 1997, **66**, 77–82.
- 21 J. R. Anaconda and C. Toledo, *Transition Met. Chem.*, 2001, **26**, 228–231.
- 22 K. D. Mjos, J. F. Cawthray, E. Polishchuk, M. J. Abrams and C. Orvig, *Dalton Trans.*, 2016, **45**, 13146–13160.
- 23 P. Fernandes, I. Sousa, L. Cunha-Silva, M. Ferreira, B. de Castro, E. F. Pereira, M. J. Feio and P. Gameiro, *J. Inorg. Biochem.*, 2014, **131**, 21–29.
- 24 M. Vincent, R. E. Duval, P. Hartemann and M. Engels-Deutsch, *J. Appl. Microbiol.*, 2018, **124**, 1032–1046.
- 25 B. Urbaniak, Y. Mrestani, Z. J. Kokot and R. H. H. Neubert, *Chromatographia*, 2007, **65**, 489–492.
- 26 T.-L. Ho, *Chem. Rev.*, 1975, **75**, 1–20.
- 27 S. C. Wallis, B. G. Charles, L. R. Gahan, L. J. Filippich, M. G. Bredhauer and P. A. Duckworth, *J. Pharm. Sci.*, 1996, **85**, 803–809.
- 28 W. Vincent, S. Schulman, J. Midgley, W. van Oort and R. Sorel, *International Journal of Pharmaceutics*, 1981, **9**, 191–198.
- 29 K. Timmers and R. Sternglanz, *Bioinorg. Chem.*, 1978, **9**, 145–155.

- 30 H. Irving, R. J. P. Williams, *J. Chem. Soc.*, 1953, 3192–3210.
- 31 N. Jiménez-Garrido, L. Perelló, R. Ortiz, G. Alzuet, M. González-Alvarez, E. Cantón, M. Liu-González, S. García-Granda and M. Pérez-Priede, *J. Inorg. Biochem.*, 2005, **99**, 677–689.
- 32 I. Turel, *Coord. Chem. Rev.*, 2002, **232**, 27–47.
- 33 S. Wu, W. Zhang, X. Chen, Z. Hu, M. Hooper, B. Hooper and Z. Zhao, *Spectrochim. Acta A Mol. Biomol. Spectrosc.*, 2001, **57**, 1317–1323.
- 34 M. Sakai, A. Hara, S. Anjo and M. Nakamura, *J. Pharm. Biomed. Anal.*, 1999, **18**, 1057–1067.
- 35 J. Al-Mustafa and Z. A. Taha, *Thermochim. Acta*, 2011, **521**, 9–13.
- 36 I. Turel, I. Leban and N. Bukovec, *J. Inorg. Biochem.*, 1997, **66**, 241–245.
- 37 H. Sun, H. Li and P. J. Sadler, *Chem. Ber./Recl.*, 1997, **130**, 669–681.
- 38 J. W. Clitherow. Salts of ranitidine and complexes of bismuth with carboxylic acids, and pharmaceutical compositions thereof. USPTO, 5008256, US Patent, 1991.
- 39 J. R. Lambert and P. Midolo, *Aliment. Pharmacol. Ther.*, 1997, 11 Suppl 1, 27–33.
- 40 Z. H. Chohan, C. T. Supuran and A. Scozzafava, *J. Enzyme Inhib. Med. Chem.*, 2005, **20**, 303–307.
- 41 A. Koppenhöfer, U. Hartmann and H. Vahrenkamp, *Chem. Ber.*, 1995, **128**, 779–785.
- 42 Z.-F. Chen, R.-G. Xiong, J. Zhang, X.-T. Chen, Z.-L. Xue and X.-Z. You, *Inorg. Chem.*, 2001, **40**, 4075–4077.
- 43 H. A. A. Ezelarab, S. H. Abbas, H. A. Hassan and G. E.-D. A. Abu-Rahma, *Arch. Pharm.*, 2018, **351**, e1800141.

- 44 T. M. E. Davis, T.-Y. Hung, I.-K. Sim, H. A. Karunajeewa and K. F. Ilett, *Drugs*, 2005, **65**, 75–87.
- 45 K. A. Gould, X.-S. Pan, R. J. Kerns and L. M. Fisher, *Antimicrob. Agents Chemother.*, 2004, **48**, 2108–2115.
- 46 Y.-Q. Hu, S. Zhang, Z. Xu, Z.-S. Lv, M.-L. Liu and L.-S. Feng, *Eur. J. Med. Chem.*, 2017, **141**, 335–345.
- 47 P. O. Brown and N. R. Cozzarelli, *Science*, 1979, **206**, 1081–1083.
- 48 A. Vanden Broeck, C. Lotz, J. Ortiz and V. Lamour, *Nat. Commun.*, 2019, **10**, 4935.
- 49 P. Heisig, *J. Antimicrob. Chemother.*, 1993, **32**, 367–377.
- 50 B. D. Bax, P. F. Chan, D. S. Eggleston, A. Fosberry, D. R. Gentry, F. Gorrec, I. Giordano, M. M. Hann, A. Hennessy, M. Hibbs, J. Huang, E. Jones, J. Jones, K. K. Brown, C. J. Lewis, E. W. May, M. R. Saunders, O. Singh, C. E. Spitzfaden, C. Shen, A. Shillings, A. J. Theobald, A. Wohlkonig, N. D. Pearson and M. N. Gwynn, *Nature*, 2010, **466**, 935–940.
- 51 The Protein Data Bank H.M. Berman, J. Westbrook, Z. Feng, G. Gilliland, T.N. Bhat, H. Weissig, I.N. Shindyalov, P.E. Bourne, *Nucleic Acids Research*, 2000, **28**: 235-242.
- 52 Designed and provided by A.-K. Duhme-Klair and A. J. Wilkinson
- 53 J. H. M. Cabral, A. P. Jackson, C. V. Smith, N. Shikotra, A. Maxwell and R. C. Liddington, *Nature*, 1997, **388**, 903–906.
- 54 R. J. Kerns, M. J. Rybak, G. W. Kaatz, F. Vaka, R. Cha, R. G. Grucz, V. U. Diwadkar and T. D. Ward, *Bioorg. Med. Chem. Lett.*, 2003, **13**, 1745–1749.
- 55 X.-M. Chu, C. Wang, W. Liu, L.-L. Liang, K.-K. Gong, C.-Y. Zhao and K.-L. Sun, *Eur. J. Med. Chem.*, 2019, **161**, 101–117.
- 56 R. J. Kerns, M. J. Rybak and C. M. Cheung, *Diagn. Microbiol. Infect. Dis.*, 2006, **54**, 305–310.

- 57 X. Zhao, B. Quinn, R. Kerns and K. Drlica, *J. Antimicrob. Chemother.*, 2006, **58**, 1283–1286.
- 58 Z. Ude, I. Romero-Canelón, B. Twamley, D. Fitzgerald Hughes, P. J. Sadler and C. J. Marmion, *J. Inorg. Biochem.*, 2016, **160**, 210–217.
- 59 K. J. Aldred, H. A. Schwanz, G. Li, B. H. Williamson, S. A. McPherson, C. L. Turnbough Jr, R. J. Kerns and N. Osheroff, *Biochemistry*, 2015, **54**, 1278–1286.
- 60 Z. Ude, K. Kavanagh, B. Twamley, M. Pour, N. Gathergood, A. Kellett and C. J. Marmion, *Dalton Trans.*, 2019, **48**, 8578–8593.
- 61 A. C. Gentry and N. Osheroff, in *Encyclopedia of Biological Chemistry* (Second Edition), eds. W. J. Lennarz and M. D. Lane, Academic Press, Waltham, 2013, pp. 163–168.
- 62 J. Azéma, B. Guidetti, A. Korolyov, R. Kiss, C. Roques, P. Constant, M. Daffé and M. Malet-Martino, *Eur. J. Med. Chem.*, 2011, **46**, 6025–6038.
- 63 G. Q. Hu, Z. Q. Zhang, S. Q. Xie and W. L. Huang, *Chin. Chem. Lett.*, 2010, **21**, 661–663.
- 64 We wish to acknowledge the use of the EPSRC funded Physical Sciences Data-science Service hosted by the University of Southampton and STFC under grant number EP/S020357/1.
- 65 M. P. López-Gresa, R. Ortiz, L. Perelló, J. Latorre, M. Liu-González, S. García-Granda, M. Pérez-Priede and E. Cantón, *J. Inorg. Biochem.*, 2002, **92**, 65–74.
- 66 L.-C. Yu, Z.-L. Tang, P.-G. Yi and S.-L. Liu, *J. Coord. Chem.*, 2009, **62**, 894–902.
- 68 D. K. Saha, S. Padhye, C. E. Anson and A. K. Powell, *Transition Met. Chem.*, 2003, **28**, 579–584.
- 69 P. Drevenšek, I. Leban, I. Turel, G. Giester and E. Tillmanns, *Acta Crystallogr. C*, 2003, **59**, m376–m378.

- 70 D. K. Saha, S. Patitungkho, S. Padhye, D. N. Deobagkar, A. Ozarkar, M. M. Bhadbhade and R. G. Gonnade, *Transition Met. Chem.*, 2005, **30**, 334–340.
- 71 J. Overgaard, I. Turel and D. E. Hibbs, *Dalton Trans.*, 2007, 2171–2178.
- 72 H. Farrokhpour, H. Hadadzadeh, F. Darabi, F. Abyar, H. A. Rudbari and T. Ahmadi-Bagheri, *RSC Adv.*, 2014, **4**, 35390–35404.
- 73 F. Rafiee, F. Haghi, R. Bikas, A. Heidari, M. Gholami, A. Kozakiewicz and H. Zeighami, *AMB Express*, 2020, **10**, 82.
- 74 D. K. Saha, S. Padhye, C. E. Anson and A. K. Powell, *Inorg. Chem. Commun.*, 2002, **5**, 1022–1027.
- 75 I. Turel, P. Živec, A. Pevec, S. Tempelaar and G. Psomas, *Eur. J. Inorg. Chem.*, 2008, 3718–3727.
- 76 L.-C. Yu, L. Lai, S.-L. Liu and Y. Xia, *J. Coord. Chem.*, 2009, **62**, 2261–2267.
- 77 Z.-F. Chen, L.-C. Yu, M. Zhang, T. Yuan, H. Liang, H.-K. Fun and Y. Zhang, *J. Coord. Chem.*, 2007, **60**, 219–228.
- 78 M. P. Chrysouli, C. N. Banti, N. Kourkoumelis, E. E. Moushi, A. J. Tasiopoulos, A. Douvalis, C. Papachristodoulou, A. G. Hatzidimitriou, T. Bakas and S. K. Hadjikakou, *Dalton Trans.*, 2020, **49**, 11522–11535.
- 79 D.-R. Xiao, E.-B. Wang, H.-Y. An, Y.-G. Li and L. Xu, *Cryst. Growth Des.*, 2007, **7**, 506–512.
- 80 S. Huang, P. Du, C. Min, Y. Liao, H. Sun and Y. Jiang, *J. Fluoresc.*, 2013, **23**, 621–627.
- 81 R. D. Shannon, *Acta Crystallogr. A*, 1976, **32**, 751–767.
- 82 X. Zhao and K. Drlica, *Curr. Opin. Microbiol.*, 2014, **21**, 1–6.
- 83 N. Abbaspour, R. Hurrell and R. Kelishadi, *J. Res. Med. Sci.*, 2014, **19**, 164–174.

- 84 K. D. Krewulak and H. J. Vogel, *Biochim. Biophys. Acta*, 2008, **1778**, 1781–1804.
- 85 M. S. Weiss and G. E. Schulz, *J. Mol. Biol.*, 1993, **231**, 817–824.
- 86 C.-E. Lin, Y.-Deng Jr, W.-S. Liao, S.-W. Sun, W.-Y. Lin and C.-C. Chen, *J. Chromatogr. A*, 2004, **1051**, 283–290.
- 87 The Cambridge Structural Database. C. R. Groom, I. J. Bruno, M. P. Lightfoot and S. C. Ward, *Acta Cryst.* (2016). B72, 171-179. DOI:10.1107/S2052520616003954.
- 88 I. Persson, *Journal of solution chemistry*, 2018, **47**, 797–805.
- 89 R. Sahu, P. Chaliha and V. Manivannan, *J. Chem. Sci.*, 2016, **128**, 37–42.
- 90 H.-J. Schneider, *Chem. Sci.*, 2012, **3**, 1381–1394.
- 91 J. A. K. Howard, V. J. Hoy, D. O'Hagan and G. T. Smith, *Tetrahedron*, 1996, **52**, 12613–12622.
- 92 Sheldrick, G.M., *Acta Cryst*, 2015, A71, 3-8.
- 93 Sheldrick, G.M, *Acta Cryst*, 2015, C71, 3-8.
- 94 N. J. Hair and J. K. Beattie, *Inorg. Chem.*, 1977, **16**, 245–250.
- 95 P. D. Robinson and J. H. Fang, *Am. Mineral.*, 1971, **56**, 1567.
- 96 K. J. Palmer, R. Y. Wong, and K. S. Lee, *Acta Crystallogr.*, 1972, **28**, 236 Sect. B.
- 97 J. N. Thomas, P. D. Robinson, and J. H. Fang, *Am. Mineral.*, 1974, **59**, 582.
- 98 P. D. Robinson and J. H. Fang, *Am. Mineral.*, 1973, **58**, 535.
- 99 J. H. Fang and P. D. Robinson, *Am. Mineral.*, 1970, **55**, 1534.
- 100 L. Fanfani, A. Nunzi, and P. F. Zanazzi, *Am. Mineral.*, 1970, **55**, 78.

- 101 M. D. Lind, *J. Chem. Phys.*, 1967, **47**, 990.
- 102 A. Ferrari, L. Cavalca and E. Tañí, *Gazz. Chim. Ital.*, 1957, **87**, 22.
- 103 I. Lindqvist, *Ark. Kemi, Mineral. Geol.*, 1947, **24**, 1.
- 104 M. D. Lind, M. J. Hamor, T. A. Hamor, and J. L. Hoard, *Inorg. Chem.*, 1964, **3**, 34.
- 105 C. H. L. Kennard, *Inorg. Chim. Acta*, 1968, **1**, 347.
- 106 P. J. Sadler, *Advances in Inorganic Chemistry*, Academic Press, 1991, vol. 36.
- 106 J.-H. He, D.-Z. Sun, D.-R. Xiao, S.-W. Yan, H.-Y. Chen, X. Wang, J. Yang and E.-B. Wang, *Polyhedron*, 2012, **42**, 24–29.
- 107 B. Lu and Y. Zhu, *Phys. Chem. Chem. Phys.*, 2014, **16**, 16509–16514.
- 108 R. A. Scott, Ed., in *Encyclopedia of Inorganic and Bioinorganic Chemistry*, John Wiley & Sons, Ltd, Chichester, UK, 2011, vol. 123, pp. 1–32.
- 109 R. J. P. Williams, *Endeavour*, 1984, **8**, 65–70.
- 110 I. Turel, P. Bukovec and M. Quirós, *Int. J. Pharm.*, 1997, **152**, 59–65.
- 111 K. D. Mjos, J. F. Cawthray, E. Polishchuk, M. J. Abrams and C. Orvig, *Dalton Trans. J. Inorg. Chem.*, 2016, **45**, 13146–13160.
- 112 S. A. Sadeek, W. H. El-Shwiniy, W. A. Zordok and A. M. El-Didamony, *Spectrochim. Acta A Mol. Biomol. Spectrosc.*, 2011, **78**, 854–867.
- 113 S. R. M. D. Saleh, 2009. Siderophore-drug conjugates as novel antibacterial agents. MPhil thesis. University of York (2009).
- 114 B. Wiedemann and P. Heisig, *Infection*, 1994, 22 Suppl 2, S73–9.
- 115 R. Pourahmad Jaktaji and E. Mohiti, *Iran. J. Pharm. Sci.*, 2010, **9**, 43–48.
- 116 D. S. Horowitz and J. C. Wang, *J. Biol. Chem.*, 1987, **262**, 5339–5344.

- 117 H Yoshida, M Bogaki, M Nakamura, S Nakamura, *Antimicrob. Agents Chemother.*, 1990, **34**, 1271–1272.
- 118 T. Paul, J. Liu, M. L. Machesky and T. J. Strathmann, *J. Colloid Interface Sci.*, 2014, **428**, 63–72.
- 119 F. Bray, J. Ferlay, I. Soerjomataram, R. L. Siegel, L. A. Torre, A. Jemal, *CA Cancer J. Clin.*, 2018, **84**, 394–424.
- 120 S. Wang, F. Zhang, G. Yu, Z. Wang, O. Jacobson, Y. Ma, R. Tian, H. Deng, W. Yang, Z.-Y. Chen and X. Chen, *Theranostics*, 2020, **10**, 6629–6637.
- 121 J. L. Nitiss, *Nat. Rev. Cancer*, 2009, **9**, 338–350.
- 122 B. Xu, X.-L. Kong, T. Zhou, D.-H. Qiu, Y.-L. Chen, M.-S. Liu, R.-H. Yang and R. C. Hider, *Bioorg. Med. Chem. Lett.*, 2011, **21**, 6376–6380.
- 123 P. Ball, in *The Quinolones (Third Edition)*, ed. V. T. Andriole, *Academic Press*, San Diego, 2000, pp. 1–31.
- 124 SciFinder, <https://scifinder.cas.org>, (accessed November 2020).
- 125 S. Garaga, A. V. R. Reddy, K. J. Prabahar, R. B. Korupolu and P. D. Sanasi, *Sci. Pharm.*, 2013, **81**, 651–662.
- 126 S. J. Milner, 2011. *Siderophore-Drug Conjugates As Novel Antimicrobial Agents*. PhD. University of York.
- 127 A. G. Al-Bakri, G. Othman and Y. Bustanji, *J. Appl. Microbiol.*, 2009, **107**, 280–286.
- 128 M. T. Arias-Moliz, C. M. Ferrer-Luque, M. Espigares-García and P. Baca, *J. Endod.*, 2009, **35**, 711–714.
- 129 R. Zhang, M. Chen, Y. Lu, X. Guo, F. Qiao and L. Wu, *Sci. Rep.*, 2015, **5**, 12944.
- 130 S. Klosek. Dual-sensitizer-containing luminescent compounds, conjugates, and uses thereof. Int. Pat., 019403, 2008.

- 131 K. Groche, U. Petersen and K. Kuck. US Pat., 4 563 459, 1986.
- 132 M. A. A. Abdel-Aal, S. A. Abdel-Aziz, M. S. A. Shaykoon and G. E.-D. A. Abuo-Rahma, *Arch. Pharm.* , 2019, **352**, e1800376.
- 133 A. M. Kamat, J. I. DeHaven and D. L. Lamm, *Urology*, 1999, **54**, 56–61.
- 134 J. Polster and H. Lachmann, *Spectrometric titrations*, VCH, Weinheim, 1989.